INTEGRATED APPROACH TOWARDS UNDERSTANDING

INTERACTIONS OF MINERAL DUST AEROSOL WITH WARM

CLOUDS

A Dissertation
Presented to
The Academic Faculty

by

Prashant Kumar

In Partial Fulfillment
of the Requirements for the Degree
Doctor of Philosophy in the
School of Chemical & Biomolecular Engineering

Georgia Institute of Technology
May 2011

INTEGRATED APPROACH TOWARDS UNDERSTANDING INTERACTIONS OF MINERAL DUST AEROSOL WITH WARM CLOUDS

Approved by:

Dr. Irina N. Sokolik, Advisor
School of Earth & Atmospheric Sciences
Georgia Institute of Technology

Dr. Athanasios Nenes, Advisor
School of Chemical & Biomolecular
Engineering and Earth & Atmospheric
Sciences
Georgia Institute of Technology

Dr. Amyn Teja
School of Chemical & Biomolecular
Engineering
Georgia Institute of Technology

Dr. Carson Meredith
School of Chemical & Biomolecular
Engineering
Georgia Institute of Technology

Dr. Rodney Weber
School of Earth & Atmospheric Sciences
Georgia Institute of Technology

Date Approved: March 21, 2011

To My Dearest Parents

ACKNOWLEDGEMENTS

This thesis would not be possible without the guidance and support of my advisors, Prof. Athanasios Nenes and Prof. Irina N. Sokolik. I thank Prof. Nenes and Prof. Sokolik for believing in my research potential, and for initiating a joint collaboration between Chemical Engineering and Atmospheric Sciences. I have learned many things from them, and those that stand out include the art of research and being one's own critique. It feels unique to be classified as a chemical engineer in climate research with both experimental and modeling skill-sets.

I would like to thank my committee members Prof. Amyn Teja, Prof. Carson Meredith, and Prof. Rodney Weber for their valuable comments and insights. The work in this thesis was funded by the NOAA ACC grant and NOAA is thanked for their support. I also extend thanks to all current members and alumni of both Nenes and Sokolik group for being great colleagues. In particular, I thank Terry Lathem, Dr. Vlassis Karydis, Dr. Donifan Barahona, Max Bangert, and Prof. Josef Dufek for collaborations on various projects during my PhD.

This work could have not been possible without the encouragement of my friends at Georgia Tech. I thank Pramod Warrier for his support during PhD qualifiers in 2008, and for being a great housemate. I also thank Dhaval Bhandari and Ashish Pande for being there when it mattered the most. I will always cherish my friendship with Siddharth Athreya, Manoj Agrawal, Divya Paruchuri, and Yanto Yanto for all the precious memories at Georgia Tech. I really enjoyed my friendship with Prabuddha Bansal, Nitesh

Bhuwania, Ambarish Kulkarni, Kiran Kambly, Pei Yoong Koh, and many other friends. I thank you all for making my four years at Georgia Tech truly memorable.

I would also like to acknowledge Prof. R P Chhabra for his guidance in 2006 when I was applying for a PhD in US. I thank Saurabh Kumar for his support in 2007 when I started at Georgia Tech.

Finally, I thank my family for their love and support throughout my life and through my PhD journey. I thank my father, Prof. Vinod Kumar Srivastava and my mother, Manju Srivastava for their continued and everlasting encouragement in the last four years. I am also thankful to my sister, Arpita Srivasatava and brother-in-law Shantanu Nigam who reside in Atlanta for their constant support and love. I feel lucky to have family away from home. My niece Siya Nigam has been my stress buster in the last two years.

I thank divine god for his blessings and for making this work possible.

TABLE OF CONTENTS

LIST OF TABLES

LIST OF FIGURES

xv

LIST OF SYMBOLS

a_w	Water activity
A_{FHH}	FHH adsorption isotherm parameter
B_{FHH}	FHH adsorption isotherm parameter
C	Power law constant
$C(D_m)$	Slip correction factor for D_m
$C(D_{ve})$	Slip correction factor for D_{ve}
c_p	Heat capacity of air
D_c	Critical wet diameter
D_{core}	Dust core diameter
D_{dry}	Dry CCN diameter
D_g	Geometric mean diameter
D_m	Electrical mobility diameter
D_n	Diameter of the sphere whose projected area is equal to that of the particle normal to the direction of flow
D_p	Droplet diameter
D_{se}	Surface-area equivalent diameter
$D_v^{'}$	Diffusivity of water vapor in air modified for non continuum effects
D_v	Diffusivity of water vapor in air
D_{ve}	Volume equivalent diameter
$D_{v,ave}$	Average mass transfer coefficient
ΔD_w	Droplet size difference at OPC
D_{H_2O}	Diameter of water molecule

e	Entrainment rate of dry air into the parcel
F_D	Drag force
F_κ	KT activation fraction
F_{FHH}	FHH-AT activation fraction
g	Acceleration due to gravity
ΔH_v	Enthalpy of vaporization of water
$I_e(0, s_{max})$	Condensation integral
M_a	Molar mass of air
M_s	Molar mass of solute
M_w	Molar mass of water
N_d	Cloud droplet number
N_d^κ	KT droplet number
N_d^{FHH}	FHH-AT droplet number
N_0	Particle concentration
$n_l^s(s)$	Critical supersaturation distribution function
n_m	number of lognormal modes in the size distribution
n_s	Moles of solute
n_T	Total moles in the aqueous phase
n_w	Moles of water in the droplet
P	Pressure
$P_{H_2O}^\circ$	Equilibrium water vapor pressure
R	Universal gas constant
s	Supersaturation
s_c	Critical supersaturation

s_{eq}	Equilibrium supersaturation
s_{max}	Parcel maximum supersaturation
S	Saturation ratio
T	Temperature
ΔT	Thermal gradient
V	Parcel updraft velocity
V_s	Solute volume
V_w	Water volume
V_T	Droplet volume
w	Updraft Velocity
w_l	Liquid water vapor mixing ratio
w_t	Total water vapor mixing ratio
w_v	Water vapor mixing ratio
w_v^*	Saturation water vapor mixing ratio
x	Power law exponent relating s_c and D_{dry}
x_{exp}	Experimental exponent
x_{FHH}	FHH-AT exponent
x_κ	KT exponent
x_i	Mass fraction of the certain compound i
x_s	Mole fraction of soluble salt
x_w	Mole fraction of water in the droplet

Greek Letters

κ	Hygroscopicity parameter
κ_{mix}	Theoretical hygroscopicity parameter
κ_{CCN}	CCN measurements derived hygroscopicity parameter
ρ_{a}	Air density
ρ_{s}	Solute density
ρ_{w}	Water density
α_{c}	Water vapor uptake coefficient
α_{T}	Thermal accommodation coefficient
σ_{w}	Surface tension of water
σ_{g}	Standard deviation
k_{a}	Thermal conductivity of air
$k_a^{'}$	Thermal conductivity of air modified for non continuum effects
χ	Dynamic shape factor
λ	Mean free path of the gas molecules
υ_{s}	Solute effective van't Hoff factor
ε_{s}	Soluble volume fraction
ε_{i}	Insoluble volume fraction
γ_{w}	Activity coefficient for water
Θ	Number of water monolayers
θ_{l}	Potential temperature in moist air

LIST OF ABBREVIATIONS

AIE	Aerosol Indirect Effect
AMMA	African Monsoon Measurements Analysis
AR	Aspect Ratio
ASTEX	Atlantic Stratocumulus Transition Experiment
AT	Adsorption Activation Theory
ATD	Arizona Test Dust
BET	Brunauer Emmett Taylor
CCN	Cloud Condensation Nuclei
CFSTGC	Continuous Flow Stream-wise Thermal Gradient CCN Chamber
CID	Canary Island Dust
CN	Condensation Nuclei
CPC	Condensation Particle Counter
CRYSTAL-FACE	The Cirrus Regional Study of Tropical Anvils and Cirrus Layers - Florida Area Cirrus Experiment
DMA	Differential Mobility Analyzer
DMT	Droplet Measurement Technology
EDX	Energy-dispersive X-ray spectroscopy
ERBE	Earth Radiation Budget Experiment
ESEM	Environmental Scanning Electron Microscopy
FHH	Frenkel Halsey Hill
GCCN	Giant Cloud Condensation Nuclei
GF	Growth Factor
HTDMA	Hygroscopicity Tandem Differential Mobility Analyzer

IC	Ion Chromatography
ICP	Inductively Coupled Plasma
IPCC	Intergovernmental Panel on Climate Change
IN	Ice Nuclei
KT	Köhler Theory
LWC	Liquid Water Content
MOUDI	Micro Orifice Uniform Deposition Impactor
OL	Owens Lake
OPC	Optical Particle Counter
RH	Relative Humidity
RMSE	Root Mean Square Error
SD	Saharan Dust
SEM	Scanning Electron Microscopy
SMCA	Scanning Mobility CCN Analysis
SMPS	Scanning Mobility Particle Sizer
TDGA	Threshold Droplet Growth Analysis

SUMMARY

Mineral dust is ubiquitous in the atmosphere and represents a dominant type of particulate matter by mass. Dust particles can serve as cloud condensation nuclei (CCN), giant CCN (GCCN), or ice nuclei (IN), thereby, affecting cloud microphysics, albedo, and lifetime. Despite its well-recognized importance, assessments of dust impacts on clouds and climate remain highly uncertain. This thesis addresses the role of dust as CCN and GCCN with the goal of improving our understanding of dust-warm cloud interactions and their representation in climate models.

Most studies to date focus on the soluble fraction of aerosol particles when describing cloud droplet nucleation, and overlook the interactions of the hydrophilic insoluble fraction with water vapor. A new approach to include such interactions (expressed by the process of water vapor adsorption) is explored, by combining multilayer Frenkel-Halsey-Hill (FHH) physical adsorption isotherm and curvature (Kelvin) effects.

The importance of adsorption activation theory (FHH-AT) is corroborated by measurements of CCN activity of mineral aerosols generated from clays, calcite, quartz, and desert soil samples from Northern Africa, East Asia/China, and Northern America. A new aerosol generation setup for CCN measurements was developed based on a dry generation technique capable of reproducing natural dust aerosol emission. Based on the dependence of critical supersaturation with particle dry diameter, it is found that the FHH-AT is a better framework for describing fresh (and unprocessed) dust CCN activity than the classical Köhler theory (KT). Ion Chromatography (IC) measurements

performed on fresh regional dust samples indicate negligible soluble fraction, and support that water vapor adsorption is the prime source of CCN activity in the dust.

CCN measurements with the commonly used wet generated mineral aerosol (from atomization of a dust aqueous suspension) are also carried out. Results indicate that the method is subject to biases as it generates a bimodal size distribution with a broad range of hygroscopicity. It is found that smaller particles generated in the more hygroscopic peak follow CCN activation by KT, while the larger peak is less hydrophilic with activation similar to dry generated dust that follow FHH-AT.

Droplet activation kinetics measurements demonstrate that dry generated mineral aerosol display retarded activation kinetics with an equivalent water vapor uptake coefficient that is 30 - 80% lower relative to ammonium sulfate aerosol. Wet generated mineral aerosols, however, display similar activation kinetics to ammonium sulfate. These results suggest that at least a monolayer of water vapor (the rate-limiting step for adsorption) persists during the timescale of aerosol generation in the experiment, and questions the atmospheric relevance of studies on mineral aerosol generated from wet atomization method.

A new parameterization of cloud droplet formation from insoluble dust CCN for regional and global climate models is also developed. The parameterization framework considers cloud droplet formation from dust CCN activating via FHH-AT, and soluble aerosol with activation described through KT. The parameterization is validated against a numerical parcel model, agreeing with predictions to within 10% ($R^2 \sim 0.98$).

The potential role of dust GCCN activating by FHH-AT within warm stratocumulus and convective clouds is also evaluated. It is found that under pristine

aerosol conditions, dust GCCN can act as collector drops with implications to dust-cloud-precipitation linkages. Biases introduced from describing dust GCCN activation by KT are also addressed.

The results demonstrate that dust particles do not require deliquescent material to act as CCN in the atmosphere. Furthermore, the impact of dust particles as giant CCN on warm cloud and precipitation must be considered. Finally, the new parameterization of cloud droplet formation can be implemented in regional and global models providing an improved treatment of mineral aerosol on clouds and precipitation. The new framework is uniquely placed to address dust aerosol indirect effects on climate.

CHAPTER 1

INTRODUCTION

1.1   Clouds, Aerosol, and Climate Change

Clouds are a key component of the climate system and play an important role in controlling the Earth's energy balance and hydrological cycle. About 60% of the Earth is covered by clouds that cool the Earth-atmosphere system on a global average (Lohmann and Feichter, 2005). Figure 1.1 shows how clouds affect the Earth's energy balance, demonstrating their central role in controlling the energy distribution in the atmosphere and between surface-and-atmosphere. Measurements of the Earth Radiation Budget Experiment (ERBE) indicate that small changes in clouds macrophysical (coverage, structure, altitude, and mixing) and microphysical (droplet number, size, phase, nucleation and growth of droplets, and ice crystals) properties have significant impacts on climate. In addition to controlling the radiation budget, clouds also play an important role in controlling the moisture in the atmosphere and the availability of fresh water. Understanding clouds, where they occur, and their characteristics, is thought to be the key to understanding the climate and climate change.
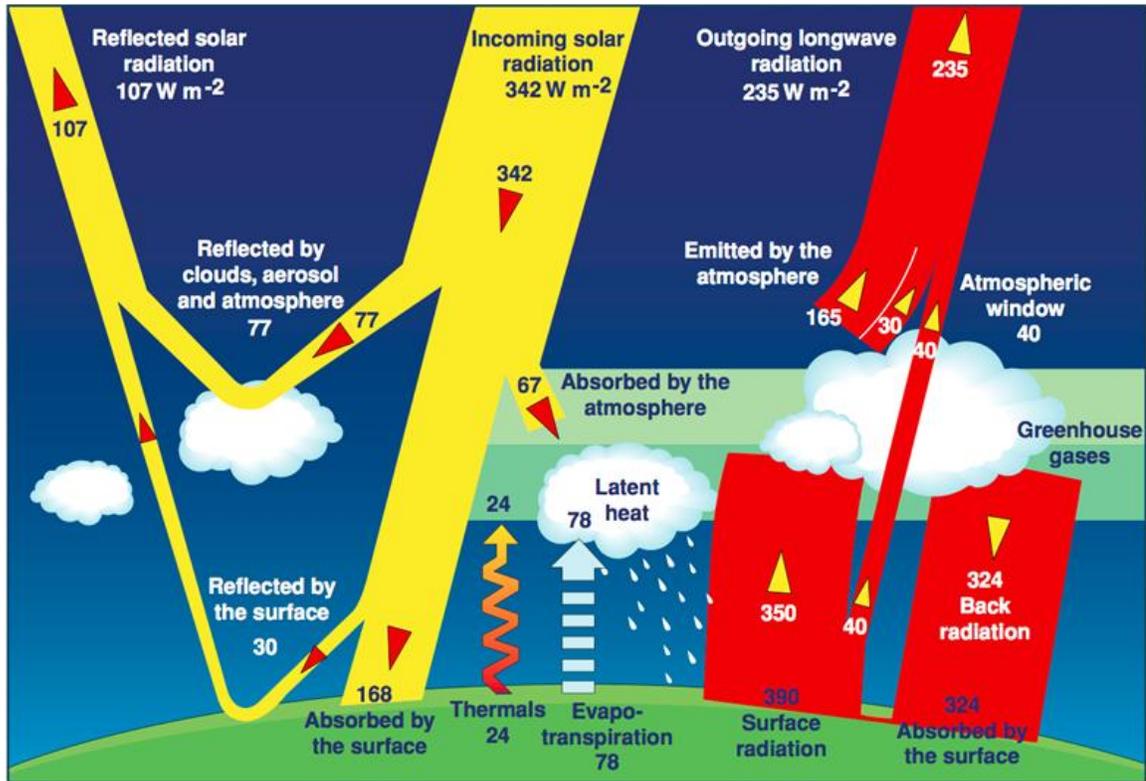
Figure 1.1: Radiative budget of the Earth (Kiehl and Trenberth, 1997).

Together with clouds, suspended atmospheric particles (or aerosols) play an important role in the climate system. Due to their ability to absorb and scatter solar and terrestrial radiation, aerosol particles have a direct influence on the radiative energy balance. Furthermore, there is mounting evidence that atmospheric aerosols interact with the climate system and impact the hydrological cycle through changes in cloud coverage, cloud properties and precipitation (Collins et al., 1994, Lohmann and Feichter, 2005, Levin and Cotton, 2008). Certain aerosols can serve as cloud condensation nuclei (CCN) upon which water vapor can condense to form cloud droplets. This link between aerosol and cloud formation is referred as the Aerosol Indirect Effect (AIE) and is a major source of uncertainty in climate change predictions. The Intergovernmental Panel on Climate Change (IPCC) in their report from 2007 (Fig. 1.2), stated that aerosols potentially have a

strong cooling effect due to AIE on climate that rivals the warming influence by the greenhouses gases. However the level of scientific understanding was low as indicated by an extremely large error bar. This uncertainty in AIE originates from poorly quantified assessments of aerosol-cloud interactions in climate models, both global and regional scales. Some of these challenges include poorly understood interactions of different types of particulate matter with atmospheric water vapor, theoretical shortcomings in physical mechanisms that explain aerosol-water vapor interactions, lack of observational data (on sources, emissions, etc.) to complexities associated with coarse grid size of global climate models. Measurements have played an important role in this research, and will need to span for regional to global scales in order to comprehensively test climate system models.

Cloud droplet activation is the direct microphysical link between aerosols and clouds, and is at the heart of the aerosol indirect effect (Nenes and Seinfeld, 2003). Droplet activation in atmospheric models is often calculated from physically-based prognostic formulations (e.g., Feingold and Heymsfield, 1992; Abdul-Razzak et al., 1998; Abdul-Razzak and Ghan, 2000; Cohard et al., 2000; Nenes and Seinfeld, 2003, Fountoukis and Nenes, 2005; Ming et al., 2006; Barahona and Nenes, 2007) that rely on Köhler theory (Köhler, 1936). Köhler theory considers curvature and solute effects on the equilibrium vapor pressure of a growing droplet, and can describe the equilibrium growth of a droplet as a function of ambient supersaturation. However, it is well known that insoluble species like dust can serve as cloud condensation nuclei (CCN), giant CCN (GCCN) (e.g., Rosenfeld et al., 2001; Levin and Cotton, 2008), or ice nuclei (IN) (e.g., DeMott et al., 2003; Field et al., 2006) thereby affecting cloud microphysics, albedo, and lifetime by serving as cloud condensation nuclei (CCN), giant CCN (GCCN) (e.g., Rosenfeld et al., 2001; Levin and Cotton, 2008), or ice nuclei (IN) (e.g., DeMott et al.,

2003; Field et al., 2006). Despite its well-recognized importance, assessing the impacts of dust on clouds and climate remains uncertain due to theoretical shortcomings in current activation theory (Köhler theory) when applied to dust aerosol. Therefore, a thorough understanding of the interactions of mineral (dust) aerosol with warm clouds is of significant importance.
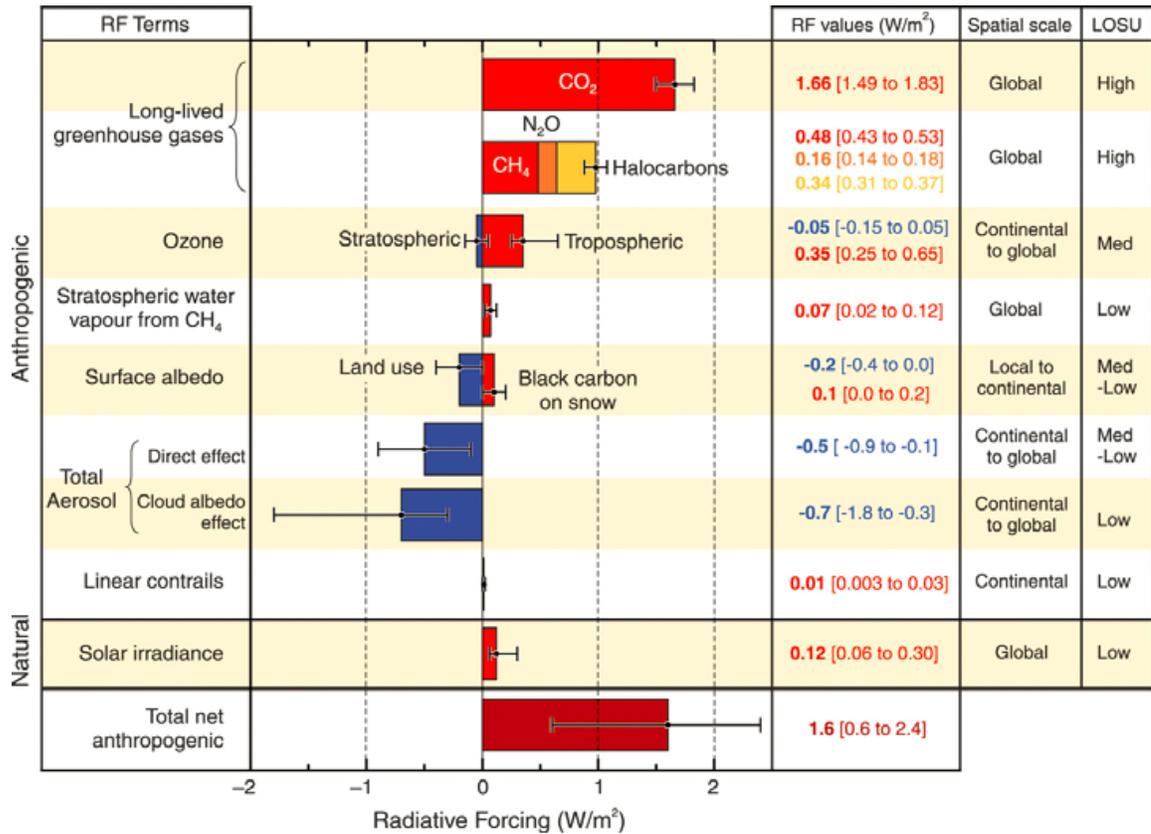
Figure 1.2: Estimated global average radiative forcing from anthropogenic and natural sources. Also shown is the spatial scale, and the level of scientific understanding. Figure obtained from IPCC, 2007 (Forster et al., 2007).

1.2   Mineral Aerosols (Dust)

Mineral aerosols represent a dominant source of particulate matter (by mass) in the atmosphere. The largest global source of wind-blown dust is desert regions with approximately 1000 - 5000 Tg of dust particles emitted annually (Schuttlefield et al., 2007). Major dust source regions extend from west coast of North Africa through the Middle East, into Central Asia and cover some of major deserts that includes the Sahara in Africa, deserts of Arabian Peninsula, Oman, dried lakebeds of Caspian and Aral Sea in Central Asia, and extending through to the Gobi and the Taklimakan in China. Outside the major dust sources, emissions are also observed from sources located in USA and Mexico in Northern America, the Great Artesian Basin of Australia, Botswana depressions and the Namibia Desert in Southern Africa, as well as the Sothern American deserts of Altiplano in Bolivia, and smaller deserts in Patagonia and in Western Argentina (Formenti et al., 2010).

Dust particles can alter the Earth's radiation budget directly because of their tendency to absorb and scatter solar and infrared radiation (Sokolik et al., 2001). They also affect the climate indirectly by interacting with water vapor and thus affecting cloud properties and precipitation (Ramanathan et al., 2001). In addition, the iron content of dust provides an importance souces of fertizer in oceans via deposition and dissolution mechanism (Duce et al., 1991). Other than the climatic impacts, mineral dust also has a direct adverse impact on human health (e.g., Kwon et al., 2002; Perez et al., 2008) by acting as a carrier of micro-organisms (Kellogg and Griffin, 2006), as well as on regional air quality because of the visibility impairment (Prospero, 1999).

Mineral dust is a complex mixture of a variety of species such as iron oxides (e.g., hematite (Fe_2O_3), goethite ($FeO(OH)$)), carbonates (e.g., calcite ($CaCO_3$), dolomite ($CaMg(CO_3)_2$)), quartz (SiO_2), and clays (kaolinite ($Al_2Si_2O_5(OH)_4$), illite ($K,H_3O)(Al,Mg,Fe)_2(Si,Al)_4O_{10}[(OH)_2,(H_2O)]$, and montmorillonite ($(Na,Ca)_{0.33}(Al,Mg)_2(Si_4O_{10})(OH)_2 \cdot nH_2O)$])) (Lafon et al., 2006; Chou et al., 2008; Coz et al., 2009; Twohy et al., 2009). Due to differences in the parent soils, dust aerosol originating from different source regions can have different chemical composition. Formenti el al. (2010) suggested that the fraction of calcite content and the ratio of illite to kaolinite clay in mineral dust samples can be used as a fingerprint to identify dust from specific source areas. For instance, a ratio of illite to kaolinite mass fraction greater than five corresponds to dust from Northern Africa while a ratio of illite to kaolinite mass fraction less than two is representative of dust originating from Eastern Asia.

Mineral dust particles can remain suspended in the atmosphere for up to several weeks and can be transported large distances downwind from the source regions. During transport, dust particles (especially the carbonate fraction which can comprise up to 30% of the total mass), provide reaction surfaces for heterogonous and multiphase reactions with anthropogenic pollutants such as nitrates and sulphates (Levin et al., 1996), resulting in modified dust properties, such as enhanced hygroscopicity (Hatch et al., 2008). Thus differences in parent soils, and emission and transport processes can cause substantial variability in size-resolved composition and morphology of dust particles (Sokolik et al., 2001; Jeong and Sokolik, 2007).

Apart from varied chemical composition, dust particles also exhibit a variety of complex shapes, of sizes varying from few hundred nanometers to hundreds of microns

that are difficult to measure or express in terms of a unique set of parameters or functions. Characterization of dust non-sphericity is often done by either (*i*) introducing a dynamic shape factor, χ, (defined as the ratio of drag force, F_D, experienced by the non-spherical particle to that experienced by a volume equivalent sphere when both move at the same velocity in the gas (e.g., DeCarlo et al., 2004), or (*ii*) providing an Aspect Ratio (*AR*), defined as the ratio of the longest dimension of particles to the orthogonal shortest length (width). Commonly, χ is obtained by tandem electrical mobility and aerodynamic particle sizing (e.g., DeCarlo et al., 2004; Kuwata and Kondo, 2009) and is an integrated measure of the three-dimensional particle shape. *AR* is measured with electron microscopy that reports two dimensional image projections of particles from which the longest dimension and width are determined (e.g., Kalashnikova and Sokolik, 2004). A number of recent studies have reported measurements of *AR* values for species considered in this study. For instance, Chou et al. (2008) report a mean *AR* equal to 1.7 for Niger dust collected during the AMMA campaign, Kandler et al. (2009) report *AR* equal to 1.64 for Saharan dust collected over Spain, and Coz et al. (2009) report *AR* equal to 1.81 for African dust. These *AR* values are somewhat higher compared to *AR* equal to 1.3 − 1.4 reported by Okada et al. (2001) for East Asian dust. *AR* can also vary with particle size (Wiegner et al., 2009). As particle size and shape are fundamental parameters that describe atmospheric lifetime, transport processes, as well aerosol direct and indirect radiative impacts, uncertainties associated with mineral dust shape further complicates understanding of impacts of mineral dust on the Earth system.

1.3 Mineral Aerosols as Cloud Condensation Nuclei

Mineral dust has been found to play an important role in both warm (liquid) and mixed-phase clouds through both direct and indirect effects. When first emitted into the atmosphere, mineral dust particles are often insoluble, but during the course of their transport (short, mid or long-range), they acquire some deliquescent material, such as $(NH_4)_2SO_4$ (Levin et al., 1996); and become efficient Cloud Condensation Nuclei (CCN), upon which cloud droplets are formed through the process of activation. Changes in the CCN concentration affect the radiative properties of clouds, known as the "cloud albedo" or "Twomey" effect of aerosols (Twomey, 1974). The enhanced number of droplets is often accompanied by a reduction in their size, thereby affecting cloud precipitation efficiency. This may result in increased cloudiness, which gives rise to the so called "cloud lifetime" or "Albrecht" effect of aerosols (Albrecht, 1989). These effects combined, are known as aerosol indirect effects.

The ability of dust particles to serve as a CCN under atmospherically relevant water vapor supersaturations depends on their mineralogy, size, morphology, and atmospheric processing (aging). Due to differences in chemical composition of the parent soils, as well as the emission and transport routes of suspended dust particles, mineral aerosol at the source region and downwind can have different chemical composition and morphology, which leads to differences in solubilities and hydrophilicities (Sokolik et al., 2001) with implications to dust CCN activation potential. Additionally, due to changes in precipitation patterns as a result of anthropogenic disturbances, the sizes of global arid regions are expected to increase by millions of hectares per year (Sheehy, 1992). All these factors combined makes mineral dust interaction with clouds even more

complicated compared to other tropospheric aerosols. Thus understanding the dust particle's ability to act as CCN, and associated impacts on clouds is essential for improved climate change predictions.

Based on modeling studies, it has been suggested that mineral dust aerosol can contribute to up to 10% of the global CCN burden (Hoose and Lohmann, 2008), with contribution being much larger in desert regions and in regions affected by dust transport. This has been confirmed by laboratory studies that demonstrated both regional dusts as well as individual clays can interact with water to act as effective CCN. For example, Koehler et al. (2009) and Herich et al. (2009) measured CCN activation of two types of regional dust samples (Northern Africa and Arizona Test Dust) and several clays (kaolinite, illite, and montmorillonite), respectively, at water vapor supersaturation relevant to atmospheric conditions. These laboratory measurements provided sufficient evidence that fresh insoluble mineral dust aerosol, even without a significant fraction of soluble material, can act as a CCN at atmospherically relevant supersaturations (Seinfeld and Pandis, 2006).

The inability and/or inconsistencies in current droplet nucleation theories to accurately describe fresh and aged dust CCN activity, makes mineral dust aerosol as one of the least understood components of the climate change. A number of models as well as modifications to the current activation theory known as Köhler theory (KT) (Köhler, 1936) have been proposed to describe insoluble particle CCN activity (e.g., Fletcher, 1958; Wexler and Ge, 1998; Abdul-Razzak and Ghan, 2000; Dusek et al., 2006; Petters and Kreidenweis, 2007). Significant discrepancies, however, exist between reported laboratory measurements and results predicted by theories. This is because current

activation theories, when applied to dust, assume that the dust CCN activity is dependent solely on the soluble fraction. Furthermore, all modifications to Köhler theory, fail to account for the interactions between hydrophilic insoluble fraction (or dust core) and water vapor, even if appreciable.

It was suggested recently that the threshold of cloud droplet nucleation substantially decreases, when water vapor adsorbs onto the surface of slightly soluble or insoluble particles, resulting in cloud droplet formation by the process of adsorption activation. The CCN activity of a fresh dust particle (i.e., without any appreciable soluble coating) can hence be described using a different activation mechanism of physical adsorption. Henson (2007) showed that BET (Brunauer, Emmett and Taylor) (Brunauer et al., 1938) isotherms can be successfully applied to represent droplet formation by adsorption activation for insoluble CCN. Similarly, Sorjamaa and Laaksonen (2007) used the Frenkel-Halsey-Hill (FHH) multilayer physical adsorption model to describe water uptake as a function of relative humidity (i.e., water activity) and applied the theory to describe the activation of perfectly wettable and insoluble hydrophilic CCN. The new formulations of activation of hydrophilic insoluble CCN as described by Henson, and Sorjamaa and Laaksonen will be referred to as the adsorption activation theory (AT).

Predicting complex effects of mineral dusts on clouds and climate requires integrating observational knowledge into theoretical descriptions or parameterizations. Laboratory studies can provide data for developing and constraining parameterizations for the use in numerical modeling of dust impacts on clouds. However, there are many challenges associated with laboratory measurements such as generating mineral dust aerosol with a distribution that resembles the size distributions of dust plumes generated

in the natural source regions, simulating atmospherically relevant water vapor supersaturations in laboratory instruments, accurately relating the composition of mineral dust CCN to its CCN activation potential, identifying the role of dust processing and transformation in the atmosphere as a consequence of long range transport, to being able to encapsulate all of this information for use in climate models.

Similarly, global aerosol-climate models so far have paid little attention to mineral dust, due to their low number concentrations and reduced hygroscopicities in comparison to other tropospheric aerosols. Because of these complexities involved in dust-cloud interactions, climate models either do not include dust or if they do, these predictions rely on overly simplified parameterizations to treat dust activation behavior. To date, only a few state-of-the art global aerosol climate models include dust in the parameterizations. For instance, ECHAM5-HAM (Lohmann et al., 2007) treats only dust particles coated with sulphates and excludes the contribution of externally mixed mineral dust to cloud droplet number. In MIRAGE (Easter et al., 2004), SPRINTARS (Takemura et al., 2005), and CAM-Oslo (Storelvmo et al., 2006) model, pure mineral dust is assigned a soluble fraction of 13%, 14%, and 1.3%, respectively. Hence, more work is desired with regards to the activation of mineral aerosol to simulate realistic dust-cloud interactions for accurate assessment of dust aerosol indirect effect.

The influence of dust particles on warm clouds can be more significant if they are large enough to act as a giant CCN (GCCN) (defined as particles with a dry diameter larger than 5 μm); thus altering precipitation efficiency (i.e., promote or suppress precipitation). For example, some studies suggest that large salt containing mineral dust particles can initiate precipitation formation by broadening the droplet spectrum and

enhancing cloud-coalescence processes in a cloud cycle (Feingold et al., 1999; Rudich et al., 2002). Yin et al. (2002) used parcel model simulations to show that mineral dust aerosol can promote precipitation due to formation of a soluble coating on its surface, causing dust particle to grow to the size of a GCCN. On the other hand, Rosenfeld et al. (2001) and Mahowald and Kiehl (2003) found using remote sensing measurements that dust particles can also decrease the collision-coalescence process, thus increasing cloud lifetime and reducing precipitation efficiency. Van den Heever et al. (2005) investigated the effects of increasing GCCN concentrations from relatively clean conditions to dusty conditions; using measurements from the CRYSAL-FACE field campaign and noted that while more liquid water was produced under dusty conditions; precipitation processes were suppressed resulting in a reduction of total precipitation reaching the ground as compared to the clean case. Teller and Levin (2006) found that increasing the GCCN concentration led to a decrease in precipitation in clean clouds but increased precipitation in polluted clouds. The enhancement in precipitation from GCCN concentrations was a result of increased graupel production within the clouds. Additionally, dust GCCN in warm clouds can also result in evaporation of cloud droplets, thus decreasing the number of collector drops and the probability of precipitation formation commonly known as the Semi-Direct effect (Huang et al., 2006). Inconsistencies in size definitions of GCCN (Levin et al., 1996; Feingold et al., 1999) as well as confusions on the ability of pristine or aged dust to act as GCCN (Yin et al., 2002) complicate the current understanding of mineral dust, and subsequent impacts on the climate and the hydrological cycle.

1.4 Thesis Outline

The goal of this thesis is to improve our current understanding of how mineral aerosols affect warm clouds through serving as CCN and GCCN. The approach is shown in Fig. 1.3, and it integrates laboratory measurements with development of numerical models of dust-cloud interactions. The major objectives of this thesis include:

1. Investigation of the importance of water vapor adsorption on hydrophilic insoluble mineral particles to describe cloud droplet nucleation and growth from dust aerosols.

2. Development of a new physically-based droplet formation parameterization framework to describe dust activation in climate models.

3. Perform laboratory measurements of CCN activity and droplet activation kinetics of regional dust samples and minerals to validate the adsorption activation theory, and to support the new droplet formation parameterization.

4. Investigation of the applicability of commonly used wet generation method to mineral (dust) aerosols.

5. Quantify the contribution of soluble salts in dust samples to dust CCN activity.

6. Formulation of a unified dust activation framework to account for the effects of solutes to dust CCN activity.

7. Examination of dust GCCN growth by adsorption activation mechanism in cloud models to address dust-cloud-precipitation linkages.

This thesis is structured as follows. Chapter 2 provides motivation behind this thesis and examines the importance of including water adsorption effects when describing the hygroscopic and cloud condensation nuclei (CCN) behavior of mineral aerosol. In Chapters 3 and 4, new laboratory measurements of cloud condensation nuclei

(CCN) activity and droplet activation kinetics of aerosols generated (dry and wet) from clays, calcite, quartz, and desert soil samples from Northern Africa, East Asia/China, and Northern America are presented. The premise of Chapters 3 and 4 is to expand the set of size resolved experimental measurements of dust (fresh and aged) CCN activity to constrain the role of dust in aerosol-cloud-climate interactions. Chapter 5 presents a new parameterization of cloud droplet formation by including effects of adsorption activation within an ascending air parcel containing insoluble (but wettable) particles externally mixed with aerosol containing an appreciable soluble fraction. Chapter 6 examines the growth of dust particles acting as GCCN and its implications for cloud precipitation processes, considering the effects of dust mineralogy, size, and adsorption parameters. Finally, Chapter 7 presents major findings, implications, and directions for future work.
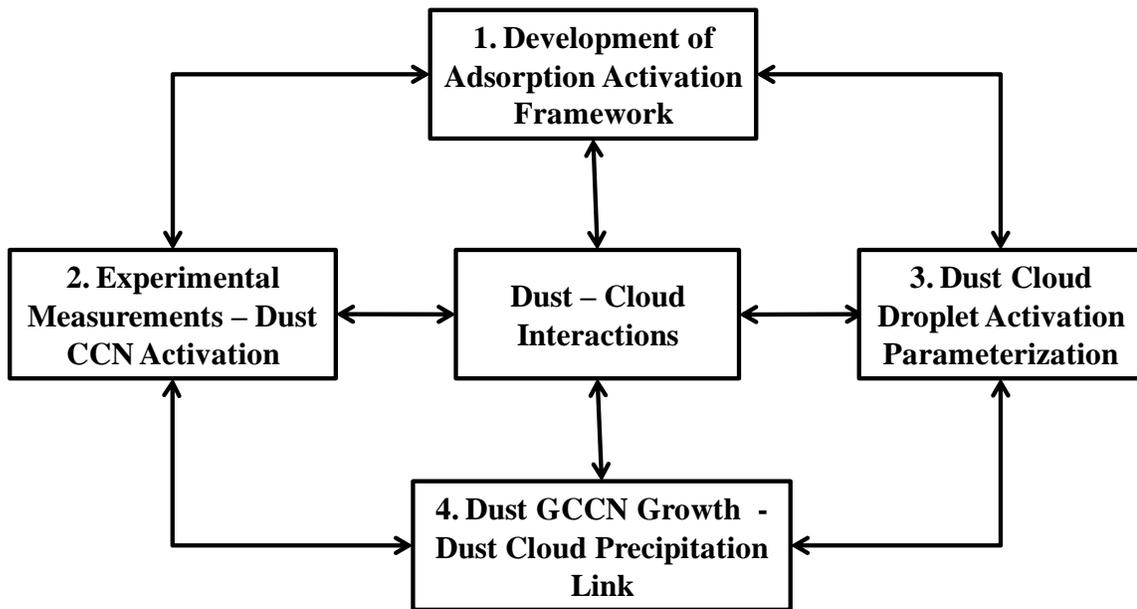
Figure 1.3: Thesis schematic with major objectives.

1.5   References

Abdul-Razzak, H. and Ghan, S. J.: A parameterization of aerosol activation: 2. Multiple aerosol types, J. Geophys. Res., 105(D6), 6837 - 6844, 2000.

Abdul-Razzak, H., Ghan, S. J., and Rivera-Carpio, C.: A parameterization of aerosol activation: 1. Single aerosol type, J. Geophys. Res., 103(D6), 6123 - 6131, 1998.

Albrecht, B. A.: Aerosols, cloud microphysics, and fractional cloudiness, Science, 245, 1227 - 1230, 1989.

Barahona, D. and Nenes, A.: Parameterization of cloud droplet formation in large-scale models: Including effects of entrainment, J. Geophys. Res., 112, D16206, doi:10.1029/2007JD008473, 2007.

Brunauer, S., Emmett, P. H., and Teller, E.: Adsorption of gases in multimolecular layers, J. Am. Chem. Soc., 60(2), 309 - 319, 1938.

Chou, C., Formenti, P., Maille, M., Ausset, P., Helas, G., Harrison, M., and Osborne, S.: Size distribution, shape, and composition of mineral dust aerosols collected during the African monsoon multidisciplinary analysis special observation period 0: dust and biomass burning experiment field campaign in Niger, January 2006, J. Geophys. Res., 113, D00C10, doi:10.1029/2008JD009897, 2008.

Cohard, J. -M., Pinty, J. -P., and Suhre, K.: On the parameterization of activation spectra from cloud condensation nuclei microphysical properties, J. Geophys. Res., 105(D9), 11,753 - 11,766, 2000.

Collins, W. D., Conant, W. C., and Ramanathan, V.: Earth Radiation Budget, Clouds, and Climate Sensitivity. The Chemistry of the Atmosphere: Its Impact on Global Change, edited by: Calvert, J. G., Blackwell Scientific Publishers, Oxford, UK, 207 - 215, 1994.

Coz, E., Gómez-Moreno, F. J., Pujadas, M., Casuccio, G. S., Lersch, T. L., and Artinano, B.: Individual particle characteristics of North African dust under different long-range transport scenarios, Atmos. Environ., 43, 1850 - 1863, 2009.

DeCarlo, P. F., Slowik, J. G., Worsnop, D. R., Davidovits, P., and Jimenez, J. L.: Particle morphology and density characterization by combined mobility and aerodynamic diameter measurements. Part 1: Theory, Aerosol Sci. Tech., 38, 1185 - 1205, 2004.

DeMott, P. J., Sassen, K., Poellot, M. R., Baumgardner, D., Rogers, D. C., Brooks, S. D., Prenni, A. J., and Kreidenweis, S. M.: African dust aerosols as atmospheric ice nuclei, Geophys. Res. Lett., 30(14), 1732, doi:10.1029/2003GL017410, 2003.

Duce, R. A., Liss, P. S., Merrill, J. T., Atlas, E. L., Buat-Ménard, P., Hicks, B. B., Miller, J. M., Prospero, J. M., Arimoto, R., Church, T. M., Ellis, W., Galloway, J. N., Hansen, L., Jickels, T. D., Knap, A. H., Reinhardt, K. H., Schneider, B., Soudine, A., Tokos, J. J., Tsunogai, S., Wollast, R., and Zhou, M.: The atmospheric input of trace species to the world ocean, Global Biogeochem. Cy., 5, 193 - 259, 1991.

Dusek, U., Reischl, G., and Hitzenberger, R.: CCN activation of pure and coated carbon black particles, Environ. Sci & Technol., 40, 1223 - 1230, 2006.

Easter, R. C., Ghan, S. J., Zhang, Y., Saylor, R. D., Chapman, E. G., Laulainen, N. S., Abdul-Razzak, H., Leung, L. R., Bian, X., and Zaveri, R. A.: MIRAGE: Model description and evaluation of aerosols and trace gases, J. Geophys. Res., 109, D20210, doi:10.1029/2004JD004571, 2004.

Feingold, G., Cotton, W. R., Kreidenweis, S. M., and Davis, J. T.: The impact of giant cloud condensation nuclei on drizzle formation in stratocumulus: implication for cloud radiative properties, J. Atmos. Sci., 56, 4100 - 4117, 1999.

Feingold, G. and Heymsfield, A. J.: Parameterization of condensational growth of droplets for use in general circulation models, J. Atmos. Sci, 49, 2325 - 2342, 1992.

Field, P. R., Möhler, O., Connolly, P., Krämer, M., Cotton, R., Heymsfield, A. J., Saathoff, H., and Schnaiter, M.: Some ice nucleation characteristics of Asian and Saharan desert dust, Atmos. Chem. Phys., 6, 2991 - 3006, 2006. http://www.atmos-chem-phys.net/6/2991/2006/.

Fletcher, N. H.: Size effect in heterogeneous nucleation, J. Chem. Phys., 29, 572 - 576, 1958.

Formenti, P., Schuetz, L., Balkanski, Y., Desboeufs, K., Ebert, M., Kandler, K., Petzold, A., Scheuvens, D., Weinbruch, S., and Zhang, D.: Recent progress in understanding physical and chemical properties of mineral dust, Atmos. Chem. Phys. Discuss., 10, 31,187 – 31,251, 2010, www.atmos-chem-phys-discuss.net/10/31187/2010/.

Forster, P., Ramaswamy, V., Artaxo, P., Berntsen, T., Betts, R., Fahey, D. W., Haywood, J., Lean, J., Lowe, D. C., Myhre, G., Nganga, J., Prinn, R., Raga, G., Schulz, M., and Van Dorland, R.: Changes in Atmospheric Constituents and in Radiative Forcing, in: Climate Change 2007: The Physical Science Basis. Contribution of Working Group I to the Fourth Assessment Report of the Intergovernmental Panel on Climate Change, edited by: Solomon, S., Qin, D., Manning, M., Chen, Z., Marquis, M., Averyt, K. B., Tignor, M., and Miller, H. L., Cambridge University Press, Cambridge, UK and New York, NY, USA, 129 - 234, 2007.

Fountoukis, C. and Nenes, A.: Continued development of a cloud droplet formation parameterization for global climate models, J. Geophys. Res., 110, D11212, doi:10.1029/2004JD005591, 2005.

Hatch, C. D., Gierlus, K. M., Schuttlefield, J. D., and Grassian, V. H.: Water adsorption and cloud condensation nuclei activity of calcite and calcite coated with model humic and fulvic acids, Atmos. Environ., 42, 5672 - 5684, 2008.

Herich, H., Tritscher, T., Wiacek, A., Gysel, M., Weingartner, E., Lohmann, U., Baltensperger, U., and Cziczo, D. J.: Water uptake of clay and desert dust aerosol particles at sub- and supersaturated water vapor conditions, Phys. Chem. Chem. Phys., 11, 7804 - 7809, doi:10.1039/b901585j, 2009.

Henson, B. F.: An adsorption model of insoluble particle activation: Application to black carbon, J. Geophys. Res., 112, D24S16, doi:10.1029/2007JD008549, 2007.

Hoose, C., and Lohmann, U.: Dust impacts on warm and cold clouds: Insights from global models, Invited contribution to the 3rd International Workshop on Mineral Dust, Leipzig, 2008.

Huang, J., Lin, B., Minnis, P., Wang, T., Wang, X., Hu, Y., Yi, Y., and Ayers, J. K.: Satellite based assessment of possible dust aerosols semi-direct effect on cloud water path over East Asia, Geophys. Res. Lett., 33, L19802, doi:10.1029/2006GL026561, 2006.

Jeong, G. -R. and Sokolik, I. N.: The effect of mineral dust aerosols on the photolysis rates in the clean and polluted marine environments, J. Geophys. Res., 112, D21308, doi:10.1029/2007JD008442, 2007.

Kalashnikova, O. V. and Sokolik, I. N.: Modeling the radiative properties of nonspherical soil-derived mineral aerosols, J. Quant. Spectrosc. Ra., 87(2), 137 - 166, 2004.

Kandler, K., Schütz, L., Deutscher, C., Ebert, M., Hofmann, H., Jäckel, S., Jaenicke, R., Knippertz, P., Lieke, M., Massling, A., Petzold, A., Schladitz, A., Weinzierl, B., Wiedensohler, A., Zorn, S., and Weinbruch, S.: Size distribution, mass concentration, chemical and mineralogical composition and derived optical parameters of the boundary layer aerosol at Tinfou, Morocco, during SAMUM 2006, Tellus, 61B, 32 - 50, doi: 10.1111/j.1600-0889.2008.00385.x, 2009.

Kellogg, C. A., and Griffin, D. W.: Aerobiology and the global transport of desert dust, Trends Ecol. Evol., 21, 638 - 644, 2006.

Kiehl, J. T., and Trenberth, K. E.: Earth's annual global mean energy budget, Bull. Amer. Meteor. Soc.,78, 197 - 208, 1997.

Koehler, K. A., Kreidenweis, S. M., DeMott, P. J., Petters, M. D., Prenni, A. J., and Carrico, C. M.: Hygroscopicity and cloud droplet activation of mineral dust aerosol, Geophys. Res. Lett., 36, L08805, doi:10.1029/2009GL037348, 2009.

Köhler, H., The nucleus in and the growth of hygroscopic droplets, Trans. Faraday Soc., 32(2), 1152 - 1161, 1936.

Kuwata, M. and Kondo, Y.: Measurements of particle masses of inorganic salt particles for calibration of cloud condensation nuclei counters, Atmos. Chem. Phys., 9, 5921 - 5932, 2009, www.atmos-chem-phys-discuss.net/9/5921/2009/.

Kwon, H., Cho, S. H., Chun, Y., Lagarde, F., and G, P.: Effects of the Asian dust events on daily mortality in Seoul, Korea, Environ. Res., 90, 1 - 5, 2002.

Lafon, S., Sokolik, I. N., Rajot, J. L., Caquineau, S., and Gaudichet, A.: Characterization of iron oxides in mineral dust aerosols: Implications to light absorption. J. Geophys. Res., 111, D21207, doi:10.1029/2005JD007016, 2006.

Levin, Z., and Cotton, W. R.: Aerosol Pollution Impact on Precipitation: A scientific review, Springer Press., pp. 382, 2008.

Levin, Z., Ganor, E., and Gladstein, V.: The effects of dust particles coated with sulfate on rain formation in the Eastern Mediterranean, J. Appl. Meteorol., 35, 1511-1523, 1996.

Lohmann, U., and Feichter, J.: Global indirect aerosol effects: a review, Atmos. Chem. Phys., 5, 715 - 737, 2005, http://www.atmos-chem-phys.net/5/715/2005/.

Lohmann, U., Stier, P., Hoose, C., Ferrachat, S., Kloster, S., Roeckner, E. and Zhang, J.: Cloud microphysics and aerosol indirect effects in the global climate model ECHAM5-HAM, Atmos. Chem. Phys., 7, 3425 - 3446, 2007, http://www.atmos-chem-phys.net/7/3425/2007/.

Mahowald, N. and Kiehl, L.: Mineral aerosols and clouds, Geophys. Res. Lett., 30(9), doi:10.1029/2002GL016762, 2003.

Ming, Y., Ramaswamy, V., Donner, L. J., and Phillips, V. T. J.: A new parameterization of cloud droplet activation applicable to general circulation models, J. Atmos. Sci., 63, 1348 - 1356, 2006.

Nenes, A. and Seinfeld, J. H.: Parameterization of cloud droplet formation in global climate models, J. Geophys. Res., 108 (D14), 4415, doi:10.1029/2002JD002911, 2003.

Okada, K., Heintzenberg, J., Kai, K., and Qin Y.: Shape of atmospheric mineral particles collected in three Chinese arid-regions, Geophys. Res. Lett., 28(16), 3123 - 3126, doi:10.1029/2000GL012798, 2001.

Perez, L., Tobias, A., Querol, X., Künzli, N., Pey, J., Alastuev, A., Viana, M., Valero, N., González-Cabré, M., and Sunyer, J.: Coarse particles from Saharan dust and daily mortality, Epidemiology, 19, 800 – 807, 2008.

Petters, M. D., and Kreidenweis, S. M.: A single parameter representation of hygroscopic growth and cloud condensation nucleus activity, Atmos. Chem. Phys., 7, 1961 – 1971, 2007, http://www.atmos-chem-phys.net/7/1961/2007/.

Prospero, J. M.: Long-range transport of mineral dust in the global atmosphere: Impact of African dust on the environment of the southeastern United States, Proc. Natl. Acad. Sci. USA, 96, 3396 - 3403, 1999.

Ramanathan, V., Crutzen, P. J., Kiehl, J. T., and Rosenfeld, D.: Atmosphere – Aerosols, climate, and the hydrological cycle, Science, 294 (5549), 2119 - 2124, 2001.

Rudich, Y., Khersonsky, O., and Rosenfeld, D.: Treating clouds with a grain of salt, Geophys. Res. Lett., 29 (22), 2060, doi:10.1029/2002GL016055, 2002.

Rosenfeld, D., Rudich, Y., and Lahav, R.: Desert dust suppressing precipitation: A possible desertification feedback loop, Proc. Natl. Acad. Sci. U.S.A., 98(11), 5975 - 5980, 2001.

Schuttlefield, J. D., Cox, D., and Grassian, V. H.: An investigation of water uptake on clays minerals using ATR-FTIR spectroscopy coupled with quartz crystal microbalance measurements, J. Geophys. Res., 112, D21303, doi:10.1029/2007JD008973, 2007.

Seinfeld, J. H., and Pandis, S. N.: Atmospheric Chemistry and Physics, John Wiley, New York, USA, 767 - 773, 2006.

Sheehy, D. P.: A perspective on desertification of grazing land ecosystems in North China, Ambio. Stockholm [AMBIO.], 21 (4), 303 - 307, 1992.

Sokolik, I. N., Winker, D. M., Bergametti, G., Gillette, D. A., Carmichael, G., Kaufman, Y. J., Gomes, L., Schuetz, L., and Penner, J. E.: Introduction to special section: outstanding problems in quantifying the radiative impacts of mineral dust, J. Geophys. Res., 106(D16), 18,015 - 18,027, 2001.

Sorjamaa, R., and Laaksonen, A.: The effect of H_2O adsorption on cloud drop activation of insoluble particles: a theoretical framework, Atmos. Chem. Phys., 7, 6175 - 6180, 2007, http://www.atmos-chem-phys.net/9/6175/2007/.

Storelvmo, T., Kristjánsson, J. E., Ghan, S. J., Kirkevåg, A., Seland, Ø., and Iversen, T.: Predicting cloud droplet number concentration in Community Atmosphere Model (CAM)-Oslo, J. Geophys. Res., 111(D24208), doi:10.1029/2005JD006300, 2006.

Takemura, T., Nozawa, T., Emori, S. Nakajima, T. Y. and Nakajima, T.: Simulation of climate response to aerosol direct and indirecteffects with aerosol transport-radiation model, J. Geophys. Res., 110(D02202), doi:10.1029/2004JD005029, 2005.

Teller, A., and Levin, Z.: The effects of aerosols on precipitation and dimensions of subtropical clouds; a sensitivity study using a numerical cloud model, Atmos. Chem. Phys., 6, 67 - 80, 2006, http://www.atmos-chem-phys.net/6/67/2006/.

Twohy, C. H., Kreidenweis, S. M., Eidhammer, T., Browell, E. V., Heymsfield, A. J., Bansemer, A. R., Anderson, B. E., Chen, G., Ismail, S., DeMott, P. J., and Van Den Heever, S. C.: Saharan dust particles nucleate droplets in eastern Atlantic clouds, Geophys. Res. Lett., 36, L01807, 1 - 6, doi:10.1029/2008GL035846, 2009.

Twomey, S.: Pollution and the planetary albedo, Atmos. Environ., 8, 1251 - 1256, 1974.

Van den Heever, S. C., Carrio, G., Cotton, W. R., DeMott, P. J., and Prenni, A. J.: Impacts of Nucleating Aerosol on Florida Storms. Part I: Mesoscale Simulations, J. Atmos. Sci., 63, 1752 - 1775, 2006.

Wexler, A. S. and Ge, Z. Z.: Hydrophobic particles can activate at lower relative humidity than slightly hygroscopic ones: a Köhler theory incorporating surface fixed charge, J. Geophys. Res., 103(D6), 6083 - 6088, 1998.

Wiegner, M., Gasteiger, J., Kandler, K., Weinzierl, B., Rasp, K., Esselborn, M., Freudenthaler, V., Heese, B., Toledano, C., Tesche, M., and Althausen, D.: Numerical simulations of optical properties of Saharan dust aerosols with emphasis on linear depolarization ratio, Tellus, 61B, 180 - 194, 2009.

Yin, Y., Wurzler, S., Levin, Z., and Reisin, T. G.: Interactions of mineral dust particles and clouds: Effects on precipitation and cloud optical properties, J. Geophys. Res., 107(D23), 4724, doi:10.1029/2001JD001544, 2002.

CHAPTER 2

MOTIVATION: IMPORTANCE OF ADSORPTION FOR CCN ACTIVITY AND HYGROSCOPIC PROPERTIES OF MINERAL DUST AEROSOL

2.1   Abstract

This chapter uses published data on dust-water interactions to examine the importance of including water adsorption effects when describing the hygroscopic and cloud condensation nuclei (CCN) behavior of mineral dust aerosol. Adsorption activation theory (AT) better represents fresh dust-water interactions than Köhler theory (KT), as *i*) a consistent set of adsorption parameters can describe the hygroscopic behavior of dust (under both sub and supersaturated conditions), *ii*) the dependence of critical supersaturation, s_c, with particle dry diameter, D_{dry}, is closer to observations. The long adsorption timescale could also contribute to the large differences observed between dry and wet generated dust hygroscopicity. If KT and AT are consistently applied to the same dust size distribution, KT predicts up to tenfold higher CCN and 40% higher droplet number concentration than AT. This profoundly different behavior between the theories suggests that both may be required for a comprehensive description of atmospheric dust CCN activity.

2.2   Introduction

Mineral dust is ubiquitous in the atmosphere and represents a dominant type of particulate matter by mass. Dust particles can act as cloud condensation nuclei (CCN), giant CCN (GCCN) (e.g., Rosenfeld et al., 2001; Levin and Cotton, 2008), or ice nuclei (IN) (e.g., DeMott et al., 2003; Field et al., 2006) affecting cloud microphysics, albedo, and lifetime. Despite its well-recognized importance, assessments of dust impacts on clouds and climate are highly uncertain. In this study, we address the role of dust as CCN with the goal to provide an improved representation of dust CCN activation in the climate models.

Dust CCN activity is currently described by Köhler theory (herein KT; Köhler, 1936), which is based solely on the contribution of the solute and curvature effects upon water equilibrium vapor pressure. KT implies that dust particles devoid of any solute would require very high ambient supersaturations (dictated by the Kelvin equation) to act as CCN. It is well known however that adsorption of water on insoluble particles (especially clays) can lead to hygroscopic growth similar to deliquescent salts (e.g., Schuttlefield et al., 2007). Past studies have demonstrated that calcite ($CaCO_3$) (a mineral with very low solubility compared to deliquescent salts) and Arizona Test Dust (ATD) can interact with water vapor and adsorb multiple layers of water under subsaturated conditions (Gustafsson et al., 2005; Vlasenko et al., 2005; Hatch et al., 2008). This interaction implies that dust mixtures and individual minerals with hydrophilic insoluble surfaces can affect water activity of aerosol (especially when the solute fraction of particles is low) with largely ignored implications for predicted CCN activity. Henson (2007) and Sorjamaa and Laaksonen (2007) recognized this gap, and developed

adsorption activation theory (AT) to describe the activation of hydrophilic insoluble CCN. The Sorjamaa and Laaksonen (2007) formulation is based on the FHH (Frenkel, Halsey and Hill) adsorption model (and constrained by two adjustable parameters, A_{FHH}, B_{FHH}). Kumar et al. (2009) incorporated FHH-AT into a droplet activation parameterization for use in regional and global models, assuming that the aerosol constitutes an external mixture of "soluble" (KT) and "insoluble" (AT) particles.

Even if constrained by the same CCN activity or hygroscopic growth data, predicted CCN concentration and cloud droplet number, N_d, can differ between using KT and FHH-AT because: i) the relationship between particle critical supersaturation, s_c, and dry diameter, D_{dry}, differs between theories, resulting in a different predicted CCN spectrum even if the same size distribution is used, and, ii) KT particles require substantially more water to activate than FHH-AT particles with the same s_c (Kumar et al., 2009). Competition for water vapor in a cloud parcel during activation of KT particles can thus be more intense than for FHH-AT particles, leading to a different parcel maximum supersaturation, s_{max}, and droplet number.

In this study, we substantiate the importance of considering water vapor adsorption effects on the activation of mineral dust particles. This is done by fitting published CCN activity and hygroscopic growth data to the KT and FHH-AT, and examining whether each theory can i) describe subsaturated hygroscopic growth and CCN activity with one set of water-interaction parameters, and, ii) reproduce the observed dependence of s_c with respect to D_{dry}. Finally, we evaluate the differences in the CCN number and droplet number concentrations predicted by KT and FHH-AT, using the consistent parameters and the same aerosol size distribution.

2.3   Comparison of Köhler and Adsorption Activation Theories

KT provides a relationship between the equilibrium vapor pressure of an aqueous droplet as a function of its wet diameter and exhibits a maximum value termed as critical supersaturation, s_c, at a characteristic critical wet diameter, D_c. Particles exposed to ambient supersaturation above s_c typically activate into cloud droplets (Nenes et al., 2001). In KT, s_c depends on the amount of solute in the dry particle, which is related to its chemical composition and size. Petters and Kreidenweis (2007) parameterized the solute term of KT in terms of a hygroscopicity parameter, κ, which was derived from the relationship between D_{dry} and s_c. κ can be used to directly compare the hygroscopicity of aerosol over a wide range of composition, with $\kappa \rightarrow 0$ for completely insoluble particles (for which $s_c \sim D_{dry}^{-1}$) to $\kappa \rightarrow 1.4$ for the most hygroscopic atmospheric aerosol (for which $s_c \sim D_{dry}^{-3/2}$). According to KT, a constant value of κ should be able to describe both aerosol subsaturated water uptake (where relative humidity, RH, is below 100%) and predict CCN activity (RH > 100%).

FHH-AT is similar to KT, except that the solute term is replaced with an adsorption term modeled by the FHH isotherm (Crittenden and Thomas, 1998). The adsorption parameter B_{FHH}, strongly affects the shape of the equilibrium curve, and largely determines the existence and value of s_c and D_c (Kumar et al., 2009). As with KT, s_c in FHH-AT can be related to D_{dry} as $s_c = CD_{dry}^x$. Particles with an appreciable soluble fraction follow KT, and $x \sim$ -1.5 when $\kappa > 0.2$. In FHH-AT, x varies between -0.8 and -1.2, depending on A_{FHH}, B_{FHH} (Kumar et al., 2009).

2.4   Evidence of Adsorption Activation

Figure 2.1a shows published data (symbols) of s_c as a function of D_{dry} (Koehler et al. 2009; Sullivan et al., 2009) for different dust types and individual mineral particles generated in the lab either with the use of a dry fluidized bed, or via wet atomization from an aqueous suspension of dust particles. The CCN activity data are fitted to a power law expression, $s_c = CD_{dry}^x$, from which the "experimental" exponent, x_{exp}, is determined (Table 2.1). A_{FHH} and B_{FHH} and the corresponding exponent, x_{FHH}, were determined from fitting the FHH-AT model (Fig. 2.1a, lines) to the experimental data via least squares minimization. The KT fits to the data (expressed in terms of κ) are given by Koehler et al. (2009) and Sullivan et al. (2009), from which the corresponding KT exponent, x_κ, is computed. The values of the exponents, adsorption parameters (A_{FHH}, B_{FHH}), and κ (determined by Koehler et al., 2009, and Sullivan et al., 2009) are presented in Table 2.1.

In Fig. 2.1b, x_κ (circles) and x_{FHH} (squares) are plotted against x_{exp} for all dust samples and individual minerals. With the exception of $CaCO_3$ and $CaSO_4$ (calcium sulphate) (where $x_\kappa \rightarrow$ -1 because of the very low κ), $x_\kappa \sim$ -1.5. $CaCO_3$ (representing fresh unprocessed dust) and $CaSO_4$, $CaC_2O_4.H_2O$ (calcium oxalate monohydrate or COH) (representing atmospherically processed mineral dust) are better described by FHH-AT, as x_{FHH} is in perfect agreement with x_{exp}. For wet generated ATD, Owens Lake (OL), Canary Island Dust (CID), and oxalic acid ($C_2O_4H_2$), x_{FHH} lies closer than x_κ to the 1:1 line. x_κ for dry Saharan Dust (SD), ATD and wet $Ca(NO_3)_2$ are closer to x_{exp} than x_{FHH}; this is expected for $Ca(NO_3)_2$ because it is highly soluble (deliquescence RH = 49%; Fountoukis and Nenes, 2007), but not for dry ATD and SD. The large scatter ($R^2 < 0.7$

25

for the s_c-D_{dry} data for dry ATD) and potential size-dependant composition (for SD) may explain this.

Another indication that KT may be an incomplete description of the dust CCN activity presents itself in the value of wet-dust κ parameters, and the implications thereof. If the aerosol can be considered as a mixture of a soluble salt with molar volume $\left[M_s / \rho_s \right]$, effective van't Hoff factor ν_s, and volume fraction ε_s, then $\kappa = \left(\dfrac{M_w}{\rho_w} \right)\left(\dfrac{\rho_s \nu_s}{M_s} \right)\varepsilon_s$, where $\left[M_w / \rho_w \right]$ is the molar volume of water. Assuming that the hygroscopic fraction of dust behaves like ammonium sulfate gives $\left(\dfrac{M_w}{\rho_w} \right)\left(\dfrac{\rho_s \nu_s}{M_s} \right) = 0.61$ (Petters and Kreidenweis, 2007). Therefore, the dust κ parameters can be used to infer an "equivalent soluble volume fraction", computed as $\varepsilon_s = \dfrac{\kappa}{0.61}$. If KT indeed applies, then ε_s should reflect the true soluble fraction of dust. From the values of κ reported in Table 2.1, $\varepsilon_s = 0.58$, 0.65 - 1.78, and 0.43 for wet ATD, OL, and CID, respectively. Such a large soluble fraction in fresh dust is much larger (or even impossible if larger than unity) than the expected 2% soluble mass fraction in ATD (Vlasenko et al., 2005) and 3 - 37% in OL (Koehler, 2008). Koehler et al. (2009) attribute this enhanced hygroscopicity to redistribution of the soluble material among the insoluble dust cores, particularly in the smaller size range. Given that KT implies $s_c \sim \varepsilon_s^{-0.5} D_{dry}^{-1.5}$, ε_s will have to scale with $D_{dry}^{0.3}$ for KT to yield $x_\kappa = x_{exp} \sim -1.36$. This means that ε_s varies more than 60% over the diameter range (40 − 200 nm) reported in the Koehler et al. (2009) experiments, so that the soluble fraction at the high s_c should be close to unity. This is certainly possible; the

26

hygroscopicity parameter, however, does not seem to change considerably when subsets of the activation data (especially in the higher supersaturation range) are separately considered. This implies that KT may not completely describe the CCN activity of dust, so that other processes, such as physisorption, could contribute to the water activity depression required to yield the observed CCN activity. The long equilibration time (minutes or more) associated with adsorption (e.g., Schuttlefield et al., 2007) may explain why the hygroscopicity of dry and wet generated dust are so different. The residence time of dust particles in the instrumentation is typically less than a minute, limiting the amount of water that can adsorb and bias the observed hygroscopicity below its equilibrium value. Wetting the dust particles prior to measurement would maximize the amount of adsorbed water and express the full extent of its hygroscopicity. One approach to modeling this system is using one value for A_{FHH}, B_{FHH} combined with a variable uptake coefficient (that is very low during formation of the monolayer, and progressively increases with the number of adsorbed layers). Another explanation is the swelling of the clays; during complete wetting, more surface area could be exposed for interaction, which would enhance dust hygroscopicity compared to the dry particle. Further work should focus on the existence and mechanism of adsorption/desorption transients.
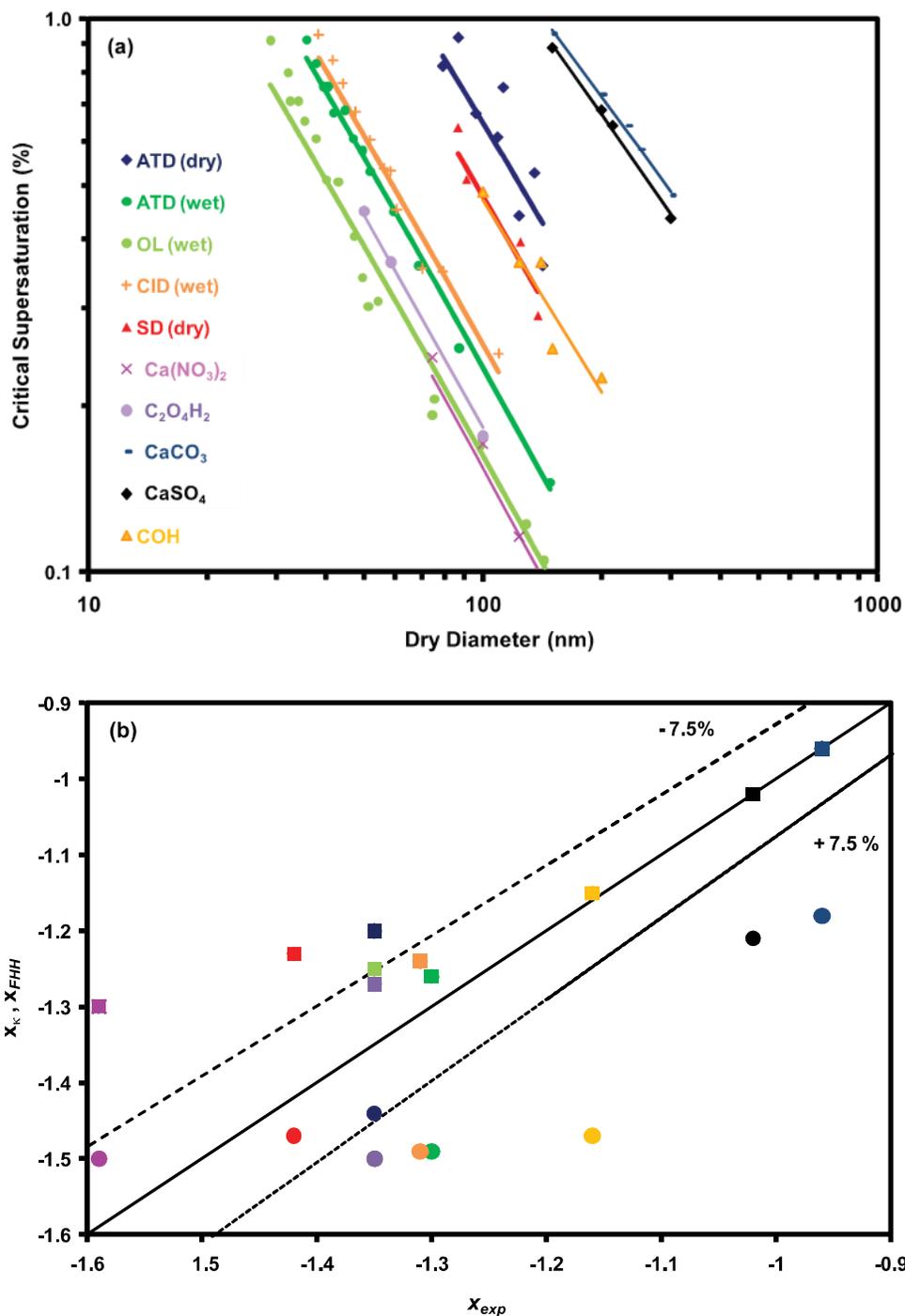
Figure 2.1: **(a)** FHH adsorption activation fits (lines) to the observed CCN activity (points) for dust types presented in Table 2.1. Data obtained from Fig. 7.1 (pp. 154) and Fig. 5 from Koehler et al. (2009) and Sullivan et al. (2009), respectively. "Dry" refers to dust particles generated with a fluidized bed, and "wet" refers to atomization from an aqueous suspension. **(b)** Comparison between x_{exp}, x_κ (circles) and x_{FHH} (squares). Color scheme identical to Fig. 2.1a. Dashed lines represent ± 7.5% deviation from 1:1 line.

Table 2.1: FHH parameters for different mineral dusts and dust related compounds composites. FHH adsorption activation fits to the experimental CCN activity data obtained from Koehler et al. (2009) and Sullivan et al. (2009)

Description (Acronym)	Generation[*]	κ	A_{FHH}	B_{FHH}	x_κ	x_{FHH}	x_{exp}
Arizona Test Dust (ATD)	Dry	0.025	0.27	0.79	-1.43	-1.20	-1.39
Arizona Test Dust (ATD)	Wet	0.35	0.85	0.88	-1.49	-1.26	-1.36
Owens Lake (OL)	Wet	0.39-1.07	1.14	0.91	-1.50	-1.25	-1.36
Canary Island Dust (CID)	Wet	0.26	0.80	0.88	-1.49	-1.24	-1.33
Saharan Dust (SD)	Dry	0.054	0.42	0.83	-1.47	-1.23	-1.42
Calcium Nitrate (Ca(NO$_3$)$_2$)	Wet	0.51	1.13	0.90	-1.50	-1.30	-1.59
Oxalic Acid (C$_2$O$_4$H$_2$)	Wet	0.50	1.02	0.90	-1.50	-1.27	-1.35
Calcium Carbonate (CaCO$_3$)	Dry	0.0011	0.25	1.19	-1.18	-0.96	-0.96
Calcium Sulfate (CaSO$_4$)	Dry	0.0016	0.10	0.91	-1.21	-1.02	-1.02
Calcium Oxalate Monohydrate (COH or CaC$_2$O$_4$.H$_2$O)	Dry	0.048	0.57	0.88	-1.47	-1.15	-1.16

[*]"Dry" refers to dust particles generated with a fluidized bed; "Wet" refers to atomization from an aqueous solution/suspension.

2.5 Reconciling Dust Hygroscopicity under Subsaturated and Supersaturated Conditions

Herich et al. (2009) measured water uptake on mineral dusts and different clays under subsaturated (with a hygroscopicity tandem differential mobility analyzer; HTDMA) and supersaturated (with a cloud condensation nuclei counter; CCNc) conditions. The hygroscopic growth factors (GF) were measured with a HTDMA, and the CCN activity was measured using a CCNc. A poor correlation in experiments (deviation larger than $\pm 50\%$) was found between κ derived from the HTDMA and CCNc. Herich et al. (2009) attributed this to resolution limitations in the HTDMA GF. Alternatively, KT may not adequately represent dust-water interactions, so that a single value of κ is not expected to describe the subsaturated water uptake and CCN activity for mineral dust aerosol. If FHH is more appropriate, then one set of A_{FHH} and B_{FHH} (neglecting the potential non-equilibrium artifacts) should reproduce both subsaturated and supersaturated properties of mineral dust aerosol, and is attempted below.

Gustafsson et al. (2005) studied the subsaturated hygroscopic uptake of ATD particles generated from suspensions in distilled water. Surface coverages as a function of RH were measured using a thermogravimetric analysis, during which multilayer adsorption (the number of water molecule layers, $\theta \sim 3 - 4$) were observed for RH greater than 50%. Under such conditions, the FHH adsorption isotherm is applicable and is fitted to the data. The optimal values for A_{FHH} and B_{FHH} are 1.16 and 0.88, respectively, versus 0.85 and 0.88 from CCN activation experiments (Table 2.1). Vlasenko et al. (2005) measured subsaturated hygroscopic growth of dry ATD; fitting a FHH adsorption isotherm to the growth data for RH > 70% gives $A_{FHH} = 0.19$ and $B_{FHH} = 0.98$ (RMSE =

0.035), which are very close to the FHH parameters obtained from CCN activation experiments for the same compound ($A_{FHH} = 0.27$ and $B_{FHH} = 0.79$; Table 2.1). Fitting FHH isotherms to the Gustafsson et al. (2005) and Hatch et al. (2008) measurements for $CaCO_3$ (different type from Table 2.1) gives $A_{FHH} = 0.83 - 1.00$ and $B_{FHH} = 0.76$. All the above suggests that the adsorption parameters for similar samples are indeed consistent across different studies.

2.6   Impact of KT and AT on CCN and Droplet Number

In this section, differences in predicted CCN concentrations and droplet number concentrations from application of KT and FHH-AT are estimated. For this, we use a single-mode lognormal aerosol obtained from in-situ measurements of SD during the NAMMA field campaign (Twohy et al., 2009) (with geometric mean diameter, $D_g = 0.10$ μm, standard deviation, $\sigma_g = 1.6$, and total particle concentration, $N_0 = 225$ per cm^3). The CCN spectra computed with KT and FHH-AT (using κ, A_{FHH}, and B_{FHH} listed in Table 2.1 and the lognormal CCN spectra formulations of Kumar et al., 2009) are presented in Fig. 2.2a. For supersaturations between 0.05% and 0.5% (a range relevant for cumulus and stratocumulus clouds), application of KT results in 8 - 12 times larger CCN that when applying FHH-AT. This is a direct consequence of $x_\kappa < x_{FHH}$, which tends to yield a larger activation fraction for KT-derived CCN spectra. For supersaturations greater than 0.5%, most aerosol in both distributions activate, so CCN computed by KT and FHH-AT converge.

The larger CCN concentrations (at a given supersaturation) associated with use of KT suggests that the calculated droplet number, compared to using FHH-AT, will be larger. KT however requires more water to activate particles than FHH-AT (Kumar et al.,

2009), so the competition for water vapor in the former particles is stronger, potentially impacting s_{max} and N_d. For example for $s_c = 0.05\%$, the ratio of water volume at D_c in KT against FHH-AT ranges from 4.83 (dry ATD) to 15.43 (wet ATD). Hence for the same size distribution, the droplet number difference from application of each theory depends on two competing factors: *i*) the stronger competition of KT CCN for water vapor, and *ii*) the typically larger activation fraction associated with KT. These factors are comprehensively accounted for in droplet number calculations carried out with the Kumar et al. (2009) parameterization. In all droplet number calculations presented, the parcel is assumed adiabatic, with initial temperature, 273 K; pressure, 600 mbar; and updraft velocity, w ranging from 0.1 m s^{-1} to 10 m s^{-1}. For each dust type, the respective κ and FHH parameters (A_{FHH} and B_{FHH}) from Table 2.1 are used.

Figure 2.2b shows the fraction of total CCN that activate using KT, F_κ, to that from FHH-AT, F_{FHH}, as a function of parcel updraft velocity (symbols) for four different dust types. The corresponding parcel s_{max} is also shown (solid lines). For wet CID and wet ATD, $\dfrac{N_d^\kappa}{N_d^{FHH}}$ is largest (~ 1.3 - 1.4) at $w \sim 0.1$ m s^{-1} and approaches 1.0 for $w > 1$ m s^{-1}. This is because the parcel $s_{max} < 1\%$ for all $w < 1$ m s^{-1} (Fig. 2.2b), where $\dfrac{F_k}{F_{FHH}} > 1$ (Fig. 2.2a) and droplet differences are dominated by the larger activation fractions associated with KT. Similarly, $\dfrac{F_k}{F_{FHH}} > 1$ for dry ATD and SD and $w < 1$ m s^{-1}. However, for $w > 1$ m s^{-1}, the competition of water vapor from KT particles is sufficiently strong so that $\dfrac{N_d^\kappa}{N_d^{FHH}} < 1$. At very high updrafts (> 3 m s^{-1}), all particles activate, and $\dfrac{N_d^\kappa}{N_d^{FHH}} \rightarrow 1$.
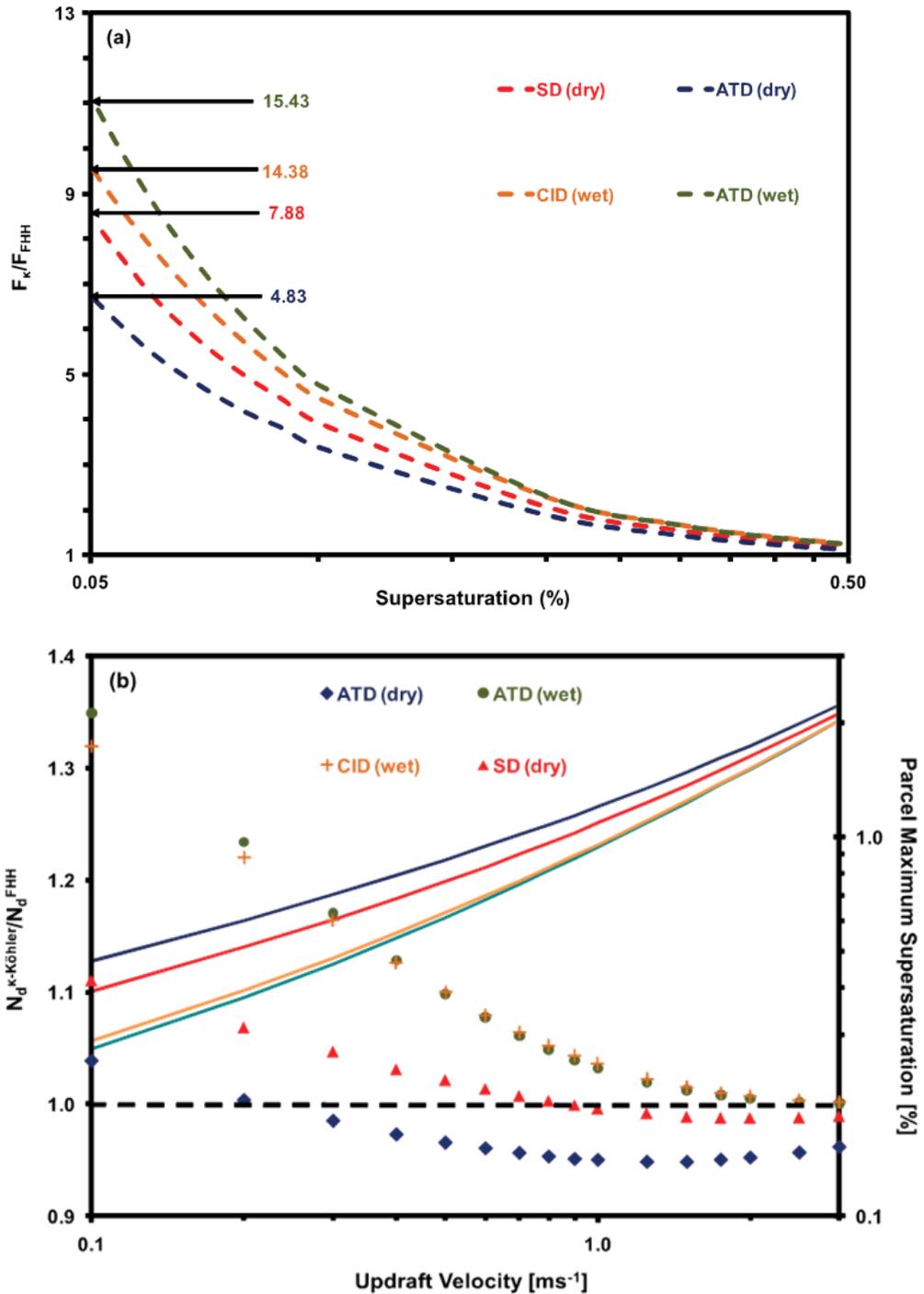
Figure 2.2: (a) Ratio of CCN spectrum given by Köhler theory to that given by FHH adsorption activation theory as a function of supersaturation. Numbers noted on each curve refer to the ratio of water volume required by KT over FHH-AT to activate a CCN with $s_c = 0.05\%$. **(b)** Ratio of parameterized activated fraction (points) for different dust types as a function of increasing updraft velocity in a cloud parcel. Also shown are the corresponding parcel s_{max} (lines) for each dust type. Color scheme identical to Fig. 2.1a. Dust types defined in Table 2.1.

2.7   Conclusions

In this study, we compared Köhler theory (KT) against FHH adsorption activation theory (FHH-AT) when applied to the activation of mineral dust aerosol. Based on published data, a number of potential issues were found with KT, suggesting it may not fully represent CCN activity of mineral dust aerosol, since *i*) a consistent set of FHH-AT adsorption parameters can be found that describe both the subsaturated hygroscopic growth and CCN activity, and, *ii*) the critical supersaturation vs. dry diameter exponents determined for FHH-AT are often closer to observations, than those from KT. Application of KT and FHH-AT leads to the differences in predicted CCN and cloud droplet number concentrations, even if consistent hygroscopicity and adsorption parameters (i.e., derived from the same experimental data) are used. For the dust samples considered here, CCN concentrations can differ by a factor of 10, and results in a 40% difference in predicted cloud droplet number concentration. Thus, a comprehensive description of CCN activity of mineral dust aerosol throughout its atmospheric lifetime may require a combination of both KT and FHH-AT.

2.8   Acknowledgements

2.9   References

Crittenden, B. D., and Thomas, W. J.: Adsorption technology and design, Butterworth - Heinemann, ISBN 0750619597, 1998.

DeMott, P. J., Sassen, K., Poellot, M. R., Baumgardner, D., Rogers, D. C., Brooks, S. D., Prenni, A. J., and Kreidenweis, S. M.: African dust aerosols as atmospheric ice nuclei, Geophys. Res. Lett., 30(14), 1732, doi:10.1029/2003GL017410, 2003.

Field, P. R., Möhler, O., Connolly, P., Krämer, M., Cotton, R., Heymsfield, A. J., Saathoff, H., and Schnaiter, M.: Some ice nucleation characteristics of Asian and Saharan desert dust, Atmos. Chem. Phys., 6, 2991 - 3006, 2006, http://www.atmos-chem-phys.net/6/2991/2006/.

Fountoukis, C., and Nenes, A.: ISORROPIA II: a computationally efficient aerosol thermodynamic equilibrium model for K^+, Ca^{2+}, Mg^{2+}, NH_4^+, Na^+, SO_4^{2-}, NO_3^-, Cl^-, H_2O aerosols, Atmos. Chem. Phys., 7, 4639 - 4659, 2007, http://www.atmos-chem-phys.net/7/4639/2006/.

Gustafsson, R. J., Orlov, A., Badger, C. L., Griffiths, P. T., Cox, R. A., and Lambert, R. M.: A comprehensive evaluation of water uptake on atmospherically relevant mineral surfaces: DRIFT spectroscopy, thermogravimetric analysis and aerosol growth measurements, Atmos. Chem. Phys., 5, 3415 – 3421, 2005, http://www.atmos-chem-phys.net/5/3415/2005/.

Hatch, C. D., Gierlus, K. M., Schuttlefield, J. D., and Grassian, V. H.: Water adsorption and cloud condensation nuclei activity of calcite and calcite coated with model humic and fulvic acids, Atmos. Environ., 42, 5672 - 5684, 2008.

Herich, H., Tritscher, T., Wiacek, A., Gysel, M., Weingartner, E., Lohmann, U., Baltensperger, U., and Cziczo, D. J.: Water uptake of clay and desert dust aerosol particles at sub- and supersaturated water vapor conditions, Phys. Chem. Chem. Phys., doi:10.1039/b901585j, 2009.

Henson, B. F.: An adsorption model of insoluble particle activation: Application to black carbon, J. Geophys. Res., 112, D24S16, doi:10.1029/2007JD008549, 2007.

Koehler, K. A.: The impact of natural dust aerosol on warm and cold cloud formation, Ph.D. dissertation thesis, 208 pp., Colo. State Univ., Fort Collins, 2008.

Koehler, K. A., Kreidenweis, S. M., DeMott, P. J., Petters, M. D., Prenni, A. J., and Carrico, C. M.: Hygroscopicity and cloud droplet activation of mineral dust aerosol, Geophys. Res. Lett., 36, L08805, doi:10.1029/2009GL037348, 2009.

Köhler, H., The nucleus in and the growth of hygroscopic droplets, Trans. Faraday Soc., 32(2), 1152 - 1161, 1936.

Kumar, P., Sokolik, I. N., and Nenes, A.: Parameterization of cloud droplet formation for global and regional models: including adsorption activation from insoluble CCN, Atmos. Chem. Phys., 9, 2517 - 2532, 2009, http://www.atmos-chem-phys.net/9/2517/2009/.

Levin, Z., and Cotton, W. R.: Aerosol pollution impact on precipitation: A scientific review, WMO/IUGG Report, 2007.

Nenes, A., Ghan, S. J., Abdul-Razzak, H., Chuang, P. Y., and Seinfeld, J. H.: Kinetic limitations on cloud droplet formation and impact on cloud albedo, Tellus, 53B, 133 - 149, 2001.

Petters, M. D., and Kreidenweis, S. M.: A single parameter representation of hygroscopic growth and cloud condensation nucleus activity, Atmos. Chem. Phys., 7, 1961 – 1971, 2007, http://www.atmos-chem-phys.net/7/1961/2007/.

Rosenfeld, D., Rudich, Y., and Lahav, R.: Desert dust suppressing precipitation: A possible desertification feedback loop, Proc. Natl. Acad. Sci. U.S.A., 98(11), 5975 - 5980, 2001.

Schuttlefield, J. D., Cox, D., and Grassian, V. H.: An investigation of water uptake on clays minerals using ATR-FTIR spectroscopy coupled with quartz crystal microbalance measurements, J. Geophys. Res., 112, D21303, doi:10.1029/2007JD008973, 2007.

Sorjamaa, R. and Laaksonen, A.: The effect of H_2O adsorption on cloud drop activation of insoluble particles: a theoretical framework, Atmos. Chem. Phys., 7, 6175 - 6180, 2007, http://www.atmos-chem-phys.net/9/6175/2007/.

Sullivan, R. C., Moore, M. J. K., Petters, M. D., Kreidenweis, S. M., Roberts, G. C., and Prather, K. A.: Effect of chemical mixing state on the hygroscopicity and cloud nucleation properties of calcium mineral dust particles, Atmos. Chem. Phys., 9, 3303 - 3316, 2009, http://www.atmos-chem-phys.net/9/3303/2009/.

Twohy, C. H., Kreidenweis, S. M., Eidhammer, T., Browell, E. V., Heymsfield, A. J., Bansemer, A. R., Anderson, B. E., Chen, G., Ismail, S., DeMott, P. J., and Van Den Heever, S. C.: Saharan dust particles nucleate droplets in eastern Atlantic clouds, Geophys. Res. Lett., 36, L01807, 1 - 6, doi:10.1029/2008GL035846, 2009.

Vlasenko, A., Sjögren, S., Weingartner, E., Gäggeler, H. W., and Ammann, M.: Generation of Submicron Arizona Test Dust Aerosol: Chemical and Hygroscopic Properties, Aerosol Sci. Tech., 39 (5), 452 - 460, 2005.

CHAPTER 3

MEASUREMENTS OF CLOUD CONDENSATION NUCLEI ACTIVITY AND DROPLET ACTIVATION KINETICS OF FRESH UNPROCESSED REGIONAL DUST SAMPLES AND MINERALS

3.1 Abstract

This study reports laboratory measurements of cloud condensation nuclei (CCN) activity and droplet activation kinetics of aerosols dry generated from clays, calcite, quartz, and desert soil samples from Northern Africa, East Asia/China, and Northern America. Based on the observed dependence of critical supersaturation, s_c, with particle dry diameter, D_{dry}, we found that FHH (Frenkel, Halsey, and Hill) adsorption activation theory is a far more suitable framework for describing fresh dust CCN activity than Köhler theory. One set of FHH parameters (A_{FHH} ~ 2.25 ± 0.75, B_{FHH} ~ 1.20 ± 0.10) can adequately reproduce the measured CCN activity for all species considered, and also explains the large range of hygroscopicities reported in the literature. Based on a threshold droplet growth analysis, mineral dust aerosols were found to display retarded activation kinetics compared to ammonium sulfate. Comprehensive simulations of mineral dust activation and growth in the CCN instrument suggest that this retardation is equivalent to a reduction of the water vapor uptake coefficient (relative to that for calibration ammonium sulfate aerosol) by 30 - 80%. These results suggest that dust particles do not require deliquescent material to act as CCN in the atmosphere.

3.2   Introduction

Clouds are an important component of the Earth's radiation budget and hydrological cycle. Even small changes in cloud properties may have significant impacts on climate (Collins et al., 1994). Perturbations in aerosol loadings can alter cloud properties, giving rise to the aerosol indirect effect on climate. Aerosol effects on clouds constitute one of the most uncertain components of anthropogenic climate change (Forster et al., 2007). Mineral aerosol (or dust) is one of the lesser understood of aerosol species in the study of aerosol-cloud-climate interactions. It has been well recognized that dust plays an important role in cold cloud processes because of its effectiveness as Ice Nuclei (IN) (DeMott et al., 2003; Field et al., 2006). Dust can also affect warm clouds by acting as Cloud Condensation Nuclei (CCN), changes of which affect their radiative (Twomey, 1974) and precipitation properties (Rosenfeld et al., 2001).

In general, the ability of dust particles to serve as CCN depends on their mineralogy, size, morphology, and atmospheric processing. Quantitative understanding of the interactions of dust with water vapor is complex because of its varying source-dependent mineralogical composition and aging during its atmospheric residence. Mineral aerosol may constitute of iron oxides (e.g., hematite, goethite), carbonates (e.g., calcite, dolomite), quartz, and clays (e.g., kaolinite, illite, and montmorillonite) (Lafon et al., 2006; Chou et al., 2008; Coz et al., 2009; Twohy et al., 2009). Dust particles mainly

originate from arid and semi-arid regions, with an annual emission of approximately 1000 - 5000 Tg (Schuttlefield et al., 2007). Differences in parent soils, and emission and transport processes cause substantial variability in size-resolved composition and morphology of dust particles (Sokolik et al., 2001; Jeong and Sokolik, 2008). Dust particles can remain suspended in the atmosphere for up to several weeks and can be transported over large distances downwind from source regions. During their transport, dust particles (especially the carbonate fraction which can comprise up to 30% of the total mass), provides reaction sites for heterogeneous chemical reactions with atmospheric trace gases and pollutants (Levin et al., 1996), resulting in modified dust properties, such as enhanced hygroscopicity (Hatch et al., 2008). However, not all dust particles undergo aging (Prospero, 1999; Ganor and Mamane, 1982; Ganor and Foner, 1996). Depending on transport routes of dust plumes and environmental conditions, dust particles can remain unprocessed and have the same properties as freshly emitted dust in source regions. Thus, it is important to understand the CCN activity of fresh dust particles as well as aged dust.

To describe the CCN activity of freshly emitted dust, two phenomena must be accounted for: *i*) the effect of solute (which may be present in freshly emitted dust or formed during atmospheric aging), and *ii*) the adsorption of water on the insoluble component of the dust particles. The former can be accounted for by using Köhler theory (KT) (Köhler, 1936) and the latter with adsorption activation theory (AT) (Henson, 2007; Sorjamaa and Laaksonen, 2007; Kumar et al., 2009a). The formulation of Henson (2007) used the BET (Brunauer, Emmett and Taylor; Brunauer et al., 1938) adsorption isotherm, while Sorjamaa and Laaksonen (2007) used the multilayer FHH (Frenkel, Halsey and

Hill) adsorption isotherm with two adjustable parameters (A_{FHH} and B_{FHH}). Based on analysis of published data on dust-water interactions, Kumar et al. (2009b) showed the importance of including water adsorption effects when describing the hygroscopic and CCN behavior of mineral aerosol. The same study found that FHH particles require less water to activate to cloud droplets than particles activating by KT; this implies that the competition for water vapor by FHH particles is less intense that KT particles to form droplets with implications for parcel maximum supersaturation, s_{max}, and cloud droplet number, N_d. Kumar et al. (2009a) addressed the need to account for adsorption activation in atmospheric models by developing a cloud droplet formation parameterization where the CCN constitutes an external mixture of soluble aerosol (that follow KT) and insoluble aerosol (that follow FHH adsorption activation theory, FHH-AT). Here, we report new measurements to further support the dust-CCN parameterization developed by Kumar et al. (2009a).

Past studies have already demonstrated that both regional dusts as well as individual clays can interact with water and act as effective CCN. For example, Koehler et al. (2009) and Herich et al. (2009) measured CCN activation of two types of regional dust samples (Northern Africa and Arizona Test Dust) and several clays (kaolinite, illite, and montmorillonite), respectively, at water vapor supersaturation relevant to atmospheric conditions. These studies, however, parameterized the observed hygroscopicity using a KT framework in terms of a hygroscopicity parameter, κ (Petters and Kreidenweis, 2007). This approach was evaluated by Kumar et al. (2009b), who, after examining the relationship between s_c and D_{dry} for the published dust samples suggested that FHH-AT is a better description of fresh dust CCN activity as the s_c-D_{dry}

exponents determined from FHH-AT were closer to observations than from KT. Furthermore, no study to date has accounted for non-sphericity effects in the CCN activity relationships, even when it is well known that dust particles are non-spherical (e.g., Okada et al., 2001; Chou et al., 2008). Further, the effect of multiple charged particles in the electrical mobility classification for measurements of size-resolved CCN activity (required for determining s_c and D_{dry}) is often addressed by removal of the secondary peaks in the activation curves (e.g., Lance et al., 2006; Rose et al., 2008). If multiply-charged particles are present in significant enough numbers (such as for dust CCN), this approach may not suffice causing biases in measured CCN activity towards higher hygroscopicity (Petters et al., 2007). A comprehensive analysis of charging efficiency (e.g., Moore et al., 2010) needs to be considered to avoid such biases in observed hygroscopicity.

In this study, we investigate the CCN-relevant properties of clays and several dust samples representative of major regional dust sources. Measurements were carried out with a Droplet Measurement Technologies Continuous-Flow Streamwise Thermal Gradient CCN (CFSTGC) counter (Roberts and Nenes, 2005; Lance et al., 2006). The CCN activation behavior of mineral aerosols generated from Northern American, African, and East Asian desert soils as well as individual clays (illite and montmorillonite), calcite ($CaCO_3$), and quartz (SiO_2) are studied. The effects of multiple charging and shape (non-sphericity) on the electrical mobility sizing of particles and activation curves are examined. The experimental results are used to infer the dominant activation physics (KT or FHH-AT) and determine the appropriate adsorption parameters (e.g., A_{FHH} and B_{FHH}) that describe the hygroscopicity of fresh dust for the use in droplet

activation parameterizations of Kumar et al. (2009a). Finally, using the method of threshold droplet growth analysis (TDGA, e.g., Asa-Awuku et al., 2010; Padró et al., 2010), potential retardations in the activation kinetics of dust (compared to calibration aerosol) are identified. A comprehensive simulation of dust activation in the CCN instrument is then performed to parameterize these kinetic delays in terms of changes in the effective water vapor uptake coefficient.

3.3   Measurements and Data Analysis

3.3.1   Regional Dust Samples and Individual Minerals

Aerosols from regional soil samples and individual minerals/clays were generated and analyzed in this study. Table 3.1 provides a summary of the analyzed samples, including information on the location of sample collection. The soil samples were collected in source regions of Northern Africa and East Asia. Commercially available Arizona Test Dust (ATD) was used as representative of North America soil. Individual minerals/clays used to generate aerosol were analyzed as purchased, with no physical and chemical treatments to resemble atmospheric behaviors.

Table 3.1: Summary of Regional Dust Samples and Clays/Minerals analyzed in this study

Sample	Abbreviation	Location/Supplier
Dust		
Niger	Niger	Sahel, 13º31' N, 2º38' E
East Asian Soil 1	Soil 1	Eastern edge of the Hexi Corridor
East Asian Soil 2	Soil 2	South-eastern edge of the Tengger Desert
East Asian Soil 3	Soil 3	Central Tengger Desert
East Asian Soil 4	Soil 4	South-eastern edge of the Taklamakan Desert
East Asian Soil 5	Soil 5	Southern edge of the Hunshandake Desert
Arizona Test Dust	ATD	Powder Technologies Inc.
Clay/Mineral		
Illite	Illite	Clay Mineral Society
Ca Montmorillonite	Ca Mont	Clay Mineral Society
Na Montmorillonite	Na Mont	Clay Mineral Society
Calcite	$CaCO_3$	OMYA
Quartz/Silica	SiO_2	GELEST

3.3.2 *Measurements of CCN Activity*

The measurement setup consists of three sections: aerosol generation, particle size selection, and CCN measurement (Fig. 3.1). To generate aerosol, approximately 3 grams of the desired sample were placed in a 1000 ml sealed Erlenmeyer flask which is connected to a Burrell-Wrist Action Shaker (Model 75). Compressed filtered air is introduced into the flask that generates polydisperse fine aerosols by mechanical disintegration ("saltation") with a distribution that resembles the size distributions of dust plumes generated in the natural source regions (Lafon et al., 2006).

The dry aerosol is then sent to the electrostatic classifier for particle size selection (TSI Model 3080) with a Differential Mobility Analyzer (DMA, TSI Model 3081). Before entering the classifier, aerosols are passed through an impactor to remove supermicro-meter size particles (i.e., size greater than 1 μm) and then charged with a series of Kr-85 neutralizers. The particles are then classified in the DMA by their electrical mobility set by the voltage applied to the DMA. The Sheath flow rate in the DMA is set to 2.3 l min^{-1}, and the monodisperse flow is set to 0.45 l min^{-1}. The classified aerosol flow is mixed with filtered air and then sampled by a Condensation Particle Counter (CPC, TSI Model 3010), and a Droplet Measurement Technologies Continuous Flow Streamwise Thermal Gradient CCN (CFSTGC) chamber.

The CPC measures the total concentration of aerosol, or condensation nuclei (CN) present in the monodisperse stream. The fraction of aerosol acting as CCN is measured by exposing particles to a constant water vapor supersaturation within the CFSTGC. This is done by flowing the aerosol in a cylindrical column with wetted walls upon which a thermal gradient, ΔT, is applied in the axial direction. The difference in diffusivity

between water vapor and heat is exploited for the generation of water vapor supersaturation, s, which reaches maximum at the column centerline. CCN flowing along the column centerline are activated to cloud droplets and are counted at the exit with an optical particle counter (OPC). Each value of ΔT generates a unique supersaturation value, which in this study varied between 0.15% and 1%. CCN activity is characterized by the dry activation diameter, D_{dry}, which corresponds to the minimum dry particle diameter that activates at the certain supersaturation of interest, s_c. D_{dry} is found by expressing the ratio of CCN to CN concentration as a function of dry particle diameter, and, determining the diameter for which 50% of the classified aerosol acts as CCN.

The calibration of the instrument supersaturation is determined from the D_{dry} of $(NH_4)_2SO_4$ calibration aerosol at a given ΔT. $(NH_4)_2SO_4$ aerosol was generated by atomizing an aqueous solution and subsequently drying the droplet stream with a series of silica-gel diffusion dryers. D_{dry} of $(NH_4)_2SO_4$ is then related to s by applying Köhler theory, assuming that $(NH_4)_2SO_4$ has a shape factor of 1.04 in the DMA (Kuwata and Kondo, 2009), density of 1760 kg m^{-3}, surface tension of water (calculated at the average column temperature), molar mass of 0.132 kg mol^{-1}, and osmotic coefficients calculated with the Pitzer activity coefficient model (Pitzer and Mayorga, 1973). A relationship between ΔT vs. instrument supersaturation is determined by repeating the above calibration procedure over a range of ΔT. This relationship is then used in all dust activation experiments. Calibration is repeated throughout the measurements, and exhibits little variability (about 5% relative uncertainty in instrument supersaturation).

Size-resolved CCN activity is carried out using the Scanning Mobility CCN Analysis (SMCA) (Moore et al., 2010), where the DMA used for aerosol classification is

operated in scanning voltage mode. This allows the concurrent determination of aerosol size distribution and size-resolved CCN activity over a voltage scan cycle. In this study, the complete range of dry particle size (20 - 850 nm) is scanned over three minutes. The CFSTGC was operated at a flowrate of 0.50 l min^{-1} and a sheath-to-aerosol ratio of 10:1 (or 7.5:1). SMCA also provides the droplet distribution of activated CCN (measured in the optical particle counter of the CCN instrument) as a function of their dry diameter. The dependence of droplet size on the supersaturation profile and dust dry particle size is used to study the dust activation kinetics.
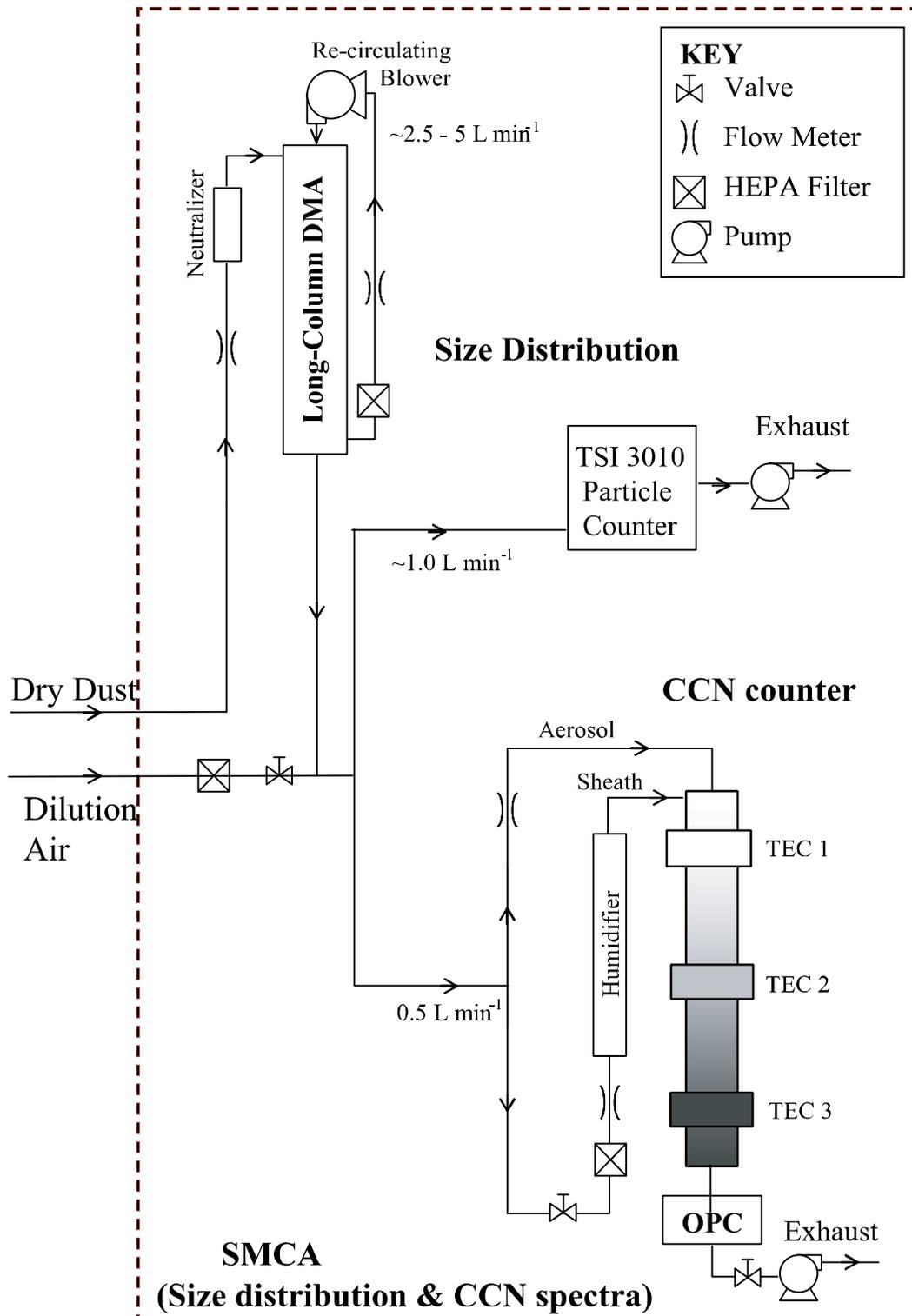
Figure 3.1: Schematic of the experimental set-up used for size resolved CCN activation and droplet growth kinetics measurements.

3.3.3 Data Analysis Methodology

The measurement of D_{dry}, and corresponding s_c, is fitted with a power law function $s_c = CD_{dry}^x$. The experimental exponent, x_{exp} (Kumar et al., 2009b), is then compared against the exponent determined from fits of KT and FHH-AT to the data. The appropriateness of each theory is evaluated based on its ability to reproduce x_{exp}. According to KT, particles with appreciable hygroscopicity exhibit $x = -3/2$. In FHH-AT, x depends on the value of A_{FHH} and B_{FHH} but generally ranges between -0.80 and -1.20 (Kumar et al., 2009a). The same fitting procedure also determines the adsorption parameters A_{FHH} and B_{FHH} (for FHH-AT), and the hygroscopicity parameter κ (for KT).

B_{FHH} strongly affects the shape of the equilibrium curve and largely determines the existence and value of s_c and critical wet diameter, D_c (described as the wet diameter of the aerosol particle at the maximum of the equilibrium curve) (Kumar et al., 2009a). A_{FHH} also affects these parameters, but to a lesser extent than B_{FHH}. Figure 3.2 shows the relationship between D_{dry} and s_c for a range of B_{FHH} values computed at surface tension of water equal to 0.072 J m^{-2}, temperature equal to 298.15 K, and A_{FHH} = 2.50. Lower B_{FHH} values correspond to more hydrophilic dust. As B_{FHH} approaches 3.0, particles become less hydrophilic (with $x \rightarrow$ -1), which corresponds to insoluble but wettable particles that follow the Kelvin equation. Similarly for KT, as κ decreases from $\kappa = 0.05$ to $\kappa = 0$ (Fig. 3.2) particles becomes less hygroscopic causing a decrease in the exponent from $x = -1.5$ to $x \rightarrow$ -1.0. It can be seen from Fig. 3.2 that the slopes determined from KT (expressed in terms of κ) are much steeper than those determined from FHH-AT (expressed in terms of B_{FHH}). This suggests that the same particle type can exhibit two different s_c-D_{dry} exponent values if described by KT or FHH-AT.

Droplet activation kinetics of aerosol inside CFSTGC depends on the supersaturation profiles, residence time, water vapor uptake coefficient, dry particle size (Nenes et al., 2001; Roberts and Nenes, 2005; Lance et al., 2006), as well as the theory used to describe the equilibrium vapor pressure for the particle (KT or FHH-AT). Activation kinetics can be characterized by the difference in droplet size, ΔD_w, between dust CCN and $(NH_4)_2SO_4$ CCN with same s_c. A negative ΔD_w implies that mineral aerosol exhibits retarded activation kinetics (the converse is typically not observed). This technique is called threshold droplet growth analysis (TDGA) and has been successfully used by a number of in-situ and laboratory studies (Asa-Awuku et al., 2010; Padró et al., 2010).

We quantitatively describe the growth of dust by simulating the process of droplet nucleation and growth within the CCN instrument using the comprehensive computational fluid dynamics model. We use the Lance et al. (2006) model, which numerically simulates the temporal and spatial distributions of velocity, pressure, temperature, and water vapor concentration throughout the growth chamber, considering the coupling of particle and gas phases through the release of latent heat and condensation/evaporation of water vapor onto the droplets. The kinetics of dust activation is then parameterized in terms of an effective uptake coefficient, which influences the mass transfer coefficient of water onto the dust CCN. Condensational growth of aerosol is computed based on a size-dependent mass transfer coefficient multiplied by the difference between gas-phase and equilibrium water vapor pressure (Nenes et al., 2001)

$$D_p \frac{dD_p}{dt} = \frac{s - s_{eq}}{\dfrac{\rho_w RT}{4 P_{H_2O}^\circ D_v' M_w} + \dfrac{\Delta H_v M_w}{4 k_a' T}\left(\dfrac{\Delta H_v \rho_w}{RT} - 1\right)} \qquad [3.1]$$

where D_p is the droplet diameter, s is the local instrument supersaturation, ρ_w is the water density, M_w is the molar mass of water, R is the universal gas constant, T is the average column temperature, $P_{H_2O}^\circ$ is the equilibrium water vapor pressure, ΔH_v is the enthalpy of vaporization of water, D_v' is the diffusivity of water vapor in air modified for non continuum effects, and k_a' is the thermal conductivity of air modified for non continuum effects. Here D_v' is defined by Fukuta and Walter (1970) as

$$D_v' = \frac{D_v}{1 + \frac{2D_v}{\alpha_c D_p}\sqrt{\frac{2\pi M_w}{RT}}} \qquad\qquad [3.2]$$

where D_v is the diffusivity of water vapor in air, α_c is the water vapor uptake coefficient. k_a' is given by

$$k_a' = \frac{k_a}{1 + \frac{2k_a}{\alpha_T D_p \rho_a c_p}\sqrt{\frac{2\pi M_a}{RT}}} \qquad\qquad [3.3]$$

where M_a is the mean molar mass of air, k_a is the thermal conductivity of air, ρ_a is the air density, c_p is the heat capacity of air, and α_T is thermal accommodation coefficient (equal to 1.0). For insoluble CCN activating according to FHH-AT, the equilibrium supersaturation of the droplet, s_{eq}, is given by Kumar et al. (2009a)

$$s_{eq} = \exp\left[\frac{4\sigma M_w}{RT\rho_w D_p} - A_{FHH}\left(\frac{D_p - D_{dry}}{2D_{H_2O}}\right)^{-B_{FHH}}\right] - 1 \qquad\qquad [3.4]$$

where σ is the CCN surface tension at the point of activation (Pruppacher and Klett, 1997), D_{dry} is the dry CCN diameter, D_{H_2O} is the diameter of water molecule equal to

2.75 Å (Kumar et al., 2009a), and A_{FHH} and B_{FHH} are adsorption parameters constrained from the activation experiments.

The instrument model was initialized using the appropriate geometric dimensions and operating conditions of DMT CFSTGC (Lance et al., 2006). A computational grid of 200 cells in the radial and 200 cells in the axial direction were used in each simulation. A Lagrangian approach is used to determine CCN growth in the CFSTGC by Eq. (3.1), assuming the particles flow along streamlines occupied by the aerosol region of the chamber (determined from the sheath-aerosol ratio) and grow according to the local water vapor saturation ratio and temperature (Roberts and Nenes, 2005; Lance et al., 2006). The droplet diameter at the exit of the flow chamber is then compared against the measured droplet size distribution, following the binning scheme used in the optical detection of the instrument. The value of uptake coefficient is then inferred by minimizing the discrepancy between predicted and observed droplet distributions in OPC.
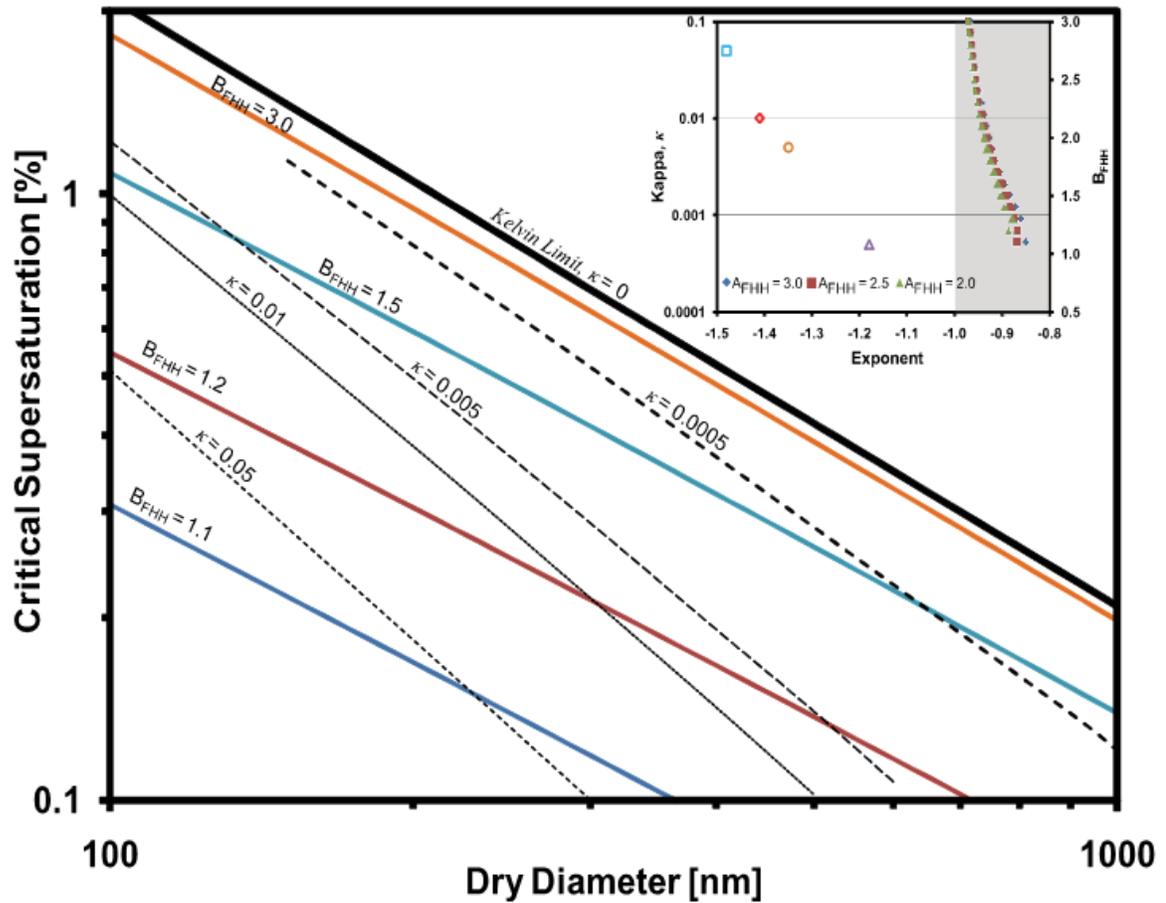
Figure 3.2: s_c-D_{dry} lines for different values of B_{FHH} computed at $\sigma = 0.072$ J m^{-2}, $T = 298.15$ K and $A_{FHH} = 2.50$. Dashed lines indicate κ isolines determined at above conditions. Also shown in black thick line is the $\kappa = 0$, Kelvin curve. The inset figure shows experimental exponent as function of B_{FHH} and κ.

3.4   Results and Discussion

3.4.1   *Effects of Multiple Charging and Dust Particle Shapes*

3.4.1.1 Correction for Multiply Charged Particles in SMCA

To account for the effect of multiply charged particles in the activation curves and observed D_{dry}, we assume an equilibrium charge distribution for the particles entering the DMA and apply a correction algorithm as described in Moore et al. (2010). The correction algorithm determines the contribution from the multiply charged (+2, +3, +4, +5 and +6 charges) particles to the total particle counts in each size bin for the CN time series and rebins respective contributions to its "true" size bin. The same procedure is applied to the CCN time series. The inversion of the CN, CCN time series determines the activation fraction and hence D_{dry}. To ensure sufficient residence time for attaining equilibrium charge distribution inside the Kr-85 neutralizers, we determine the number of neutralizers beyond which the inverted size distribution does not change. Test results indicate that 3 Kr-85 neutralizers in series (with a total nominal activity of 10 mCi) were sufficient to completely neutralize the surface charges and attain the Boltzmann equilibrium distribution.

The impact of multiply charged particles is shown in Fig. 3.3, which presents the activation curves (with and without multiple charging corrections) at 0.30% supersaturation for aerosol generated from the Soil 2 sample. D_{dry} increases from ~170 nm to ~247 nm upon application of the multiple charge correction. The effect on D_{dry} is further enhanced at lower supersaturations (e.g., $s_c = 0.15\%$ and $s_c = 0.20\%$) that correspond to large particles with a pronounced probability of multiple charging. The uncertainty in the activation efficiency due to counting statistics uncertainty and flow rate

variability (expressed as error bars in Fig. 3.3) were accounted for using the procedure of

Moore et al. (2010).
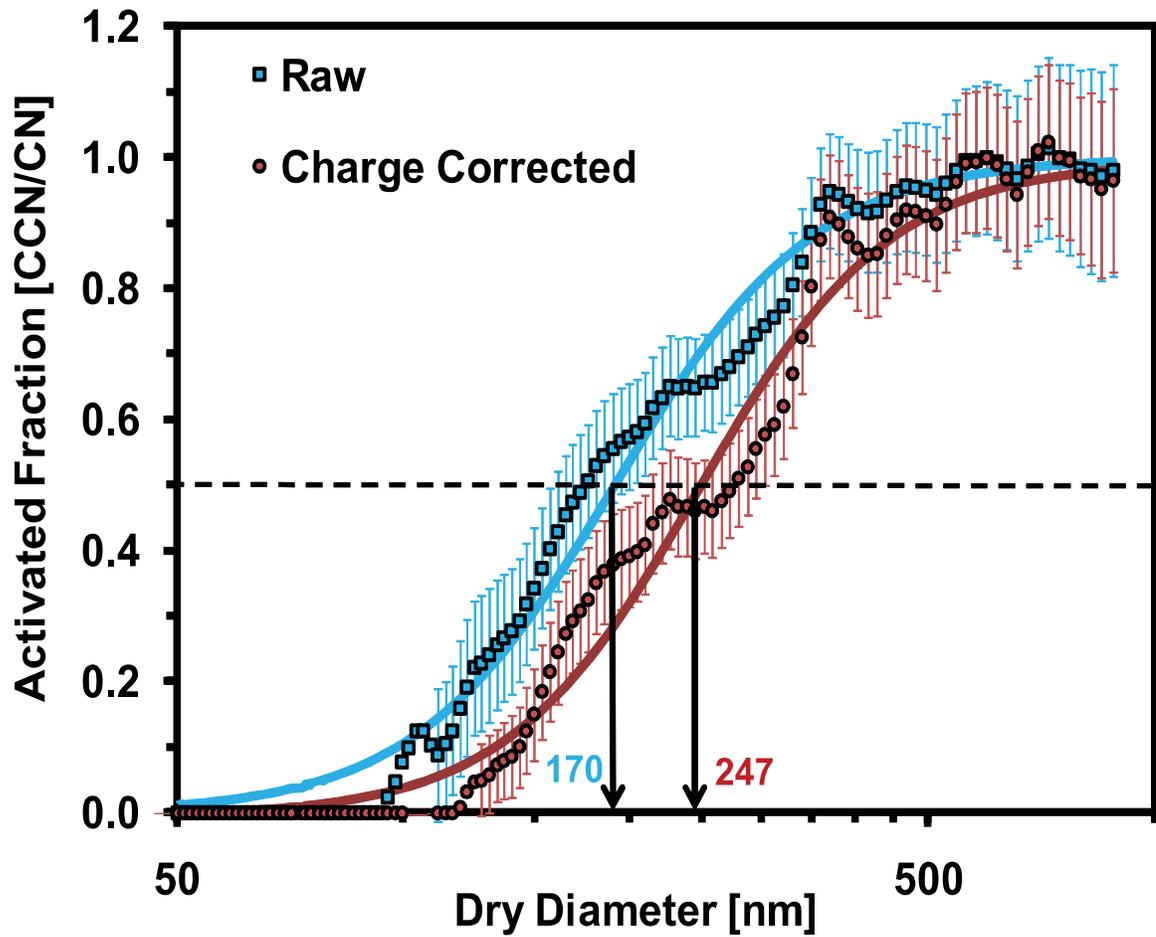
Figure 3.3: Activation curves for Soil 2 at $s_c = 0.3\%$. Shown are inversions without (blue) and with multiple charge corrections (brown). Error bars represent uncertainty of activation efficiency as a result of counting efficiency and flow rate uncertainty at different diameters.

3.4.1.2 Accounting for Dust Non-Sphericity

Dust particles exhibit a variety of complex shapes that are difficult to measure or express in terms of a unique set of parameters or functions. Characterization of dust non-sphericity is often done by either *i*) introducing a dynamic shape factor, χ, (defined as the ratio of drag force, F_D, experienced by the non-spherical particle to that experienced by a volume equivalent sphere when both move at the same velocity in the gas; e.g., DeCarlo et al., 2004), or *ii*) providing an Aspect Ratio (*AR*), defined as the ratio of the longest dimension of particles to the orthogonal shortest length (width). Commonly, χ is obtained by tandem electrical mobility and aerodynamic particle sizing (e.g., DeCarlo et al., 2004; Kuwata and Kondo, 2009) and is an integrated measure of the three-dimensional particle shape. *AR* is measured with electron microscopy that reports two dimensional image projections of particles from which the longest dimension and width are determined (e.g., Kalashnikova and Sokolik, 2004).

Here we assess the effect of dust non-sphericity in CCN activity measurements by considering the range of values of *AR* or χ reported in the literature for different types of mineral aerosol. A number of recent studies have reported measurements of *AR* values for species considered in this study. For instance, Chou et al. (2008) report a mean *AR* equal to 1.7 for Niger dust collected during the AMMA campaign, Kandler et al. (2009) report *AR* equal to 1.64 for Saharan dust collected over Spain, and Coz et al. (2009) report *AR* equal to 1.81 for African dust. The *AR* values for African soils are slightly higher compared to *AR* of 1.3 - 1.4 reported by Okada et al. (2001) for East Asian dust. *AR* can also vary with particle size (Wiegner et al., 2009). To account for this, we considered those values of *AR* that are most relevant for this study (i.e., particles less than 1µm).

Furthermore, the extent of non-sphericity can be affected by the aerosol generation method (Sullivan et al., 2010) which can give rise to very different particle morphologies from those generated with the dry soft-saltation technique used in this study. Some of the other techniques of aerosol generation include a fluidized bed (Koehler et al., 2009), dry dust generator (Herich et al., 2009), and atomization of a dust aqueous suspension (Koehler et al., 2009; Herich et al., 2009). All above factors can contribute to uncertainty in χ for similar aerosol types. For instances for ATD, Möhler et al. (2008) reported $\chi = 1.3$ while Endo et al. (1998) reported $\chi = 1.5$. Similarly for illite, Hudson et al. (2008) and Möhler et al. (2008) reported $\chi = 1.3 \pm 0.02$ and $\chi = 1.3$ respectively. For other clays and minerals analyzed in this study such as montmorillonite, Hudson et al. (2008) reported $\chi = 1.11 \pm 0.03$, while Hinds (1999) report a value of $\chi = 1.36$ for quartz.

In this study, we use the published range of dust non-sphericity. As most of the recent studies on African and Asian mineral dust aerosol have quantified dust non-sphericity based on AR, we initially started with the Fuchs (1964) approach to convert from AR to χ assuming mineral aerosol as a spheroid. However, we found that using the Fuchs (1964) approach results in much lower values of χ ($\sim 1.007 - 1.034$) than those determined from direct measurements of χ ($\sim 1.11 - 1.50$). According to Davies (1979), sand particles composed of a mixture of different minerals have a dynamic shape factor of $1.3 - 1.6$. Therefore, in this study non-sphericity corrections are performed for all species considering $\chi = 1.3 \pm 0.2$ as this covers as possible values of measured χ. Further, we examine the importance of this uncertainty in χ (between $\chi = 1.1$ and $\chi = 1.5$) for dust-CCN measurements by evaluating its effect on x_{exp} and FHH parameters, A_{FHH} and B_{FHH}.

Size selection in this study is performed using the DMA that classifies a particle by its electric mobility. Electrical mobility can then be related to the physical diameter if the number of elementary charges per particle and χ are known (together with the strength of the electric field and other operational parameters in the DMA). Often χ is assumed unity. For mineral dust, however, $\chi > 1$ which translates into a larger drag force than expected for spherical particles; when neglected, the nonsphericity would eventually lead to underestimation of the particle surface area. In this study, we account for dust non-sphericity by correcting for the surface area of the particle available for water vapor adsorption. This is performed by converting from electrical mobility diameter, D_m, to surface-area equivalent diameter, D_{se}, so that the CCN activity data is expressed in terms of the s_c-D_{se} relationship. By converting from D_{dry} to D_{se}, the aerosol physical size is expressed in terms of the characteristic length responsible for controlling surface water vapor adsorption. D_{se} is determined by converting the electrical mobility diameter (D_m), to particle volume equivalent diameter (D_{ve}), and from there to D_{se}.

Determining D_{ve} from D_m

D_{ve} is determined from D_m by iterative solution of the dynamic shape factor equation (DeCarlo et al., 2004)

$$\chi = \frac{D_m C(D_{ve})}{D_{ve} C(D_m)} \qquad [3.5]$$

where $C(D_m)$ and $C(D_{ve})$ are the slip correction factors for D_m and D_{ve}, respectively. $C(D_m)$ and $C(D_{ve})$ can be approximated from the correlation of Willeke and Baron, (2001)

$$C(D_i) = 1 + \frac{2\lambda}{D_i}\left(1.142 + 0.558\exp\left(-0.999\frac{D_i}{2\lambda}\right)\right)$$ [3.6]

where λ is the mean free path of the gas molecules and D_i corresponds to either of D_m or D_{ve}. Application of Eq. (3.5) to determine D_{ve} requires knowledge of χ.

Determining D_{se} from D_{ve}

When χ is known (or estimated), the correlation of Leith (1987) is used to relate χ, D_{se}, and D_{ve}

$$\chi = \frac{1}{3}\left(\frac{D_n}{D_{ve}}\right) + \frac{2}{3}\left(\frac{D_{se}}{D_{ve}}\right)$$ [3.7]

where D_n is the diameter of the sphere whose projected area is equal to that of the particle normal to the direction of flow. For the DMA, $D_n = D_m$, hence Eq. (3.7) can be rearranged to express D_{se} as

$$D_{se} = \frac{3\chi D_{ve} - D_m}{2}$$ [3.8]

Despite involved uncertainties, accounting for dust non-sphericity provides more realistic representation of dust particles as well as enables us to determine non-sphericity effects on the physics controlling the activation of insoluble dust particles.

3.4.1.3 Effect of Charge and Shape Correction on Dust CCN Activation

The largest change in dry critical activation diameter from multiple charging corrections is observed at the point of lowest supersaturation (corresponding to the largest activation diameters with highest probability of multiple charging). For all species considered in this study (regional dusts and clays/minerals), $\chi = 1.3$ was used to convert from charge corrected electrical mobility diameter, D_m to the shape corrected surface-area

equivalent diameter, D_{se}. The error bars on D_{se} represent the range using $\chi = 1.1$ as the lower limit and $\chi = 1.5$ as the upper limit. We found that accounting for non-sphericity using $\chi = 1.3$, can result in an increase in activation diameters by up to $18 - 20\%$ when converting from D_m to D_{se} using the procedure outlined above. Based on Fig. 3.4, as the final activation diameters (after including both charge and shape corrections) lie outside the experimental error bars (or region of experimental uncertainty) determined from the raw data, the essence of including the charge and shape corrections is justified and hence performed for all the samples studied here.

We also found that introducing both multiple charging and shape correction changes the dry activation diameters significantly and hence the exponents determined from the s_c-D_{dry} relationship. For example in the case of ATD, $x_{exp} = -1.23$ for the uncorrected data; after applying charge corrections, $x_{exp} = -0.78$; with shape and charge corrections, $x_{exp} = -0.82$. This is a very large and important difference, enough to shift the implied activation mechanism from a regime where both FHH-AT and KT may be active ($x_{exp} = -1.23$) to a regime where FHH-AT dominates ($x_{exp} = -0.82$). This example emphasizes the importance of applying corrections (especially for multiple charges) for adequate interpretation of the activation data.

It is also noted that the effect of particle non-sphericity must be incorporated into the diameter used in the Kelvin term at the point of activation if only a few monolayers are adsorbed at activation (Romakkaniemi et al., 2001). We find that for all regional samples considered in our study, the number of adsorbed water vapor monolayers layers range from 100 - 500 at the point of activation. This implies that at the point of activation, non-spherical dust aerosol has sufficiently high water coverage so that the

droplet shape is spherical, and, the molar volume and gas-liquid surface tension of the adsorbed H_2O approaches that for the bulk water.
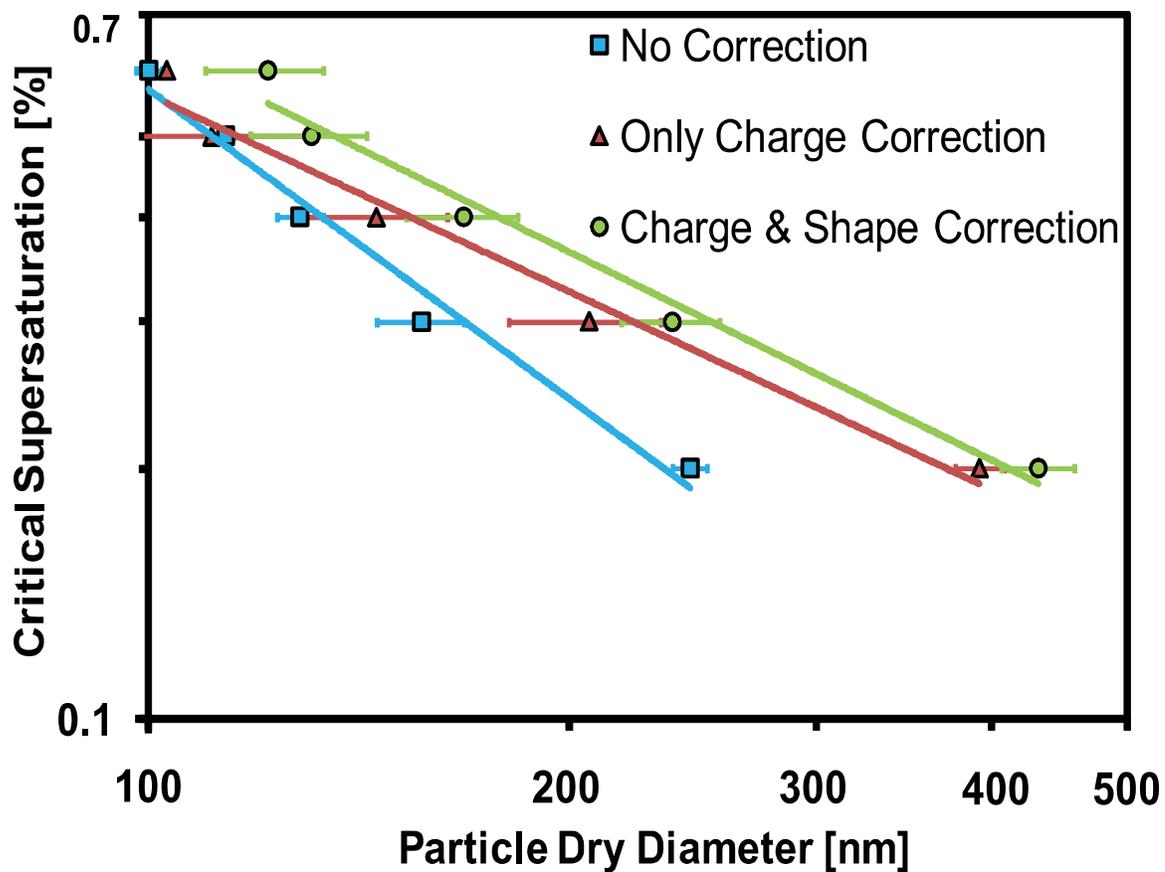
Figure 3.4: CCN activation curves (s_c-D_{dry}) for ATD ($\chi = 1.3 \pm 0.2$) showing the effect of including charge and shape corrections on the raw data. Blue shows curve with no correction, brown shows the results with charging corrections and green shows curve after including both charge and shape corrections. Error bars represent experimental uncertainty and numerical uncertainty in D_{dry} at same instrument supersaturation.

3.4.2 *Results of Dust CCN Activation Measurements*

The CCN activation curves for dry generated dust and mineral/clay samples are shown in Fig. 3.5 and 3.6, respectively. CCN activity is presented in terms of dry activation diameter (D_{se}, given by Eq. 3.8) against instrument supersaturation. The CCN activity data (points) are fit to a power law expression from which the experimental exponent, x_{exp}, is determined. The A_{FHH}, B_{FHH}, and corresponding exponent, x_{FHH}, were determined from fitting the FHH-AT model (lines) to the experimental data via least squares minimization. The dry generation method used in this study did not produce sufficient number concentrations of particles with sizes smaller than 100 nm. Hence the CCN activity is restricted to supersaturations 0.7% and below (corresponding to D_{dry} ~ 100 nm and above).

Figure 3.5 clearly demonstrates that dust aerosols are CCN at atmospherically relevant supersaturations. It also indicates that soft saltation technique can generate mineral dust in the fine mode (with D_{dry} between 100 nm and 500 nm) which may contribute to CCN. The measured D_{dry} for different dust samples are much larger than expected for $(NH_4)_2SO_4$, suggesting that dust has a lower CCN activation potential than what is expected for soluble aerosol like $(NH_4)_2SO_4$. Figure 3.5 suggests that dust aerosols collected from different regions of the globe can have different activation properties which are attributed to the physical properties, morphology and the chemical composition of the parent soils. The CCN activity comparisons amongst different regional dust samples indicate that East Asian soils have a range of CCN activity potentials with B_{FHH} ~ 1.1 - 1.3. In comparison, Niger Soil (representative of North African dust) and ATD (representative of North American dust) were found to exhibit

less variability, with $B_{FHH} = 1.25 - 1.28$. The range in CCN activity of East Asian soils is most likely reflective of the compositional variability. Differences in CCN activity amongst samples collected in the same region likely reflect the chemical heterogeneity within the dust samples. We found that the experimental data (points) can be described by FHH-AT fits (lines) well, with $A_{FHH} \sim 2.25 \pm 0.75$ and $B_{FHH} \sim 1.20 \pm 0.10$ for all dust types considered in this study. A direct comparison of CCN activity against data published in the literature is done by expressing our results (for particles of a given dry diameter) in terms of a hygroscopicity parameter, κ. CCN activity results for regional soils, and minerals and clays indicate a $\kappa \leq 0.05$ for all samples considered in this study. It is also noted that the differences in values of the adsorption parameters determined in this study with those determined by Kumar et al. (2009b) for ATD, and likely arise from the application of multiple charge and dust non-sphericity corrections. Furthermore, the ATD experimental data used by Kumar et al (2009b) in the predictions of adsorption parameters were taken from Koehler et al. (2009) that used a fluidized bed to generate aerosols, while in this study measurements were performed using a dry generation technique.

Figure 3.6 presents the CCN activity of all the minerals and clays considered. The activation diameters obtained for different dusts (Fig. 3.5) are within the range of those observed for different clays and minerals (Fig. 3.6). This suggests that dust CCN activity is controlled by adsorption of water onto the clay and mineral components in the dust samples. Comparison between CCN activities for different clays indicates montmorillonite (both Na and Ca rich) is more hydrophilic than illite, which agrees with the findings of Herich et al. (2009). Higher CCN activation potential for montmorillonite

can be attributed to the mineralogy of the sample; the presence of unbounded Na and Ca cations allows water to penetrate the interlayer molecular space, which together with adsorption results in the clay swelling to several times its original volume. In the case of illite, the interlayer space is mainly occupied by poorly hydrated potassium cations that prevent these clay types from expanding, thus reducing the amount of water that can adsorb on the surface and its CCN activation potential.

The CCN activity of SiO_2 and $CaCO_3$ was also measured (Fig. 3.6). As expected, SiO_2 was the least CCN active of species considered with $B_{FHH} = 1.36$ versus $B_{FHH} < 1.30$ for the other clays and minerals (Table 3.2). This is because the majority of the silica surface does not interact strongly with water vapor since physisorption occurs primarily on the limited number of silanol sites (Young, 1958). We also find that the charged-corrected activation curves in our study differ from published CCN activation data for $CaCO_3$ (Sullivan et al., 2009), montmorillonite, and illite (Herich et al., 2009). For example, charge-corrected activation curves for clays (illite and Na-montmorillonite) exhibited $\kappa = 0.02$ - 0.04, versus 0.002 - 0.003 in Herich et al. (2009). In addition, (OMYA) $CaCO_3$ in this study was found to exhibit multiple κ values, 0.02 at $s_c = 0.4\%$ - 0.5% and 0.003 - 0.007 at $s_c = 0.2\%$ - 0.3%, higher than found by Sullivan et al. (2009) for (Solvay) $CaCO_3$ ($\kappa = 0.0011$). Our results for (OMYA) $CaCO_3$ at low s_c ($\kappa = 0.003$ - 0.007) compare well with results obtained for (Baker) $CaCO_3$ ($\kappa = 0.008$) (Sullivan et al., 2010). Similarly, we find a good comparison in CCN activity measurements based on κ values for regional dust samples considered in this study (for activation curves with and without multiple charging corrections) and past studies. For dry generated ATD (non-corrected), $\kappa = 0.04$ determined in this study compares well with non-corrected $\kappa = 0.025$

found by Koehler et al. (2009). Similarly, a good comparison for African dust samples was found with charge-corrected $\kappa = 0.023$ (Herich et al., 2009) and non-corrected $\kappa = 0.054$ (Koehler et al., 2009) determined for Saharan Dust, and charge-corrected and non-corrected $\kappa = 0.02 - 0.04$ for Niger dust data.

The differences cited above for $CaCO_3$ can be attributed to factors such as sample-to-sample variability (as confirmed by Sullivan et al., 2010) and method of aerosol generation. The soft saltation technique may yield very different particles from studies using a custom-built dry dust generator (Herich et al., 2009) or fluidized bed (Koehler et al., 2009). Furthermore, the lack of charge correction (in previous studies) will provide activation curves sensitive to the aerosol size distribution (as it determines the fraction of multiply charged particles with same mobility diameter), so differences in the dust size distribution will lead to variable biases in D_{dry}. Unfortunately, absence of number size distributions of the CCN in the published studies precludes a conclusive attribution of these differences to multiple charging biases.

Table 3.2 shows the values of the experimental exponent, determined from the s_c-D_{dry} data for all dust samples and individual minerals/clays. The x_{exp} values determined in this study are much lower than those reported by Kumar et al. (2009b) that were determined from the experimental data of Koehler et al. (2009) and Sullivan et al. (2009). This is a result of experimental measurements performed in this study at much lower supersaturations, as well as the application of multiple charge and shape factor corrections to the activation curves that tend to further shift D_{dry} and x_{exp} (as illustrated in Fig. 3.4).

In Fig. 3.7, x_{FHH} is plotted against x_{exp} for all dust samples and individual minerals/clays. For $CaCO_3$, the value of x_{exp} from the uncorrected s_c-D_{dry} data equals -0.81. The value of x_{exp} after charge and shape correction reduces further to -0.75. As x_{exp} for $CaCO_3$ is outside the range of exponents that can be predicted by FHH-AT, x_{FHH} deviates from x_{exp} by more than 10%. For Na-montmorillonite, Ca-montmorillonite, Soil 1 and Soil 3, x_{FHH} is in excellent agreement with x_{exp} suggesting that the above can be parameterized using FHH-AT. This suggests that the CCN activity of clays is consistent with multilayer adsorption activation theory. In the case of illite, SiO_2, ATD, Niger, Soil 2, Soil 4, and Soil 5, x_{FHH} lies within the variability of x_{exp}, suggesting that FHH-AT also is an excellent description of CCN activity. Considering the uncertainty observed in experimental exponents (Fig. 3.7), it can be argued that the dust samples considered in this study are in excellent agreement with FHH-AT. Furthermore, x_{exp} for all samples are found to be between -0.80 and -1.20 (range relevant for adsorption activation as given by Kumar et al., 2009a) as well as between -0.75 (determined for $CaCO_3$) and -0.93 (determined for Na-montmorillonite) providing support that nucleation of freshly generated regional dust aerosols is controlled by water vapor adsorption on clays and minerals. This confirms the conclusions of Kumar et al. (2009b) that *i*) using the KT framework for parameterizing dust-CCN interactions is inappropriate, and, *ii*) adsorption effects must be included when describing the hygroscopic and CCN behavior of mineral aerosol.

It can also be seen from the insert in Fig. 3.2, that for KT to predict the correct exponent determined from the experimental s_c-D_{dry} relationships on dust and clays (shown as shaded region), the values of κ must be very low (less than 0.0005), much

lower than those determined in previous studies (Koehler et al., 2009; Herich et al., 2009; Sullivan et al., 2009). On the contrary, FHH-AT can predict experimental exponents obtained from dust and clays s_c-D_{dry} relationships (Table 3.2) using a single set of values for A_{FHH} and B_{FHH}. Furthermore, the predicted water vapor uptake under sub-saturated conditions is very low, and can explain the very low apparent hygroscopicity measured (using the hygroscopic tandem DMA technique) for dust aerosol (Herich et al., 2009). This strongly supports that FHH-AT describes fresh dust-CCN interactions better than KT for the samples considered in this study.

While the application of the shape factor corrections to CCN activation data changes the dry activation diameters considerably, it does so uniformly so that the exponent derived from the s_c-D_{dry} relationship (hence the implied activation physics) is not substantially affected. This can be seen from Table 2. Applying $\chi = 1.3 \pm 0.2$, changes x_{exp} by as little as 5% from charge corrected x_{exp}. Using $\chi = 1.3 \pm 0.2$ has a minor effect on dust hydrophilicity (indicated by a small range of B_{FHH}; Table 3.2). The omission of multiple-charging corrections to the activation curves, however, has a profound effect on the implied activation physics, as the dust appears significantly more CCN active than it really is.
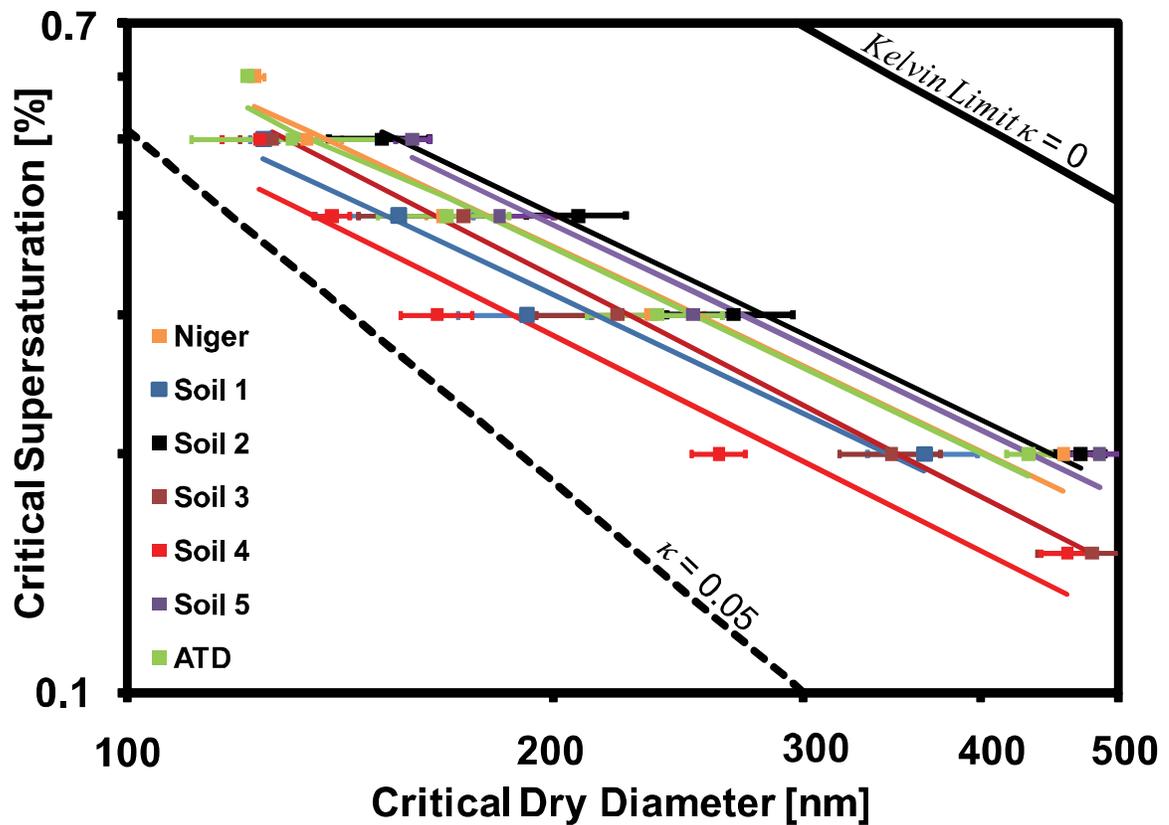
Figure 3.5: CCN activation curves for different dust types presented in Table 3.1. Symbols show experimentally determined CCN activity and lines show FHH adsorption activation fits. Error bars represent measurement uncertainty in D_{dry}. Also shown in black thick line is the $\kappa = 0$, Kelvin curve. Black dashed line corresponds to $\kappa = 0.05$.
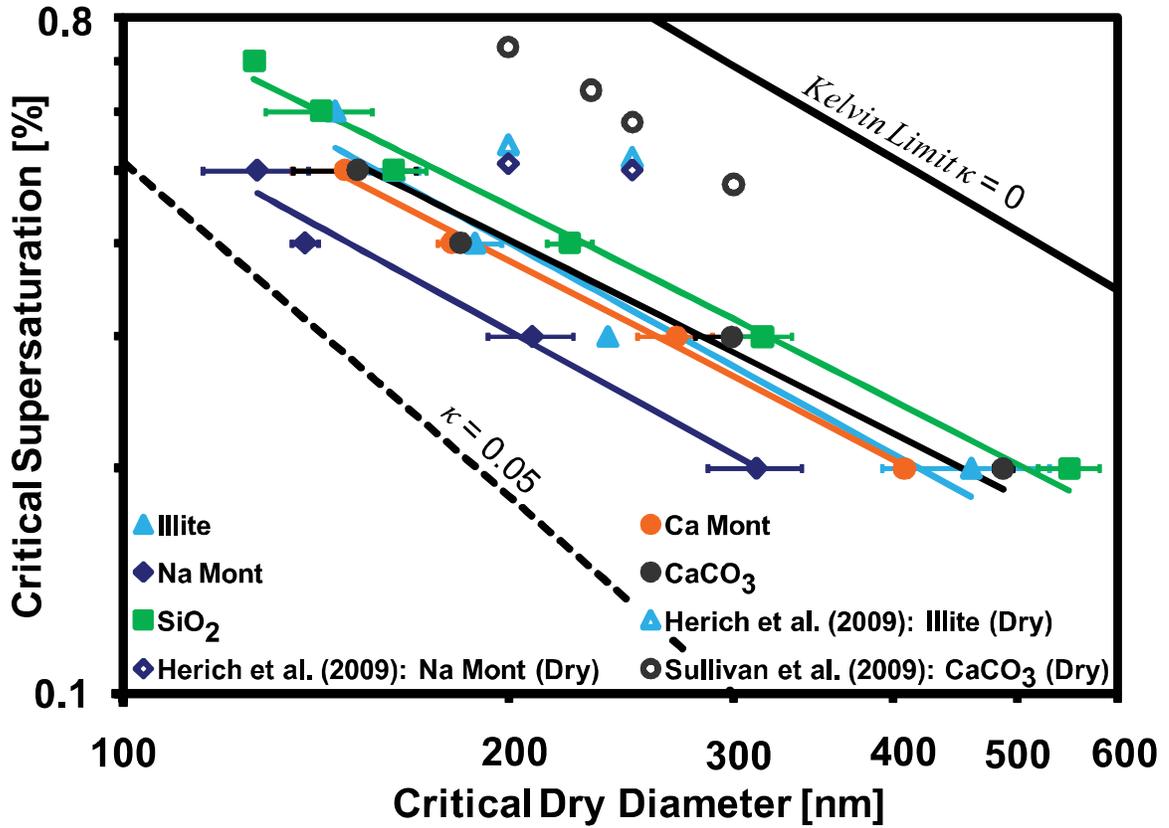
Figure 3.6: CCN activation curves for different mineral types presented in Table 3.1. Symbols (filled) are experimentally determined CCN activity, and lines represent FHH adsorption activation fits. Open symbols represent data obtained from Sullivan et al. (2009) and Herich et al. (2009). Color scheme of open symbols identical to CCN activity observed with measurements in this study. Error bars represent measurement uncertainty in D_{dry}. Also shown in black thick line is the $\kappa = 0$, Kelvin curve. Black dashed line corresponds to $\kappa = 0.05$.

Table 3.2: FHH parameters and exponent comparisons for different regional dusts and individual clays/minerals

Sample	A_{FHH}	B_{FHH}	x_{exp}	x_{FHH}
Dust				
Niger	2.94 ± 0.06	1.27 ± 0.02	$-0.79 \pm 0.02 + (0.04)$	-0.87
Soil 1	2.94 ± 0.06	1.24 ± 0.02	$-0.84 \pm 0.02 + (0.05)$	-0.84
Soil 2	2.88 ± 0.11	1.30 ± 0.04	$-0.82 \pm 0.02 + (0.05)$	-0.85
Soil 3	1.36 ± 0.49	1.12 ± 0.03	$-0.92 \pm 0.03 + (0.05)$	-0.92
Soil 4	1.82 ± 0.39	1.13 ± 0.02	$-0.88 \pm 0.03 + (0.04)$	-0.89
Soil 5	2.91 ± 0.09	1.30 ± 0.03	$-0.78 \pm 0.03 + (0.05)$	-0.85
ATD	2.96 ± 0.03	1.28 ± 0.03	$-0.82 \pm 0.02 + (0.04)$	-0.83
Clay/Mineral				
Illite	1.02 ± 0.38	1.12 ± 0.04	$-0.92 \pm 0.03 + (0.05)$	-0.93
Ca Mont	2.06 ± 0.72	1.23 ± 0.04	$-0.88 \pm 0.02 + (0.05)$	-0.88
Na Mont	1.23 ± 0.31	1.08 ± 0.03	$-0.93 \pm 0.02 + (0.04)$	-0.93
$CaCO_3$	3.00 ± 0.04	1.30 ± 0.03	$-0.75 \pm 0.02 + (0.05)$	-0.85
SiO_2	2.95 ± 0.05	1.36 ± 0.03	$-0.82 \pm 0.03 + (0.04)$	-0.86

Values in parentheses indicate change in magnitude of x_{exp} from change in χ between 1.1 and 1.5

Figure 3.7: Comparison of x_{exp} and x_{FHH} for dust and clay/mineral types presented in Table 3.1. Dashed line represents + 10% deviation from the 1:1 line. Error bars represent deviation in x_{exp} due to the uncertainty in D_{dry}.

72

3.4.3 Droplet Growth Kinetics

In addition to CCN activity, the optical particle counter of CFSTGC measures droplet sizes that can be used to explore CCN activation kinetics of mineral dust. This is carried out using TDGA, by comparing droplet diameter, D_w, from the sample CCN against that of $(NH_4)_2SO_4$ calibration aerosol with same critical supersaturation and maintaining identical instrument conditions (flow rates, pressure, and inlet temperature). If the droplet sizes from mineral aerosol are smaller than that observed from calibration aerosol (for conditions of identical instrument supersaturation, i.e., with same s_c), the activation kinetics of mineral dust is likely slower than the calibration aerosol. However, if activated droplet sizes are indistinguishable (to within experimental uncertainty) from $(NH_4)_2SO_4$ droplet size, mineral dust exhibits the same activation kinetics as the reference aerosol.

Figure 3.8 presents the droplet diameters observed at OPC that are activated from regional dust aerosols as a function of instrument supersaturation. For comparison, droplet sizes are presented for pure $(NH_4)_2SO_4$ aerosol with s_c equal to the instrument supersaturation. It is evident that droplet growth for mineral aerosol at same s_c is lower than that determined for $(NH_4)_2SO_4$ calibration aerosol. The difference in outlet size suggests a delay in activation kinetics as both particles are exposed to the same supersaturation profile during their transit through the CFSTGC. This behavior is consistent with the slower time scales associated with water vapor adsorption (Kumar et al., 2009b). A similar behavior of reduced growth is also observed for different clays and minerals (Fig. 3.9).

Reduced growth at same s_c observed for the mineral aerosol inside the CFTSGC can be attributed to three potential factors: *i*) different shape of the equilibrium curve (FHH-AT vs. KT), *ii*) different mass transfer coefficient (or α_c) of water vapor to the growing droplet, and *iii*) dry particle size. To compare the effect of theory (KT or FHH-AT) used to describe equilibrium vapor pressure, we simulated droplet sizes at the exit of CFSTGC column for different α_c and s_c. Simulations suggest that the size of activated droplets at the exit of the growth column, originating from particles activating at same s_c and with same α_c are almost identical, suggesting that the activation theory has an almost negligible effect on the final droplet size (not shown). Simulations (not shown) indicate that dry CCN size has a negligible effect on final droplet sizes. Based on the above, the droplet size difference between dust CCN and $(NH_4)_2SO_4$ calibration aerosol is primarily driven by the intrinsic activation kinetics of the aerosol (which here is parameterized as difference in water vapor mass transfer coefficients (hence α_c)). This is consistent with a slower timescale associated with adsorption of additional multi-layers of water vapor than absorption of water from deliquesced aerosol (Seinfeld and Pandis, 2006; Pruppacher and Klett, 1997).

Data shown in Fig. 3.8 can be used to infer the water vapor uptake coefficient for dust by simulating dust CCN growth within the CFSTGC. Figure 3.10 shows values of α_c determined for different regional dust aerosols relative to $(NH_4)_2SO_4$. Compared to $(NH_4)_2SO_4$ calibration aerosol (that activates according to classical KT), mineral dust CCN grows to smaller droplet sizes that implies slower growth rate. When expressed in terms of α_c, it corresponds to an average 50% reduction in α_c. In absolute terms, if α_c of water upon deliquesced $(NH_4)_2SO_4$ aerosol is of order 0.2 (Davidovits et al., 2006), a

50% reduction would give α_c of water upon dust $\sim$ 0.1. The α_c tends to decrease as instrument supersaturation increases; at the highest supersaturation, the amount of water adsorbed at D_c is much lower than for larger particles (low critical supersaturation). The kinetics of adsorption accelerates as the amount of adsorbed water increases (Pruppacher and Klett, 1997), so it is expected that α_c would decrease with particle size. The literature value of $(6.3 \pm 0.7) \times 10^{-2}$ determined for the water vapor uptake coefficient on mineral dust (Seisel et al., 2005) is in agreement with the inferred α_c from the highest critical supersaturation ($\alpha_c \sim 0.065$). The diversity of inferred uptake coefficients could also be related to the chemical heterogeneity between samples.

Retarded activation kinetics may have an impact on the activated droplet number in clouds that contain significant concentrations of dust CCN. It is shown by Nenes et al. (2002) that a reduced α_c affects the water uptake in the early stages of cloud formation (since droplets do not grow as rapidly); this leads to a higher parcel maximum supersaturation and hence a higher cloud droplet number. The extent of the impact depends on the vertical velocity, CCN concentration and the relative proportion of KT to FHH-AT particles. A thorough assessment will be the focus of a future study.
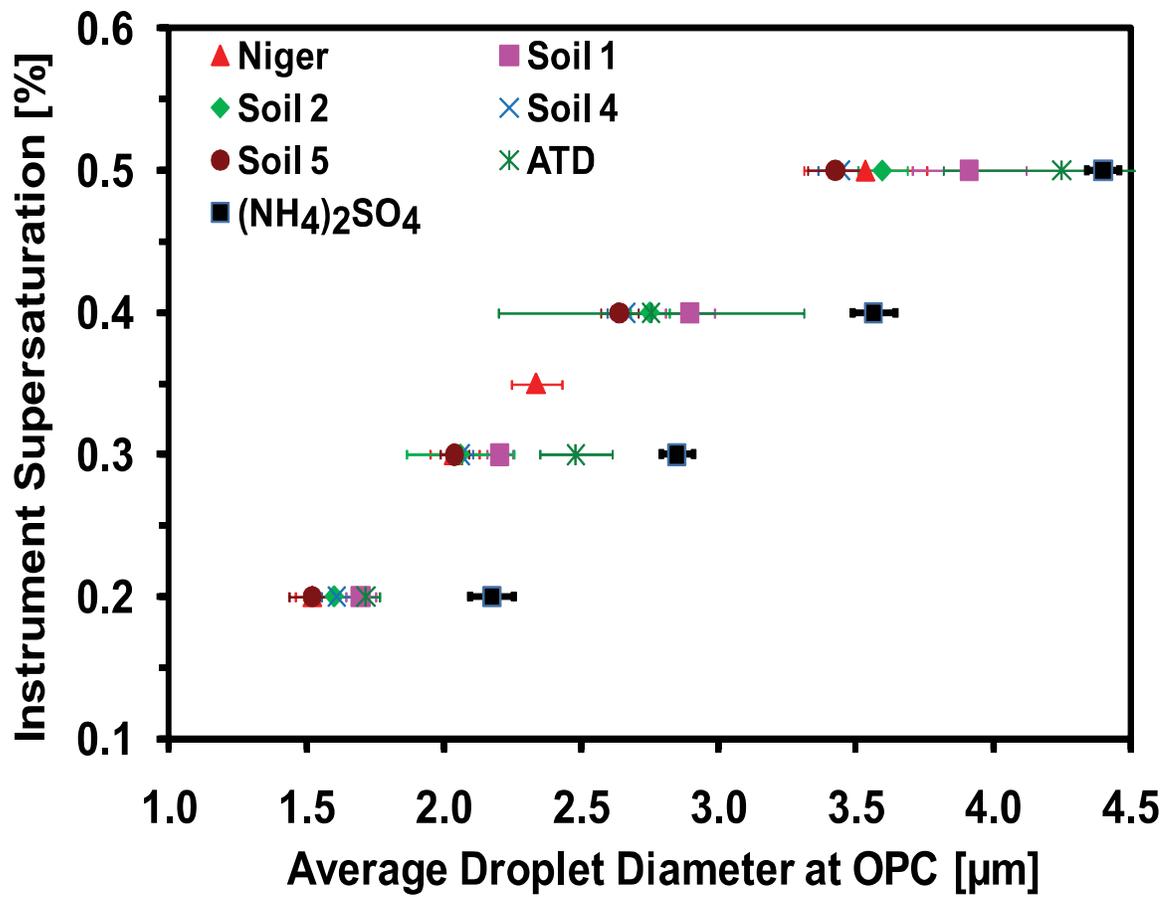
Figure 3.8: Activated droplet sizes of mineral dust CCN with s_c equal to the instrument supersaturation shown as symbols. Error bars represent experimental uncertainty in droplet size as observed by the OPC at same instrument supersaturation.
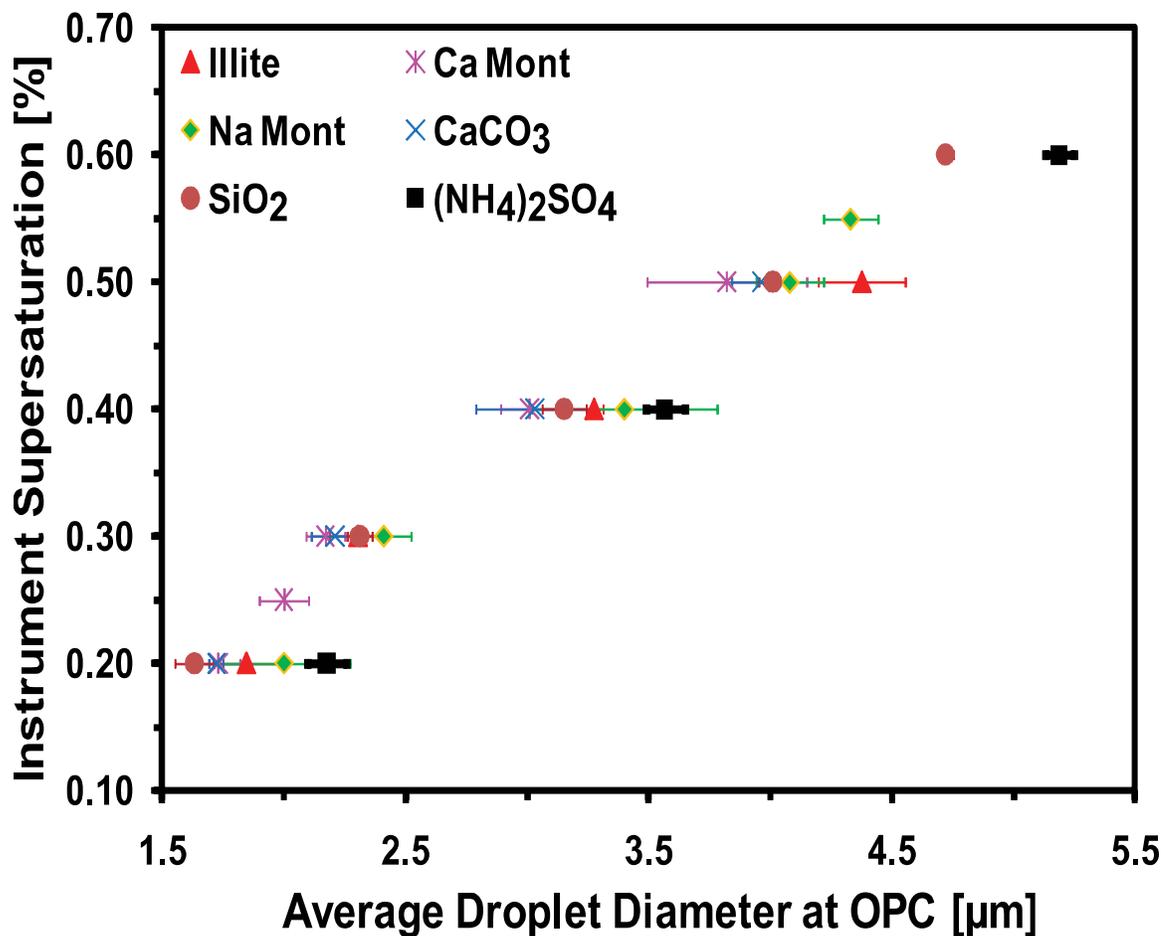
Figure 3.9: Activated droplet sizes of different minerals and clay CCN with s_c equal to the instrument supersaturation shown as symbols. Error bars represent experimental uncertainty in droplet size as observed by the OPC at same instrument supersaturation.
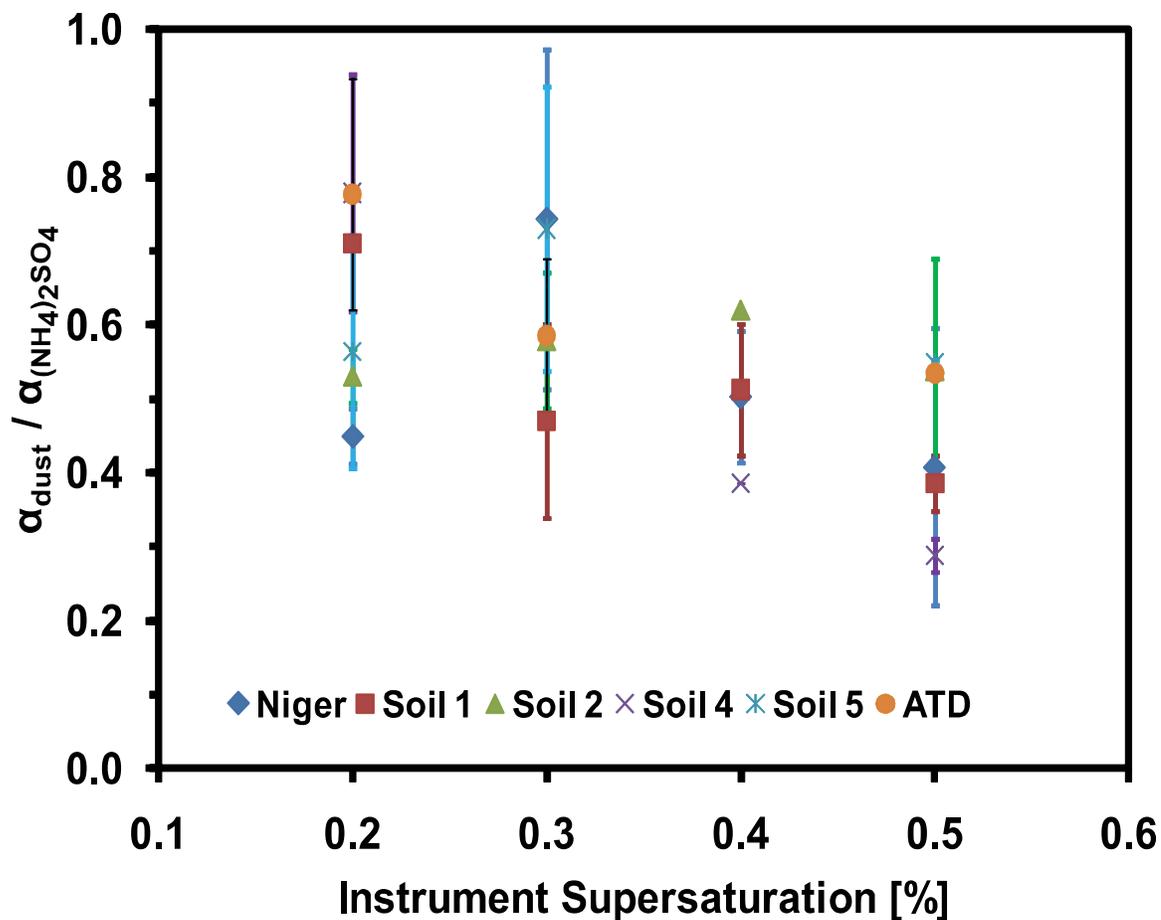
Figure 3.10: Inferred water vapor uptake coefficients for the growth kinetics data of Fig. 3.8 normalized to that of $(NH_4)_2SO_4$ calibration aerosol as a function of different instrument supersaturation. Error bars represent experimental uncertainty in determination of water vapor uptake coefficients arising due to differences in droplet sizes measured by the OPC.

3.5   Conclusions

In this study, the CCN properties and droplet activation kinetics of aerosol generated from regional dust samples and individual minerals (clays, calcite, and quartz) were measured. The aerosols were generated dry in the lab, and properties were measured using the Scanning Mobility CCN Analysis (Moore et al., 2010). Including multiple charge corrections significantly increased D_{dry} and decreased x_{exp}. Dust non-sphericity was accounted for by converting from electrical mobility diameter, D_m, to surface area equivalent diameter such that the surface area available for adsorption can be accounted for. Non-sphericity corrections were accounted for by using the dynamic shape factor, $\chi = 1.3 \pm 0.2$ as this range covered published data for species considered in this study. It was found that while the application of the shape factor corrections to CCN activation data changes the dry activation diameters, it does so uniformly so that the magnitude of the exponent derived from the s_c-D_{dry} relationship (hence the implied activation physics) is not substantially affected with a deviation of as low as 5%.

The x_{exp} for regional dust samples and mineral aerosols investigated in this study was found to be in excellent agreement with FHH-AT (mostly agreeing to within 10%) and one set of adsorption parameters ($A_{FHH} \sim 2.25 \pm 0.75$, $B_{FHH} \sim 1.20 \pm 0.10$). In contrast, KT cannot capture x_{exp} without a hygroscopicity parameter that exhibits very strong size-dependence. This confirms the assessment of Kumar et al. (2009b) and further supports that FHH-AT provides more realistic representation of fresh dust CCN activity than KT.

Using threshold droplet growth analysis, dust CCN was found to have a reduced growth compared to $(NH_4)_2SO_4$ calibration aerosol at the same instrument

supersaturation. This implies slower activation kinetics of dust relative to $(NH_4)_2SO_4$ aerosol. These delays in activation by dust CCN, when parameterized in terms of the water vapor uptake coefficient, α_c, translates to a 30 - 80% (average = 50%) reduction in α_c (relative to the $(NH_4)_2SO_4$ aerosol).

The samples studied here are representative of major regional dust sources, and the adsorption activation parameters determined can be used to express their CCN potential in cloud droplet formation parameterizations developed by Kumar et al. (2009a). These parameterizations are valid for fresh dust in the dust source regions and for transported dust if it will not undergo significant atmospheric processing. A combined KT and FHH-AT framework, however, may be needed to accurately describe the CCN activity of aged dust, dry lakebed dust mixed with salts (e.g., Owens Lake, Texcoco, and Aral Sea), and more generally dust particles with significant amounts of soluble materials.

A major implication of this study is that freshly-emitted dust and mineral aerosols can act as CCN through the effects of water adsorption alone. In some cases, 100 nm dust particles can exhibit comparable hygroscopicity to an organic species with $\kappa \sim 0.05$ or a particle with $(NH_4)_2SO_4$ volume fraction of 10%. Dust particles in the Giant CCN (GCCN) size range will exhibit much lower apparent hygroscopicity because of their lower surface-to-volume ratio. Whether the effects of adsorption is sufficient to make freshly emitted dust GCCN act as a good collector drop is an open question left for a future study. Nevertheless, this study reshapes the conceptual notion of dust CCN activity to one where freshly emitted insoluble dust particles can have an appreciable

hygroscopicity (that depends on their surface-to-volume ratio) which can be augmented through atmospheric processing.

3.6   Acknowledgements

3.7   References

Asa-Awuku, A., Nenes, A., Gao, S., Flagan, R. C., and Seinfeld, J. H.: Water-soluble SOA from Alkene ozonolysis: composition and droplet activation kinetics inferences from analysis of CCN activity, Atmos. Chem. Phys., 10, 1585 - 1597, 2010, http://www.atmos-chem-phys.net/10/1585/2010/.

Brunauer, S., Emmett, P. H., and Teller, E.: Adsorption of gases in multimolecular layers, J. Am. Chem. Soc., 60(2), 309 - 319, 1938.

Chou, C., Formenti, P., Maille, M., Ausset, P., Helas, G., Harrison, M., and Osborne, S.: Size distribution, shape, and composition of mineral dust aerosols collected during the African Monsoon Multidisciplinary Analysis Special Observation Period 0: Dust and Biomass-Burning Experiment field campaign in Niger, January 2006, J. Geophys. Res., 113, D00C10, 2008.

Collins, W. D., Conant, W. C., and Ramanathan, V.: Earth radiation budget, clouds, and climate sensitivity. The chemistry of the atmosphere: Its impact on global change, edited by: J. G. Calvert, 207 - 215, Blackwell Scientific Publishers, Oxford, UK, 1994.

Coz, E., Gómez-Moreno, F. J., Pujadas, M., Casuccio, G. S., Lersch, T. L., and Artinano, B.: Individual particle characteristics of North African dust under different long-range transport scenarios, Atmos. Environ., 43, 1850 - 1863, 2009.

Davidovits P., Kolb, C. E., Williams, L. R., Jayne, J. T., and Worsnop, D. R.: Mass accommodation and chemical reactions at gas-liquid interfaces, Chem. Rev., 106(4), 1323 - 1354, 2006.

Davies, C. N.: Particle-fluid interaction, J. Aerosol Sci. 10,477 - 10,513, 1979. DeCarlo, P. F., Slowik, J. G., Worsnop, D. R., Davidovits, P., and Jimenez, J. L.: Particle morphology and density characterization by combined mobility and aerodynamic diameter measurements. Part 1: Theory, Aerosol Sci. Tech., 38, 1185 - 1205, 2004.

DeMott, P. J., Sassen, K., Poellot, M. R., Baumgardner, D., Rogers, D. C., Brooks, S. D., Prenni, A. J., and Kreidenweis, S. M.: African dust aerosols as atmospheric ice nuclei, Geophys. Res. Lett., 30(14), 1732, doi:10.1029/2003GL017410, 2003.

Endo, Y., Chen, D. -R., and Pui, D. Y. H.: Effects of particle polydispersity and shape factor during dust cake loading on air filters, Powder Technol., 98(3), 241 - 249, 1998.

Field, P. R., Möhler, O., Connolly, P., Krämer, M., Cotton, R., Heymsfield, A. J., Saathoff, H., and Schnaiter, M.: Some ice nucleation characteristics of Asian and Saharan desert dust, Atmos. Chem. Phys., 6, 2991 - 3006, 2006, http://www.atmos-chem-phys.net/6/2991/2006/.

Forster, P., Ramaswamy, V., Artaxo, P., Berntsen, T., Betts, R., Fahey, D. W., Haywood, J., Lean, J., Lowe, D. C., Myhre, G., Nganga, J., Prinn, R., Raga, G., Schulz, M., and Van Dorland, R.: Changes in Atmospheric Constituents and in Radiative Forcing, in: Climate Change 2007: The Physical Science Basis. Contribution of Working Group I to the Fourth Assessment Report of the Intergovernmental Panel on Climate Change, edited by: Solomon, S., Qin, D., Manning, M., Chen, Z., Marquis, M., Averyt, K. B., Tignor, M., and Miller, H. L., Cambridge University Press, Cambridge, UK, and New York, NY, USA, 129 - 234, 2007.

Fuchs, N. A.: The Mechanics of Aerosols, Dover Publications, Inc., New York, USA, 37 - 43, 1964.

Fukuta, N. and Walter, L. A.: Kinetics of hydrometer growth from the vapor; spherical model, J. Atmos. Sci., 27, 1160 - 1172, 1970.

Ganor, E., and Foner, H: The mineralogical and chemical properties and behavior of Aeolian Saharan dust over Israel, in The Impact of Desert Dust Across the Mediterranean, edited by S. Guerzoni and R. Chester, pp. 163 - 172, Springer, New York, 1996.

Ganor, E., and Mamane, Y.: Transport of Saharan dust across the eastern Mediterranean, Atmos. Environ., 16, 581 - 587, 1982.

Hatch, C. D., Gierlus, K. M., Schuttlefield, J. D., and Grassian, V. H.: Water adsorption and cloud condensation nuclei activity of calcite and calcite coated with model humic and fulvic acids, Atmos. Environ., 42, 5672 - 5684, 2008.

Herich, H., Tritscher, T., Wiacek, A., Gysel, M., Weingartner, E., Lohmann, U., Baltensperger, U., and Cziczo, D. J.: Water uptake of clay and desert dust aerosol particles at sub- and supersaturated water vapor conditions, Phys. Chem. Chem. Phys., 11, 7804 - 7809, doi:10.1039/b901585j, 2009.

Henson, B. F.: An adsorption model of insoluble particle activation: Application to black carbon, J. Geophys. Res., 112, D24S16, doi:10.1029/2007JD008549, 2007.

Hinds, W. C.: Aerosol Technology, John Wiley & Sons, Inc., New York, USA, 1999.

Hudson, P., Gibson, E. R., Young, M. A., Kleiber, P. D., and Grassian, V. H.: Coupled infrared extinction and size distribution measurements for several clay components of mineral dust aerosol, J. Geophys. Res., 113, D01201, doi:10.1029/2007JD008791, 2008.

Jeong, G. R., and Sokolik, I. N.: The effect of mineral dust aerosols on the photolysis rates in the clean and polluted marine environments. J. Geophys. Res., 112, D21308, doi:10.1029/2007JD008442, 2007.

Kandler, K., Schütz, L., Deutscher, C., Ebert, M., Hofmann, H., Jäckel, S., Jaenicke, R., Knippertz, P., Lieke, M., Massling, A., Petzold, A., Schladitz, A., Weinzierl, B., Wiedensohler, A., Zorn, S., and Weinbruch, S.: Size distribution, mass concentration, chemical and mineralogical composition and derived optical parameters of the boundary layer aerosol at Tinfou, Morocco, during SAMUM 2006, Tellus , 61B, 32 - 50, doi:10.1111/j.1600-0889.2008.00385.x, 2009.

Kalashnikova, O. V., and Sokolik, I. N.: Modeling the radiative properties of nonspherical soil-derived mineral aerosols, J. Quant. Specrtrocs. Radiat. Transfer, 87(2), 137 - 166, 2004.

Koehler, K. A., Kreidenweis, S. M., DeMott, P. J., Petters, M. D., Prenni, A. J., and Carrico, C. M.: Hygroscopicity and cloud droplet activation of mineral dust aerosol, Geophys. Res. Lett., 36, L08805, doi:10.1029/2009GL037348, 2009.

Köhler, H., The nucleus in and the growth of hygroscopic droplets, Trans. Faraday Soc., 32(2), 1152 - 1161, 1936.

Kumar, P., Sokolik, I. N., and Nenes, A.: Parameterization of cloud droplet formation for global and regional models: including adsorption activation from insoluble CCN, Atmos. Chem. Phys., 9, 2517 - 2532, 2009a, http://www.atmos-chem-phys.net/9/2517/2009/.

Kumar, P., Nenes, A., and Sokolik, I. N.: Importance of adsorption for CCN activity and hygroscopic properties of mineral dust aerosol, Geophys. Res. Lett., 36, L24804, doi:10.1029/2009GL040827, 2009b.

Kuwata, M., and Kondo, Y.: Measurements of particle masses of inorganic salt particles for calibration of cloud condensation nuclei counters, Atmos. Chem. Phys., 9, 5921 - 5932, 2009, http://www.atmos-chem-phys.net/9/5921/2009/.

Lafon, S., Sokolik, I. N., Rajot, J. L., Caquineau, S., and Gaudichet, A.: Characterization of iron oxides in mineral dust aerosols: Implications to light absorption. J. Geophys. Res., 111, D21207, doi:10.1029/2005JD007016, 2006.

Lance, S., Medina, J., Smith, J. N., and Nenes, A.: Mapping the operation of the DMT continuous flow CCN counter, Aerosol Sci. Tech., 40, 242 - 254, 2006.

Lance, S., Nenes, A., and Rissman, T.: Chemical and dynamical effects on cloud droplet number: Implications for estimates of the aerosol indirect effect., J. Geophys. Res., 109, D22208, doi:10.1029/2004JD004596, 2004.

Leith, D.: Drag on nonspherical objects, Aerosol Sci. Tech., 6, 153 - 161, 1987.

Levin, Z., Ganor, E., and Gladstein, V.: The effects of dust particles coated with sulfate on rain formation in the Eastern Mediterranean, J. Appl. Meteorol., 35, 1511 - 1523, 1996.

Möhler, O., Benz, S., Saathoff, H., Schnaiter, M., Wagner, R., Schneider, J., Walter, S., Ebert, V., and Wagner, S.: The effect of organic coating on the heterogeneous ice nucleation efficiency of mineral dust aerosols, Environ. Res. Lett., 3, 2008.

Moore, R., Nenes, A., and Medina, J.: Scanning Mobility CCN Analysis - A method for fast measurements of size resolved CCN distributions and activation kinetics, Aerosol Sci. Tech., 44, 861 - 871, 2010.

Nenes, A., Charlson, R. J., Facchini, M. C., Kulmala, M., Laaksonen, A., and Seinfeld, J. H.: Can chemical effects on cloud droplet number rival the first indirect effect?, Geophys. Res. Lett., 29 (17), 1848, doi: 10.1029/2002GL015295, 2002.

Nenes, A., Ghan, S. J., Abdul-Razzak, H., Chuang, P. Y., and Seinfeld, J. H.: Kinetic limitations on cloud droplet formation and impact on cloud albedo, Tellus, 53B, 133 - 149, 2001.

Okada, K., Heintzenberg, J., Kai, K., and Qin Y.: Shape of atmospheric mineral particles collected in three Chinese arid-regions, Geophys. Res. Lett., 28(16), 3123 - 3126, doi:10.1029/2000GL012798, 2001.

Padró, L.T., Tkacik, D., Lathem, T., Hennigan, C., Sullivan, A. P., Weber, R. J., Huey, L. G., and Nenes, A.: Investigation of CCN relevant properties and droplet growth kinetics of water-soluble aerosol fraction in Mexico City, J. Geophys. Res, 115, D09204, doi:10.1029/2009JD013195, 2010.

Petters, M. D., and Kreidenweis, S. M.: A single parameter representation of hygroscopic growth and cloud condensation nucleus activity, Atmos. Chem. Phys., 7, 1961 - 1971, 2007, http://www.atmos-chem-phys.net/7/1961/2007/.

Petters, M. D., Prenni, A. J., Kreidenweis, S. M., and DeMott, P. J.: On measuring the critical diameter of cloud condensation nuclei using mobility selected aerosol, Aerosol Sci.Tech., 41, 907 - 913, 2007.

Pitzer, K. S., and Mayorga, G.: Thermodynamics of electrolytes. II. Activity and osmotic coefficients for strong electrolytes with one or both ions univalent, J. Phys. Chem., 77(19), 2300 - 2308, 1973.

Prospero, J. M.: Long-range transport of mineral dust in the global atmosphere: Impact of African dust on the environment of the southeastern United States, Proc. Natl. Acad. Sci. USA, 96, 3396 - 3403, 1999.

Pruppacher, H. R., and Klett, J. D.: Microphysics of clouds and precipitation 2nd ed., Kluwer Academic Publishers, Boston, MA, 1997.

Roberts, G., and Nenes, A.: A continuous-flow streamwise thermal gradient CCN chamber for atmospheric measurements, Aerosol Sci. Tech., 39, 206 - 221, 2005.

Romakkaniemi, S., Hämeri, K., Väkevä, M., and Laaksonen, A.: Adsorption of water on 8-15 nm NaCl and $(NH_4)_2SO_4$ aerosols measured using an ultrafine tandem differential mobility analyzer, J. Phys. Chem. A, 105, 8183 - 8188, 2001.

Rose, D., Gunthe, S. S., Mikhailov, E., Frank, G. P., Dusek, U., Andreae, M., and Pöschl, U.: Calibration and measurement uncertainties of a continuous-flow cloud condensation nuclei counter (DMT-CCNC): CCN activation of ammonium sulfate and sodium chloride aerosol particles in theory and experiment, Atmos. Chem. Phys., 8, 1153 - 1179, 2008, http://www.atmos-chem-phys.net/8/1153/2008/.

Rosenfeld, D., Rudich, Y., and Lahav, R.: Desert dust suppressing precipitation: A possible desertification feedback loop, Proc. Natl. Acad. Sci. U.S.A., 98(11), 5975 - 5980, 2001.

Schuttlefield, J. D., Cox, D., and Grassian, V. H.: An investigation of water uptake on clays minerals using ATR-FTIR spectroscopy coupled with quartz crystal microbalance measurements, J. Geophys. Res., 112, D21303, doi:10.1029/2007JD008973, 2007.

Seisel, S., Pashkova, A., Lian, Y., and Zellner, R.: Water uptake on mineral dust and soot: A fundamental view of hydrophilicity of atmospheric particles?, Faraday Discuss., 130, 437 - 451, 2005.

Seinfeld, J. H., and Pandis, S. N.: Atmospheric Chemistry and Physics, John Wiley, New York, USA, 767 - 773, 2006.

Sokolik, I. N., Winker, D. M., Bergametti, G., Gillette, D. A., Carmichael, G., Kaufman, Y. J., Gomes, L., Schuetz, L., and Penner, J. E.: Introduction to special section: Outstanding problems in quantifying the radiative impacts of mineral dust, J. Geophys. Res., 106(D16), 18,015 - 18,027, 2001.

Sorjamaa, R. and Laaksonen, A.: The effect of H_2O adsorption on cloud drop activation of insoluble particles: a theoretical framework, Atmos. Chem. Phys., 7, 6175 - 6180, 2007, http://www.atmos-chem-phys.net/9/6175/2007/.

Sullivan, R. C., Moore, M. J. K., Petters, M. D., Kreidenweis, S. M., Roberts, G. C., and Prather, K. A.: Effect of chemical mixing state on the hygroscopicity and cloud nucleation properties of calcium mineral dust particles, Atmos. Chem. Phys., 9, 3303 - 3316, 2009, http://www.atmos-chem-phys.net/9/3303/2009/.

Sullivan, R. C., Moore, M. J. K., Petters, M. D., Kreidenweis, S. M., Qafoku, O., Laskin, A., Roberts, G. C., and Prather, K. A.: Impact of particle generation method on the apparent hygroscopicity of insoluble mineral particles, Aerosol Sci. Tech., 44, 10, 830 - 846, 2010.

Twohy, C. H., Kreidenweis, S. M., Eidhammer, T., Browell, E. V., Heymsfield, A. J., Bansemer, A. R., Anderson, B. E., Chen, G., Ismail, S., DeMott, P. J., and Van Den Heever, S. C.: Saharan dust particles nucleate droplets in eastern Atlantic clouds, Geophys. Res. Lett., 36, L01807, 1 - 6, doi:10.1029/2008GL035846, 2009.

Twomey, S.: Pollution and the planetary albedo, Atmos. Environ., 8, 1251 - 1256, 1974.

Wiegner, M., Gasteiger, J., Kandler, K., Weinzierl, B., Rasp, K., Esselborn, M., Freudenthaler, V., Heese, B., Toledano, C., Tesche, M., and Althausen, D.: Numerical simulations of optical properties of Saharan dust aerosols with emphasis on linear depolarization ratio, Tellus, 61B, 180 - 194, 2009.

Willeke, K., and Baron, P. A.: Aerosol Measurement: Principles, Techniques, and Applications. (2nd ed.). New York: John Wiley & Sons, Inc., 2001.

Young, G. J.: Interaction of water vapor with silica surfaces, J. Colloid Sci., 13(1), 67 - 85, 1958.

CHAPTER 4

MEASUREMENTS OF CLOUD CONDENSATION NUCLEI ACTIVITY AND DROPLET ACTIVATION KINETICS OF WET PROCESSED REGIONAL DUST SAMPLES AND MINERALS

4.1   Abstract

This study reports laboratory measurements of particle size distributions, cloud condensation nuclei (CCN) activity, and droplet activation kinetics of wet generated aerosols from clays, calcite, quartz, and desert soil samples from Northern Africa, East Asia/China, and Northern America. The dependence of critical supersaturation, s_c, on particle dry diameter, D_{dry}, is used to characterize particle-water interactions and assess the ability of Frenkel-Halsey-Hill adsorption activation theory (FHH-AT) and Köhler theory (KT) to describe the CCN activity of the considered samples. Regional dust samples produce unimodal size distributions with particle sizes as small as 40 nm, CCN activation consistent with KT, and exhibit hygroscopicity similar to inorganic salts. Clays and minerals produce a bimodal size distribution; the CCN activity of the smaller mode is consistent with KT, while the larger mode is less hydrophilic, follows activation by FHH-AT, and displays almost identical CCN activity to dry generated dust. Ion Chromatography (IC) analysis performed on regional dust samples indicates a soluble fraction that cannot explain the CCN activity of dry or wet generated dust. A mass balance and hygroscopicity closure suggests that the small amount of ions (of low solubility compounds like calcite) present in the dry dust dissolve in the aqueous

suspension during the wet generation process and give rise to the observed small hygroscopic mode. Overall these results identify an artifact that may question the atmospheric relevance of dust CCN activity studies using the wet generation method.

Based on a threshold droplet growth analysis, wet generated mineral aerosols display similar activation kinetics compared to ammonium sulfate calibration aerosol. Finally, a unified CCN activity framework that accounts for concurrent effects of solute and adsorption is developed to describe the CCN activity of aged or hygroscopic dusts.

Citation: Kumar, P., Sokolik, I. N., and Nenes, A.: Measurements of cloud condensation nuclei activity and droplet activation kinetics of wet processed regional dust samples and minerals, Atmos. Chem. Phys. Discuss., 2011 (submitted).

4.2   Introduction

The ability of aerosols to act as cloud condensation nuclei (CCN) can be characterized based on their size, chemical composition, and the level of water vapor supersaturation in ambient clouds. The mineral aerosol (or dust) has been recognized as an important atmospheric specie because of its ability to act as CCN, giant CCN (GCCN) (e.g., Rosenfeld et al., 2001; Levin and Cotton, 2008), or ice nuclei (IN) (e.g., DeMott et al., 2003; Field et al., 2006). Despite its well recognized importance, mineral aerosol poses a challenge in atmospheric models due to its compositional complexity, non-sphericity and atmospheric lifetime leading to poorly quantified dust-cloud interactions.

Mineral aerosol originates mainly from arid and semi-arid desert regions of the world (e.g., Sahara, Taklamakan, and Gobi) and consists of clays (e.g., kaolinite, illite,

and montmorillonite), carbonates (e.g., calcite, dolomite), iron oxides (e.g., hematite, goethite) and quartz (Lafon et al., 2006). Dust particles are often transported over long distances downwind from their source regions. During their transport, dust particles undergo atmospheric processing to form soluble species (like sulfates) on the dust surface (e.g., Levin et al., 1996) that have important impacts on dust CCN activity (Kelly et al., 2007).

Two classes of theory have been proposed to describe the CCN activity of mineral aerosol: Köhler theory (KT) (Köhler, 1936), where hygroscopicity is driven by the amount of solute in the dust, and, by more recent FHH (Frenkel, Halsey, and Hill) adsorption activation theory (AT) (Sorjamaa and Laaksonen, 2007; Kumar et al., 2009a,b) that explicitly considers the effect of water vapor adsorption on the dust surface. Almost all published experimental studies on CCN activity of fresh dust (e.g., Koehler et al., 2009; Herich et al., 2009) parameterize laboratory observations using the KT framework on the assumption that dust CCN activity is controlled solely by the amount of soluble salts in the mineral aerosol, with the insoluble fraction not affecting water activity. However, studies that measured soluble ions composition on dust samples collected from various dust source regions (e.g., Song et al., 2004; Radhi et al., 2010) indicated negligible amounts of soluble salts. In a recent study, Kumar et al. (2010) compared the power law exponent derived from the experimental s_c-D_{dry} relationship with those determined from FHH-AT and KT, and suggested that FHH-AT is a better representation than KT for CCN activity of dry generated dust devoid of a soluble fraction. However, Kumar et al. (2009a) found that KT applies for dusts with a considerable salt fraction such as those generated from dry lakebed mixed with salts (e.g.,

Owens Lake; Koehler et al., 2009) or mineral dust exposed to considerable cloud processing or aging (Levin et al., 1996). Based on this, Kumar et al. (2009a) suggested combining KT and FHH-AT to comprehensively describe CCN activity of mineral aerosol (with droplet nucleation occurring via both adsorption and solute effects) throughout its atmospheric lifetime. To account for adsorption activation CCN in atmospheric models, Kumar et al. (2009b) developed a cloud droplet formation parameterization where the CCN constitutes an external mixture of soluble aerosol (that follow KT) and insoluble aerosol (that follow FHH-AT).

Recent laboratory measurements of CCN activity of dust and calcium minerals (Hatch et al., 2008; Koehler et al., 2009; Herich et al., 2009; Sullivan et al., 2009), subsaturated hygroscopicity measurements (Gustafsson et al., 2005; Vlasenko et al., 2005; Herich et al., 2009), size distributions and chemical reactivity (Hudson et al., 2008; Gibson et al., 2006), and ice cloud particle nucleation (e.g., Koehler et al., 2009) have utilized the well-established technique of generating aerosol via atomization from an aqueous dust suspension. Recently, Sullivan et al. (2010), however, suggested that wet atomization of calcium minerals with considerably low solubility in water (typical of mineral aerosol composition) can induce artifacts in the dust properties to the point where they may not represent dust aerosols in the atmosphere. This has not been explored for atmospheric dusts and minerals or clays.

In this study, CCN activity and droplet activation kinetics measurements of regional dust and mineral aerosol generated by wet atomization technique are performed to quantify biases introduced in the observed CCN activity and physical properties of dusts, and selected minerals and clays. Contribution of the soluble salts present in fresh

dust samples to dust CCN activity is also investigated. The results obtained here are then compared against properties of fresh dust dry generated by a soft-saltation technique (Kumar et al., 2010). The effect of wetting dust and mineral samples in aqueous solution to generate aerosol and its implication to particles number size distributions, CCN activation, and droplet activation kinetics is provided in sections 4.5.1, 4.5.2, and 4.5.3, respectively. The contribution of soluble salts to dust CCN activity is also evaluated in section 4.5.4. Finally, section 4.6 discusses implications for dust-warm cloud interactions and presents a new CCN activity framework that combines both solute and water vapor adsorption effects for dust-cloud interactions. The conclusions and summary of this work is presented in section 4.7.

4.3   Experimental Methods

4.3.1   Regional Dust Samples and Individual Minerals

Aerosols from regional soil samples and individual minerals/clays were generated and characterized in this study. Niger soil collected from the Sahel source region ($13^o31'$N, $2°38'$E) was used as representative of African dust. Asian soil samples were collected from five different East Asia (China) desert locations (Soil 1, eastern edge of the Hexi corridor; Soil 2, south-eastern edge of the Tengger Desert; Soil 3, central Tengger Desert; Soil 4, south-eastern edge of the Taklamakan Desert; Soil 5, southern edge of the Hunshandake Desert). Commercially available Arizona Test Dust was also used in measurements. Analyzed individual minerals included several clays (kaolinite, illite, and montmorillonite) and calcite. These minerals were aerosolized as purchased, with no subsequent treatment prior to atomization.

4.3.2 *Measurements of CCN Activity and Droplet Activation Kinetics*

The laboratory setup employed to characterize the CCN activity and droplet activation kinetics of the regional dust samples is described in detail by Kumar et al. (2010) and Padró et al. (2010) and briefly summarized here. Aerosol is generated by atomization of a dust-water suspension containing 2.0 ± 0.4 gram of regional dust (mineral/clay) in 100 ml of high purity DI (18 q-grade) water. The atomized droplets are then dried by passing through two silica gel diffusion dryers that maintain a relative humidity less than 5%. The resulting polydisperse dry aerosol is then passed through a 1 μm impactor and a series of Kr-85 bipolar chargers to achieve an equilibrium charge distribution. The aerosol is then sent to a Differential Mobility Analyzer (DMA, TSI Model 3081) that classifies and size-selects the aerosol based on their electrical mobility. The aerosol sample flow rate of $1.0 \, l \, min^{-1}$ is used with a sheath flow rate of $5 \, l \, min^{-1}$ to select particle sizes up to 500 nm in electrical mobility diameter. The classified aerosol is then mixed with filtered air before being split into two streams. One stream is sent to a Condensation Particle Counter (CPC, TSI Model 2010) that measures Condensation Nuclei (CN) concentration. The second stream is sent to a Droplet Measurement Technology (DMT) Continuous Flow Streamwise Thermal Gradient Chamber (CFSTGC; Roberts and Nenes, 2005; Lance et al., 2006) to measure the fraction of aerosol that act as a CCN for supersaturations ranging between 0.2% and 1.0%. The CCN instrument supersaturation was calibrated with $(NH_4)_2SO_4$ aerosol using the procedure described by Kumar et al. (2010).

CCN activation curves, aerosol size distribution and droplet size distributions are obtained using Scanning Mobility CCN Analysis (SMCA) (Moore et al., 2010). SMCA

relies on the principle of continuously scanning DMA voltage over time to determine particle size based on electrical mobility. During SMCA, the supersaturation in the CFSTGC is maintained constant (between 0.2% and 1.0%) with aerosol flow rate set to $0.5 \, \mathrm{l \, min^{-1}}$ and sheath-to-aerosol ratio of 10:1.

CCN activity is expressed in terms of minimum dry diameter, D_{dry} of particles that activate into cloud droplets at a critical supersaturation, s_c. D_{dry} is determined by fitting a sigmoid curve to the experimentally determined CCN to CN concentration ratio with respect to dry particle diameter. Dry critical diameter, D_{dry} is then the diameter for which 50% of the particles activate at s_c equal to the instrument supersaturation. The contribution from larger multiple charged particles (in this study, up to +3) are accounted for using the approach of Moore et al. (2010).

Droplet activation kinetics for dust CCN is also inferred using SMCA. This is done by comparing the droplet size, D_w, at the optical particle counter (OPC) of CFSTGC for particles generated from regional dusts with that from calibration $(NH_4)_2SO_4$ aerosol with s_c equal to instrument supersaturation. The calibration is used as a standard of activation kinetics. If D_w is lower than the calibration, the dust may be subject to kinetic retardations. This technique is called "Threshold Droplet Activation Kinetics (TDGA)", and has been successfully used in a number of in-situ and laboratory studies (Bougiatioti et al. 2009; Padró et al., 2010, Kumar et al., 2010). As the comparison is made against $(NH_4)_2SO_4$ aerosol that activates according to KT, uncertainty is introduced in the determination of activation kinetics by TDGA, (owing to the difference in critical wet diameter between KT and FHH-AT particles). However, if retarded activation kinetics suggested by TDGA is not due to differences in activation physics, a computational fluid

dynamics model of the CCN instrument (Kumar et al., 2010) can be used to comprehensively simulate the growth of CCN and appropriately account for size shifts from differences in KT and FHH-AT. Any residual droplet size difference can be attributed to delayed activation kinetics and parameterized as changes in the water vapor uptake coefficient, α_c.

4.3.3 Soluble Ions Measurements

4.3.3.1 Particle Sample Collection

A 12 stage Micro Orifice Uniform Deposition Impactor (MOUDI, Model 110, MSP Corp.) was used to collect dry generated and size-resolved particles to determine their soluble fraction. The stage cuts of MOUDI are 18.0, 10.0, 5.6, 3.2, 1.8, 1.0, 0.56, 0.32, 0.18, 0.1, and 0.056 μm aerodynamic diameter, plus an after filter (< 0.056 μm). The flowrate of the MOUDI is set to 30 l min^{-1}. The collection substrates used in the first 11 stages include 47 mm Aluminium foil disks (0.001″, regular strength Reynolds wrap). A thin layer of Heavy-Duty Silicone Spray (MSP corp.) is applied to the foil substrates to minimize particle bounce. The substrates were weighed before and after the sampling using weighing scale (OHAUS Corp., AR0640) to determine the mass of dust deposited at each impactor stage. To ensure sufficient mass for composition measurements, sample collection is done for several hours, and grouping of substrates was performed. Stages corresponding to aerodynamic diameters greater than 1.0 μm were grouped and will be referred to as coarse mode. Aerosol particles collected at stages with aerodynamic diameters equal to and less than 1.0 μm will be referred to as fine mode.

The dry aerosol collected in the MOUDI was generated following Kumar et al. (2010). Approximately 10 - 15 grams of the desired sample was introduced in the 1000

94

ml sealed Erlenmeyer flask attached to a Burrell-Wrist Action Shaker (Model 75). Compressed filtered air is introduced into the flask that generates polydisperse fine aerosols by mechanical disintegration (saltation) with a distribution that resembles the natural size distributions of dust particles generated in source regions (Lafon et al., 2006).

4.3.3.2 Ion Chromatography Analysis

After particle collection, the substrates were placed in a Nalgene HDPE bottle with 20 - 24 ml of 18 q-grade deionized (DI) water for extraction. Each bottle was sonicated and heated in a water bath (at ~ 60°C, Padró et al., 2010) for 75 minutes. The solution was then allowed to cool for 3 hours and filtered through a 0.45 μm pore syringe filter to remove the insoluble particles suspended in solution.

The concentration of major ions in the filtered extract solution was measured with Ion Chromatography (IC, Dionex Model DX500). The IC used in this study has two channels allowing concurrent measurements of anions and cations. Anions were measured using an AS11 column, an ASRS ultra-suppressor, and a gradient elute of sodium hydroxide. Cations were determined using a CS12 column and CSRS ultra-suppressor and methanesulfonate acid eluent. Anions measured included acetate ($C_2H_3O_2^-$), chloride (Cl^-), formate ($HCOO^-$), nitrate (NO_3^-), nitrite (NO_2^-), oxalate ($C_2O_4^{2-}$) and sulfate (SO_4^{2-}). The cations measured were ammonium (NH_4^+), calcium (Ca^{2+}), potassium (K^+) and sodium (Na^+). The ion concentrations obtained from IC measurements were then used as input for the ISORROPIA-II thermodynamic equilibrium model (Fountoukis and Nenes, 2007) to predict the mixture of inorganic salts present in the samples.

4.4　Experimental Analysis

To describe the CCN activity of dust particles, two phenomena must be accounted for: *i*) the effect of adsorption of water vapor on the insoluble dust particles represented by the adsorption activation theory (AT) (Kumar et al., 2009a,b), and, *ii*) the effect of solute (which may be present in freshly emitted dust or formed during atmospheric aging) represented by the Raoult effect in Köhler Theory (KT) (Köhler, 1936).

4.4.1　*Adsorption Activation Theory (AT)*

The AT used here is developed with the multilayer FHH adsorption isotherm model (Sorjamaa and Laaksonen, 2007; Kumar et al., 2009a,b) and contains two adjustable parameters (A_{FHH} and B_{FHH}) that describe the contribution of water vapor adsorption on CCN activity. A_{FHH}, B_{FHH} are determined by least squares fitting of the observed s_c, D_{dry} to the maxima of the FHH-AT water vapor equilibrium curves (Sorjamaa and Laaksonen, 2007; Kumar et al., 2009b)

$$s = \frac{4\sigma_w M_w}{RT\rho_w D_p} - A_{FHH}\left(\frac{D_p - D_{dry}}{2D_{H_2O}}\right)^{-B_{FHH}} \qquad [4.1]$$

where s is the supersaturation, D_{dry} is the dry CCN diameter, D_{H_2O} is the diameter of water molecule (equal to 2.75 Å, Kumar et al., 2009b), D_p is the droplet diameter, σ_w is the CCN surface tension at the point of activation (Pruppacher and Klett, 1997), ρ_w is the water density, M_w is the molar mass of water, R is the universal gas constant, and T is the average column temperature. The value of B_{FHH} is a measure of the particle hydrophilicity with lower B_{FHH} values corresponding to a more hydrophilic particle. As B_{FHH} increases, particles become less hydrophilic and resemble insoluble (but wettable) particles that follow the Kelvin equation (Kumar et al., 2010). Kumar et al. (2010) found

that the CCN activity of dry generated aerosols from regional dust samples considered in this work, are well described by FHH-AT with $A_{FHH} = 2.25 \pm 0.75$ and $B_{FHH} = 1.20 \pm 0.10$.

4.4.2 κ-Köhler Theory (κ-KT)

The CCN activity of an aerosol particle with appreciable amounts of solute can be described using Köhler theory (KT). In this study, solute effects are parameterized using the hygroscopicity parameter, κ, approach (Petters and Kreidenweis, 2007) that collectively accounts for the density, molar mass, and dissociation effects of solute on water activity (the Raoult term in the Köhler equation). The κ can be used to directly compare the hygroscopicity of aerosol over a wide range of composition, with $\kappa \to 0$ for completely insoluble material to $\kappa \to 1.4$ for NaCl (the most hygroscopic of atmospheric aerosol species).

When $\kappa > 0.2$, κ can be obtained from s_c-D_{dry} pairs given by the following approximate expression

$$\kappa = \frac{4A^3}{27D_{dry}^3 s_c^2} \qquad [4.2]$$

where $A = \dfrac{4\sigma_w M_w}{\rho_w RT}$, s_c is the instrument supersaturation, and D_{dry} is the minimum dry particle activation diameter at s_c. Lower values of κ (e.g., $\kappa < 0.05$) that are more relevant to the dust s_c-D_{dry} experimental relationships are calculated from the numerical solution of

$$s = \frac{4\sigma_w M_w}{RT\rho_w D_p} - \frac{D_{dry}^3 \kappa}{D_p^3 - D_{dry}^3(1-\kappa)} \qquad [4.3]$$

All studies on dust CCN activation, with the exception of Kumar et al. (2010), have parameterized dust CCN activity using the κ-KT approach, implicitly assuming that CCN activity of dust is governed by its small soluble fraction.

4.5 Results and Discussion

4.5.1 Size Distributions

Figure 4.1a compares the particle number size distribution of aerosols generated from the Niger dust sample (brown squares) and Soil 2 (blue circles). Size distributions were generated using either the dry soft-saltation method (open symbols) described in Kumar et al. (2010) or the wet atomization method (solid symbols). While both generation methods produce particles with a unimodal size distribution (Fig. 4.1a), the sizes of particles are significantly different. For instance, wet generated Niger dust (brown curve) has a mean diameter of ~ 40 nm while dry generated dust peaks at ~ 450 nm. Similar differences are observed for Soil 2 (blue curve) where median diameters are 41 nm and 400 for wet and dry generated dust, respectively. This demonstrates that particles generated via wet atomization technique can be up to ten times smaller than those generated by the dry saltation technique.

In the case of ATD, the wet atomization method generated a bimodal dry size distribution (Fig. 4.1b) with a dominant first peak centered at a modal diameter of ~ 35 nm, and a second peak with reduced number concentration centered at a modal diameter ~ 240 nm. For comparison, the number size distribution for ATD generated by the dry technique (Fig. 4.1b) produces a peak centered at ~ 340 nm. This suggests that the second observed peak in the wet generation method could be primarily dust particles internally mixed with material from the first hygroscopic peak. Similar behavior was also observed

for kaolinite particles (Fig. 4.1b). Dry and wet generated size distributions are provided as inset in Fig. 4.1b; bimodal distribution with peaks at ~ 34 nm and ~ 300 nm are seen. For dry generated kaolinite aerosol, however, a unimodal distribution is observed with a peak centered at ~ 500 nm. A similar behavior in terms of the bimodal distribution with the dominant smaller peak and minor bigger peak was observed by Sullivan et al. (2010) for the Solvay calcite system.

Like in the case of ATD and kaolinite, a bimodal size distribution is observed for wet generated illite and $CaCO_3$ particles (Fig. 4.1c). However, the relative strength of both modes is reversed, with the peak at ~ 37 nm diameter being less prominent than that observed at ~ 160 nm. Similarly for wet generated $CaCO_3$ aerosol (solid blue circle), the minor and major peaks were centered at ~ 33 nm and ~ 200 nm, respectively. Dry generated illite (open brown) and $CaCO_3$ (open blue) aerosols exhibit a unimodal size distribution with a mean diameter ~ 460 nm and ~ 250 nm, respectively.

Most commonly found clay minerals in regional dust samples are kaolinite, illite, and montmorillonite (Usher et al., 2003). Depending on the aluminosilicate layer-layer interactions (charge-countering cations, van der Waals forces, or hydrogen bonds), clays can be classified as swelling or non-swelling (Farmer, 1974). Illite and kaolinite are non-swelling clays because of strong inter-ionic and hydrogen bond interactions that prevent expansion in the presence of water. In contrast, montmorillonite can contain unbounded Na^+ and Ca^+ ions that can hydrate in the presence of water and make clays swell. The differences in interactions of water with the internal clay structure may lead to large changes in the particle size distributions for montmorillonite clay (Na-rich and Ca-rich) generated via the wet atomization and dry soft-saltation techniques (Fig. 4.1d). It can be

also inferred that swelling (montmorillonite) and non-swelling (illite and kaolinite) clays produce the systems with different particle-water interactions in aqueous solutions. This difference in water interaction is also consistent with previous studies on hygroscopicity measurements where water uptake ability of montmorillonite was found to be similar to that of the zeolite sample that contains internal pores for water adsorption (Schuttlefield et al., 2007). Observed differences in water interactions also manifest as differences in CCN activity between swelling and non-swelling clays (shown in Sect. 4.5.2.2).
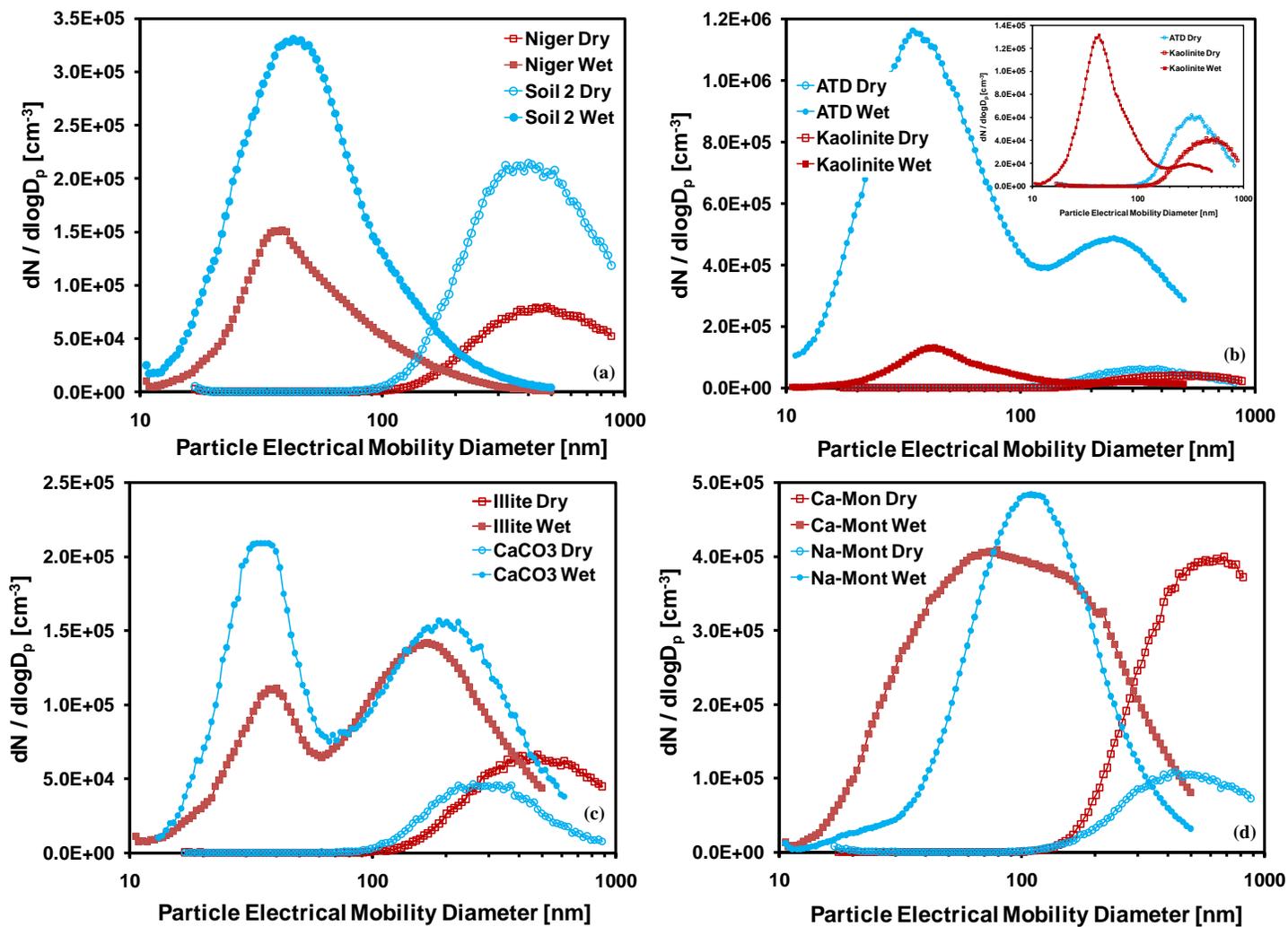
Figure 4.1: Particle number size distribution measured by the SMPS system via dry generated and wet generated techniques for **(a)** Niger Soil and East Asian Soil 2, **(b)** ATD and Kaolinite, **(c)** Illite and $CaCO_3$ and **(d)** Montmorillonite (Na-rich and Ca-rich).

101

4.5.2 CCN Activation Results

4.5.2.1 Regional Dust Samples

The dust CCN activity (s_c versus D_{dry}) measured for wet generated dust aerosol is presented in Fig. 4.2. The KT fits to the experimental data are shown with solid lines. For comparison, the CCN activation curves for dry generated dust (open symbols) are also shown with their corresponding FHH-AT fits. It is evident that the wet generated particles were significantly more CCN active than those generated from the dry soft-saltation technique. For all wet samples, κ ranges between 0.15 - 0.61, which is considerably higher than the equivalent κ (= 0.05) for dry generated dust (Kumar et al., 2010). Increased hygroscopicity after wetting is consistent with previous studies on dust-CCN activity that used similar wet generation techniques (e.g., Koehler et al., 2009; Herich et al., 2009).

It can be seen that within experimental uncertainty, x_{exp} for all dust types (with the exception of ATD) is about -1.5. This suggests that KT provides a good framework for representing CCN activity in this case. The hygroscopicity parameter, κ, for Niger, Asian and ATD samples were found to be slightly below that of $(NH_4)_2SO_4$ ($\kappa = 0.61$). In the case of ATD, a bimodal size distribution was obtained (Fig. 4.1b). While performing CCN activation measurements on wet generated ATD aerosol, almost all particles of the second peak activated (with an activation fraction ~ 1.0). Therefore, in this analysis we fit a sigmoid curve to the experimental points of activation fraction generated from the dominant first mode. Results indicated that the CCN activity of wet generated ATD can be parameterized with $\kappa = 0.40$ (compared to $\kappa < 0.05$ for dry generated ATD). As x_{exp} is expected to range between -0.8 (corresponding to FHH-AT) and -1.5 (corresponding to

KT), the unusual x_{exp} (equal to -2.15) for ATD can be a consequence of sparingly soluble species such as $CaSO_4$ (Padró and Nenes, 2007), a strong size-dependant composition or activation physics (AT vs. KT).

Kumar et al. (2009a, 2010) showed that the value of x_{exp} can be used to infer the mechanism that dominates particle-water interaction (i.e., adsorption or solute). $x_{exp} \sim$ -1.5 indicates that the solute effect dominates (hence KT applies), while x_{exp} between -0.8 and -1.2 indicates the dominance of the water vapor adsorption effect (hence FHH-AT applies). When this is applied to the wet generated data, it is seen from Table 4.1 that x_{exp} differs significantly from those determined by dry generation (Kumar et al., 2010). For almost all wet generated regional dust aerosols, x_{exp} is $\sim$ -1.5 (with the exception of ATD; Table 4.1), while a much lower $x_{exp} \sim -(0.9 \pm 0.2)$ was observed for dry generated dust aerosol. Thus FHH-AT describes fresh dry dust-CCN activation, while KT describes wet generated dust CCN activity. An $x_{exp} \sim$ -1.5 and $\kappa \sim 0.4$ correspond to an aerosol mostly composed of soluble salt. The IC analysis, however, shows negligible amounts of soluble salts present in the dust (Section 4.5.4). This, together with the very small size of the particles generated confirms that the process of wet generation for mineral aerosol leads to particles that do not resemble the dust suspended in the atomizer (likely composed of soluble salts leached off the original dust), hence the measured physical and chemical properties are likely subject to significant artifacts. A possible explanation for differences in activation mechanisms between dry and wet generated dust is provided in section 4.5.4.

4.5.2.2 Individual Minerals and ATD Samples

The CCN activation curves for wet generated illite, ATD, kaolinite and montmorillonite aerosols are shown in Fig. 4.3. Two sets of CCN activation data were obtained for illite and calcite, reflecting the size-dependent change in composition confirmed by the presence of bimodal size distribution (Fig. 4.1c) and double activation curve (Fig. 4.3a). A similar behavior was observed for kaolinite and ATD (activation curves shown in Fig. 4.3b). However for kaolinite and ATD, the CCN data (s_c-D_{dry} relationships) could only be determined from the dominant first peak. This is because for kaolinite, too few particles were generated in the minor second peak, while for ATD, almost all particles of the second peak activated with an activation fraction of ~ 1.0. For swelling montmorillonite clays (both Na-rich and Ca-rich), only one set of activation data points was obtained as a unimodal size distribution (Fig. 4.1d) that produced broad activation curves (Fig. 4.3c). This is consistent with the broad size distributions obtained for wet generated montmorillonite aerosol (Fig. 4.1d).

Figure 4.4 presents the CCN activity for wet generated calcite and clays considered in this study (solid and open squares). For comparison, the CCN activity for dry generated minerals (open triangles) is also shown. For samples with evident multi-modal activation, the most hygroscopic mode can readily be parameterized by κ-KT, while the second peak is well parameterized by FHH-AT and is in agreement with the CCN activity of dry generated species. This suggests that the particles generated in the second peak of wet distributions may be closer to the dry generated aerosol as discussed below. The intrinsic hygroscopicity, κ_{int} (Sullivan et al., 2010) of a limited solubility compound such as $CaCO_3$ is equal to 0.97. This value compares well with $\kappa = 1.0$ for the

more hygroscopic wet generated $CaCO_3$ peak (Fig. 4.4) and provides a potential cause for the more hygroscopic KT-like CCN activation data for wet generated regional dusts.

Table 4.2 shows the values of the experimental exponent, x_{exp}, determined from measurements of the s_c-D_{dry} relationships for individual minerals and clays generated by wet atomization method. Here κ was obtained by fitting κ-KT to the CCN activation data corresponding to the more hygroscopic peak and adsorption parameters (A_{FHH} and B_{FHH}) determined from fitting FHH-AT to the less hydrophilic peak. Similar to wet generated regional dust aerosol, clays and calcite yield κ approaching values characteristic of soluble inorganic salts (with κ for the first peak of $CaCO_3$ being as high as 1.0). The x_{exp} from the s_c-D_{dry} relationship from the CCN activation of the fist peak is also $\sim$ -1.5 (Table 4.2). This suggests that particles generated in the more hygroscopic peak follow activation according to KT. The x_{exp} from the s_c-D_{dry} data of the less hydrophilic peak is much lower and closer ($\pm$ 10%) to x_{exp} determined from dry generated dust that follow FHH-AT. Furthermore, B_{FHH} obtained from wet generated dust is 1.20 $\pm$ 0.20. This value is similar to B_{FHH} equal to 1.20 $\pm$ 0.10 for dry generated dust (Kumar et al., 2010). This relates to the process of reversible water vapor adsorption on dust, and represents the fate of the dust particle in the atmosphere if it is subjected to multiple evaporation/activation cycles.
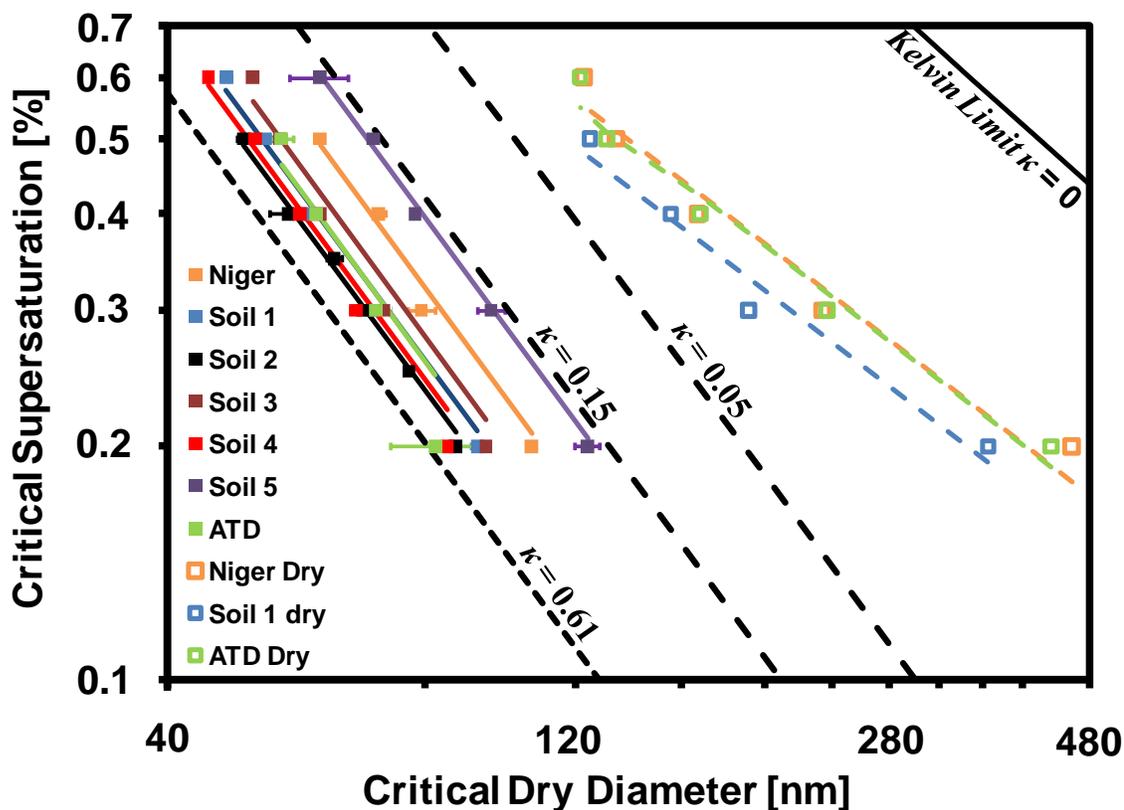
Figure 4.2: CCN activation curves for different dust types considered in this study. Solid symbols refer to wet generated CCN activity and solid lines show κ-KT fits. Open symbols refer to dry generated CCN activity and dashed line are FHH adsorption activation fits (Data obtained from Kumar et al., 2010). Also shown in black dashed lines are κ-KT lines.
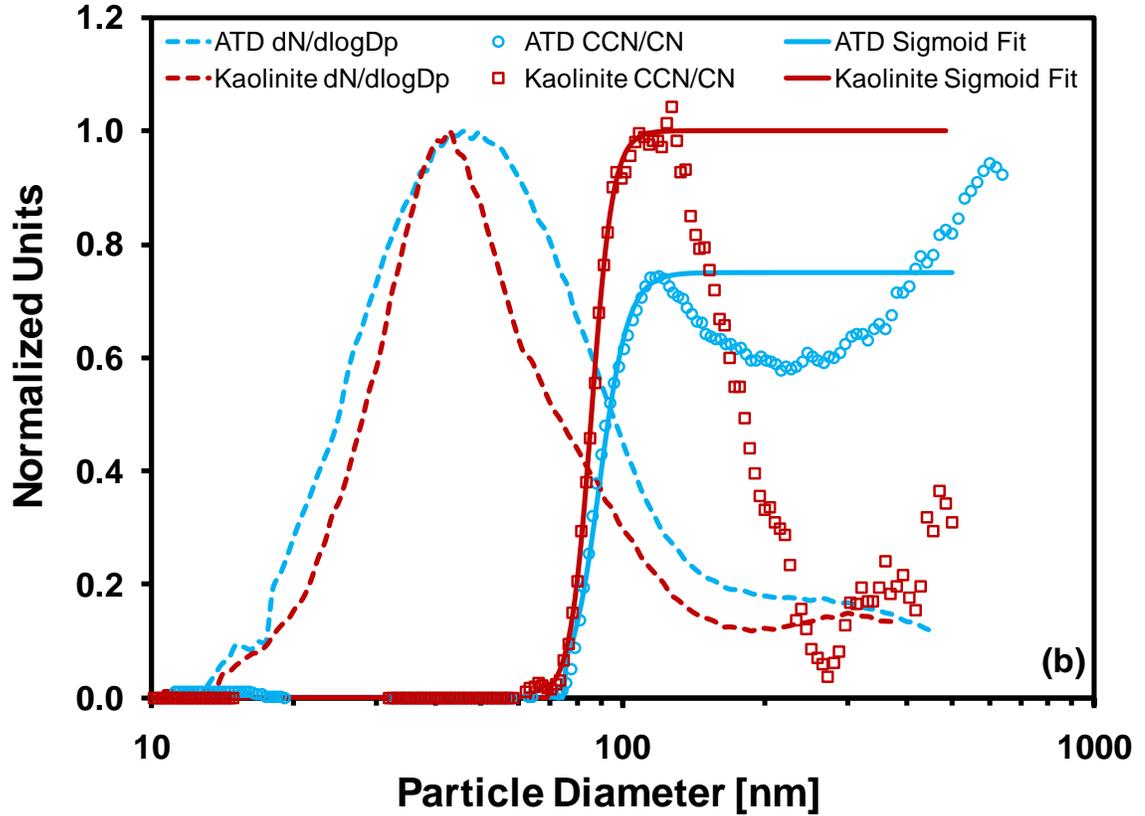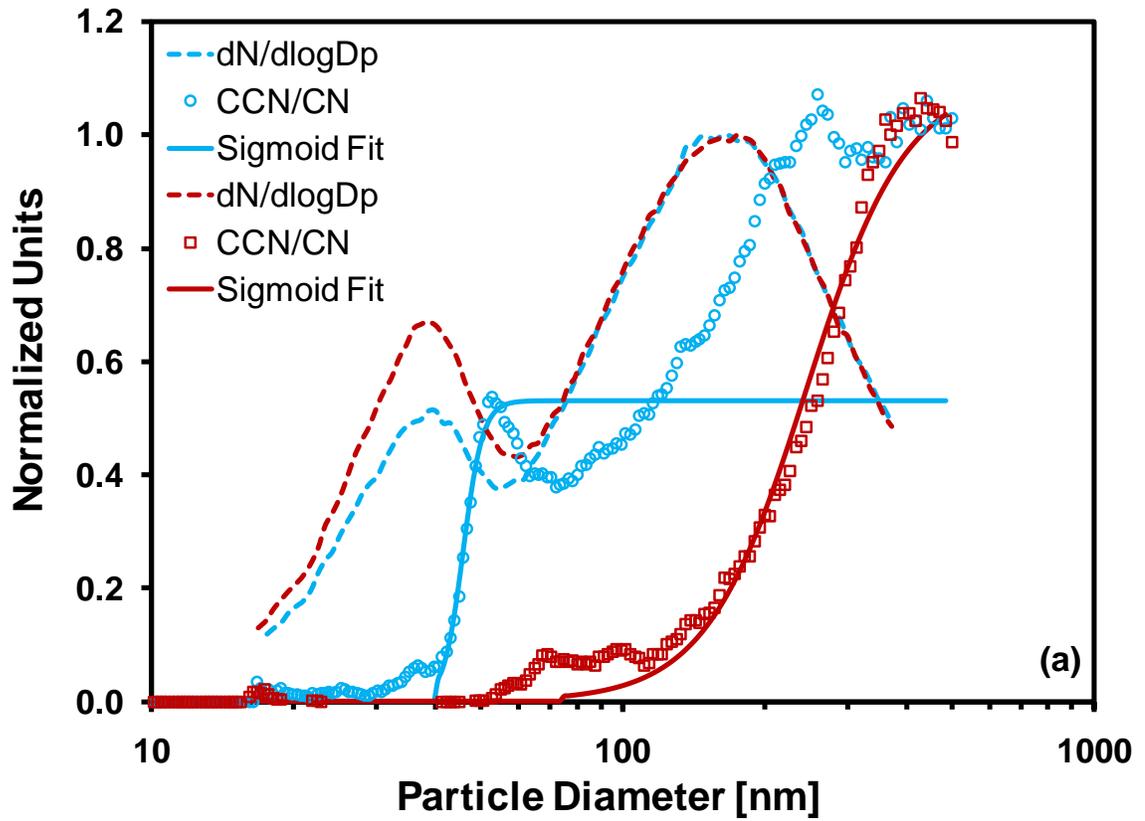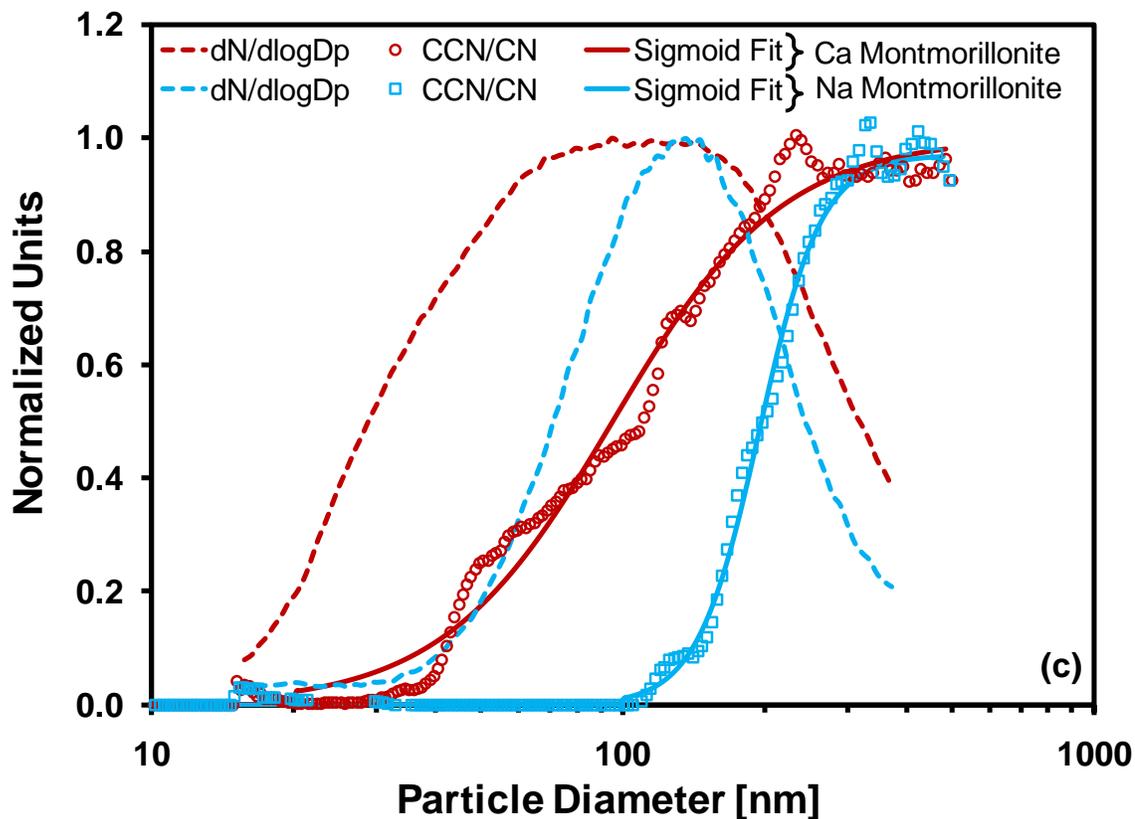
Figure 4.3: CCN activation curves for wet generated **(a)** Illite at supersaturation equal to 0.5% (open blue square) and supersaturation equal to 0.3% (open brown square), **(b)** ATD (open blue square) and Kaolinite (open brown circle) at supersaturation equal to 0.2%, and **(c)** Na-Montmorillonite and Ca-Montmorillonite at supersaturation equal to 0.3% (open blue square) and supersaturation equal to 0.55% (open brown circle). Also shown in dashed lines are normalized particle number size distributions for wet generated sample. The sigmoid curve (thick line) is fit to CCN activation data points.
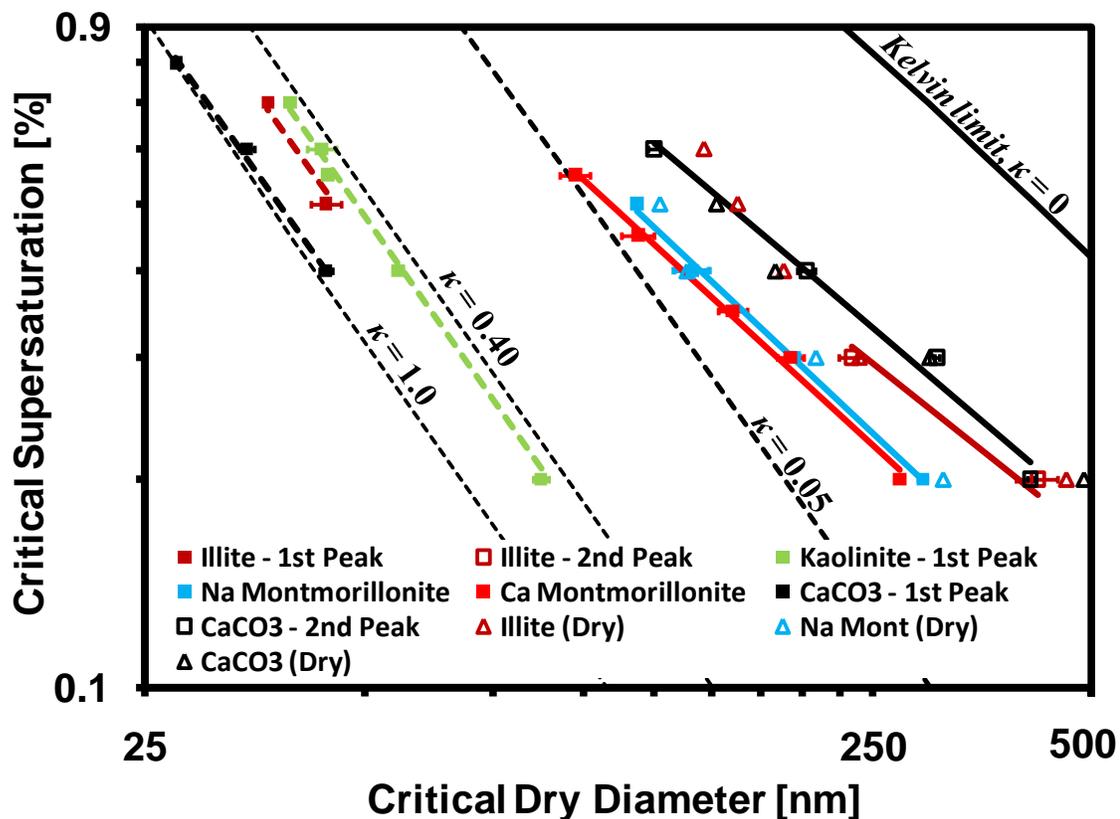
Figure 4.4: CCN activation curves for different mineral and clays types considered in this study. Solid and open square (■, □) symbols refer to wet generated CCN activity and dashed lines show κ-KT fits. Open triangle (Δ) refers to dry generated CCN activity and solid lines are FHH adsorption activation fits (obtained from Kumar et al., 2010).

Table 4.1: CCN activation results – experimental exponents, and hygroscopicity parameter (κ) for regional dust samples generated from wet atomization method

Soil	x_{exp}	κ	$x_{exp}*$
Niger	-1.63	0.26	$-0.79 \pm 0.02 + (0.04)$
Soil 1	-1.63	0.39	$-0.84 \pm 0.02 + (0.05)$
Soil 2	-1.56	0.48	$-0.82 \pm 0.02 + (0.05)$
Soil 3	-1.71	0.34	$-0.92 \pm 0.03 + (0.05)$
Soil 4	-1.73	0.44	$-0.88 \pm 0.03 + (0.04)$
Soil 5	-1.53	0.17	$-0.78 \pm 0.03 + (0.05)$
ATD[+]	-2.16	0.40	$-0.82 \pm 0.02 + (0.04)$

* represents experimental exponent determined from dry generation method (Kumar et al., 2010). Values in parentheses indicate change in magnitude of x_{exp} from change in χ between 1.1 and 1.5.

[+] Two peaks were observed for ATD. Values here represent experimental results from the first peak.

Table 4.2: CCN activation results – experimental exponent, hygroscopicity parameter (κ), Adsorption parameters (A_{FHH}, B_{FHH}) for clays and calcite sample generated from wet atomization method

Mineral	x_{exp}	κ	A_{FHH}	B_{FHH}	x_{exp}*
Illite (Peak 1)	-1.63	0.58			$-0.92 \pm 0.03 + (0.05)$
Illite (Peak 2)	-0.60		3.00	1.27	$-0.92 \pm 0.03 + (0.05)$
Kaolinite	-1.57	0.47			
Ca Mont	-0.76		1.09	1.04	$-0.88 \pm 0.02 + (0.05)$
Na Mont	-0.99		0.87	1.00	$-0.93 \pm 0.02 + (0.04)$
$CaCO_3$ (Peak 1)	-1.46	1.00			$-0.75 \pm 0.02 + (0.05)$
$CaCO_3$ (Peak 2)	-0.89		1.74	1.22	$-0.75 \pm 0.02 + (0.05)$

* represents experimental exponent determined from dry generation method (Kumar et al., 2010). Values in parentheses indicate change in magnitude of x_{exp} from change in χ between 1.1 and 1.5

4.5.3 *Droplet Activation Kinetics*

TDGA is used to study the CCN activation kinetics of wet dust and is based on comparing D_w measured by the OPC at the base of CFSTGC for the sample CCN against that of $(NH_4)_2SO_4$ calibration aerosol. If droplet sizes (D_w) from dust CCN are smaller than those from calibration aerosol (with same s_c and for identical conditions of instrument supersaturation), this suggests that mineral aerosol may experience slower growth during their residence time in the instrument. However, if activated droplet sizes are indistinguishable (within experimental uncertainty) from $(NH_4)_2SO_4$ data, wet generated mineral aerosol would exhibit activation kinetics similar to $(NH_4)_2SO_4$ calibration aerosol.

Activated droplet sizes obtained for the wet generated regional dusts are shown in Fig. 4.5. Droplet sizes similar to those generated by $(NH_4)_2SO_4$ aerosol were observed. This suggests that wet generated dust aerosol exhibits activation kinetics similar to $(NH_4)_2SO_4$. In some cases, droplets generated from wet dust aerosol appear to grow 5% larger compared to pure $(NH_4)_2SO_4$ aerosol. Given the 0.5 µm uncertainty (associated with the binning scheme) of the OPC, this larger size is statistically insignificant. A similar behavior was also observed for clays and calcite wet generated (Fig. 4.6). The CCN number concentrations in the experiments (either calibration or dust activation) was at most ~ 1000 - 1500 cm^{-3} at D_{dry} (and definitely less than 5000 cm^{-3}) so that water vapor depletion effects on CCN concentration and wet droplet diameter are negligible (Lathem and Nenes, 2010) and thus not attributing to increased droplet sizes for dust CCN.

The results presented here suggest that the activation kinetics of wet generated dust is distinctly faster than for dry generated dust (expressed by a 30 - 80% reduction in

effective water vapor uptake coefficient relative to $(NH_4)_2SO_4$ aerosol). This result suggests that dust particles that already have been wetted in the atomizer have sufficient water coverage to display rapid activation kinetics. It is possible that the wet generated aerosol is not aggressively dried; it may therefore retain a few monolayers of water on its surface and accelerate the rapid re-condensation of water in the CFSTGC (as the water uptake, hence growth kinetics, becomes progressively more rapid with amount of adsorbed water; Kumar et al., 2009a). Rapid activation kinetics is expected for particles primarily composed of soluble salt (which correspond to the high κ particles in Fig. 4.2 and 4.4).

Faster activation kinetics of wet generated dust (compared to dry dust) would imply that the fresh dust in the source regions would behave differently to cloud processed dust downwind of its source region that has undergone multiple activation/evaporation cycles. This would also mean that fresh and cloud processed dust would behave differently even when exposed to the same levels of cloud supersaturation. This is of significance for both Saharan and Asian dusts given that large regions of the world are affected by their mid- and long-range transport. Whether a fresh or cloud processed dust has more significant impact on cloud droplet number would also depend on activation physics and time scales of cloud formation. These issues are further addressed in section 4.6.
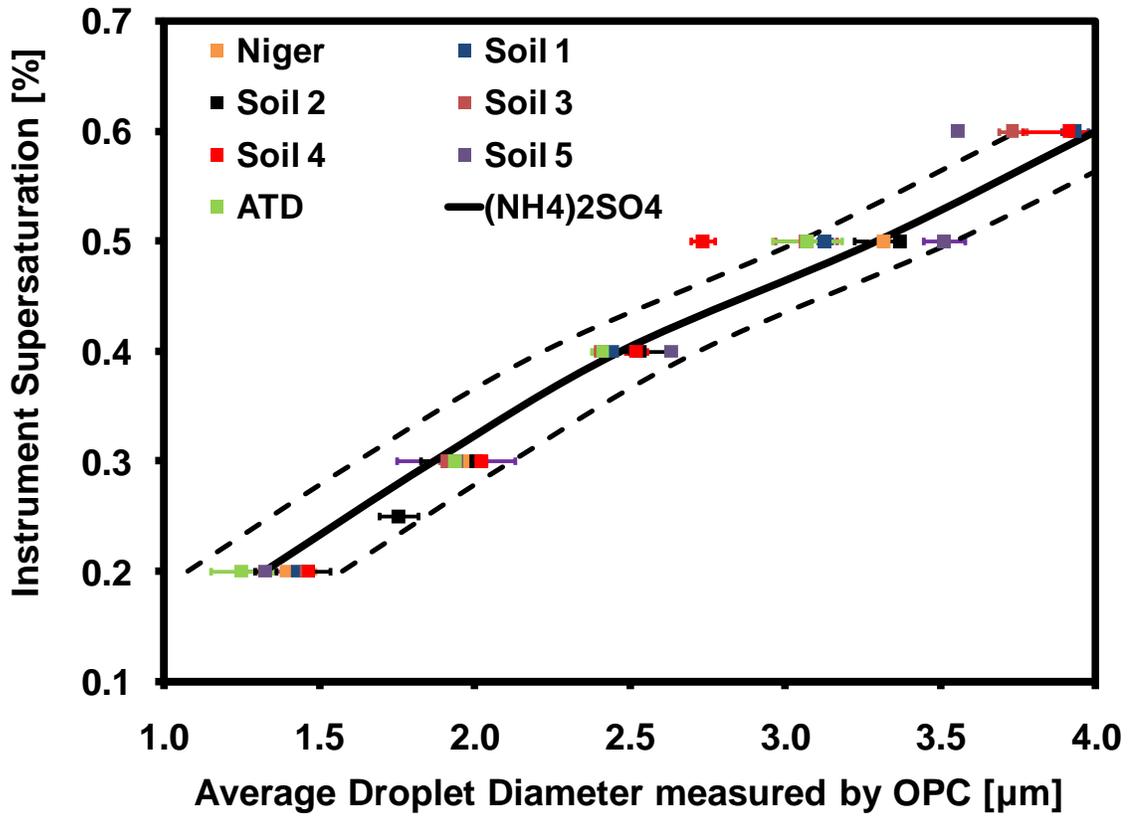
Figure 4.5: Activated droplet sizes of wet generated mineral dust CCN with s_c equal to the instrument supersaturation. Error bars represent variability in droplet sizes as measured by the OPC at same instrument supersaturation. Dashed lines represent $\pm$ 0.25 μm variability in $(NH_4)_2SO_4$ droplet sizes.
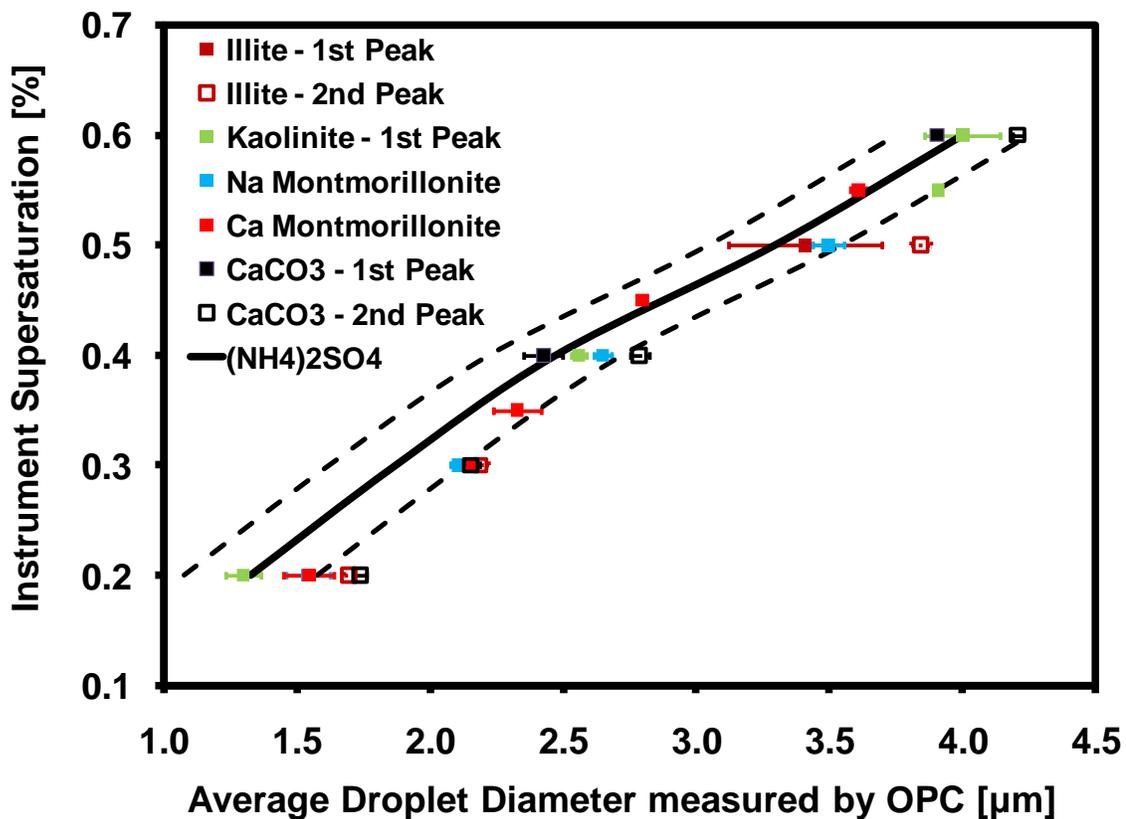
Figure 4.6: Activated droplet sizes of wet generated clays and calcite CCN with s_c equal to the instrument supersaturation. Error bars represent variability in droplet sizes as measured by the OPC at same instrument supersaturation. Dashed lines represent ± 0.25 μm variability in $(NH_4)_2SO_4$ droplet sizes.

4.5.4 Contribution of Soluble Ions to Hygroscopicity

Previous studies on the dust CCN activity (Koehler et al., 2009; Herich et al., 2009) attributed increased hygroscopicity of the wet generated dust aerosol to the presence of soluble salts on dust particles. Kumar et al. (2009a) raised doubts to this based on the slope of the s_c-D_{dry} relationship. Sullivan et al. (2010) confirmed this for calcite as a negligible mass fraction of soluble salts in calcite aerosol was found using ICP and SEM-EDX. Here we further address this issue by examining the soluble fraction of the regional dust and clay samples and relating it to dust CCN activation.

The IC analysis was performed on the ATD, Niger, Soil 4, and Soil 5 samples as they represent the important dust source regions. For fine (≤ 1 μm) and coarse (>1 μm) samples, the ionic concentration obtained from IC (in terms of mg l^{-1}) is converted to dry ionic mass composition (based on the amount of DI water used to prepare the aqueous extracts) and converted to a mixture of salts, each with a mass fraction x_i by applying the ISORROPIA-II model (Fountoukis and Nenes, 2007) as described in Padró et al. (2010). The volume fraction of substance i, ε_i, is computed as follows

$$\varepsilon_i = \frac{x_i / \rho_i}{\sum_j (x/\rho)_j}$$ [4.4]

where j refers to all substances present in the aerosol (soluble and insoluble). Table 4.3 contains information on the properties (molar mass, M_s, density, ρ_s, and hygroscopicity parameter, κ) of salts that may be present in the mineral aerosol.

A closure analysis for κ was performed by comparing the measured κ_{CCN} against predictions (κ_{mix}) using a volume-average mixing rule (Petters and Kreidenweis, 2007)

$$\kappa_{mix} = \sum_i \varepsilon_i \kappa_i$$ [4.5]

where i refers to all soluble salts.

For all of the eight samples analyzed in this study, an excess of cations was found, with Ca^{2+} being the most dominant unbalanced cation. Since IC analysis did not measure CO_3^{2-}, we postulate that all of the excess cations were balanced by CO_3^{2-}, resulting in carbonate salts in the form of $CaCO_3$. This is consistent with findings of Claquin et al. (1999) that show calcite to make up to 30% of the dust composition. Table 4.4 shows the inferred volume fractions of soluble salt and insoluble species from ISORROPIA-II along with the corresponding hygroscopicity parameter (κ) determined using Eq. (4.5). It can be seen from Table 4.4 that the inferred κ_{mix} for all samples is much smaller than that determined from the observed CCN activity of dry generated dust aerosol. This confirms that the presence of soluble fractions alone cannot explain hygroscopicity observed in the original dust samples, further supporting that the CCN activity observed by Kumar et al. (2010) for dry generated dust aerosol originated from water vapor adsorption onto the insoluble dust surface.

It was previously suggested by Koehler et al. (2009) that the presence of soluble contaminants in dust can be attributed to enhanced hygroscopicities in CCN activation measurements performed on wet generated dust aerosol. For the above statement to hold true for the dust samples analyzed in this study, dust and mineral aerosols would have to be composed of $\geq$ 25 - 80% by volume of soluble salts like $(NH_4)_2SO_4$ ($\kappa = 0.61$) to display κ of ~ 0.2 – 0.5 (Table 4.1 and Table 4.2). However, IC analysis performed on all eight samples did not reveal significant amounts of soluble salts in the bulk samples with a soluble volume fraction of less than 1% (Table 4.4). Sullivan et al. (2010) provided a possible explanation regarding the presence of particles produced in the first peak of

calcite and ATD, and attributed those to a mixture of parent mineral particles plus secondary calcium bicarbonates, calcium hydrates as well as contributions from other undetected impurities that may have formed amorphous precipitates (given that we observe substantially smaller aerosol than in dry generation, it is likely that parent mineral particles are seldomly present). It may also be possible that slightly soluble compounds (such as $CaCO_3$) can form metastable aerosol (e.g., Raymond and Pandis, 2002; Padró and Nenes, 2007) due to insufficient drying inside the diffusion dryers so that all of the material is available for solvation. This has been seen in our measurements, where assuming $CaCO_3$ is fully soluble yields $\kappa \sim 0.97$ (vs. observed $\kappa_{CCN} \sim 1.0$ and x_{exp} $\sim$ -1.5). This suggests that the same behavior may also be occurring in regional dust samples when dissolved in water resulting in a high value of κ. It can be also argued that presence of dissolved soluble contaminants in the DI water can also result to the formation of the first hygroscopic peak. However, results from IC performed on DI water (blank sample) indicated negligible presence of dissolved ions impurities. For instance, the concentration of Na^+, K^+ and NH_4^+ was below the detection limit, while the concentration of Ca^{2+} was lower by a factor of 10^3 when compared to the IC results of dust samples. Similarly for anions, the only concentration detected by IC was for $SO4^{2-}$ and that was again lower by a factor of $\sim 300 - 2,000$. Therefore, residual ions in pure DI water are an unlikely contributor to the observed hygroscopicity of the first peak.

The analysis performed above questions the atmospheric relevance of CCN activity experiments using wet generated dust, and the usage of κ-KT for parameterizing its hygroscopicity. It also supports the approach of Kumar et al. (2009a,b, 2010) of using the exponents derived from the scale dependence of s_c on D_{dry} to reveal the dominant

activation physics. Since that large-mode aerosol (whenever present during wet generation) closely matches the activation behavior of dry generated dust, we postulate that wetting of fresh dust does not irreversibly change its CCN activity. The activation kinetics however can be accelerated with dust cloud cycling.

Table 4.3: Properties of inorganic salts potentially extracted from regional soil samples. Properties obtained from Padró et al. (2010)

Salt	Chemical Formula	Molar Mass (g mol^{-1})	ρ (g cm^{-3})	κ
Sodium Nitrate	$NaNO_3$	84.99	2.25	0.88
Sodium Sulphate	Na_2SO_4	142.04	2.68	0.85
Sodium Bisulphate	$NaHSO_4$	120.06	2.74	0.82
Sodium Chloride	$NaCl$	58.44	2.16	1.40
Ammonium Chloride	NH_4Cl	53.49	1.52	1.46
Ammonium Nitrate	NH_4NO_3	80.04	1.50	0.64
Ammonium Sulphate	$(NH_4)_2SO_4$	132.14	1.77	0.60
Ammonium Bisulphate	NH_4HSO_4	115.11	1.79	0.53
Calcium Sulphate	$CaSO_4$	136.14	2.32	0.01
Calcium Nitrate	$Ca(NO_3)_2$	164.00	1.82	0.40
Calcium Chloride	$CaCl_2$	110.98	2.15	0.70
Potassium Sulphate	K_2SO_4	174.27	2.66	0.69
Potassium Bisulphate	$KHSO_4$	136.17	2.24	0.59
Sodium Carbonate	Na_2CO_3	105.98	2.54	1.30
Ammonium Carbonate	$(NH_4)_2CO_3$	96.09	1.50	0.84
Potassium Carbonate	K_2CO_3	138.20	2.29	0.90
Calcium Carbonate	$CaCO_3$	100.08	2.71	0.001

Table 4.4: Soluble volume fraction (ε_s), insoluble volume fraction (ε_s), and inferred hygroscopicity parameter (κ) for mineral dust aerosol samples. Uncertainties in volume fractions are estimated to being less than 0.3%

Sample	$\varepsilon_{soluble}$	$\varepsilon_{insoluble}$	κ_{mix}
ATD – Coarse	0.007	0.993	0.003
ATD – Fine	0.009	0.991	0.004
Niger – Coarse	0.004	0.996	0.001
Niger – Fine	0.003	0.997	0.001
Soil 4 – Coarse	0.014	0.986	0.003
Soil 4 – Fine	0.086	0.914	0.016
Soil 5 – Coarse	0.003	0.997	0.001
Soil 5 – Fine	0.003	0.997	0.002

4.6   Implications for Dust - Warm Cloud Interactions

Droplet activation in large-scale atmospheric models is often calculated from physically-based prognostic parameterizations (e.g., Abdul-Razzak and Ghan, 2000; Ming et al., 2006; Nenes and Seinfeld, 2003, Kumar et al., 2009b) that rely on solving the supersaturation balance equation (for a 1-D parcel) to determine parcel maximum supersaturation, s_{max}. The s_{max} corresponds to the point where droplet activation terminates in the cloud, and occurs when supersaturation generated from expansion cooling balances supersaturation depletion from condensation of water vapor on pre-existing aerosol particles. The level of s_{max} in clouds depends on the competition between CCN for available water vapor that is required to activate CCN to cloud droplets.

Kumar et al. (2009a) found that the volume of water required by particles to activate to cloud droplets at a given supersaturation can vary significantly between KT and FHH-AT. This behavior is also shown in Fig. 4.7 which compares the ratio of water volume at the critical wet diameter, D_c, required by KT over FHH-AT for supersaturations between 0.05% and 0.6%. The A_{FHH}, B_{FHH}, and κ used in Fig. 4.7 are representative of dust samples analyzed in this study and by Kumar et al. (2010). It can be seen from Fig. 4.7 that for a particle to activate by KT, up to 15 times more water volume is required for activation compared to particles activating via FHH-AT at the same critical supersaturation. A high value of water volume at D_c implies that large amount of water vapor would be required by the CCN to form a cloud droplet. Integration over the entire CCN population would increase competition for water vapor, lead to a decrease in s_{max}, and cause a decrease in cloud droplet number, N_d.

Based on the above, it becomes clear that the choice of activation theory can have a strong impact on s_{max} and N_d. For an externally mixed population of KT and FHH-AT particles, the treatment of Kumar et al. (2009b) is sufficient. However, during atmospheric transport, fresh dust undergoes aging and acquires soluble species like $(NH_4)_2SO_4$ on its surface (Levin et al., 1996). Similarly, dust generated from dry dust lake beds (or playas) are known to contain significant amounts of soluble salts (Pratt et al., 2010). The presence of such soluble salts on dust surface can affect water-particle interactions with implication to the dust CCN activity. Below, we address the effect of soluble salts on dust surface to droplet equilibrium behavior.

We adopt a shell-and-core model with the core representing insoluble dust and shell consisting of a layer of soluble salt. Based on laboratory dust CCN activation measurements, Kumar et al. (2010) found typical fresh dust sizes to range between 100 and 500 nm. As ageing occurs, it is expected that dry particle size will increase; therefore in our approach we consider a core-shell model where the insoluble core does not go below 50 nm (a lower limit of fresh dust). The water vapor saturation ratio, S, of an aerosol particle in equilibrium with surrounding water vapor can be expressed as (Seinfeld and Pandis, 2006)

$$S = a_w \gamma_w \exp\left(\frac{4\sigma_w M_w}{RT\rho_w D_p} \right) \qquad [4.6]$$

where a_w is the water activity of the particle, γ_w is the activity coefficient for water, and other parameters as defined above. The exponential in Eq. (4.6) is commonly referred to as the curvature or the Kelvin effect. For a completely insoluble aerosol particle like fresh dust, a_w, is controlled by the adsorption of the water vapor on the insoluble surface such

that Eq. (4.6) reduces to Eq. (4.1) (when adsorption is modeled using the FHH adsorption isotherm).

Given that the water adsorbed on the surface must be in equilibrium with the surrounding aqueous phase and the water vapor in the gas, the a_w that accounts for both the Raoult and adsorption effects is given as

$$a_w = x_w f(\Theta) \hspace{4cm} [4.7]$$

where x_w is the mole fraction of water in the droplet and represents water activity depression due to solute effects. $f(\Theta)$ represents water vapor adsorption effect on a_w, where Θ is the number of water monolayers adsorbed on the dry particle core.

x_w is related to the mole fraction of the soluble salt, x_s, as $x_w = 1 - x_s$. Invoking the dilute approximation gives $x_s = \dfrac{n_s}{n_T} \approx \dfrac{n_s}{n_w}$, where n_s is the moles of solute, n_T is the total moles in the aqueous phase, and n_w is the moles of water in the droplet. Therefore,

$$x_s = \frac{n_s}{n_w} = \frac{\left(\dfrac{V_s \rho_s \upsilon}{M_s}\right)}{\left(\dfrac{V_w \rho_w}{M_w}\right)} \hspace{4cm} [4.8]$$

where ρ_s, M_s, and υ are density, molecular mass and effective van't Hoff factor of the solute, respectively. V_s and V_w are the volume of the salt and water in the aqueous phase, respectively.

For a given insoluble volume fraction, ε_i and diameter of the dust core, D_{core}, the size of the dry particle, D_{dry}, can be estimated as

$$D_{dry} = D_{core} / \varepsilon_i^{1/3} \hspace{4cm} [4.9]$$

The volume of the soluble fraction, ε_s, is available as $\varepsilon_s = 1 - \varepsilon_i$. Therefore, the volume of the soluble fraction, V_s, can be defined as

$$V_s = \varepsilon_s \left(\frac{\pi}{6} \right) D_{dry}^3 \qquad [4.10]$$

Substituting V_s from Eq. (4.10) into Eq. (4.8) and expressing $V_w = V_T - V_i$ where V_w is the volume of water in droplet, V_T is the droplet volume and V_i is the volume of the insoluble core gives

$$x_s = \frac{\left(\dfrac{\varepsilon_s (\pi/6) D_{dry}^3 \rho_s \upsilon}{M_s} \right)}{\left(\dfrac{(V_T - V_i) \rho_w}{M_w} \right)} = \frac{\varepsilon_s D_{dry}^3 \rho_s \upsilon M_w}{M_s \left(D_P^3 - \varepsilon_i D_{dry}^3 \right) \rho_w} \qquad [4.11]$$

Substituting the hygroscopicity parameter, κ, as $\kappa = \dfrac{\rho_s \upsilon M_w}{M_s \rho_w}$ into Eq. (4.11) gives

$$x_s = \frac{\varepsilon_s D_{dry}^3 \kappa}{\left(D_P^3 - \varepsilon_i D_{dry}^3 \right)}. \text{ Now expressing } x_w \text{ in terms of } x_s \text{ gives } x_w = 1 - x_s = 1 - \frac{\varepsilon_s D_{dry}^3 \kappa}{\left(D_P^3 - \varepsilon_i D_{dry}^3 \right)}.$$

Kumar et al. (2009a) defined surface coverage, Θ, as the number of monolayers of water adsorbed on the particle. As water vapor is adsorbed only on the dry insoluble core, Θ is given as

$$\Theta = \left(\frac{D_p - \varepsilon_i^{1/3} D_{dry}}{2 D_{H_2O}} \right) \qquad [4.12]$$

where $\varepsilon_i^{1/3} D_{dry}$ is the diameter of the insoluble core and D_{H_2O} is the diameter of the water molecule. According to Kumar et al. (2009a), $f(\Theta) = \exp\left(- A_{FHH} \Theta^{-B_{FHH}}\right)$. Substituting into Eq. (4.12) gives

125

$$f(\Theta) = \exp\left[-A_{FHH}\left(\frac{D_p - \varepsilon_i^{1/3}D_{dry}}{2D_{H_2O}}\right)^{-B_{FHH}}\right] \qquad [4.13]$$

Thus combined a_w can be obtained using Eq. (4.7), (4.11) and (4.13) as

$$a_w = \left[1 - \frac{\varepsilon_s D_{dry}^3 \kappa}{\left(D_P^3 - \varepsilon_i D_{dry}^3\right)}\right]\exp\left[-A_{FHH}\left(\frac{D_p - \varepsilon_i^{1/3}D_{dry}}{2D_{H_2O}}\right)^{-B_{FHH}}\right] \qquad [4.14]$$

Substituting a_w from Eq. (4.14) into Eq. (4.6), assuming ideality (γ_w = 1) and expanding the exponential and taking the first order terms gives

$$s = \frac{4\sigma M_w}{\rho_w RTD_p} - \frac{\varepsilon_s D_{dry}^3 \kappa}{\left(D_P^3 - \varepsilon_i D_{dry}^3\right)} - A_{FHH}\left(\frac{D_p - \varepsilon_i^{1/3}D_{dry}}{2D_{H_2O}}\right)^{-B_{FHH}} \qquad [4.15]$$

where s is the equilibrium supersaturation defined as $s = S - 1$.

Equation (4.15) represents water vapor supersaturation over an aerosol particle (consisting of insoluble core with a soluble coating) in equilibrium with the surrounding water vapor. As Eq. (4.15) is specific to an aerosol particle with a finite insoluble core but variable soluble coating, it reduces to Eq. (4.1) for a completely insoluble particle as $\varepsilon_i \rightarrow$ 1. In this study, Eq. (4.15) will be referred to as the Unified Dust Activation Framework.

Figure 4.8 shows the relationship between dry diameter, D_{dry}, and critical supersaturation, s_c, for different insoluble volume fractions, ε_i, computed for κ = 0.10, average adsorption parameters of fresh dust (A_{FHH} = 2.25, B_{FHH} = 1.20), surface tension of water, σ_w = 0.072 N m^{-1}, and temperature, T = 298.15 K. It can be seen from Fig. 4.8 that as the insoluble volume fraction, ε_i, of the dry aerosol decreases from 1.0 to 0.5, the threshold of cloud droplet nucleation on pre-existing aerosol particles increases significantly. Furthermore, as ε_i starts decreasing from 1.0, the exponent derived from the

s_c-D_{dry} relationships changes from -0.85 (representative of FHH-AT) and starts approaching that of the completely soluble particle with exponent equal to -1.50 (shown by inset Table in Fig. 4.8). This implies that the activation mechanism changes from a FHH-AT regime (-1.25 < exponent < -0.85) to the regime where both KT and FHH-AT may be applicable with exponent between -1.25 and -1.50.

Figure 4.9 shows the effect of ε_i on the magnitude of derived exponent for three different values of κ equal to 0.1, 0.61, and 1.0 computed at $A_{\mathrm{FHH}} = 2.25$ and $B_{\mathrm{FHH}} = 1.20$. It can be seen that as ε_i starts decreasing from 1.0, the magnitude of the exponent also starts changing from -0.85 (representative of FHH-AT) and starts approaching that of KT with exponent equal to -1.5. The effect of different solute type (representative of different κ) to a_w, and its corresponding, ε_s ($= 1 - \varepsilon_i$), to the derived exponent is also addressed by Fig. 4.9. It can be seen that as κ increases from 0.1 (representative of dust containing oxidized organics) to 0.61 (representative of dust containing $(NH_4)_2SO_4$), even a small decrease in ε_i can cause an appreciable change in the exponent magnitude, with implications to particle water interactions. Similar behavior is seen when going from $\kappa = 0.61$ to $\kappa = 1.0$. The results shown in Fig. 4.8 and Fig. 4.9 further substantiate the findings by Kumar et al. (2009a, 2010) that CCN activity of fresh dust ($\varepsilon_s \sim 0.0$) can be parameterized by FHH-AT and suggested a combined framework may be required to describe CCN activity of dust with a significant soluble fraction.

The proposed unified framework (Eq. 4.15) is evaluated against experimental measurements of CCN activity of Canary Island Dust (CID) and Owens Lake (OL) dust samples that are known to contain high concentration of soluble salts as high as 37% by mass in Owens Lake (Reheis, 1997) and about 14% sulphates and 5% Calcium-rich salts

by volume in dust samples collected around Canary Island (Kandler et al., 2009). Kumar et al. (2009a) found x_{exp} equal to -1.33 and -1.36 for CID and OL that could not be reconciled by KT or FHH-AT alone. A revised analysis of the exponents for CID and OL dust based on approximate salt volume fractions determined from the literature demonstrates that the unified approach (Eq. 4.15) can be used to reconcile such exponents (also shown in Fig. 4.9). A thorough assessment of the framework world require size resolved composition and CCN activation measurement of dust samples with significant solutes and is left to be addressed by future studies.
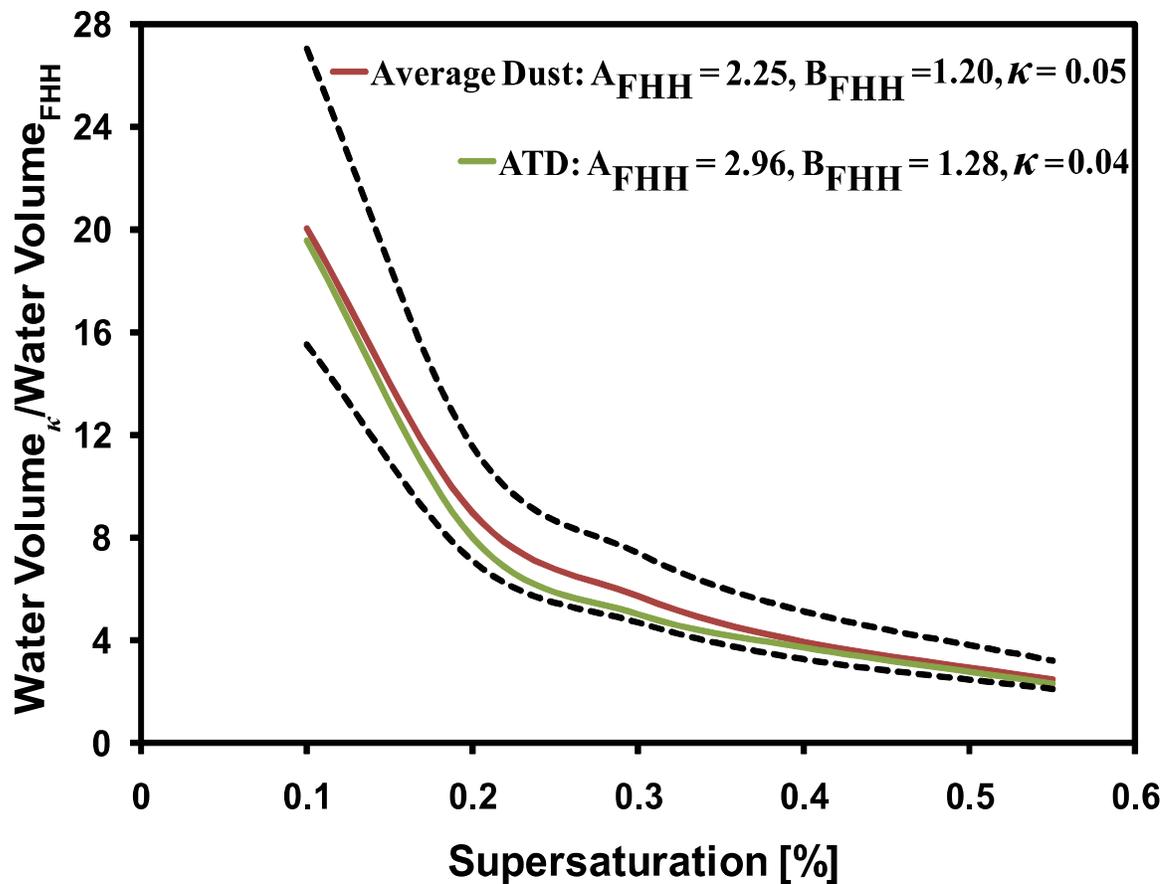
Figure 4.7: Ratio of water volume required by KT over FHH-AT to activate CCN as a function of supersaturation. Simulations are performed with values of adsorption (A_{FHH}, B_{FHH}) and κ for average dust aerosol. Dashed lines represent simulation representing upper and lower limit of dust relevant adsorption parameters.
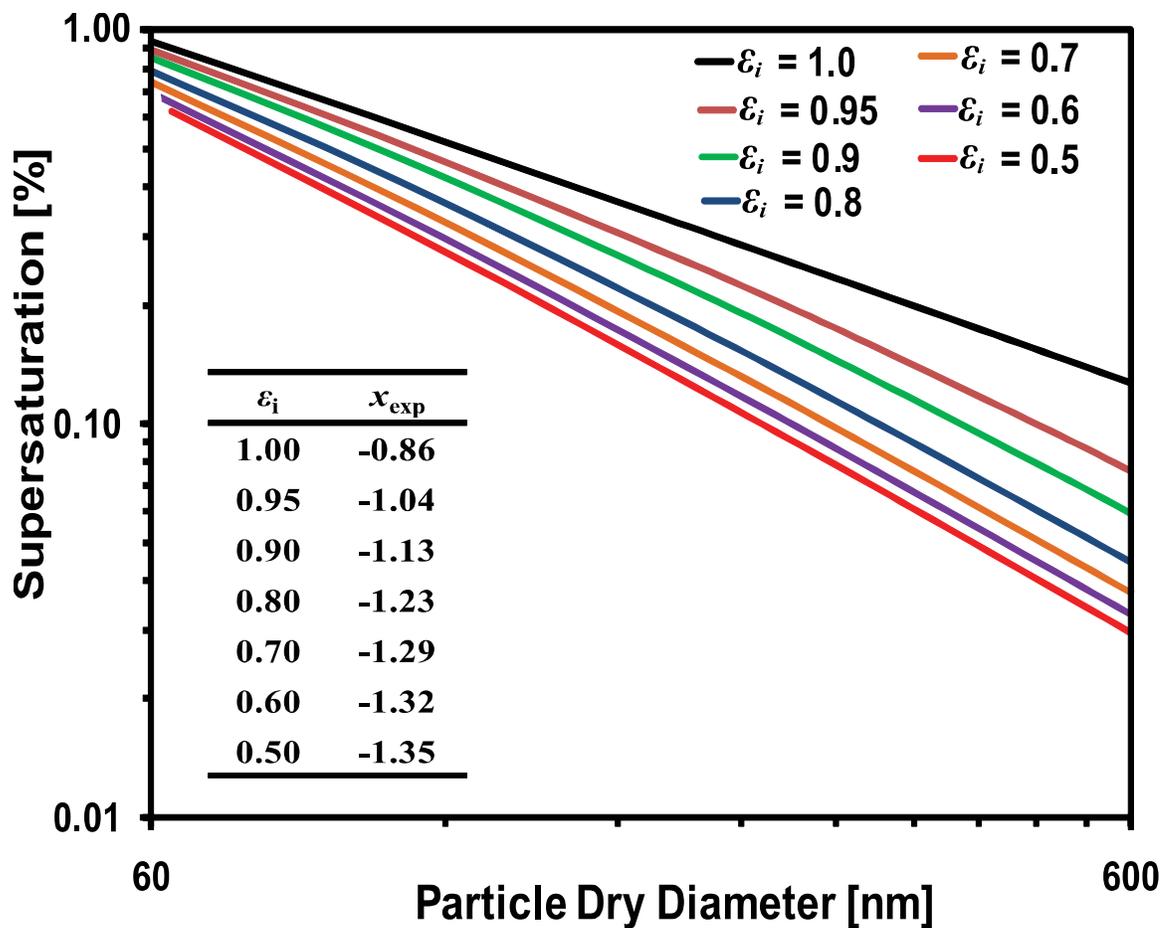
Figure 4.8: s_c–D_{dry} lines for different values of ε_i computed at $\sigma_w = 0.072$ N m^{-1}, $T =$ 298.15 K, $A_{FHH} = 2.25$, $B_{FHH} = 1.20$, $\kappa = 0.01$. The inset table shows theoretical exponent associated with s_c-D_{dry} lines shown in the main figure.
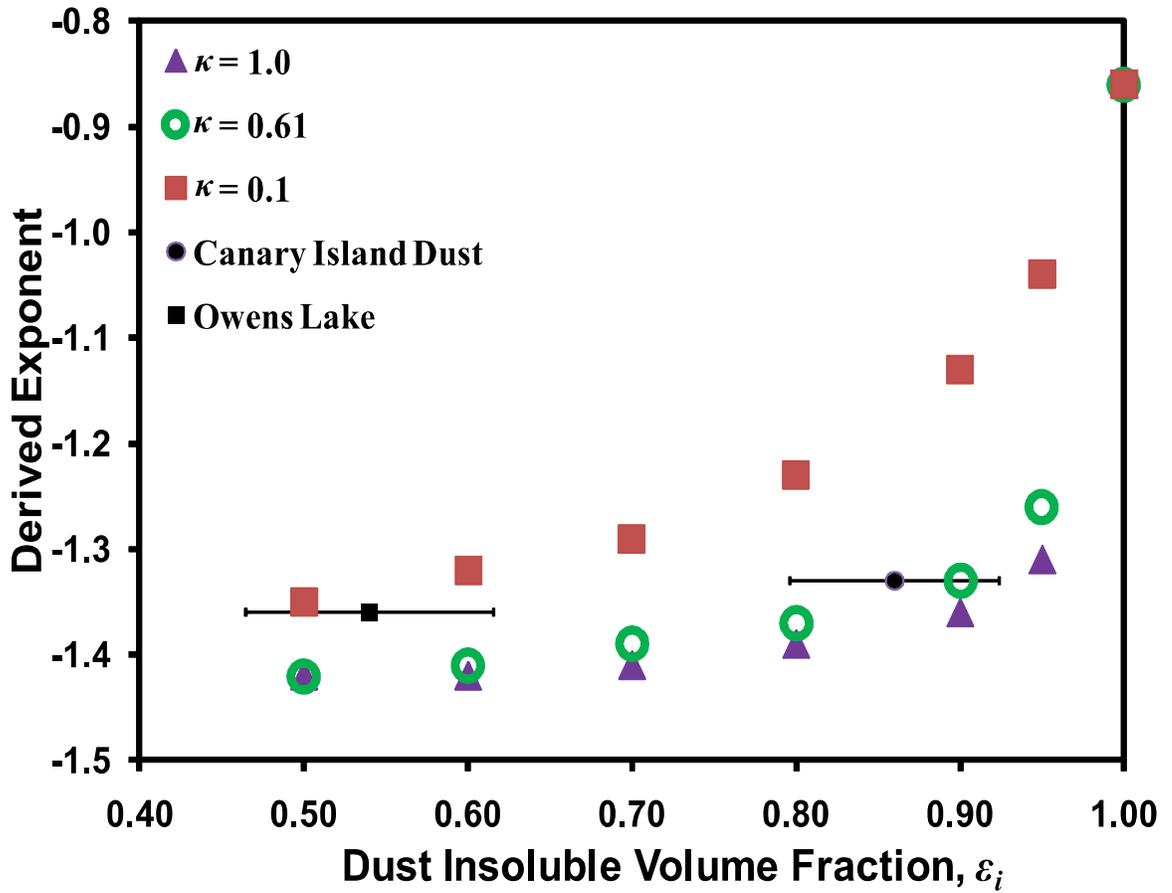
Figure 4.9: Derived theoretical exponent as a function of ε_i for different values of κ computed at $A_{FHH} = 2.25$ and $B_{FHH} = 1.20$. Also shown are data points for Canary Island Dust and Owens Lake dust (data obtained from Kumar et al., 2009a).

131

4.7   Conclusions

In this study, the CCN properties and droplet activation kinetics of aerosol wet generated from regional dust samples and individual minerals (clays, calcite, and quartz) were measured. The aerosols were generated wet in the lab, and properties were measured using the Scanning Mobility CCN Analysis (Moore et al., 2010). Measurement of dust size distributions indicated unimodal distributions for regional dust samples with particle sizes observed as low as 40 nm. These measurements demonstrate that particles generated via wet atomization are up to ten times smaller those generated by the dry soft-saltation technique. For most minerals (ATD, calcite, illite, and kaolinite) a bimodal dry size distribution was obtained. Comparisons with the number size distribution generated by the dry technique suggests that the second observed peak in the wet generation method could be a consequence of the external mixture containing more hygroscopic particles and the less hydrophilic particle mode. Montmorillonite clays were found to behave differently when mixed with water as a unimodal size distribution was obtained with the wet generation technique. This difference in patterns of number size distribution between montmorillonite (unimodal) and illite, kaolinite (bimodal) is related to the aluminosilicate layer-layer interactions.

Measurements of dust CCN activity indicated that the wet generated particles were significantly more CCN active than those generated from the dry soft-saltation technique with κ ranging between 0.15 – 0.61. For almost all wet generated regional dust aerosols, x_{exp} is ~ -1.5 (with the exception of ATD), while a much lower x_{exp} ~ -(0.9 ± 0.2) was observed for dry generated dust aerosol. Ion Chromatography (IC) analysis performed on regional dust samples indicates negligible soluble fractions. The expected

hygroscopicity from this composition was much lower than observed for both wet and dry generated aerosol. All together, these results confirm that the presence of soluble fractions alone cannot explain fresh dust CCN activity, and the effects of water vapor adsorption must be included to comprehensively describe the CCN activity of dry dust. These results also question the atmospheric relevance of past studies that used mineral dust aerosol generated with the wet atomization method.

Based on threshold droplet growth analysis, we found that wet generated dust aerosol does not exhibit delayed activation kinetics. This behavior of similar activation kinetics for wet generated dust (compared to $(NH_4)_2SO_4$) is different from that observed for dry generated mineral aerosol that exhibits retarded activation kinetics and a reduced effective water vapor uptake coefficient (by 30 - 80%) that is consistent with longer timescale associated with adsorption than absorption.

To account for the CCN activity of dust containing soluble salt fraction, we propose a new framework of CCN activation that accounts for concurrent effects of solute and water vapor adsorption. This unified framework is based on the core-and-shell model and describes equilibrium supersaturation as a function of adsorption parameters, hygroscopicity parameter of the soluble fraction, size of the dry particle, and insoluble and soluble volume fractions. As expected, the framework predicts that as ε_i decreases, x_{exp} changes from -0.85 (FHH-AT limit) and to -1.50 (KT limit). The new framework predicts values of x_{exp} consistent with published CCN activity of playa salts that tend to contain a substantial soluble fraction.

An important finding of this study is that the process of wet generation tends to generate hygroscopic particles that are not representative of the parent dust. Therefore,

published work showing an augmented CCN activity from wetting may be affected by an artifact induced by the wet generation method. The method, however, can still generate a less hydrophilic peak, with a size and degree of hydrophilicity similar to dry generated dust; this implies that the process of wetting and drying of dust particles may not irreversibly change its hydrophilicity. The wet generation method however can still be used to explore the dependence of x_{exp} on A_{FHH}, B_{FHH} and soluble volume fraction if the size-dependent composition of the particles generated can be measured, and will be the subject of future study.

4.8   Acknowledgements

4.9   References

Abdul-Razzak, H. and Ghan, S. J.: A parameterization of aerosol activation: 2. Multiple aerosol types, J. Geophys. Res., 105(D6), 6837 – 6844, 2000.

Bougiatioti, A., Fountoukis, C., Kalivitis, N., Pandis, S. N., Nenes, A., and Mihalopoulos, N.: Cloud Condensation Nuclei Measurements in the Marine Boundary Layer of the Eastern Mediterranean: CCN closure and droplet growth kinetics, Atmos. Chem. Phys., 9, 7053 - 7066, 2009, http://www.atmos-chem-phys.net/9/7066/2009/.

Claquin, T., Schulz, M., and Balkanski, Y. J.: Modeling the mineralogy of atmospheric dust sources. J. Geophys. Res., 104(D18), 22,243–22,256, 1999.

DeMott, P. J., Sassen, K., Poellot, M. R., Baumgardner, D., Rogers, D. C., Brooks, S. D., Prenni, A. J., and Kreidenweis, S. M.: African dust aerosols as atmospheric ice nuclei, Geophys. Res. Lett., 30(14), 1732, doi:10.1029/2003GL017410, 2003.

Farmer, V. C.: Mineralogical Society Monograph 4: The Infrared Spectra of Minerals, pp 539, 1974.

Field, P. R., Möhler, O., Connolly, P., Krämer, M., Cotton, R., Heymsfield, A. J., Saathoff, H., and Schnaiter, M.: Some ice nucleation characteristics of Asian and Saharan desert dust, Atmos. Chem. Phys., 6, 2991 - 3006, 2006, http://www.atmos-chem-phys.net/6/2991/2006/.

Fountoukis, C., and Nenes, A.: ISORROPIA II: a computationally efficient aerosol thermodynamic equilibrium model for K^+, Ca^{2+}, Mg^{2+}, NH_4^+, Na^+, SO_4^{2-}, NO_3^-, Cl^-, H_2O aerosols, Atmos. Chem. Phys., 7, 4639 - 4659, 2007, http://www.atmos-chem-phys.net/7/4639/2007/.

Gibson, E. R., Hudson, P. K., and Grassian, V. H.: Aerosol chemistry and climate: Laboratory studies of carbonate component of mineral dust and its reaction products, Geophys. Res. Lett., 33, L13811, doi:10.1029/2006GL026386, 2006.

Gustafsson, R. J., Orlov, A., Badger, C. L., Griffiths, P. T., Cox, R. A., and Lambert, R. M.: A comprehensive evaluation of water uptake on atmospherically relevant mineral surfaces: DRIFT spectroscopy, thermogravimetric analysis and aerosol growth measurements, Atmos. Chem. Phys., 5, 3415 – 3421, 2005, http://www.atmos-chem-phys.net/5/3415/2005/.

Hatch, C. D., Gierlus, K. M., Schuttlefield, J. D., and Grassian, V. H.: Water adsorption and cloud condensation nuclei activity of calcite and calcite coated with model humic and fulvic acids, Atmos. Environ., 42, 5672 - 5684, 2008.

Herich, H., Tritscher, T., Wiacek, A., Gysel, M., Weingartner, E., Lohmann, U., Baltensperger, U., and Cziczo, D. J.: Water uptake of clay and desert dust aerosol particles at sub- and supersaturated water vapor conditions, Phys. Chem. Chem. Phys., 11, 7804 - 7809, doi:10.1039/b901585j, 2009.

Hudson, P., Gibson, E. R., Young, M. A., Kleiber, P. D., and Grassian, V. H.: Coupled infrared extinction and size distribution measurements for several clay components of mineral dust aerosol, J. Geophys. Res., 113, D01201, doi:10.1029/2007JD008791, 2008.

Kandler, K., Schütz, L., Deutscher, C., Ebert, M., Hofmann, H., Jäckel, S., Jaenicke, R., Knippertz, P., Lieke, M., Massling, A., Petzold, A., Schladitz, A., Weinzierl, B., Wiedensohler, A., Zorn, S., and Weinbruch, S.: Size distribution, mass concentration, chemical and mineralogical composition and derived optical parameters of the boundary layer aerosol at Tinfou, Morocco, during SAMUM 2006, Tellus , 61B, 32 - 50, doi: 10.1111/j.1600-0889.2008.00385.x, 2009.

Kelly, J. T., Chuang, C. C., and Wexler, A. S.: Influence of dust composition on cloud droplet formation, Atmos. Environ., 41, 2904 - 2916, 2007.

Koehler, K. A., Kreidenweis, S. M., DeMott, P. J., Petters, M. D., Prenni, A. J., and Carrico, C. M.: Hygroscopicity and cloud droplet activation of mineral dust aerosol, Geophys. Res. Lett., 36, L08805, doi:10.1029/2009GL037348, 2009.

Köhler, H., The nucleus in and the growth of hygroscopic droplets, Trans. Faraday Soc., 32(2), 1152 - 1161, 1936.

Kumar, P., Sokolik, I. N., and Nenes, A.: Parameterization of cloud droplet formation for global and regional models: including adsorption activation from insoluble CCN, Atmos. Chem. Phys., 9, 2517 - 2532, 2009a, http://www.atmos-chem-phys.net/9/2517/2009/.

Kumar, P., Nenes, A., and Sokolik, I. N.: Importance of adsorption for CCN activity and hygroscopic properties of mineral dust aerosol, Geophys. Res. Lett., 36, L24804, doi:10.1029/2009GL040827, 2009b.

Kumar, P., Sokolik, I. N., and Nenes, A.: Measurements of cloud condensation nuclei activity and droplet activation kinetics of fresh unprocessed regional dust samples and minerals, Atmos. Chem. Phys. Discuss., 10, 31039 – 31081, 2010, www.atmos-chem-phys-discuss.net/10/31039/2010/.

Lafon, S., Sokolik, I. N., Rajot, J. L., Caquineau, S., and Gaudichet, A.: Characterization of iron oxides in mineral dust aerosols: Implications to light absorption. J. Geophys. Res., 111, D21207, doi:10.1029/2005JD007016, 2006.

Lance, S., Medina, J., Smith, J. N., and Nenes, A.: Mapping the operation of the DMT continuous flow CCN counter, Aerosol Sci. Tech., 40, 242 – 254, 2006.

Levin, Z., and Cotton, W. R.: Aerosol Pollution Impact on Precipitation: A scientific review, Springer Press., 2008

Levin, Z., Ganor, E., and Gladstein, V.: The effects of dust particles coated with sulfate on rain formation in the Eastern Mediterranean, J. Appl. Meteorol., 35, 1511 - 1523, 1996.

Möhler, O., Benz, S., Saathoff, H., Schnaiter, M., Wagner, R., Schneider, J., Walter, S., Ebert, V., and Wagner, S.: The effect of organic coating on the heterogeneous ice nucleation efficiency of mineral dust aerosols, Environ. Res. Lett., 3, 2008.

Moore, R., Nenes, A., and Medina, J.: Scanning Mobility CCN Analysis - A method for fast measurements of size resolved CCN distributions and activation kinetics, Aerosol Sci. Tech., 44, 861 - 871, 2010.

Ming, Y., Ramaswamy, V., Donner, L. J., and Phillips, V. T. J.: A new parameterization of cloud droplet activation applicable to general circulation models, J. Atmos. Sci., 63, 1348 – 1356, 2006.

Nenes, A. and Seinfeld, J. H.: Parameterization of cloud droplet formation in global climate models, J. Geophys. Res., 108(D14), 4415, doi:10.1029/2002JD002911, 2003.

Padró, L. T., and Nenes, A.: Cloud droplet activation: solubility revisited, Atmos. Chem. Phys. Discuss., 7, 2325 - 2355, 2007, http://www.atmos-chem-phys-discuss.net/7/2325/2007/.

Padró, L. T., Tkacik, D., Lathem, T., Hennigan, C., Sullivan, A. P., Weber, R. J., Huey, L. G., and Nenes, A.: Investigation of CCN relevant properties and droplet growth kinetics of water-soluble aerosol fraction in Mexico City, J. Geophys. Res, 115, D09204, doi:10.1029/2009JD013195, 2010.

Petters, M. D., and Kreidenweis, S. M.: A single parameter representation of hygroscopic growth and cloud condensation nucleus activity, Atmos. Chem. Phys., 7, 1961 - 1971, 2007, http://www.atmos-chem-phys.net/7/1961/2007/.

Pratt, K. A., et al.: Observation of playa salts as nuclei in orographic wave clouds, J. Geophys. Res., 115, D15301, doi:10.1029/2009JD013606, 2010.

Pruppacher, H. R., and Klett, J. D.: Microphysics of clouds and precipitation 2nd ed., Kluwer Academic Publishers, Boston, MA, 1997.

Radhi, M., Box, M. A., Box,G. P., Mitchell, R. M., Cohen, D. D., Stelcer, E., and Keywood, M. D.: Optical, physical and chemical characteristics of Australian Desert dust aerosols: results from a field experiment, Atmos. Chem. Phys., 10, 5925 - 5942, 2010, http://www.atmos-chem-phys.net/10/5925/2010/.

Raymond, T. M., and Pandis, S. N.: Cloud activation of single-component organic aerosol particles, J. Geophys. Res, 107, D24, 4787, doi:10.1029/2009JD002159, 2002.

Reheis, M. C.: Dust deposition downwind of Owens (Dry) Lake, 1991-1994— Preliminary findings, 102, D22, 25999 - 26008, 1997.

Roberts, G., and Nenes, A.: A continuous-flow streamwise thermal gradient CCN chamber for atmospheric measurements, Aerosol Sci. Tech., 39, 206 – 221, 2005.

Rosenfeld, D., Rudich, Y., and Lahav, R.: Desert dust suppressing precipitation: A possible desertification feedback loop, Proc. Natl. Acad. Sci. U.S.A., 98(11), 5975 - 5980, 2001.

Schuttlefield, J. D., Cox, D., and Grassian, V. H.: An investigation of water uptake on clays minerals using ATR-FTIR spectroscopy coupled with quartz crystal microbalance measurements, J. Geophys. Res., 112, D21303, doi:10.1029/2007JD008973, 2007.

Seinfeld, J. H., and Pandis, S. N.: Atmospheric Chemistry and Physics, John Wiley, New York, USA, 767 – 773, 2006.

Song, C. H., Maxwell-Meier, K., Weber, R. J., Kapustin, V., and Clarke, A.: Dust composition and mixing state inferred from airborne composition measurements during ACE-Asia C130 Flight #6, Atmos. Environ., 39, 359 - 369, 2005.

Sorjamaa, R. and Laaksonen, A.: The effect of H_2O adsorption on cloud drop activation of insoluble particles: a theoretical framework, Atmos. Chem. Phys., 7, 6175 - 6180, 2007, http://www.atmos-chem-phys.net/9/6175/2007/.

Sullivan, R. C., Moore, M. J. K., Petters, M. D., Kreidenweis, S. M., Roberts, G. C., and Prather, K. A.: Effect of chemical mixing state on the hygroscopicity and cloud nucleation properties of calcium mineral dust particles, Atmos. Chem. Phys., 9, 3303 - 3316, 2009, http://www.atmos-chem-phys.net/9/3303/2009/.

Sullivan, R. C., Moore, M. J. K., Petters, M. D., Kreidenweis, S. M., Qafoku, O., Laskin, A., Roberts, G. C., and Prather, K. A.: Impact of particle generation method on the apparent hygroscopicity of insoluble mineral particles, Aerosol Sci. Tech., 44, 10, 830 - 846, 2010.

Twohy, C. H., Kreidenweis, S. M., Eidhammer, T., Browell, E. V., Heymsfield, A. J., Bansemer, A. R., Anderson, B. E., Chen, G., Ismail, S., DeMott, P. J., and Van Den Heever, S. C.: Saharan dust particles nucleate droplets in eastern Atlantic clouds, Geophys. Res. Lett., 36, L01807, 1 - 6, doi:10.1029/2008GL035846, 2009.

Usher, C. R., Michel, A. E., and Grassian, V. H.: Reactions on mineral dust, Chem. Rev., 103, 4883 – 4939, 2003.

Vlasenko, A., Sjögren, S., Weingartner, E., Gäggeler, H. W., and Ammann, M.: Generation of Submicron Arizona Test Dust Aerosol: Chemical and Hygroscopic Properties, Aerosol Sci. Tech., 39 (5), 452 - 460, 2005.452 - 460, 2005.

CHAPTER 5

PARAMETERIZATION OF CLOUD DROPLET FORMATION FOR GLOBAL AND REGIONAL MODELS: INCLUDING ADSORPTION ACTIVATION FROM INSOLUBLE CCN

5.1   Abstract

Dust and black carbon aerosol have long been known to have potentially important and diverse impacts on cloud droplet formation. Most studies to date focus on the soluble fraction of these particles, and overlook interactions of the insoluble fraction with water vapor (even if known to be hydrophilic). To address this gap, we developed a new parameterization framework that considers cloud droplet formation within an ascending air parcel containing insoluble (but wettable) particles externally mixed with aerosol containing an appreciable soluble fraction. Activation of particles with a soluble fraction is described through well-established Köhler theory, while the activation of hydrophilic insoluble particles is treated by "adsorption-activation" theory. In the latter, water vapor is adsorbed onto insoluble particles, the activity of which is described by a multilayer Frenkel-Halsey-Hill (FHH) adsorption isotherm modified to account for particle curvature. We further develop FHH activation theory and find i) combinations of the adsorption parameters A_{FHH}, B_{FHH} which yields atmospherically-relevant behavior, and, ii) express activation properties (critical supersaturation) that follow a simple power law with respect to dry particle diameter.

Parameterization formulations are developed for sectional and lognormal aerosol size distribution functions. The new parameterization is tested by comparing the parameterized cloud droplet number concentration against predictions with a detailed numerical cloud model, considering a wide range of particle populations, cloud updraft conditions, water vapor condensation coefficient and FHH adsorption isotherm characteristics. The agreement between parameterization and parcel model is excellent, with an average error of 10% and $R^2 \sim 0.98$. A preliminary sensitivity study suggests that the sublinear response of droplet number to Köhler particle concentration is not as strong for FHH particles.

Citation: Kumar, P., Sokolik, I. N., and Nenes, A.: Parameterization of cloud droplet formation for global and regional models: including adsorption activation from insoluble CCN, Atmos. Chem. Phys., 9, 2517 - 2532, 2009, www.atmos-chem-phys.net/9/2517/2009/.

5.2 Introduction

It is well established that atmospheric aerosols are often hydrophilic, and can serve as Cloud Condensation Nuclei (CCN), upon which cloud droplets are formed through the process of activation. Changes in CCN concentration affect the radiative properties of clouds, known as the "cloud albedo" or "Twomey" effect of aerosols (Twomey, 1974). The enhanced number of droplets is often accompanied by a reduction in their size, there by affecting cloud precipitation efficiency. This may result in increased cloudiness, which gives rise to the so called "cloud lifetime" or "Albrecht" effect of aerosols (Albrecht, 1989). Combined, these "aerosol indirect effects" on clouds

perturb the Earth's radiative budget and constitute one of the most uncertain components of anthropogenic climate change (Forster et al., IPCC, 2007).

Cloud droplet activation is the direct microphysical link between aerosols and clouds, and is at the heart of the indirect effect (Nenes and Seinfeld, 2003). Droplet activation in atmospheric models is calculated from parameterizations whose sophistication ranges from empirical correlations (relating aerosol mass or number concentration to cloud droplet number concentration) to physically-based prognostic formulations (e.g., Feingold and Heymsfield, 1992; Boucher and Lohmann, 1995; Gultepe and Isaac, 1996; Abdul-Razzak et al., 1998; Abdul-Razzak and Ghan, 2000; Cohard et al., 2000; Nenes and Seinfeld, 2003, Fountoukis and Nenes, 2005; Ming et al., 2006; Barahona and Nenes, 2007). All physically-based parameterizations developed to date rely on Köhler theory (Köhler, 1936), which considers curvature and solute effects on the equilibrium vapor pressure of a growing droplet. Most often, this equilibrium curve exhibits a maximum in supersaturation known as critical supersaturation, s_c, at a critical wet droplet diameter, D_c. According to Köhler theory, when a particle is exposed to supersaturation above s_c for long enough to exceed D_c, it is in unstable equilibrium and can nucleate a cloud droplet. For atmospherically-relevant conditions of cloud formation, it is sufficient to say that a particle acts as a CCN when is exposed to supersaturation above s_c (Nenes et al., 2001).

Insoluble atmospheric particles, like mineral dust and soot, can also act as efficient cloud condensation nuclei (e.g., Seisel et al., 2005), if they acquire some amount of deliquescent material, such as $(NH_4)_2SO_4$. The threshold of nucleation substantially decreases when water interacts (adsorbs) onto slightly soluble particles giving rise to the

process of adsorption activation (Sorjamaa and Laaksonen, 2007; Henson, 2007). Henson (2007) showed that a number of existing adsorption models (e.g., Fletcher, 1958; Wexler and Ge, 1998) for slightly soluble and insoluble particles can be successfully applied to represent droplet formation from adsorption activation. Similarly, Sorjamaa and Laaksonen (2007) used the Frenkel-Halsey-Hill (FHH) multilayer physical adsorption model to describe water uptake as a function of relative humidity (i.e., water activity) and applied the theory to describe the activation of perfectly wettable and insoluble hydrophilic CCN. As with Köhler theory, adsorption of water can result in equilibrium curves with a critical supersaturation of atmospheric relevance (Henson, 2007; Sorjamaa and Laaksonen, 2007).

To date, there is no parameterization framework that can concurrently treat the competition of insoluble and soluble CCN in the cloud droplet formation process; this gap is addressed in this study. This new activation parameterization builds upon the frameworks of Nenes and Seinfeld (2003), Fountoukis and Nenes (2005) and Barahona and Nenes (2007) to include the effects of adsorption activation, based on the formulation of Sorjamaa and Laaksonen (2007). The insoluble particles (referred to in this study as FHH particles) are considered to be externally mixed with hydrophilic deliquescent particles (referred to as Köhler particles) all of which compete for water vapor in a cloud updraft, thus allowing for the comprehensive treatment of kinetic limitations, chemical effects (i.e., slow water vapor condensation and surface tension depression) and entrainment effects on cloud droplet formation.

A brief discussion of FHH adsorption activation and Köhler theory is given in section 5.3. Section 5.4 describes the formulation of the new parameterization for

sectional and lognormal representation of the aerosol size distribution. An evaluation of the parameterization by comparing against predictions of a numerical cloud parcel model is done in section 5.5. Section 5.6 provides insight into the competition effects of FHH with Köhler particles. Finally, section 5.7 summarizes the major achievements of this chapter.

5.3   Theory of Adsorption Activation

A number of adsorption isotherm models exist to describe the process of physisorption of gas-phase species onto solid surfaces, such as Langmuir (Langmuir, 1916), BET (Brunauer, Emmet and Taylor) (Brunauer et al., 1938), and FHH (Frenkel, Halsey and Hill) (e.g., Lowell et al., 2004) isotherms. The Langmuir isotherm is the first and perhaps the most studied adsorption model developed until to date. However, it is limited to describing the adsorption of a monolayer of water vapor, and hence it is not applicable to atmospheric particles (where the vapor pressure is high enough to form multiple layers of water vapor adsorbed onto the CCN). BET and FHH adsorption isotherm models were developed to treat multilayer adsorption, and have been explored to study adsorption activation, or, the process of cloud droplet formation from adsorption of water vapor onto insoluble particles (e.g., Henson, 2007; Sorjamaa and Laaksonen, 2007).

5.3.1 *FHH Adsorption Theory*

FHH adsorption theory (Sorjamaa and Laaksonen, 2007) describes the process of adsorption activation in which the water vapor saturation ratio, S, of an insoluble particle in equilibrium with surrounding water vapor can be expressed as

$$S = \alpha_w \exp\left(\frac{4\sigma_w M_w}{RT\rho_w D_p}\right) \qquad [5.1]$$

where α_w is the activity of the water in the particle, σ_w is the surface tension at the particle-gas interface, M_w is the molar mass of water, R is the universal gas constant, T is the temperature, ρ_w is the density of water, and D_p is the equivalent particle diameter. The exponential in Eq. (5.1) is commonly referred to as the curvature, or Kelvin effect. For irregularly shaped insoluble particles (such as dust), curvature along the surface varies, hence it cannot be described in terms of a single characteristic particle diameter. In this study, we consider only the average curvature, as expressed by the equivalent particle diameter. Furthermore, the insoluble particle surface is completely wettable (i.e., the contact angle between the particle and water is zero), resulting in a uniform distribution of water molecules over the particle surface. In the limit of a monolayer, water forms a contiguous film, and its activity, α_w, can be written as $\alpha_w = \exp(-A_{FHH}\Theta^{-B_{FHH}})$ (Sorjamaa and Laaksonen, 2007); substitution in Eq. (5.1) then gives

$$S = \exp\left(\frac{4\sigma_w M_w}{RT\rho_w D_p}\right)\exp(-A_{FHH}\Theta^{-B_{FHH}}) \qquad [5.2]$$

where A_{FHH}, B_{FHH} are empirical constants, and Θ is the surface coverage (defined as the number of adsorbed water molecules divided by the number of molecules in a monolayer, i.e., the number of adsorbed layers of water). A_{FHH} characterizes interactions of adsorbed

molecules with the aerosol surface and adjacent adsorbate molecules (i.e., those in the first monolayer). B_{FHH} characterizes the attraction between the aerosol surface and the adsorbate in subsequent layers; the smaller the value of B_{FHH}, the greater the distance at which the attractive forces act (Sorjamaa and Laaksonen, 2007). A_{FHH} and B_{FHH} are compound-specific and determined experimentally. A_{FHH} has been experimentally found to range from 0.1 to 3.0 while B_{FHH} ranges from 0.5 to 3.0 (Sorjamaa and Laaksonen, 2007).

Equation (5.2) expresses S in terms of D_p and Θ. However, Θ can be expressed in terms of D_{dry} and D_p as (Sorjamaa and Laaksonen, 2007)

$$\Theta = \frac{D_p - D_{dry}}{2 D_{H_2O}} \qquad [5.3]$$

where D_{dry} is the dry particle diameter and D_{H_2O} = 2.75 Å is the diameter of a water molecule adsorbed on the particle surface. Substituting Eq. (5.3) into Eq. (5.2), expressed in terms of equilibrium supersaturation, $s = S - 1$, gives an equation that depends only on D_p,

$$s = \exp\left[\frac{4\sigma_w M_w}{RT\rho_w D_p} - A_{FHH} \left(\frac{D_p - D_{dry}}{2 D_{H_2O}} \right)^{-B_{FHH}} \right] - 1$$

$$\cong \frac{4\sigma_w M_w}{RT\rho_w D_p} - A_{FHH} \left(\frac{D_p - D_{dry}}{2 D_{H_2O}} \right)^{-B_{FHH}} \qquad [5.4]$$

The activation behavior of particles following FHH theory can be rationalized by analyzing the derivative of s with respect to D_p

$$\frac{ds}{dD_p} = \left(-\frac{4\sigma_w M_w}{RT\rho_w D_p^2} \right) + \left(\frac{A_{FHH} B_{FHH}}{2 D_{H_2O}} \left(\frac{D_p - D_{dry}}{2 D_{H_2O}} \right)^{-B_{FHH}-1} \right) \qquad [5.5]$$

where the first and second terms in the right hand side of Eq. (5.5) correspond to the contribution due to Kelvin and adsorption effect, respectively. If B_{FHH} is large enough, both terms in Eq. (5.5) can become equal for a characteristic wet diameter, D_c, so that

$\left. \dfrac{ds}{dD_p} \right|_{D_p = D_c} = 0$. Under such conditions, FHH particles behave much like those following

Köhler theory, with a characteristic maximum s (the critical supersaturation, s_c) at the

critical wet diameter D_c. s_c is determined by solving $\dfrac{ds}{dD_p} = 0$ so Eq. (5.5) becomes

$$\left(-\frac{4\sigma_w M_w}{RT\rho_w D_c^2} \right) + \left(\frac{A_{FHH} B_{FHH}}{2D_{H_2O}} \left(\frac{D_c - D_{dry}}{2D_{H_2O}} \right)^{-B_{FHH}-1} \right) = 0 \qquad [5.6]$$

Numerically solving Eq. (5.6) gives D_c, which can then be substituted in Eq. (5.4) to obtain s_c. Figure 5.1a presents equilibrium curves for combinations of A_{FHH}, B_{FHH} that exhibit a maximum s_c and its corresponding D_c.

If B_{FHH} is small enough so that left hand side of Eq. (5.6) is larger than zero for all values of D_p, then the derivative of the equilibrium curve is dominated by the adsorption term and the particle either (a) is always in stable equilibrium with the environment, i.e., the particles never activate into cloud droplets, or, (b) spontaneously activate at RH less than 100% (depending on the asymptotic value of s at very large D_p). Figure 5.1b presents examples of such curves, the equilibrium supersaturation does not exhibit a maximum, but rather asymptotes to a value, s_∞, less than zero. If the ambient relative humidity is such that $s < s_\infty$, the particle is always in stable equilibrium with the environment. Conversely, if $s > s_\infty$, the particle spontaneously activates into a cloud droplet (even for a relative humidity less than 100%). Such phenomena (i.e. deliquescent

clays) have not been observed hence this region of parameter space is considered irrelevant for the atmosphere.
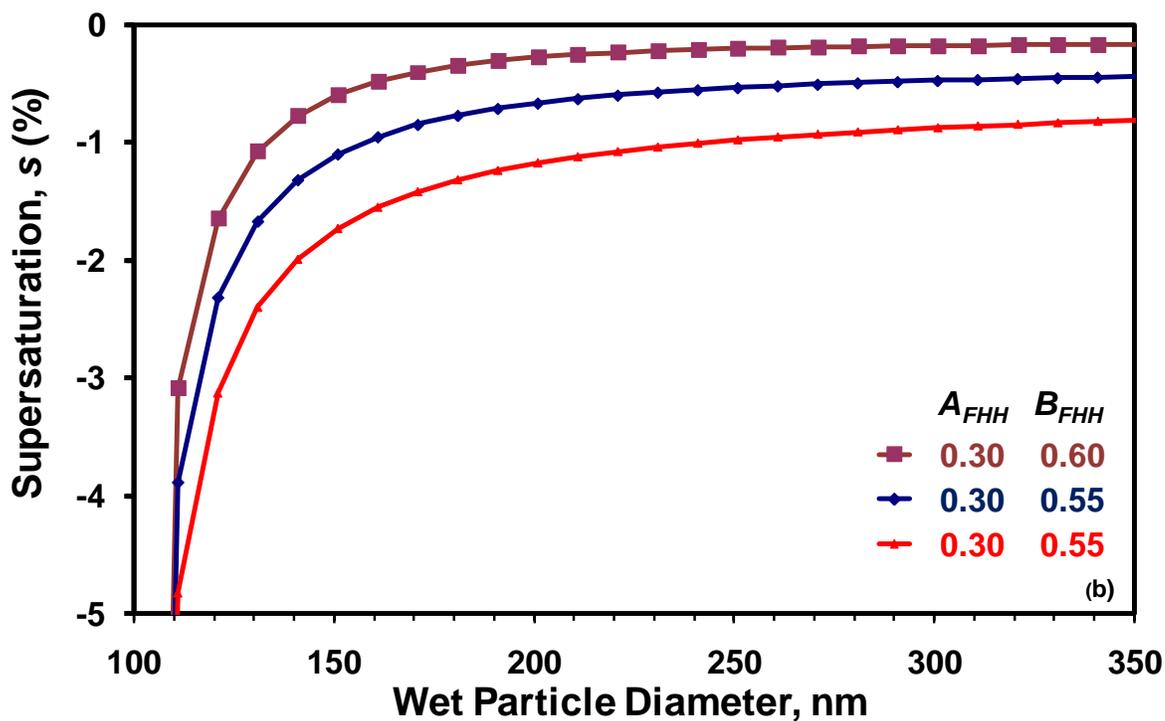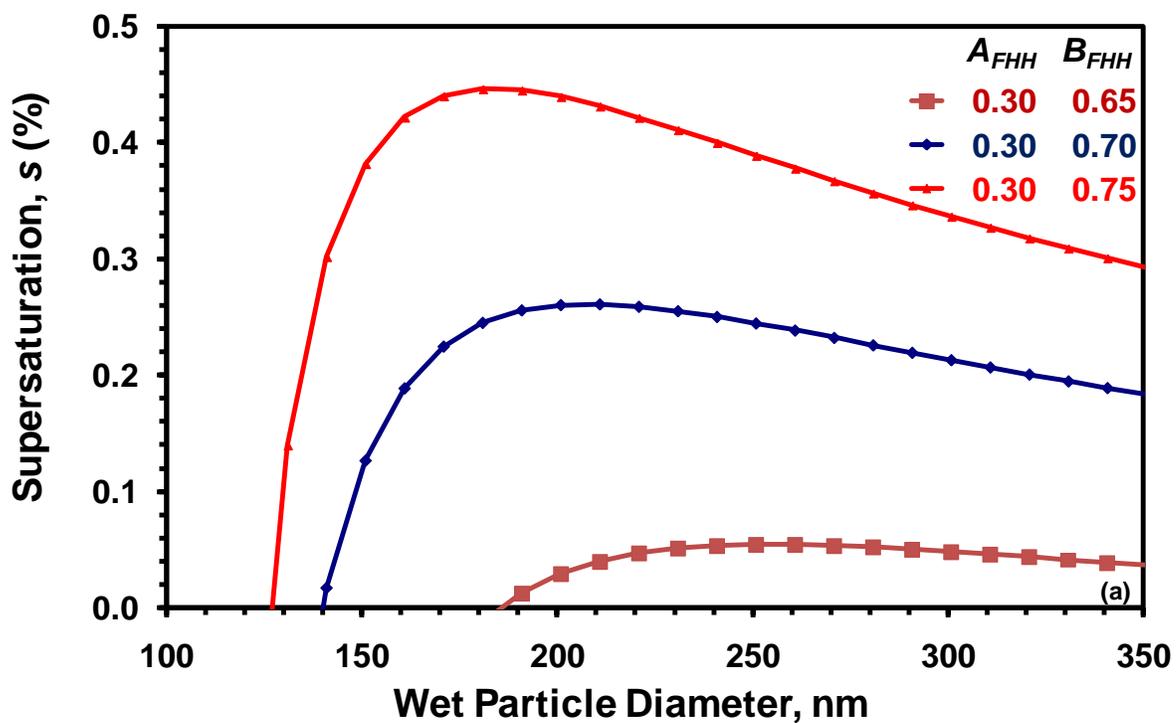
Figure 5.1: Equilibrium curves for a FHH-type particle of 100 nm dry diameter, and combinations of A_{FHH}, B_{FHH} that represent **(a)** atmospherically-relevant behavior, and, **(b)** spontaneous activation (for RH < 100%).

5.3.2 Activation characteristics of Köhler and FHH Particles

The activation of particles containing soluble material is described by Köhler theory (Köhler, 1936; Seinfeld and Pandis, 2006) in which equilibrium supersaturation is given by

$$s = \frac{A}{D_p} - \frac{B}{D_p^3}$$ [5.7]

where $A = \dfrac{4M_w\sigma_w}{RT\rho_w}$ and $B = \dfrac{6n_sM_w\nu}{\pi\rho_w}$. Here n_s are the moles of solute in the particle and ν is the effective van't Hoff factor of the solute. The s_c and D_c for Köhler particles are then given by

$$s_c = \left(\frac{4A^3}{27B}\right)^{1/2}$$ [5.8]

$$D_c = \left(\frac{3B}{A}\right)^{1/2}$$ [5.9]

The above analytical expressions for s_c and D_c neglect the insoluble CCN fraction in the denominator of the second term on the right hand side of Eq. (5.7), also known as "Raoult" term and should not be used for particles with very small soluble fractions (e.g., Khvorostyanov and Curry, 2007).

For FHH particles, it is important to know of the range of A_{FHH} and B_{FHH} which give equilibrium curves with a maximum (like in Fig. 5.1a) and therefore are potentially relevant for the atmosphere. This is done by determining the range of A_{FHH}, B_{FHH}, and D_{dry} for which a solution to Eq. (5.6) exists, for the reported range for A_{FHH} and B_{FHH} (0.1 - 3.0 and 0.5 - 3.0, respectively; Sorjamaa and Laaksonen, 2007), and, D_{dry} between 0.03

μm and 150 μm. When a solution for D_c is found, we normalize it with D_{dry} to express the growth required for FHH particles to activate into cloud droplets.

Figure 5.2 shows contour plots of D_c/D_{dry} for the D_{dry} equal to 0.25 μm and 20 μm. Depending on the existence and value of D_c/D_{dry}, each plot of Fig. 5.2 can be divided into three separate regions: "Region 1" (area filled with purple color, corresponding to $B_{FHH} < 0.6 - 0.7$ for any value of A_{FHH}), where equilibrium curves are like in Fig. 5.1b and a D_c could not be found. "Region 2" (corresponding to $0.7 < B_{FHH} < 1.0$), where equilibrium curves resemble those of Fig. 5.1a, for $D_c/D_{dry} > 2$. Finally, "Region 3" (area filled with red color, corresponding to $B_{FHH} > 1.0$), where equilibrium curves resemble those in Fig. 5.1a, and $D_c/D_{dry} < 2$. Figures 5.2a and 5.2b, are very similar, despite that they correspond to particles with two orders of magnitude difference in dry particle size. This suggests that D_c/D_{dry} has a weak dependence on D_{dry}. Furthermore, most of the atmospherically-relevant combinations of A_{FHH} and B_{FHH} lie in "Region 3", the value of D_c/D_{dry} lies between 1 - 2. Given that the size of activated droplets at the cloud parcel s_{max} are typically much larger than D_{dry} (Nenes and Seinfeld, 2003), this implies $D_p \gg D_c$ for FHH particles at s_{max}. This is an important observation that facilitates the computation of the condensation rate of water, required in the development of the droplet activation parameterization (Section 5.7). Another implication is that the amount of water required to activate FHH particles is often much smaller than for Köhler particles of same D_{dry} (Table 5.1) or same s_c (not shown).

The most appropriate activation theory for a particle depends on the relative importance of adsorption vs. solute on water activity. The theory that gives the lowest s_c

will, in general, be the most appropriate. A quantitative evaluation requires an extensive set of simulations and will be the focus of a future study.

Table 5.1: Comparison of critical to dry particle diameter for FHH and Köhler particles

D_{dry} (μm)	$\left(D_c / D_{dry}\right)_{FHH^a}$	$\left(D_c / D_{dry}\right)_{Kohler^b}$
0.01	1.81	3.13
0.025	1.86	4.80
0.05	1.91	7.00
0.075	1.93	8.53
1.00	2.13	31.31
2.50	2.23	49.48
5.00	2.30	70.01
7.50	2.32	85.75
10.00	2.38	99.02
15.00	2.44	121.27
20.00	2.48	140.03

[a] D_c calculated from Equation (5.6), $A_{FHH} = 0.68$, $B_{FHH} = 0.93$, $D_{H_2O} = 2.75$ Å

[b] D_c calculated from Equation (8b), $v = 3$, $\sigma_w = 0.072$ N m^{-1}, $M_w = 18.0$ g mol^{-1}, $M_{(NH_4)_2SO_4} = 132.14$ g mol^{-1}, $\rho_w = 1000$ kg m^{-3}

The results are provided for $(NH_4)_2SO_4$
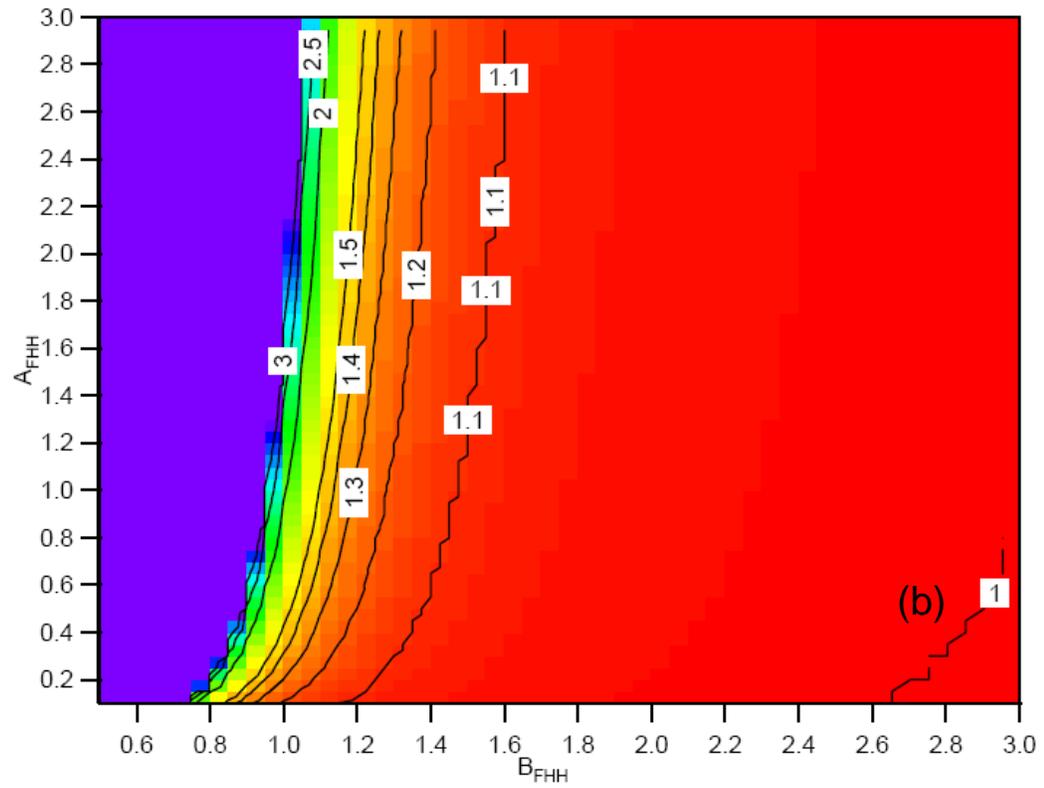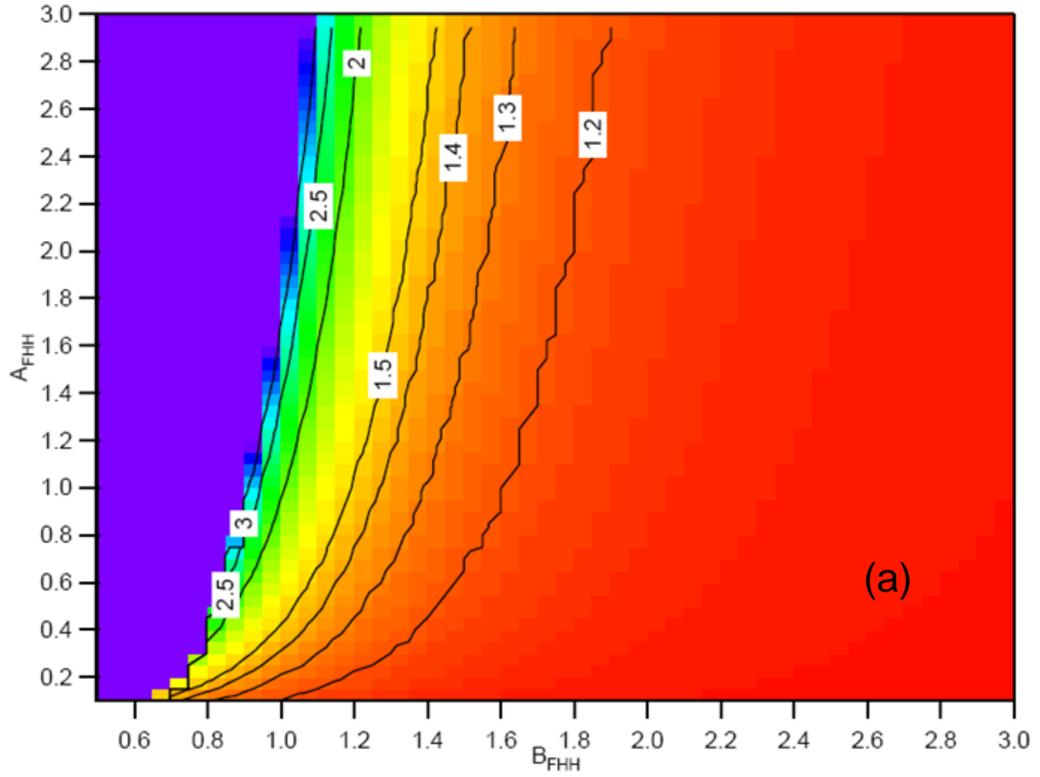
Figure 5.2: D_c/D_{dry} contours as a function of A_{FHH} and B_{FHH} for **(a)** $D_{dry} = 0.25$ μm and **(b)** $D_{dry} = 20$ μm.

5.4   Formulation of Activation Parameterization

The aerosol activation parameterization is based on the cloud parcel framework, in which a parcel of air containing an external mixture of Köhler and FHH particles is lifted and cooled. When supersaturation develops, droplets begin forming (by the process of activation) up to the point where supersaturation generation from cooling balances depletion from condensation water; this corresponds to the point of maximum parcel supersaturation, s_{max}, and is where droplet activation ceases. If the CCN spectrum (i.e., the number of CCN as a function of ambient supersaturation) and s_{max} are known, the droplet number, N_d, in the parcel can be computed as the number of CCN that activate at s_{max} (Nenes et al., 2001). The new parameterization provides a formulation to determine both s_{max} and N_d. Since sectional and lognormal representations of the aerosol particle size distribution are most frequently used in the models, formulations are developed for both.

5.4.1   Sectional Representation of CCN Spectrum

The sectional representation uses discrete size classes (bins or sections) for the aerosol distribution. Each section can have its own chemical composition. If the aerosol mixture is composed of k populations (i.e., aerosol types), then a separate binning is assigned to each type. The cumulative size distribution is then determined by summing over all the populations (Nenes and Seinfeld, 2003)

$$F^d(d) = \sum_{l=1}^{k} \int_0^d n_l^d(D_p') d(D_p') = \sum_{l=1}^{k} \left[\sum_{j=1}^{m(l)-1} N_{j,l} + N_{m(l),l} \left(\frac{d - D_{p,m(l)-1}^l}{D_{p,m(l)}^l - D_{p,m(l)-1}^l} \right) \right] \qquad [5.10]$$

where m is the section of population l that contains particles of size d with bin size limits $D_{p,m(l)-1}^l$ and $D_{p,m(l)}^l$, and $N_{m(l),l}$ is the aerosol number concentration of section m.

The aerosol critical supersaturation distribution function, $n_l^s(s)$, is then determined by mapping the aerosol particle size distribution onto supersaturation coordinates (Nenes and Seinfeld, 2003),

$$n_l^s(s) = \frac{dN}{ds} = \sum_{l=1}^{k} \frac{N_{i(l),l}}{s_{c,i(l)} - s_{c,i(l)-1}}, \qquad s_{c,i(l)-1} \leq s \leq s_{c,i(l)} \tag{5.11}$$

where $s_{c,i(l)}$ and $s_{c,i(l)-1}$ are the critical supersaturations corresponding to the boundaries of section i and population l, and $N_{i(l),l}$ is the concentration of CCN between $s_{c,i(l)}$ and $s_{c,i(l)+1}$. The CCN spectrum, $F^s(s)$, is then obtained by integration of $n^s(s')$ from $s' = 0$ to $s' = s$:

$$F^s(s) = \sum_{l=1}^{k} \int_0^s n_l^s(s') ds' = \sum_{l=1}^{k} \left[\sum_{j=1}^{i(l)-1} N_{j,l} + N_{i(l),l} \left(\frac{s - s_{c,i(l)-1}^l}{s_{c,i(l)}^l - s_{c,i(l)-1}^l} \right) \right] \tag{5.12}$$

The relationship between $s_{c,i(l)}^l$ and $d_{p,m(l)}^l$ depends on the theory used for describing activation. For Köhler particles, Eq. (5.8) is used, while for FHH particles, the procedure outlined in section 5.3.1 is used.

5.4.2 Lognormal Representation of CCN Spectrum

A lognormal distribution is often expressed as sum of several lognormal functions (or "modes")

$$\frac{dN}{d \ln D_{dry}} = \sum_{i=1}^{n_m} \frac{N_i}{\sqrt{2\pi} \ln \sigma_i} \exp \left[-\frac{\ln^2 (D_{dry} / D_{g,i})}{2 \ln^2 \sigma_i} \right] \tag{5.13}$$

where σ_i and $D_{g,i}$ are the geometric standard deviation and median diameter, respectively, for the ith lognormal mode, and n_m is the number of lognormal modes in the size distribution. Assuming each mode (or population) has uniform chemical composition, a

power law function can be used to express $D_{dry}/D_{g,i}$ in terms of a critical supersaturation ratio, $s/s_{g,i}$,

$$\frac{D_{dry}}{D_{g,i}} = \left[\frac{s}{s_{g,i}}\right]^{\frac{1}{x}}$$

[5.14]

where s and $s_{g,i}$ are critical supersaturations of CCN with dry diameter D_{dry} and $D_{g,i}$ respectively, and x is an exponent that depends on the activation theory used. For particles following Köhler theory, $x = -3/2$ (Fountoukis and Nenes, 2005), while for FHH particles, x depends on A_{FHH} and B_{FHH} (see section 5.4.3).

The aerosol critical supersaturation distribution function, $n^s(s)$, can then be calculated as follows (Fountoukis and Nenes, 2005)

$$n^s(s) = \frac{dN}{ds} = -\frac{dN}{d\ln D_{dry}} \cdot \frac{d\ln D_{dry}}{ds}$$

[5.15]

where the negative sign in the right hand side of Eq. (5.15) has been applied to reflect that s_c decreases as D_{dry} increases. Implicit is the division of D_{dry} with 1 μm to nondimensionalize the argument in $\ln D_{dry}$. Substituting $D_{dry}/D_{g,i}$ from Eq. (5.14) into Eq. (5.13) gives

$$\frac{dN}{d\ln D_{dry}} = \sum_{i=1}^{n_m} \frac{N_i}{\sqrt{2\pi}\ln\sigma_i} \exp\left[-\frac{\ln^2(s/s_{g,i})^{\frac{1}{x}}}{2\ln^2\sigma_i}\right]$$

[5.16]

Differentiating Eq. (5.14) also gives

$$\frac{d\ln D_{dry}}{ds} = \frac{1}{xs}$$

[5.17]

Substituting Eq. (5.16) and Eq. (5.17) into Eq. (5.15) gives

$$n^s(s) = \sum_{i=1}^{n_m} -\frac{N_i}{\sqrt{2\pi} \ln \sigma_i} \frac{1}{xs} \exp\left[-\frac{\ln^2(s/s_{g,i})^{\frac{1}{x}}}{2\ln^2 \sigma_i}\right] \qquad [5.18]$$

The CCN spectrum, $F^s(s)$ is then obtained by integration of $n^s(s')$ from $s'= 0$ to $s'= s$

$$F^s(s) = \int_0^s n^s(s')ds' = \sum_{i=1}^{n_m} \frac{N_i}{2} erfc\left[-\frac{\ln(s_{g,i}/s)}{x\sqrt{2}\ln \sigma_i}\right] \qquad [5.19]$$

Equation (5.19) is the generalized form of a CCN spectrum for the lognormal particle size distribution, and the value of x encompasses the physics behind the aerosol-water vapor interaction (i.e., Köhler or FHH). For $x = -3/2$ (Köhler particles), Eq. (5.19) reduces to the formulation given by Fountoukis and Nenes, (2005)

$$F^s(s) = \int_0^s n^s(s')ds' = \sum_{i=1}^{n_m} \frac{N_i}{2} erfc\left[\frac{2\ln(s_{g,i}/s)}{3\sqrt{2}\ln \sigma_i}\right] \qquad [5.20]$$

5.4.3   Relating s_c with D_{dry} for FHH particles

In determining the value of x in Eq. (5.14) for FHH particles, we computed numerically the ratio of $s/s_{g,i}$ (using the procedure in section 5.3.1) for a wide range of $D_{g,i}$ (0.03 μm – 10 μm), D_{dry} (0.05 μm – 0.8 μm), and A_{FHH} and B_{FHH} (10 different combinations as shown in Table 5.2). As can be seen in Fig. 5.3, for given values of A_{FHH} and B_{FHH}, $s/s_{g,i}$ and $D_{dry}/D_{g,i}$, exhibit a power-law dependence. This dependence holds for the entire range of $D_{g,i}$ and D_{dry} considered. Power law fits to these calculations can then be used to describe x as a function of A_{FHH} and B_{FHH}, some results of which are shown in Fig. 5.4. For each A_{FHH}, x has a maximum at $B_{FHH} \sim$ 1.3 - 1.4, while x is always negative, varying from -1.2 to -0.8, depending on the value of A_{FHH}.

Multivariate least squares regression was performed on the activation data for all the conditions in Table 5.2 to determine an analytical relationship between x, A_{FHH} and B_{FHH}

$$x = A_{FHH}^{P_1} \left[\frac{P_2}{B_{FHH}^{P_3}} - \frac{P_4}{B_{FHH}^{P_5}} \right]$$ [5.21]

where P_1, P_2, P_3, P_4, P_5 are fitting parameters, and are given in Table 5.3. Equation (5.21) reproduces the fitted x data with a root mean square error of 0.00996 (Fig. 5.4).

Equation (5.14) suggests that s_c of FHH particles can be written as $s_c = C D_{dry}^x$; C is a constant that depends on A_{FHH} and B_{FHH} and is numerically equal to the critical supersaturation of a particle of a reference dry diameter. In this study, the reference diameter is taken to be 0.1 μm; C is then determined by computing s_c (Section 5.3.1) over a range of A_{FHH} and B_{FHH}. This is presented in Fig. 5.5 where C (shown as symbols) are plotted together with a multivariate least squares regression to the following function (shown as lines)

$$C = 10^{-8} A_{FHH}^k \left[\frac{-21}{B_{FHH}^l} + \frac{1.3}{B_{FHH}^m} + \frac{p}{B_{FHH}^n} \right]$$ [5.22]

where C is expressed in μm^{-x}, and k, l, m, n, p are fitting constants given in Table 5.4. Equation (5.22) reproduces the fitted data with a root mean square error of 0.034.

Table 5.2: Cloud formation conditions considered in this study

Property	Values
α_c	0.042, 0.06, 1.0
V (m s^{-1})	0.1, 0.5, 1.0, 5.0, 10.0
T_{parcel} (K)	298
P_{parcel} (mbar)	900
$(A_{\text{FHH}}, B_{\text{FHH}})$ combinations considered for FHH particles	(0.25 , 2.00) , (0.50 , 1.00) , (0.50 , 1.75) , (0.68 , 0.93) , (0.75 , 2.00) , (0.85 , 1.00) , (1.00 , 2.00) , (1.50 , 1.50) , (2.00 , 1.00) , (2.00 , 2.50)
Soluble Fraction properties	Species considered: $(NH_4)_2SO_4$ Soluble Mass Fraction, ε: 0.5 Density, ρ: 1760 kg m^{-3} Van't Hoff Factor, ν: 3 Molar Mass: 0.132 kg mol^{-1}
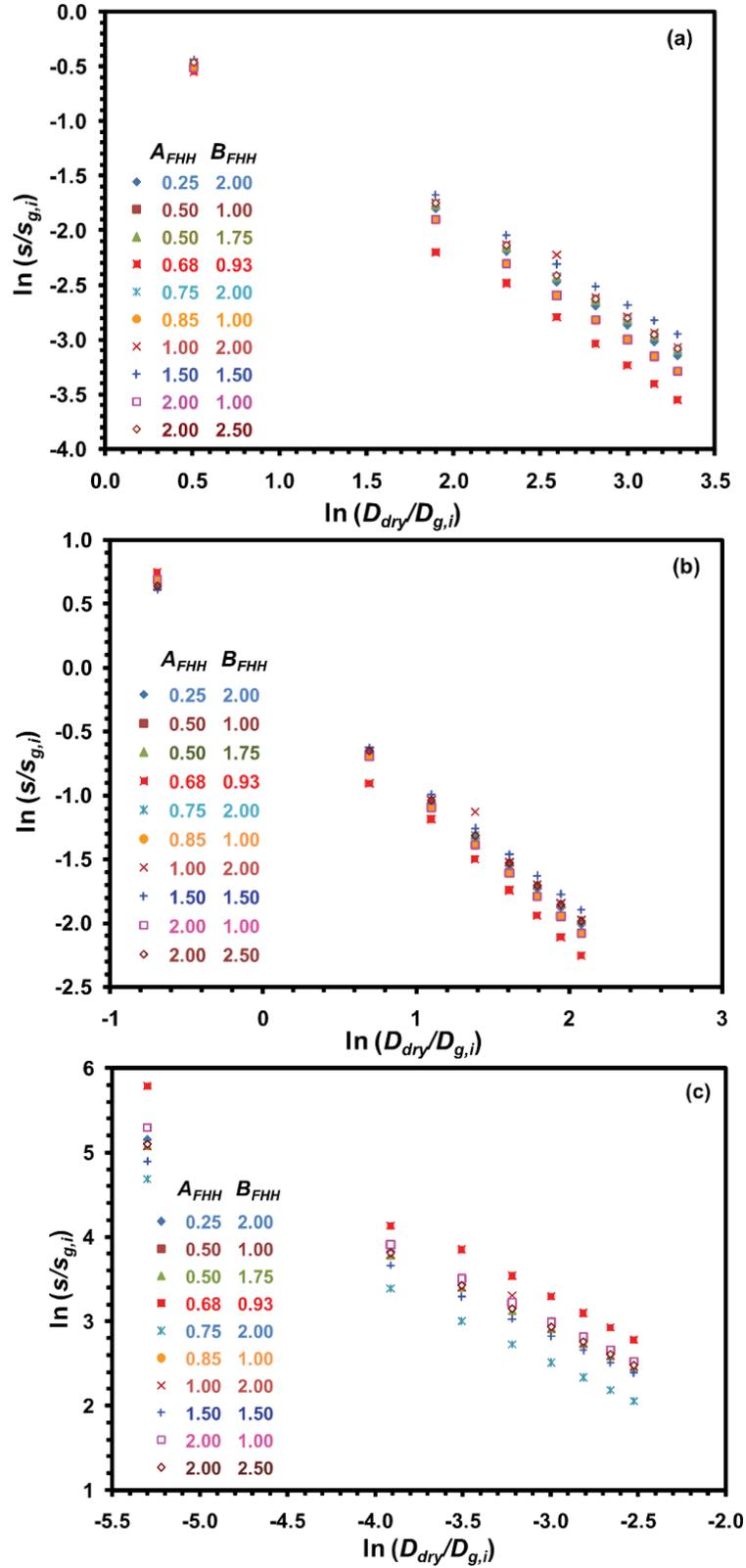
Figure 5.3: Plot of $\ln(s/s_{\mathrm{g,i}})$ versus $\ln(D_{\mathrm{dry}}/D_{\mathrm{g,i}})$ for **(a)** $D_{\mathrm{g,i}} = 0.03$ μm, **(b)** $D_{\mathrm{g,i}} = 0.1$ μm, and **(c)** $D_{\mathrm{g,i}} = 10.0$ μm.

160
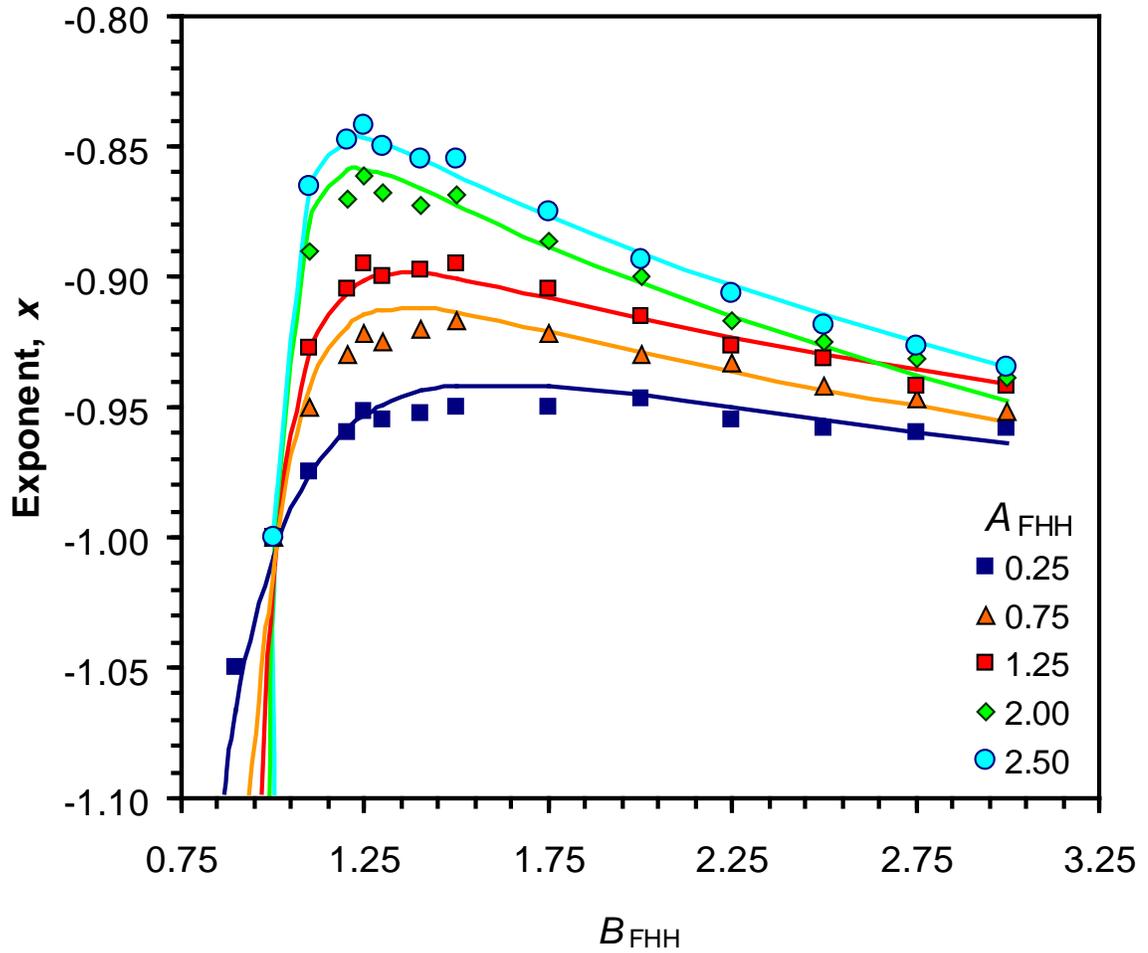
Figure 5.4: Exponent x for FHH particles as a function of B_{FHH} for different values of A_{FHH}. Shown are values computed using the procedure of section 5.3.1(symbols) and the functional fit (line), given by Eq. (5.21).

Table 5.3: Fitting parameters in Eq. (5.21)

A_{FHH}	P_1	P_2	P_3	P_4	P_5
$A_{FHH} \le 0.5$	-0.01061	-0.101038	4.6382	0.89161	-0.05708
$0.5 < A_{FHH} \le 1.5$	-0.02848	-0.124812	9.4907	0.87878	-0.06849
$1.5 < A_{FHH}$	-0.05994	-0.185129	16.2757	0.86681	-0.11858
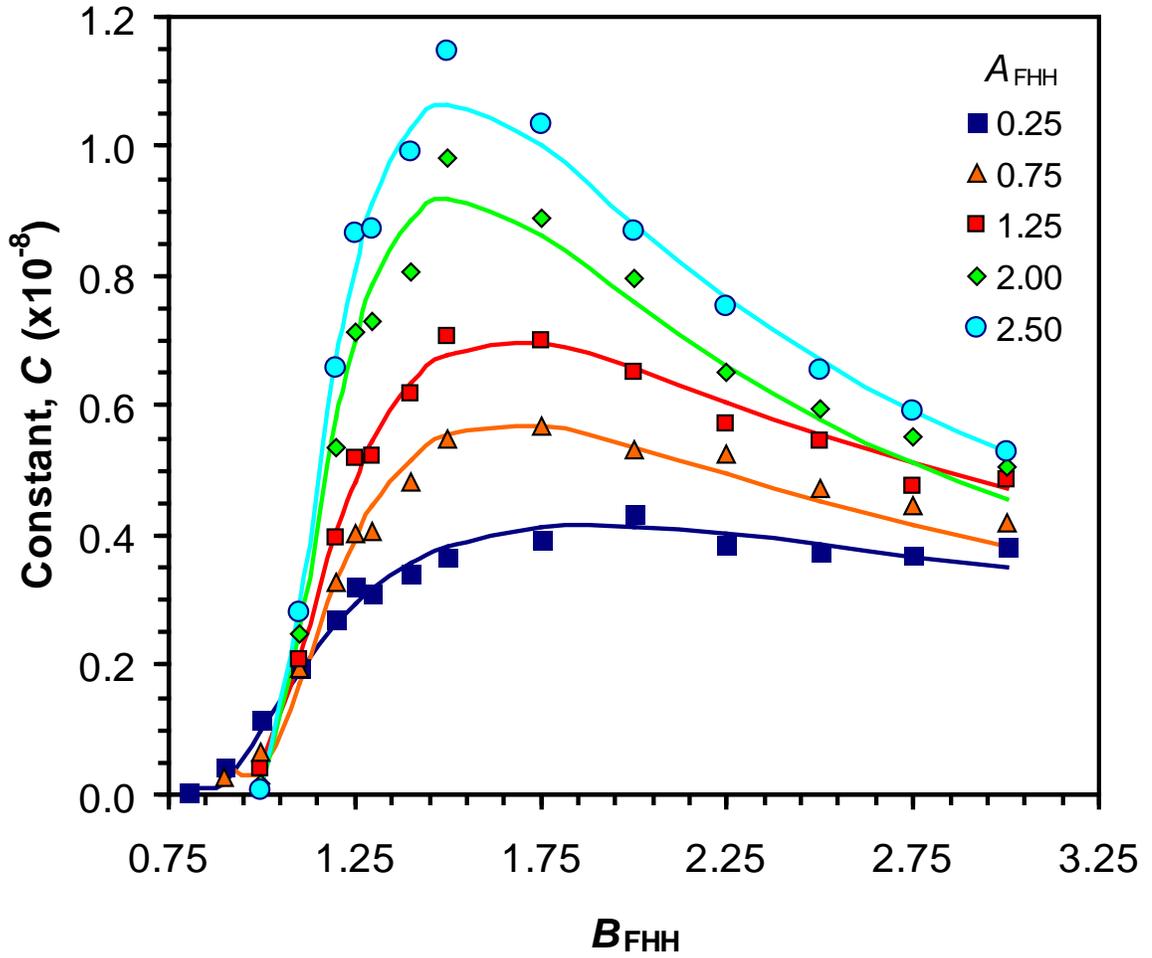
Figure 5.5: Constant C (μm^{-x}), which relates s_c of FHH particles to D_{dry} as $s_c = CD_{dry}^x$. C is presented for the atmospherically-relevant range of B_{FHH} and A_{FHH}; shown are calculations using the procedure of section 5.4.3 (symbols) and the functional fit (line), given by Eq. (5.22).

Table 5.4: Fitting parameters in Eq. (5.22)

A_{FHH}	k	l	m	n	p
$A_{FHH} \leq 0.5$	0.211	4.038	0.849	4.156	19.835
$0.5 < A_{FHH} \leq 1.5$	0.398	6.706	0.994	7.039	19.742
$1.5 < A_{FHH}$	0.656	8.270	1.364	8.739	19.705

5.4.4 Computation of s_{max} and N_d

The s_{max} in a cloud corresponds to the point where supersaturation generation from cooling balances depletion from condensation of water vapor, as well as characterizes the point where droplet activation terminates. For a non-adiabatic (entraining) cloud parcel ascending with constant velocity V, s_{max} can be determined from the solution of the following equation (Barahona and Nenes, 2007)

$$\frac{2\alpha V \rho_a}{\pi \gamma \rho_w} - G s_{max} \int_0^{s_{max}} \left(D_p^2(\tau) + 2G \int_\tau^{t_{max}} s \, dt \right)^{1/2} n^s(s') ds' = 0 \qquad [5.23]$$

where $D_p(\tau)$ is the size of CCN when exposed to $s = s_c$, τ is the time where the parcel supersaturation exceeds the CCN critical supersaturation, $\gamma = \dfrac{pM_a}{p^s M_w} + \dfrac{M_w \Delta H_v^2}{c_p R T^2}$,

$\alpha = \dfrac{g M_w \Delta H_v}{c_p R T^2} - \dfrac{g M_a}{RT} + e\left[\dfrac{\Delta H_v M_w}{R T^2}(T - T') - (1 - RH) \right]$, ΔH_v is the latent heat of condensation of water, g is the acceleration due to gravity, T is the temperature of the parcel, M_w is the molar mass of water, M_a is the molar mass of air, c_p is the heat capacity of air, p^s is the water saturation vapor pressure, p is the ambient pressure, e is the entrainment rate of dry air into the parcel (m^{-1}), and T' and RH are the ambient temperature and fractional relative humidity, respectively and R is the universal gas constant . G in Eq. (5.23) is given by

$$G = \frac{4}{\dfrac{\rho_w RT}{p^s D_v' M_w} + \dfrac{\Delta H \rho_w}{k_a T}\left(\dfrac{\Delta H_v M_w}{RT} - 1 \right)} \qquad [5.24]$$

where k_a is the thermal conductivity of air, and D_v' is the water vapor mass transfer coefficient from the gas to droplet phase corrected for non-continuum effects (calculated

as discussed in section 5.4.5). For an adiabatically rising parcel, $e = 0$, and hence Eq. (5.23) can be simplified to,

$$\frac{2\alpha V \rho_a}{\pi \gamma \rho_w} - I_e(0, s_{max}) = 0 \qquad [5.25]$$

where $I_e(0, s_{max})$ is the "condensation integral", given by

$$I_e(0, s_{max}) = G s_{max} \int_0^{s_{max}} \left(D_p^2(\tau) + 2G \int_\tau^{t_{max}} s\, dt \right)^{1/2} n^s(s')\, ds' \qquad [5.26]$$

Calculation of $I_e(0, s_{max})$ is detailed in section 5.4.6, which is then substituted in Eq. (5.25) and subsequently solved for s_{max}. The number of cloud droplets that form in the parcel is

$$N_d = F^s(s_{max}) \qquad [5.27]$$

5.4.5 *The water vapor mass transfer coefficient*

It is well known that the mass transfer coefficient of water vapor onto droplets (otherwise known as the effective diffusivity), D_v', varies with particle size (Fukuta and Walter, 1970),

$$D_v' = \frac{D_v}{1 + \frac{2D_v}{\alpha_c D_p} \sqrt{\frac{2\pi M_w}{RT}}} \qquad [5.28]$$

where D_v is the water vapor diffusivity in air, and α_c is the water vapor uptake coefficient. The α_c is a kinetic parameter, expressing the probability of water vapor molecules of being incorporated into droplet upon collision. However, processes other than accommodation can control the condensation of water vapor (e.g., dissolution kinetics, Asa-Awuku and Nenes, 2007). Thus, α_c can be used to express collectively all

related processes in terms of an effective uptake coefficient. Neglecting to account for the size dependency in D_v' results in overestimating water vapor condensation in the initial stages of cloud formation (Feingold and Chuang, 2002; Nenes et al., Fountoukis and Nenes, 2005; Ming et al., 2006), which can lead to an underestimation of s_{max} and N_d.

An analytical form of the condensation integral cannot be derived by substituting Eq. (5.28) into Eq. (5.24). Instead, Fountoukis and Nenes (2005) suggested to use an average mass transfer coefficient, $D_{v,ave}$, for the growing droplet population. Assuming that α_c is constant for all CCN, and $D_{p,low}$ and $D_{p,big}$ express the upper and lower size of droplets responsible for the condensation of water vapor (hence mass transfer), $D_{v,ave}$ can be expressed as (Fountoukis and Nenes, 2005)

$$D_{v,ave} = \frac{D_v}{D_{p,big} - D_{p,low}} \left[\left(D_{p,big} - D_{p,low} \right) - B' \ln \left(\frac{D_{p,big} + B'}{D_{p,low} + B'} \right) \right]$$ [5.29]

where $B' = \frac{2D_v}{\alpha_c} \left(\frac{2\pi M_w}{RT} \right)^{1/2}$. Based on numerical simulations for a wide range of values of conditions, Fountoukis and Nenes, (2005) suggest $D_{p,big} = 5\mu m$ and $D_{p,low} = \min \left\{ 0.207683 \alpha_c^{-0.33048}, 5.0 \right\}$ where $D_{p,low}$ is given in μm.

5.4.6 *Computing the condensation integral $I_e(0, s_{max})$*

To compute the condensation integral (Eq. 5.26), we first express it as the sum of two terms. The first one gives the contribution from particles that follow Köhler theory, $I_K(0, s_{max})$, whereas the second one from FHH particles, $I_{FHH}(0, s_{max})$

$$I_e(0, s_{max}) = I_K(0, s_{max}) + I_{FHH}(0, s_{max})$$ [5.30]

Using the population splitting approach of Nenes and Seinfeld (2003), $I_K(0, s_{max})$ is calculated as

$$I_K(0, s_{max}) = I_{K,1}(0, s_{part}) + I_{K,2}(s_{part}, s_{max})$$ [5.31]

where $I_{K,1}(0, s_{part})$ corresponds to Köhler CCN that, at the instant of parcel maximum supersaturation, either do not strictly activate ($D_p << D_c$), or experience significant growth beyond their critical diameter ($D_p >> D_c$). The $I_{K,2}(s_{part}, s_{max})$ corresponds to CCN that have not grown significantly beyond their critical diameter and for which $D_p^2(\tau) >> 2G \int_\tau^{t_{max}} s dt$ (Nenes and Seinfeld, 2003). Calculations of the partitioning supersaturation, s_{part}, and $I_{K,1}(0, s_{part})$ and $I_{K,2}(s_{part}, s_{max})$ for sectional and lognormal size distribution formulations are presented in detail by Nenes and Seinfeld (2003), Fountoukis and Nenes (2005), and Barahona and Nenes (2007), and are not repeated here.

$I_{FHH}(0, s_{max})$ in Eq. (5.30) represents the contribution of FHH particles to the condensation integral. According to section 5.3.2, $D_c/D_{dry} < 2$ for most atmospherically-relevant combinations of A_{FHH} and B_{FHH}, and is much smaller that (D_c/D_{dry}) for Köhler particles with similar dry diameters. Compared to FHH particles, Köhler particles may require 8 to 125000 times more water (i.e., 2 to 50 times more in diameter) to become activated (Table 5.1). Given that all activated droplets at s_{max} grow to much larger sizes than their dry diameter, and that $D_c \sim D_{dry}$ for FHH particles, hence $D_p >> D_c$, i.e.

$D_p^2(\tau) << 2G \int_\tau^{t_{max}} s dt$, and the corresponding condensation integral is

$$I_{FHH}(0,s_{max}) = Gs_{max}\int_0^{s_{max}}\left(2G\int_\tau^{t_{max}}sdt\right)^{1/2}n^s(s')ds' \approx Gs_{max}\int_0^{s_{max}}\left(2G\frac{1}{2\alpha V}\left(s_{max}^2-s(\tau)^2\right)\right)^{1/2}n^s(s')ds'$$

[5.32]

where $s(\tau)$ is parcel supersaturation at time τ and $\int_\tau^{t_{max}}sdt$ in Eq. (5.32) is evaluated using

the lower bound of Twomey (1959) (Nenes and Seinfeld, 2003).

For sectional representation of aerosol size distributions, $I_{FHH}(0,s_{max})$ is computed by substituting Eq. (5.11) into Eq. (5.32), and performing the integration as follows

$$I_{FHH}(0,s_{max}) = Gs_{max}\left(\frac{G}{\alpha V}\right)^{1/2}\sum_{j=1}^{i_{max}}\frac{N_j}{s_c^j-s_c^{j-1}}\left[\frac{y}{2}\left(s_{max}^2-y^2\right)^{1/2}+\frac{s_{max}^2}{2}\arcsin\frac{y}{s_{max}}\right]_{y=s_c^{j-1}}^{y=s_c^j}$$ [5.33]

where i_{max} is the boundary closest to s_{max}.

For lognormal representation of aerosol size distribution, $I_{FHH}(0,s_{max})$ is computed by substituting Eq. (5.18) into Eq. (5.32), and integrating

$$I_{FHH}(0,s_{max}) = G\left(\frac{G}{\alpha V}\right)^{1/2}\frac{N_i s_{max}^2}{2}\left[1-\left(\frac{s_{g,i}}{s_{max}}\right)^2\frac{\exp(2x^2\ln^2\sigma_i)\left(erf(\sqrt{2}x\sigma_i-u_{max})+1\right)}{2}-erf(u_{max})\right]$$

[5.34]

where $u_{max} = \dfrac{\ln(s_{g,i}/s_{max})^{-\frac{1}{x}}}{\sqrt{2}\ln\sigma_i}$. In the case of multiple lognormal modes, the right-hand

side of Eq. (5.34) is summed over all lognormal modes.

5.4.7 Using the Parameterization

The parameterization algorithm is illustrated in Fig. 5.6, and consists of two steps. First, Eq. (5.25) is numerically solved for s_{max} using the bisection method

$$\frac{\pi \gamma \rho_w}{2 \alpha V \rho_a} \left[I_{K,1}(0, s_{part}) + I_{K,2}(s_{part}, s_{max}) + I_{FHH}(0, s_{max}) \right] - 1 = 0 \qquad [5.35]$$

where the condensation integral is substituted with the desirable formulation (sectional or lognormal). Physical properties are evaluated at the cloud base conditions for adiabatic updrafts (i.e., $e = 0$). For entraining parcels (i.e., $e > 0$), properties are evaluated at the critical entrainment rate following the procedure of Barahona and Nenes (2007). Once s_{max} is determined, N_d is obtained from Eq. (5.27).

Input: P, T, updraft velocity, aerosol properties
(Size distribution, Köhler particle composition, A_{FHH}, B_{FHH} for FHH particles)

Compute CCN spectrum, $F^s(s)$, for Köhler and FHH particles

Estimate s_{max}

Re-estimate s_{max}

FHH Population

Köhler Population

Size Distribution?

Determine s_{part}
(Nenes and Seinfeld, 2003)

Lognormal

Sectional

Determine x
Use Equation 20

$$I_{K,1}(0, s_{part}) = C_1 \int_0^{s_{part}} f_1(s)ds$$

$$I_{K,2}(s_{part}, s_{max}) = C_2 \int_{s_{part}}^{s_{max}} f_2(s)ds$$

$I_{FHH}(0, s_{max})$ from
Equation 5.33

$I_{FHH}(0, s_{max})$ from
Equation 5.32

$$\frac{\pi \gamma \rho_w}{2 \alpha V \rho_a}\left[I_{K,1}(0, s_{part}) + I_{K,2}(s_{part}, s_{max}) + I_{FHH}(0, s_{max})\right] - 1 \overset{?}{=} 0$$

NO

YES

Output: $N_d = F^s(s_{max}), s_{max}$

Figure 5.6: Parameterization Algorithm. C_1, C_2, $f_1(s)$, $f_2(s)$ depend on the aerosol representation (sectional, lognormal) and are defined in Nenes and Seinfeld (2003).

5.5   Evaluation of the parameterization

5.5.1   *Method*

We first test the sectional formulation against the lognormal formulation to show the equivalence between the two. Then, we evaluate the accuracy of the parameterization by comparing the predicted droplet number concentration and maximum supersaturation against the numerical parcel model of Nenes et al. (2001) (modified to include FHH particles) for a wide range of size distributions representative of global aerosols.

5.5.2   *Evaluation of the involved parameters*

Nenes and Seinfeld (2003), Fountoukis and Nenes (2005) and Barahona and Nenes (2007) have extensively evaluated the parameterization for aerosol composed of only Köhler particles. Therefore, the focus of this evaluation is on the performance of the parameterization when FHH particles are externally mixed with Köhler particles, considering a wide range of A_{FHH}, B_{FHH}, water vapor accommodation coefficient, α_c, and parcel updraft velocity, V. The values of α_c and V were selected to represent typical conditions encountered in low - level cumulus and stratocumulus clouds of marine and continental origin (Pontikis et al., 1987; Conant et al., 2004; Meskhidze et al., 2005; Peng et al., 2005, Fountoukis et al., 2007). In total, 6600 different simulations were performed (see Table 5.2, 5.5, and 5.6).

For this comparison, we selected four Whitby (1978) trimodal size distributions, namely marine, clean continental, average background, and urban (Table 5.5). In addition, we selected four aerosol distributions that are representative of ambient dust (Jeong and Sokolik, 2007), the properties of which are given in Table 5.6, and are C04 (Clarke et al., 2004), D87 (D'Almeida, 1987), O98 (Hess et al., 1998), and W08

(Wiegner et al., 2008). As expected, the distributions given by Whitby have smaller median diameters in comparison to typical dust distributions. For each aerosol size distribution, we consider a parcel of externally mixed Köhler and FHH particles, allowing the proportion to vary from 0% (pure Köhler particles) to 100% (pure FHH particles) by number. For each FHH particle, we assume 100% of the mass is insoluble with activating properties given by A_{FHH} and B_{FHH}. Each Köhler particle has a 50% soluble $(NH_4)_2SO_4$ and 50% insoluble material by mass. A_{FHH} was varied between 0.25 to 2.0, while B_{FHH} from 0.93 to 2.50. The parcel pressure and temperature were 900 mbar and 298 K, respectively, and droplet concentration was computed at 350 m above the cloud base.

Table 5.5: Whitby (Whitby, 1978) Aerosol lognormal size distributions used in this study

Aerosol Type	Nuclei Mode			Accumulation Mode			Coarse Mode		
	D_{g1}	σ_1	N_1	D_{g2}	σ_2	N_2	D_{g3}	σ_3	N_3
Marine	0.010	1.6	340	0.070	2.0	60	0.62	2.7	3.1
Continental	0.016	1.6	1000	0.068	2.1	800	0.92	2.2	0.72
Background	0.016	1.7	6400	0.076	2.0	2300	1.02	2.16	3.2
Urban	0.014	1.8	106000	0.054	2.16	32000	0.86	2.21	5.4

D_{gi} is the median diameter (μm), N_i is the number of dry particles (cm^{-3}), and σ_i is the geometric standard deviation of the ith mode.

Table 5.6: Aerosol lognormal size distributions used in this study that are representative of mineral dust aerosol (see Jeong and Sokolik, 2007)

Size Distribution	Mode 1			Mode 2			Mode 3			Mode 4		
	D_{g1}	σ_1	$MF_1\%$	D_{g2}	σ_2	$MF_2\%$	D_{g3}	σ_3	$MF_3\%$	D_{g4}	σ_4	$MF_4\%$
C04 (Clarke et al., 2004)	0.69	1.46	1.8	1.77	1.85	69.4	8.67	1.50	28.8	-	-	-
D87 (D'Almeida, 1987)	0.16	2.10	1.0	1.40	1.90	95.3	9.98	1.60	3.7	-	-	-
O98 (Hess et al., 1998)	0.14	1.95	3.4	0.78	2.00	76.1	3.80	2.15	20.5	-	-	-
W08 (Wiegner et al., 2008)	0.078	2.2	2.93	0.495	1.7	0.81	1.40	1.9	31.53	6.50	1.7	64.73

D_{gi} is the median diameter (μm), σ_i is the geometric standard deviation, and $MF_i \%$ is the percentage mass fraction of dry particles of the ith mode. Particle number concentration was calculated from percentage mass fraction by assuming a total mass equal to 4000 μg m^{-3} and particle density equal to 2.5 g cm^{-3} in the first three distributions. For Wiegner et al. (2008), number concentration was converted to percentage mass fraction of dry particles in each mode.

5.5.3   *Comparison of sectional against lognormal formulation*

The sectional formulation is evaluated against the lognormal formulation by comparing N_d predicted by the application of each formulation to the activation of lognormal aerosol size distributions shown in Tables 5.5 and 5.6. In applying the sectional formulation, 75 sections per mode were used to discretize the lognormal distributions. The intercomparison is shown in Fig. 5.7, which depicts the parameterized N_d using the sectional versus the lognormal formulation. Figure 5.7a compares Whitby (1974) aerosol size distributions, for $\alpha_c = 0.042$, A_{FHH} equal to 0.68, and B_{FHH} equal to 0.93 while Fig. 5.7b shows comparisons for $\alpha_c = 0.06$, A_{FHH} equal to 2.00, and B_{FHH} equal to 1.00. An excellent agreement between the two formulations is obtained for all cases considered ($R^2 = 0.9998$ and $R^2 = 0.998$), suggesting both formulations are equivalent.
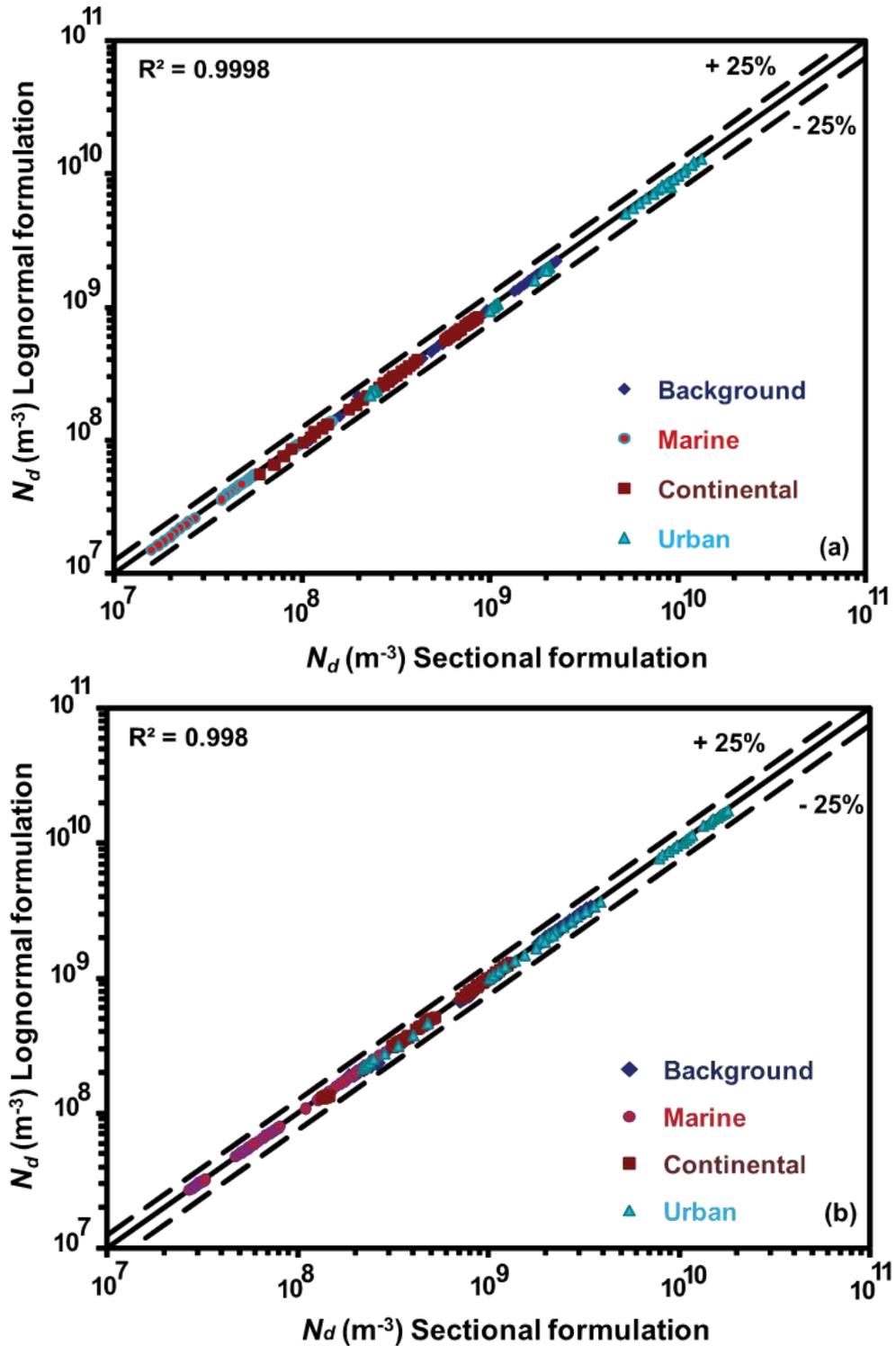
Figure 5.7: Droplet number concentration, N_d (m^{-3}), predicted by the sectional and the lognormal formulations for Whitby (1978) distributions and for the cloud formation conditions of Table 5.2. Results are shown for **(a)** $\alpha_c = 0.042$, and $A_{FHH} = 0.68$ and $B_{FHH} = 0.93$ and **(b)** $\alpha_c = 0.06$, and $A_{FHH} = 2.00$ and $B_{FHH} = 1.00$. Dashed lines represent $\pm 25\%$ deviation.

5.5.4 *Comparison of sectional parameterization with parcel model*

5.5.4.1 *Whitby aerosol distribution*

Figure 5.8 shows that the predicted droplet number from parameterization closely follows the predicted droplet number from the parcel model for all conditions of Table 5.2, thus indicating that there are no regions with systematic biases in the predictions (Fig. 5.8a: average relative error: 0.37% ± 16%, and, Fig. 5.8b: average relative error: 0.15% ± 17%). Figure 5.9 shows the comparison for the predicted droplet number between the parameterization and the parcel model for individual Whitby (1978) distributions. An excellent agreement is apparent, with an average relative error of less than 10% (Table 5.7). The only exception is the case of the marine aerosol size distribution, where a minor systematic overprediction in parameterized N_d is observed. According to Barahona and Nenes (2007), this systematic bias results from an underestimation of the droplet size that causes a consequent underestimation of surface area available for water vapor condensation. This forces an underestimation of the condensation integral, thereby resulting in an overestimation in s_{max}, and hence N_d.
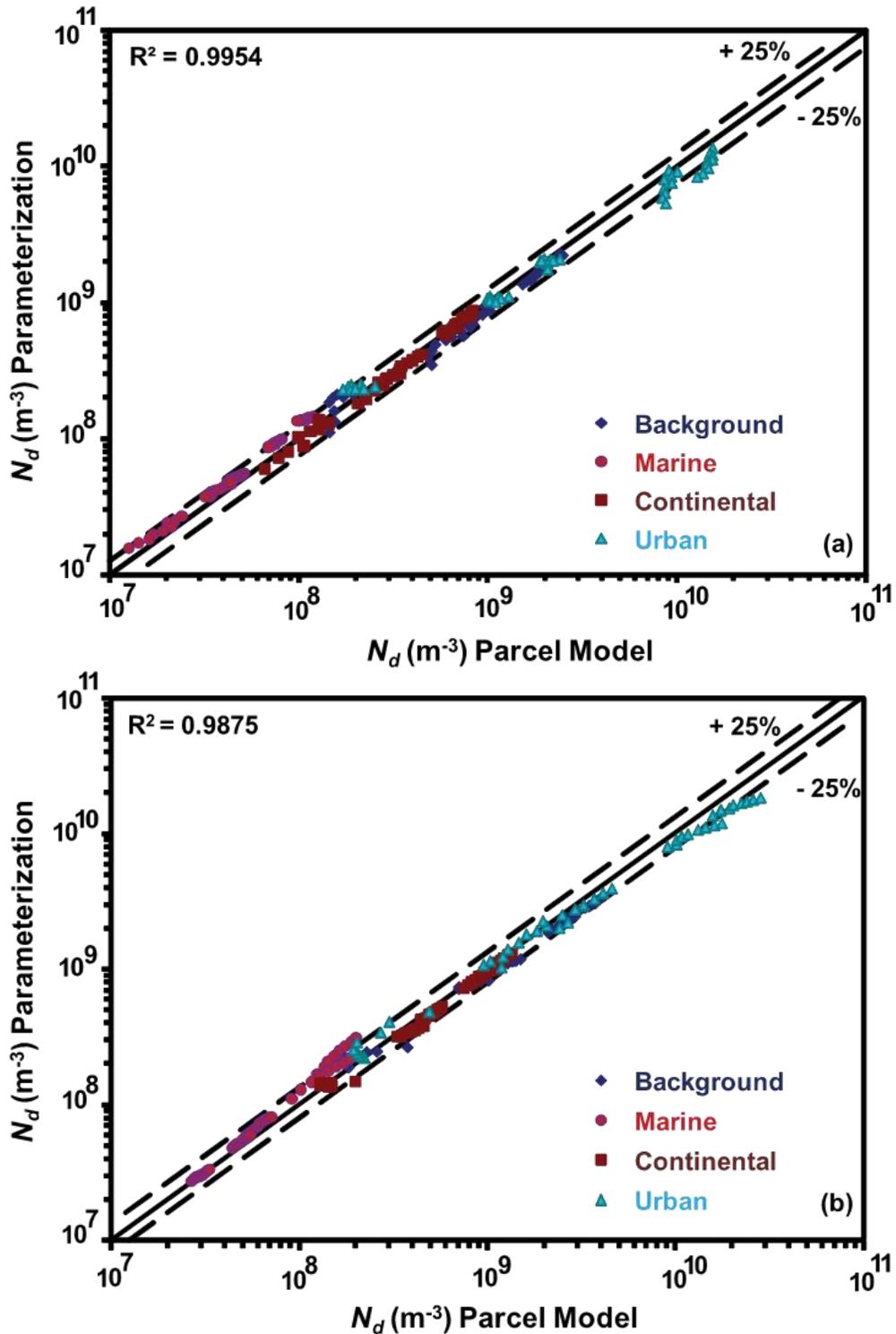
Figure 5.8: Droplet number concentration, N_d (m^{-3}), predicted by parameterization and the parcel model for Whitby (1978) distributions, for the cloud formation conditions of Table 5.2. Results are shown for **(a)** $\alpha_c = 0.042$, and $A_\mathrm{FHH} = 0.68$ and $B_\mathrm{FHH} = 0.93$ and **(b)** $\alpha_c = 0.06$, and $A_\mathrm{FHH} = 2.0$ and $B_\mathrm{FHH} = 1.0$. Dashed lines represent $\pm 25\%$ deviation.
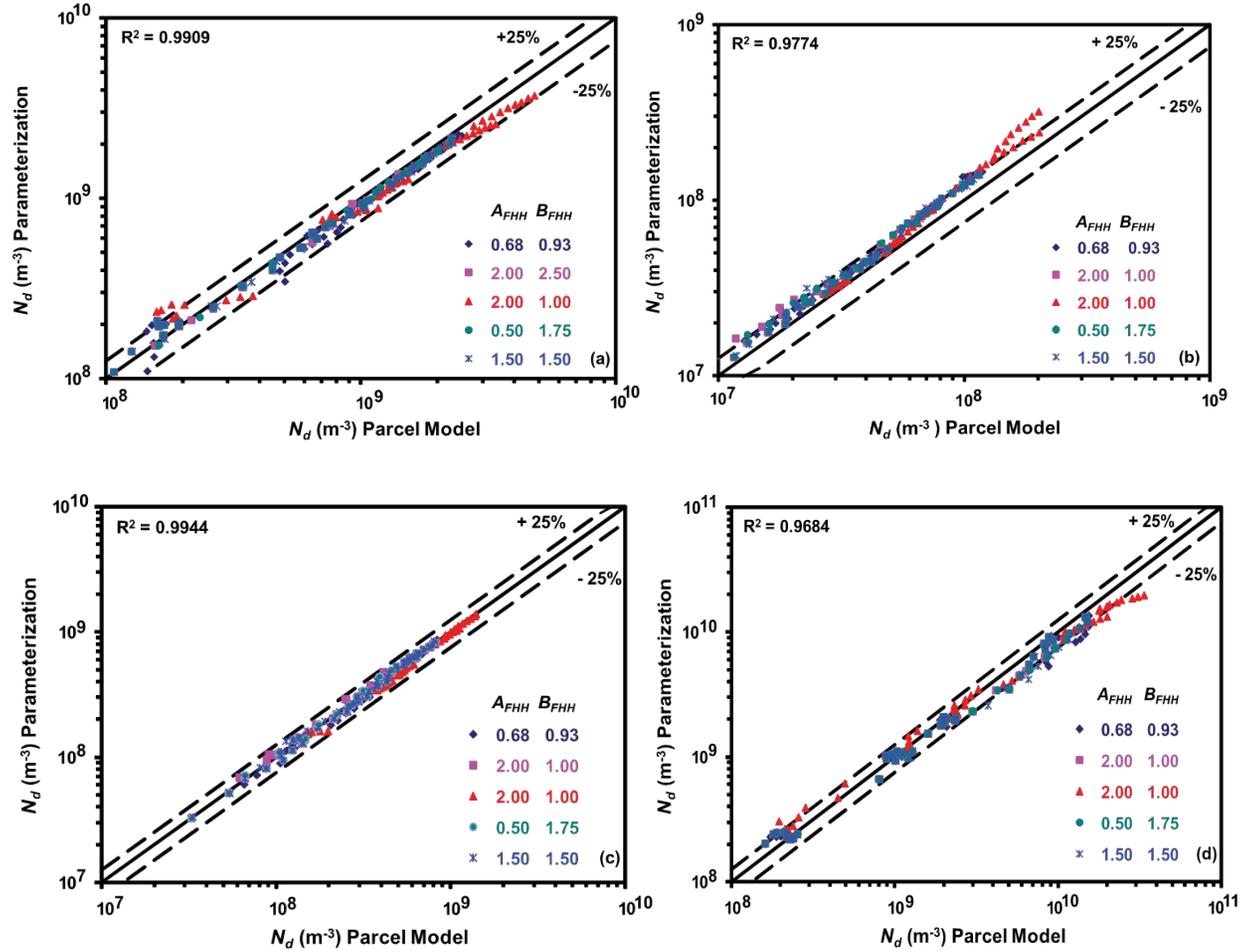
Figure 5.9: Droplet number concentration, N_d (m^{-3}), predicted by parameterization and the parcel model for Whitby (1978) distributions, **(a)** Background, **(b)** Marine, **(c)** Continental, and **(d)** Urban, for the cloud formation conditions of Table 5.2. Results are shown for $\alpha_c = 0.042$ and five different combination of A_{FHH} and B_{FHH}. Dashed lines represent $\pm 25\%$ deviation.

Table 5.7: Droplet number agreement between the parameterization and parcel model, for each aerosol type and conditions in Table 5.2

Aerosol Type	Relative Error	(%) Standard Deviation
Whitby Background (Whitby, 1978)	+ 5	± 12
Whitby Marine (Whitby, 1978)	- 20	± 10
Whitby Continental (Whitby, 1978)	+ 2	± 6
Whitby Urban (Whitby, 1978)	+ 7	± 17
C04 (Clarke et al., 2004)	+ 2	± 5
D87 (D'Almeida, 1987)	+ 8	± 12
O98 (Hess et al., 1998)	+ 2	± 15
W08 (Wiegner et al., 2008)	+ 4.5	± 25

5.5.4.2 Dust size distribution

To test the applicability of this new parameterization to distributions representative of dust, we performed an extensive analysis on droplet number predictions comparisons between this parameterization and the parcel model on aerosol distributions suggested by C04 (Clarke et al., 2004), D87 (D'Almeida, 1987), O98 (Hess et al., 1998) and W08 (Wiegner et al., 2008) for the cloud conditions of Table 5.2.

Figure 5.10 shows predictions of droplet number concentration for all conditions of parcel updrafts, uptake coefficients, and for different dust distributions, assuming A_{FHH} equal to 0.68, and B_{FHH} equal to 0.93. A good agreement is observed between parameterization and the parcel model for different updrafts and $\alpha_c = 0.042$ (Fig. 5.10a), $\alpha_c = 0.06$ (Fig. 5.10b), and, $\alpha_c = 1.0$ (Fig. 5.10c). The agreement is best at high updrafts (5 m s^{-1}, 10 m s^{-1}); at low updrafts (0.1 m s^{-1}, 0.5 m s^{-1}) overprediction by the parameterized N_d was observed. This is because of the overprediction in maximum parcel supersaturation, s_{max} (Fig. 5.11), from an underprediction in droplet size, as explained in section 5.5.4.1. The best performance is seen using the W08 (Wiegner et al., 2008) dust distribution (Fig. 5.11d). This may be attributed to smaller median diameters for the W08 (Wiegner et al., 2008) distribution in comparison to the much larger fraction of particles greater than 1 micron present in the C04 (Clarke et al., 2004), D87 (D'Almeida, 1987), and O98 (Hess et al., 1998) distributions.

Figure 5.11 compares parcel maximum supersaturation, s_{max}, between the parcel model and the parameterization for three different values of accommodation coefficients. At low values of α_c, a greater overprediction in s_{max} is observed. This consequently results in overprediction in the number of activated droplets, and manifests because of the

underestimation of surface area available for water vapor condensation for the largest size of CCN as explained in section 5.5.4.1. However, this overestimation in cloud droplet number becomes important only for very large values of s_{max} that are not found in clouds. Inspite of this overprediction in the cloud droplet number, we find that the average relative error for all dust representative distributions (Table 5.6) is well below 10% (Table 5.7).
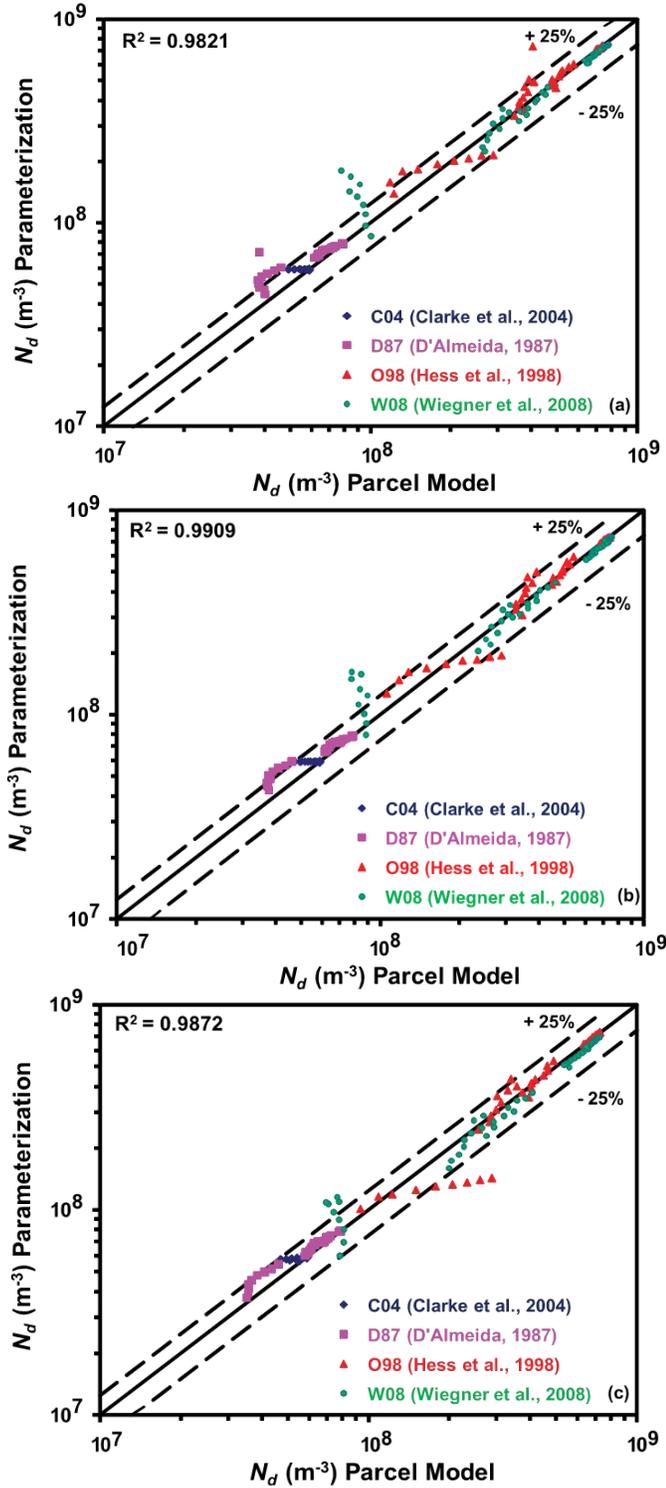
Figure 5.10: Droplet number concentration, N_d (m^{-3}), predicted by the parameterization and the parcel model for the dust size distributions of Table 5.6, and the cloud formation conditions of Table 5.2. Results are shown for $A_{FHH} = 0.68$ and $B_{FHH} = 0.93$ and **(a)** $\alpha_c = 0.042$, **(b)** $\alpha_c = 0.06$, and **(c)** $\alpha_c = 1.0$. Dashed lines represent $\pm$ 25% deviation.
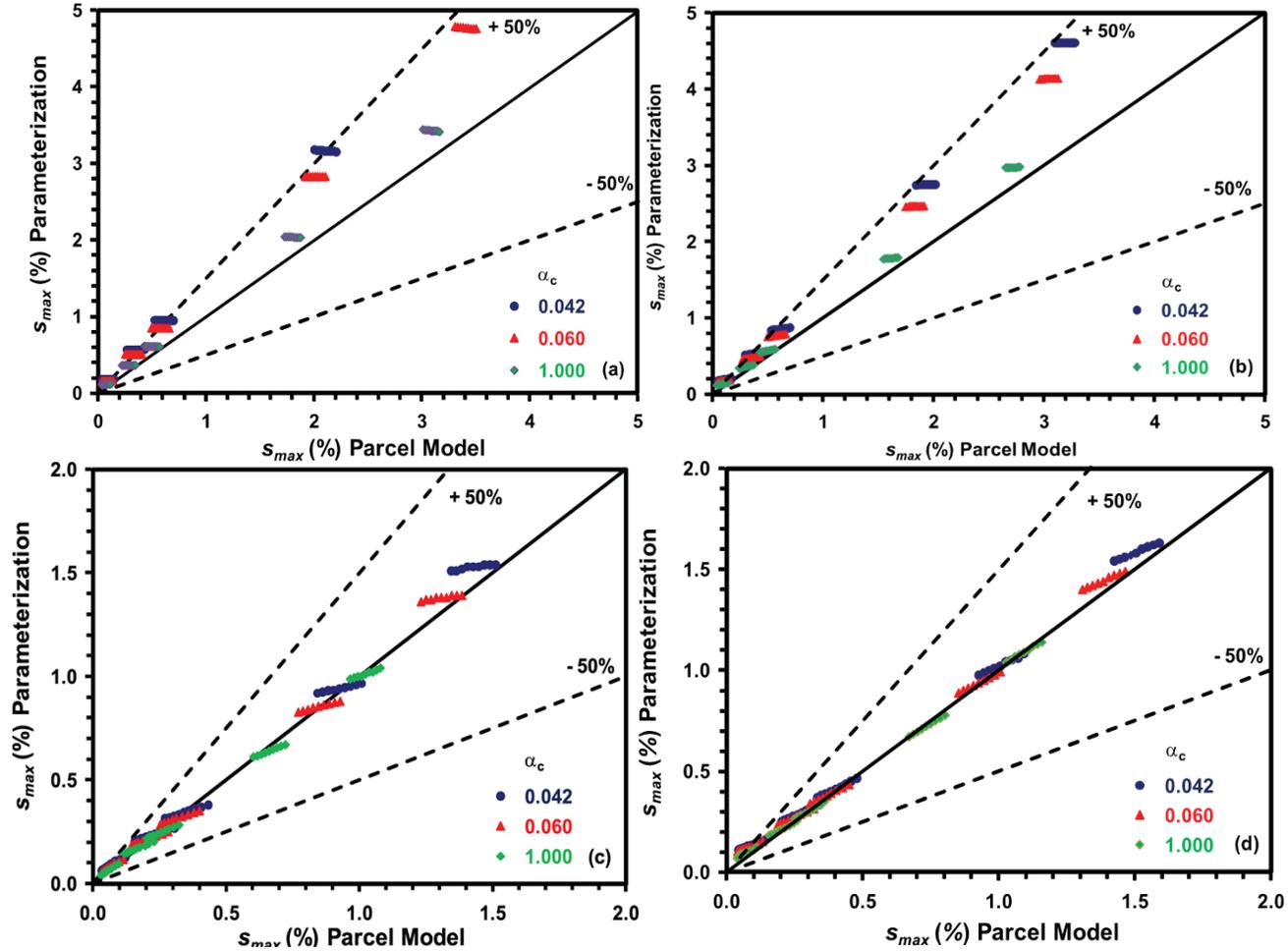
Figure 5.11: Parcel maximum supersaturation, s_{max}, predicted by the parameterization and the parcel model, for the V, α_c conditions of Table 5.2, and dust size distributions of **(a)** C04 (Clarke et al., 2004), **(b)** D87 (D'Almeida, 1987), **(c)** O98 (Hess et al., 1998), and **(d)** W08 (Wiegner et al., 2008) for $A_{FHH} = 0.68$ and $B_{FHH} = 0.93$ in all simulations. Dashed lines represent $\pm 50\%$ deviation.

5.6 On the competition of FHH with Köhler particle for water vapor

In this section, we provide a first evaluation of the potential impact of adsorption activation on cloud droplet number. For this, it is assumed that the aerosol is an external mixture of Köhler and FHH particles, both of which are described with a single-mode lognormal size distribution obtained from in-situ measurements during the NAMMA campaign (Twohy et al, 2009). The geometric mean diameter, D_g, and standard deviation, σ_g, were identical for both particle types ($D_g = 0.10$ μm, $\sigma_g = 1.6$); the total concentration of Köhler particles were maintained constant in all simulations, equal to 225 cm^{-3}, while the concentration of FHH particles was varied from 22.5 to 2250 cm^{-3}. The Köhler particles were assumed to be composed of pure $(NH_4)_2SO_4$, while size-resolved activation data of Arizona Test dust (Twohy et al, 2009) were used to constrain values of A_{FHH}, B_{FHH} (through least squares fitting to Eq. 5.14) for the FHH particles. In all simulations presented, the updraft velocity in the cloud parcel is set to 0.5 m s^{-1}, and initial pressure and temperature are 298 K and 900 mbar, respectively.

Figure 5.12 shows the predicted total cloud droplet number (blue curve) as a function of FHH to Köhler particle concentration ratio. Also shown are the contribution of Köhler (cyan curve) and FHH (green curve) particles to the droplet number, as well as the maximum supersaturation (red curve) that develops in the parcel. At low FHH/Köhler concentration ratio, all of the droplets in the cloud parcel originate from the Köhler particles. As the number concentration of FHH particles increases, the number of droplets from adsorption activation increases; the resulting competition for water vapor depresses s_{max} and slightly decreases the droplet number forming from Köhler particles. The competition effect however of FHH particles water vapor is weaker compared to similar

effects from Köhler particles (Ghan et al., 1998), because the amount of water required for activation of the former ($D_c/D_{dry} \sim 1$) is much smaller than for the latter ($D_c \gg D_{dry}$). As a result, droplet number responds much more strongly to increases in FHH aerosol number than for Köhler aerosol. A thorough quantification requires a comprehensive investigation and will the subject of a future study.
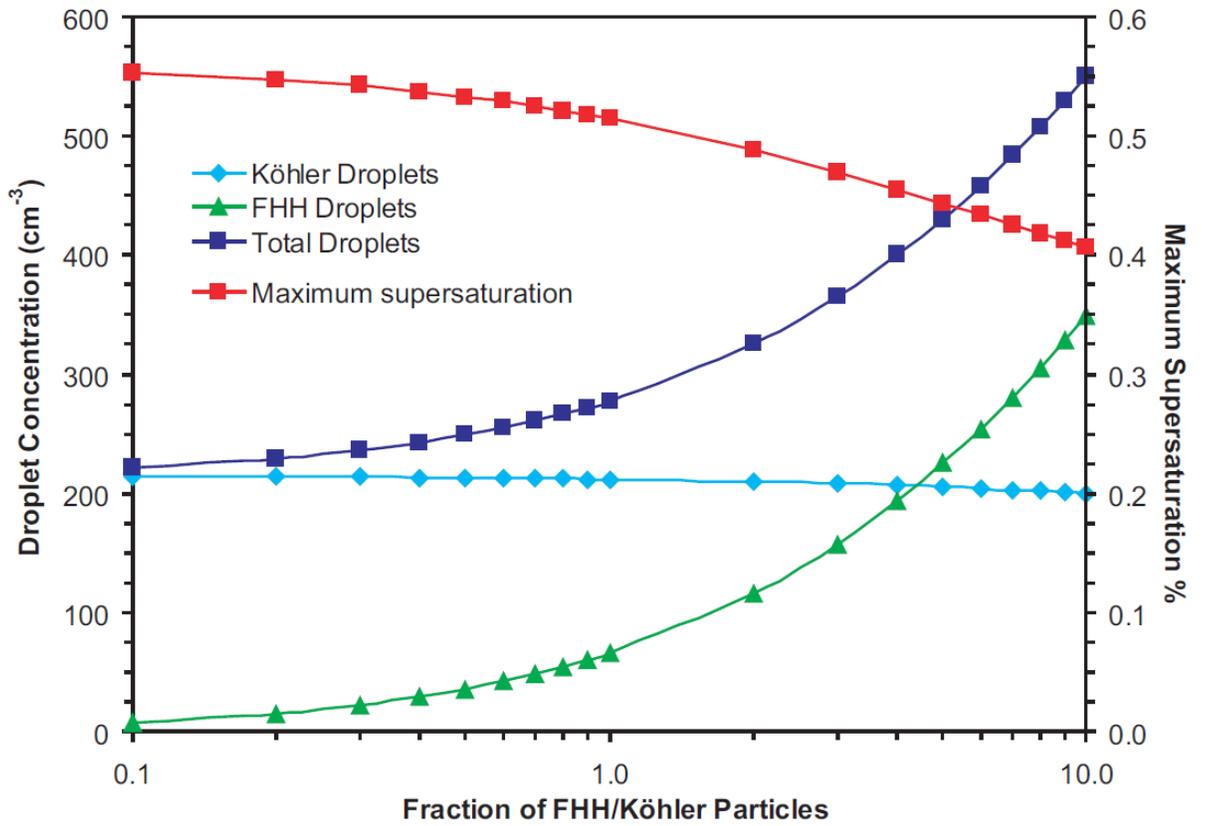
Figure 5.12: Predicted total number of cloud droplets (blue curve) as a function of FHH to Köhler particle concentration ratio, for the conditions describes in section 5.6. Also shown are the contribution of Köhler (cyan curve) and FHH (green curve) particles to the droplet number, as well as the maximum supersaturation (red curve) that develops in the parcel.

5.7   Summary

This study presents a new parameterization of cloud droplet formation for an external mixture of soluble particles that activate according to Köhler theory, and, completely insoluble, wettable particles that form droplets through adsorption activation (following FHH adsorption theory). This new parameterization is the first of its kind and is built upon previous work of Nenes and Seinfeld (2003), Fountoukis and Nenes (2005), and Barahona and Nenes (2007).

Formulation of the parameterization is developed for sectional and lognormal representations of the aerosol size distribution. To facilitate the analytical development of the parameterization, we have further developed FHH activation theory by *i*) determining the combinations of A_{FHH} and B_{FHH} for atmospherically-relevant behavior, and, *ii*) linking critical supersaturation with dry diameter using a simple power law expression, determined from numerical solutions to the FHH equilibrium curves.

The parameterization is tested by comparing predictions of droplet number and s_{max} against detailed cloud parcel model simulations. The evaluations are performed for a range of updraft velocities, water vapor uptake coefficients, ambient temperature, relative humidity, parameters of aerosol size distributions, and A_{FHH} and B_{FHH}. The parameterization closely follows the parcel model simulations with a mean relative error varying between 2% and 20% depending on aerosol distribution type with an average relative error of 10% and $R^2 \sim 0.98$.

5.8   Acknowledgements

5.9   References

Abdul-Razzak, H. and Ghan, S. J,: A parameterization of aerosol activation: 2. Multiple aerosol types, J. Geophys. Res., 105(D6), 6837 - 6844, 2000.

Abdul-Razzak, H., Ghan, S. J., and Rivera-Carpio, C.: A parameterization of aerosol activation: 1. Single aerosol type, J. Geophys. Res., 103(D6), 6123 - 6131, 1998.

Albrecht, B. A.: Aerosols, cloud microphysics, and fractional cloudiness, Science, 245, 1227-1230, 1989.

Asa-Awuku, A. and Nenes, A.: The effect of solute dissolution kinetics on cloud droplet formation: Extended Köhler theory, J. Geophys. Res., 112, D22201, doi:10.1029/2005JD006934, 2007.

Barahona, D. and Nenes, A.: Parameterization of cloud droplet formation in large-scale models: Including effects of entrainment, J. Geophys. Res., 112, D16206, doi:10.1029/2007JD008473, 2007.

Boucher, O. and Lohmann, U.: The sulfate-CCN-cloud albedo effect: A sensitivity study with 2 general circulation models, Tellus, Ser. B, 47, 281 - 300, 1995.

Brunauer, S., Emmett, P. H., and Teller, E.: Adsorption of gases in multimolecular layers, J. Am. Chem. Soc., 60(2), 309 - 319, 1938.

Clarke, A. D., Shinozuka, Y., Kapustin, V. N., Howell, S., Huebert, B., Doherty, S., Anderson, T., Covert, D., Anderson, J., Hua, X., Moore II, K. G., McNaughton, C., Carmichael, G., and Weber, R.: Size distributions and mixtures of dust and black carbon aerosol in Asian outflow: Physiochemistry and optical properties, J. Geophys. Res., 109, D15S09, doi:10.1029/2003JD004378, 2004.

Cohard, J. -M., Pinty, J. -P., and Suhre, K.: On the parameterization of activation spectra from cloud condensation nuclei microphysical properties, J. Geophys. Res., 105(D9), 11,753 - 11,766, 2000.

Conant, W. C., VanReken, T. M., Rissman, T. A., Varutbangkul, V., Jonsson, H. H., Nenes, A., Jimenez, J. L., Delia, A. E., Bahreini, R., Roberts, G. C., Flagan, R. C., and Seinfeld, J. H.: Aerosol-cloud drop concentration closure in warm cumulus, J. Geophys. Res., 109, D13204, doi:10.1029/2003JD004324, 2004.

D'Almeida, G. A.: On the variability of desert aerosol radiative characteristics, J. Geophys. Res., 92, 3017 – 3027, 1987.

Feingold, G. and Chuang, P.: Analysis of the Influence of Film-Forming compounds on Droplet Growth: Implications for Cloud Microphysical Processes and Climate, J. Atmos. Sci., 59, 2006 - 2018, 2002.

Feingold, G. and Heymsfield, A. J.: Parameterization of condensational growth of droplets for use in general circulation models, J. Atmos. Sci, 49, 2325 - 2342, 1992.

Fletcher, N. H.: Size effect in heterogeneous nucleation, J. Chem. Phys., 29, 572 - 576, 1958.

Forster, P., Ramaswamy, V., Artaxo, P., Berntsen, T., Betts, R., Fahey, D. W., Haywood, J., Lean, J., Lowe, D. C., Myhre, G., Nganga, J., Prinn, R., Raga, G., Schulz, M., and Van Dorland, R.: Changes in Atmospheric Constituents and in Radiative Forcing. In: Climate Change 2007: The Physical Science Basis. Contribution of Working Group I to the Fourth Assessment Report of the Intergovernmental Panel on Climate Change, edited by: Solomon, S., Qin, D., Manning, M., Chen, Z., Marquis, M., Averyt, K. B., Tignor, M., and Miller, H. L. Cambridge University Press, Cambridge, United Kingdom and New York, NY, USA, 2007.

Fountoukis, C. and Nenes, A.: Continued development of a cloud droplet formation parameterization for global climate models, J. Geophys. Res., 110, D11212, doi:10.1029/2004JD005591, 2005.

Fukuta, N. and Walter, L. A.: Kinetics of hydrometer growth from the vapor; spherical model, J. Atmos. Sci., 27, 1160 - 1172, 1970.

Ghan, S., G. Guzman, and H. Abdul-Razzak, Competition between sea-salt and sulfate particles as cloud condensation nuclei, J. Atmos. Sci., 55, 3340 – 3347, 1998.

Gultepe, I. and Isaac, G. A.: The relationship between cloud droplet and aerosol number concentrations for climate models, Int. J. Climatol., 16, 941 - 946, 1996.

Henson, B. F.: An adsorption model of insoluble particle activation: Application to black carbon, J. Geophys. Res., 112, D24S16, doi:10.1029/2007JD008549, 2007.

Hess, M., Koepke, P., and Schult, I.: Optical Properties of Aerosols and Clouds: The Software Package OPAC, Bull. Am. Meteorol. Soc., 79, 831-844, 1998.

Jeong, G.-R. and Sokolik, I. N.: Effect of mineral dust aerosols on photolysis rates in clean and polluted marine environments, J. Geophys. Res., 112, D21308, doi:10.1029/2007JD008442, 2007.

Khvorostyanov, V. I. and Curry, J. A.: Refinements to the Köhler's theory of aerosol equilibrium radii, size spectra and droplet activation: Effects of humidity and insoluble fraction, J. Geophys. Res., 112, D05206, doi:10.1029/2006JD007672, 2007.

Köhler, H.: The nucleus in and the growth of hygroscopic droplets, Trans. Faraday Soc., 32(2), 1152 - 1161, 1936.

Langmuir, J.: The constitution and fundamental properties of solids and liquids. Part I. Solids, J. Am. Chem. Soc., 38, 2221 - 2295, 1916.

Lowell, S., Shields, J. E., Thomas, M. A., and Thommes, M.: Characterization of Porous Solids and Powders: Surface Area, Pore Size and Density, Kluwer Academic Publishers, Netherlands, 2004.

Meskhidze, N., Nenes, A., Conant, W. C., and Seinfeld, J. H.: Evaluation of a new cloud droplet activation parameterization with in situ data from CRYSTAL-FACE and CSTRIPE, J. Geophys. Res., 110, D16202, doi:10.1029/2004JD005703, 2005.

Ming, Y., Ramaswamy, V., Donner, L. J., and Phillips, V. T. J.: A new parameterization of cloud droplet activation applicable to general circulation models, J. Atmos. Sci., 63, 1348 - 1356, 2006.

Nenes, A., Ghan, S. J., Abdul-Razzak, H., Chuang, P. Y., and Seinfeld, J. H.: Kinetic limitations on cloud droplet formation and impact on cloud albedo, Tellus, Ser. B, 53, 133 - 149, 2001.

Nenes, A. and Seinfeld, J. H.: Parameterization of cloud droplet formation in global climate models, J. Geophys. Res., 108 (D14), 4415, doi:10.1029/2002JD002911, 2003.

Nenes, A., Charlson, R. J., Facchini, M. C., Kulmala, M., Laaksonen, A., and Seinfeld, J. H.: Can chemical effects on cloud droplet number rival the first indirect effect?, Geophys. Res. Lett., 29(17), 1848, doi:10.1029/2002GL015295, 2002.

Peng, Y., Lohmann, U., and Leaitch, W. R.: Importance of vertical velocity variations in the cloud droplet nucleation process of marine stratocumulus, J. Geophys. Res., 110, D21213, doi:10.1029/2004JD004922, 2005.

Pontikis, C. A., Rigaud, A., and Hicks, E. M.: Entrainment and mixing as related to the microphysical properties of shallow warm cumulus clouds, J. Atmos. Sci., 44, 2150 - 2165, 1987.

Seinfeld, J. H., and Pandis, S. N.: Atmospheric Chemistry and Physics, John Wiley, New York, USA, 767 – 773, 2006.

Seisel, S., Pashkova, A., Lian, Y., and Zellner, R.: Water uptake on mineral dust and soot: A fundamental view of hydrophilicity of atmospheric particles?, Faraday Discuss., 130, 437 - 451, 2005.

Sorjamaa, R. and Laaksonen, A.: The effect of H2O adsorption on cloud drop activation of insoluble particles: a theoretical framework, Atmos. Chem. Phys., 7, 6175 - 6180, 2007, www.atmos-chem-phys.net/7/6175/2007/.

Twohy, C. H., Kreidenweis, S. M., Eidhammer, T., Browell, E. V., Heymsfield, A. J., Bansemer, A. R., Anderson, B. E., Chen, G., Ismail, S., DeMott, P. J., and Van Den Heever, S. C.: Saharan dust particles nucleate droplets in eastern Atlantic clouds, Geophys. Res. Lett., 36(L01807), 1 - 6, 2009.

Twomey, S.: The nuclei of natural cloud formation part II: The supersaturation in natural clouds and the variation of cloud droplet concentration, Pure Appl. Geophys., 43, 243 - 249, 1959.

Twomey, S.: Pollution and the planetary albedo, Atmos. Environ., 8, 1251 - 1256, 1974.

Wexler, A. S. and Ge, Z. Z.: Hydrophobic particles can activate at lower relative humidity than slightly hygroscopic ones: a Köhler theory incorporating surface fixed charge, J. Geophys. Res., 103(D6), 6083 - 6088, 1998.

Whitby, K. T.: The physical characteristics of sulfur aerosols, Atmos. Environ., 12, 135 - 139, 1978.

Wiegner, M., Gasteiger, J., Kandler, K., Weinzierl, B., Rasp, K., Esselborn, M., Freudenthaler, V., Heese, B., Toledano, C., Tesche, M., and Althausen, D.: Numerical simulations of optical properties of Saharan dust aerosols with emphasis on linear depolarization ratio, Tellus, 61B, in press, 2008.

CHAPTER 6

ADSORPTION ACTIVATION OF DUST GIANT CLOUD CONDENSATION NUCLEI (GCCN): IMPLICATIONS FOR CLOUD MICROPHYSICS

6.1   Abstract

The growth of dust giant cloud condensation nuclei (GCCN) by adsorption activation mechanism within low-level stratocumulus and deep convective clouds is evaluated by its ability to act as a collector drop. It is found that under pristine aerosol conditions, dust GCCN has the potential to act as collector drops compared to polluted aerosol conditions for both cloud types investigated here. Biases introduced in dust GCCN growth by Köhler theory (KT) activation are discussed, and compared against those with adsorption activation theory (AT). The effect of dust hydrophilicity on dust GCCN growth is also assessed, and is found to effect cloud microphysics of stratocumulus clouds, with negligible impact on convective clouds. We also explore water vapor accommodation properties associated with dust aerosol and find negligible impact on GCCN size. The major conclusion of this study is that dust GCCN growth by AT under clean aerosol conditions may affect dust aerosol-cloud-precipitation linkage with implications to microphysical evolution of stratocumulus and convective clouds.

6.2   Introduction

The impact of aerosol on precipitation is one of the largest sources of uncertainties in climate change modeling (Levin and Cotton, 2008). The uncertainties are caused by a number of factors ranging from aerosol concentration, size and chemical composition, type of clouds that are involved (e.g., warm, mixed-phase, or ice) to processes that influence precipitation formation. Any mechanism that affects the precipitation efficiency ranging from cloud droplet formation to drizzle production is thus of significant importance.

The cloud droplet formation process depends on the concentration of atmospheric aerosols that have the ability to serve as cloud condensation nuclei (CCN), upon which water vapor can condense to form a cloud droplet. This phenomenon can increase the cloud albedo, and is commonly referred to as the first aerosol indirect effect (Twomey, 1977). High CCN concentrations can further enhance the production of more but smaller cloud droplets, resulting in increased cloud lifetime and its consequent effect on reduced precipitation. This effect is known as the second aerosol indirect effect (or the cloud life time effect; Albrecht, 1989). Due to their small size and relative abundance in the atmosphere, the role of CCN to droplet formation and its consequent effect on precipitation has been a focus of many studies (e.g., Rosenfeld, 1999, 2000; Andreae et al., 2004). However, much less understood is the effect of giant cloud condensation nuclei (GCCN) on cloud droplet nucleation and drizzle formation. In literature, GCCN is

vaguely defined as particles with dry particle diameter greater than 5 µm and are considered equally important due to their effect on cloud microphysics and precipitation.

Amongst atmospheric aerosols, mineral dust represents the dominant fraction of particulate by mass in the atmosphere. Due to its large size compared to other tropospheric aerosols, mineral dust is one of the major sources of natural coarse mode aerosol in the atmosphere (Kouimtzis and Samara, 1995). However, there still exists a big gap in the understanding of mineral dust as a GCCN.

The influence of dust CCN on warm clouds can be more significant if they are large enough to act as a GCCN thus altering precipitation efficiency (i.e., promote or suppress precipitation). Some studies suggest that large salt containing dust particles can initiate precipitation formation by broadening the droplet spectrum and enhancing cloud-coalescence processes in a cloud cycle (Feingold et al., 1999; Rudich et al., 2002). Yin et al. (2002) used parcel model simulations to show that dust GCCN can promote precipitation due to formation of a soluble coating on particle surface, causing dust GCCN to grow by collection. On the other hand, some satellite-based studies (e.g., Rosenfeld et al., 2001; Mahowald and Kiehl, 2003) suggested that dust particles can also decrease the collision-coalescence process, thus increasing cloud lifetime and reducing precipitation efficiency.

A number of studies have also addressed the impact of the GCCN concentrations on precipitation efficiency. Van den Heever et al. (2006) investigated the effects of increasing GCCN concentrations from relatively clean conditions to dusty conditions, using measurements from the CRYSAL-FACE field campaign. Their study concluded that while more liquid water was produced under dusty conditions, precipitation

processes were suppressed resulting in a reduction of total precipitation reaching the ground compared to the clean case. Teller and Levin (2006) found that increasing GCCN concentration led to a decrease in precipitation in clean clouds but increased precipitation in polluted clouds. The enhancement in precipitation from GCCN concentrations was a result of increased graupel production within the clouds. Additionally, dust GCCN in warm clouds can also evaporate cloud droplets, thus decreasing the number of collector drops and the probability of precipitation formation. This effect is commonly known as the Semi-Direct effect (Huang et al., 2006). Inconsistencies in defining size of GCCN (Levin et al., 1996; Feingold et al., 1999) as well as confusions on the ability of pristine or aged dust to act as GCCN (Yin et al., 2002) further complicate the understanding of dust-cloud-precipitation interactions, and their subsequent impacts on the climate and the hydrological cycle.

It has been well recognized that dust originating from major desert regions (e.g., Sahara, Gobi, and Taklamakan) can be transported large distances with implications to aerosol and cloud properties. Saharan dust from northern Africa can travel across the Atlantic Ocean (Karyampudi, 1979; Karyampudi et al., 1999) and can affect parts of Barbados as well as the eastern and southeastern parts of the United States (Li et al., 1996; Savoie and Prospero, 1997). Prospero (1999) also concluded based on the 23 years record that large concentrations of Saharan dust are transported from North Africa into Florida every year with daily concentrations ranging from $10 - 100$ µg m^{-3}. Similarly, significant amounts of Saharan dust were also observed across the Eastern Mediterranean into Europe during the circulation period of the year (Kallos et al., 2007). In turn, Asian dust can also travel across the Pacific Ocean, regularly affecting Hawaii and the western

United States (Perry et al., 1999; Sassen, 2002). Thus it is important to quantify the interactions of dust with different cloud types that are encountered along the route of dust transport, and their consequent effects on cloud dynamics and precipitation.

One such campaign that focused on understanding the interactions of aerosols with low level stratocumulus clouds was the Atlantic Stratocumulus Transition Experiment (ASTEX) (Albrecht et al., 1995) that was conducted off the northwest coast of Africa. As this location coincides with the major transport route of Saharan dust to Europe and southeastern United States, appreciable amounts of dust embedded in lower levels of shallow clouds were detected during ASTEX (Clarke et al., 1996; Chazette et al., 2001). Thus low level marine stratocumulus clouds observed during the ASTEX campaign provide an ideal framework to investigate the interaction of dust GCCN with cloud and its effect on cloud dynamics. The relevance of this case study to dust GCCN-cloud interactions is further substantiated by the impact of stratocumuli on boundary layer (BL) dynamics through the vertical distribution of heat and water vapor (Paluch and Lenschow, 1991; Feingold et al., 1996; Stevens et al., 1998), and because of the modest amounts of precipitation from such clouds to the Earth's surface.

More recently during the Cirrus Regional Study of Tropical Anvils and Cirrus Layers – Florida Area Cirrus Experiment (CRYSTAL-FACE) (Jensen et al., 2004) over the Florida peninsula, high aerosol concentrations associated with the transport of Saharan dust were observed (DeMott et al., 2003; Sassen et al., 2003). Majority of studies associated with dust during CRYSTAL-FACE have focused on understanding the effects of dust as Ice Nuclei (IN) during cirrus clouds formation; with only a few addressing the impact of dust as CCN and GCCN (Van Den Heever et al., 2006; Toon, 2003). Therefore,

CRYSTAL-FACE provides another ideal case study to evaluate the impacts of long-range transport dust GCCN at high altitudes on the deep convective clouds.

In this chapter, the effect of dust GCCN on droplet growth and its implications to cloud precipitation processes will be addressed. The growth of dust GCCN is simulated using a trajectory ensemble model (TEM) approach of Stevens et al. (1996) that employs a large eddy simulation (LES) of a cloud field coupled with a cloud parcel model. The effect of adsorption activation on the dust GCCN growth within the low level stratocumulus and deep convective clouds is investigated considering ASTEX and CRYSTAL-FACE campaigns, respectively. This study focuses on the examination of the efficiency of dust GCCN to precipitation processes by studying the effects of mineral aerosol FHH adsorption parameters (A_{FHH} and B_{FHH}), sensitivity to the dry GCCN size, and the effective water vapor uptake coefficients.

The chapter is organized as follows. Section 6.3 describes the TEM model and the steps of GCCN growth calculations. In section 6.4, some details on TEM simulations used in this study are provided. Section 6.5 presents the results of simulations. Finally, section 6.6 summarizes major findings of this work.

6.3   TEM Model

The growth of dust GCCN within a cloud type is simulated using the trajectory Ensemble model (TEM) approach of Stevens et al. (1996). The TEM employs a large eddy simulation (LES) of a cloud field to obtain a set of Lagrangian trajectories that captures the variability of thermodynamic properties and dynamics within the cloud. The time evolution of the parcel thermodynamic state is then used to drive a parcel model; which computes the liquid water content, water vapor supersaturation profiles, parcel

temperature, and activation and droplet growth of GCCN in the parcel. A horizontal ensemble average GCCN size throughout the boundary layer is calculated.

6.3.1 TEM Model Equations

Each trajectory contains information that characterizes the thermodynamic state of a material point as it is advected through a flow field. The information contained in each trajectory includes time, t, position coordinates, x, y, and z, pressure, P, potential temperature in moist air, θ_l, and the total (liquid and vapor) water mass mixing ratio, w_t. The time step between two consecutive trajectory points is 2 seconds. All material points are initially taken below cloud level to ensure that their initial liquid water content (LWC) is approximately zero. The tendencies of x, y, z, P, θ_l, and w_t are calculated by the finite difference between two consecutive time steps.

The information on parcel temperature, T, is not directly available from the trajectories and is computed from θ_l as

$$\theta_l = T\left(\frac{P^o}{P}\right)^{\frac{R}{C_p}} + \Delta H_V \left(\frac{P^o}{P}\right)^{\frac{R}{C_p}} w_l \qquad [6.1]$$

where ΔH_v is the latent heat of vaporization of water, C_p is the molar heat capacity of air, w_l is the liquid water mass mixing ratio, P^o is the reference pressure equal to 1000 mbar, and R is universal gas constant. Equation (6.1) is solved for T as

$$T = \theta_l \left(\frac{P}{P^o}\right)^{\frac{R}{C_p}} - \frac{\Delta H_V}{C_p} w_l \qquad [6.2]$$

The rate of change T with t is calculated from Eq. (6.2) as

$$\frac{dT}{dt} = \left(\frac{P}{P^o}\right)^{\frac{R}{C_p}} \frac{d\theta_l}{dt} + \theta_l \left(\frac{1}{P^o}\right)^{\frac{R}{C_p}} \left(\frac{R}{C_p}\right) P^{\frac{R}{C_p}-1} \frac{dP}{dt} - \frac{\Delta H_V}{C_p} \frac{dw_l}{dt} \qquad [6.3]$$

200

where $\dfrac{d\theta_l}{dt}$ and $\dfrac{dP}{dt}$ in Eq. (6.3) are approximated using $\dfrac{\Delta\theta_l}{\Delta t}$ and $\dfrac{\Delta P}{\Delta t}$ from the trajectory output.

Parcel water vapor supersaturation, S, is calculated from the water vapor mass mixing ratio, w_v (Seinfeld and Pandis, 2006) as

$$S = \frac{w_v}{w_v^*} = \frac{P M_a}{P^o M_w} w_v \qquad [6.4]$$

where w_v^* is the saturation water vapor mixing ratio, M_w and M_a are the molar masses of water and air respectively. w_v is calculated from the conservation of water in the parcel as

$$w_t = w_v + w_l \qquad [6.5]$$

Solving for the rate of change of w_v and using the trajectory output $\dfrac{\Delta w_l}{\Delta t}$ for $\dfrac{dw_l}{dt}$ gives

$$\frac{dw_v}{dt} = \frac{dw_t}{dt} - \frac{dw_l}{dt} \approx \frac{\Delta w_t}{\Delta t} - \frac{dw_l}{dt} \qquad [6.6]$$

The liquid condensation rate is given as (Seinfeld and Pandis, 2006)

$$\frac{dw_l}{dt} = \frac{\pi}{2} \sum N_i D_{pi}^2 \rho_w \frac{dD_{pi}}{dt} \qquad [6.7]$$

where N_i is the number of droplets in each size class, i per unit mass of air, ρ_w is the density of water, and D_{pi} is the droplet diameter of each size class.

The growth of GCCN is determined by solving the droplet growth/evaporation rate equation given by (Seinfeld and Pandis, 2006)

$$D_{pi} \frac{dD_{pi}}{dt} = \frac{s - s_{eq}}{\dfrac{\rho_w RT}{4 P_{H_2O}^\circ D_v' M_w} + \dfrac{\Delta H_v M_w}{4 k_a' T}\left(\dfrac{\Delta H_v \rho_w}{RT} - 1\right)} \qquad [6.8]$$

where D_{pi} is the droplet diameter, s is the parcel supersaturation, ρ_w is the water density, M_w is the molar mass of water, R is the universal gas constant, T is the average parcel temperature, $P_{H_2O}^{\circ}$ is the equilibrium water vapor pressure, ΔH_v is the enthalpy of vaporization of water, D_v' is the diffusivity of water vapor in air modified for noncontinuum effects, and k_a' is the thermal conductivity of air modified for non-continuum effects. Here D_v' is defined as (Fukuta and Walter, 1970)

$$D_v' = \frac{D_v}{1 + \frac{2D_v}{\alpha_c D_p}\sqrt{\frac{2\pi M_w}{RT}}} \qquad [6.9]$$

where D_v is the diffusivity of water vapor in air and α_c is the water vapor uptake coefficient. k_a' is given by

$$k_a' = \frac{k_a}{1 + \frac{2k_a}{\alpha_T D_p \rho_a c_p}\sqrt{\frac{2\pi M_a}{RT}}} \qquad [6.10]$$

where M_a is the mean molar mass of air, k_a is the thermal conductivity of air, ρ_a is the air density, c_p is the heat capacity of air, and α_T is thermal accommodation coefficient (equal to 1.0).

The non-modified water vapor diffusivity, D_v, and the thermal conductivity of air, k_a, are given by

$$D_v = \frac{0.211 \times 10^5}{P}\left(\frac{T}{273}\right)^{1.94} \qquad [6.11]$$

$$k_a = 10^{-3}(4.39 + 0.071 \times T) \qquad [6.12]$$

For insoluble dust GCCN activating according to FHH-AT, the equilibrium supersaturation of the droplet, s_{eq}, is given by Kumar et al. (2009)

$$s_{eq} = \frac{4\sigma_w M_w}{RT\rho_w D_p} - A_{FHH}\left(\frac{D_p - D_{dry}}{2D_{H_2O}}\right)^{-B_{FHH}}$$ [6.13]

where σ_w is the CCN surface tension at the point of activation (Pruppacher and Klett, 1997), D_{dry} is the dry CCN diameter, D_{H_2O} is the diameter of water molecule equal to 2.75 Å (Kumar et al., 2009), and A_{FHH} and B_{FHH} are adsorption parameters constrained from the activation experiments (Kumar et al., 2010).

To summarize, parcel T is calculated using Eq. (6.2) from initial conditions of θ_l, P and w_t assuming that w_l is negligible. The initial S is calculated using Eq. (6.4). The initial D_{pi} is calculated using Eq. (6.8), assuming the aerosol is in equilibrium with S.

6.3.2 Calculation of Supersaturation Profiles

The supersaturation profiles associated with each trajectory set are derived using a parcel model initialized with a prescribed set of CCN distributions, constrained by the thermodynamic information contained in trajectories. In this study, two sets of supersaturation histories, one characteristic of a pristine environment (marine size distribution of Whitby, 1978) and another representing polluted environments (urban size distribution of Whitby 1978) were derived for each LES trajectory set. Table 6.1 contains information on CCN distribution parameters. A simple aerosol chemical composition of $(NH_4)_2SO_4$ is assumed for the aerosol size distribution while calculating the supersaturation profiles. Using $(NH_4)_2SO_4$ aerosol chemical composition to represent clean and urban aerosol conditions is explained below.

Ideally, the supersaturation profiles should be generated using size distributions that are typical of the mineral dust aerosol and activation being described by FHH-AT. However, since two extreme CCN conditions (pristine vs. urban) are considered with activation being described by KT, the resulting competition for water vapor will be more intense between KT particles that between FHH-AT particles of same size (Kumar et al., 2009). Therefore, it is unlikely that the ideal cloud supersaturation levels will lie outside of the two cases and hence the approach should suffice.

Table 6.1: Aerosol size distributions from Whitby (1978) used in this study

Aerosol Type	Nuclei Mode			Accumulation Mode			Coarse Mode		
	D_{g1}	σ_1	N_1	D_{g2}	σ_2	N_2	D_{g3}	σ_3	N_3
Marine	0.010	1.6	340	0.070	2.0	60	0.62	2.7	3.1
Urban	0.014	1.8	106000	0.054	2.16	32000	0.86	2.21	5.4

D_{gi} is the median diameter (μm), N_i is the number of dry particles (cm^{-3}), and σ_i is the geometric standard deviation of the ith mode.

6.3.3   Calculations of GCCN Growth

The model algorithm illustrating the procedure used in calculating the growth of GCCN within a cloud field is presented in Medina and Nenes (2004), and hence it is only briefly described here. The Lagrangian trajectories obtained from LES simulations together with information of CCN size distribution are used as inputs into the cloud parcel model to derive supersaturation history for each trajectory set. Dust GCCN with a certain composition (given by A_{FHH} and B_{FHH}) is introduced into the cloud field and grows according the Eq. (8). The effect of small scale local fluctuations on individual droplets is neglected. The droplet is allowed to traverse the cloud field, and horizontally averaged GCCN size is then calculated to represent the average vertical profiles of GCCN size.

6.4   Simulation Setup

6.4.1   Stratocumulus Clouds

The Lagrangian trajectories of cloud fields observed during the ASTEX Campaign were used as representative of low level stratocumulus clouds. The trajectories describe two marine stratocumulus cloud simulations namely ASTEX-1 and ASTEX-2 under conditions observed during the campaign. ASTEX-1 represents a non-precipitating cloud, while ASTEX-2 is a heavily drizzling cloud. The stratocumulus clouds considered here cover the entire simulation domain ($2.8 \times 2.8 \ km^2$) and persist for the duration of the simulation time (Zhu et al., 2004). 500 trajectories covering 1 hour of simulation time were derived for each cloud type. Output was saved every 2 seconds. Important characteristics of each cloud have been described in detail by Medina and Nenes (2004)

and are not repeated here. However, we note that both clouds are energetic enough to maintain droplets of sizes up to 80 μm in diameter.

6.4.2 Deep Convective Clouds

Trajectories representing deep convective clouds observed during CRYSTAL-FACE were used to study the interaction of long-range transported African dust GCCN with high level clouds. This cloud field covered only 22% of the 6.0×6.0 km^2 of the simulation domain and dissipated on the time scale of ~ 30 minutes. The 61 convective trajectories covering 30 minutes of simulation time were used and the output was saved every 10 seconds.

6.4.3 Composition and Size of GCCN

Mineral aerosol representing GCCN is considered with properties given by the adsorption parameters A_{FHH} and B_{FHH}. Kumar et al. (2010) found on average for dusts, $A_{FHH} = 2.25 \pm 0.75$ and $B_{FHH} = 1.20 \pm 0.10$. Therefore in this study, we explore the sensitivity to the range of ± 0.75 for A_{FHH} and ± 0.10 for B_{FHH} relevant to mineral aerosol. We also consider several initial dry dust GCCN diameters (1 μm, 2.5 μm, 5 μm, and 10 μm) to test the sensitivity of GCCN growth to its initial dry size. The chosen size range is representative of dust sizes expected to be found in low level stratocumulus and deep convective clouds. Finally, the effect of water vapor mass transfer uptake coefficient, α_c, on the growth of GCCN is also explored. Kumar et al. (2010) suggested that α_c, for dust aerosol is 30 – 80% lower than what is expected for $(NH_4)_2SO_4$. Hence, simulations are designed to test GCCN growth sensitivity with α_c equal to 0.1, 0.042, and 0.025.

6.5   Simulation Results

6.5.1   *Comparison of Cloud Types Scenarios*

Important characteristics associated with each cloud observed and simulated during ASTEX-1, ASTEX-2, and CRYSTAL-FACE are shown in Fig. 6.1. It can be seen from Fig. 6.1a that LWC (liquid water content) in the ASTEX-2 case is ~ 0.8 g m^{-3}, which is higher than that observed for ASTEX-1 with LWC ~ 0.4 g m^{-3}. This is consistent with cloud types observed during the campaign, with ASTEX-2 representative of heavily drizzling cloud, and ASTEX-1 representing non-drizzling cloud. It can be also seen that ASTEX-1 has a higher cloud base (~ 400 m) compared to ASTEX-2 with cloud base at ~ 200 m. Figure 6.1a also shows the LWC profile for CRYSTAL-FACE that is representative of a deep convective cloud. It can be seen that CRYSTAL-FACE has a cloud base at ~ 400 m and extends much higher up to as high as 2200 m.

The characteristic supersaturation profiles derived for the clean and polluted environments that will be investigated in this study are also shown in Fig. 6.1. Supersaturation profiles generated for the two conditions derived for stratocumulus clouds during ASTEX-1 are shown in Fig. 6.1b. It can be seen that the derived supersaturation profile (used to drive GCCN growth in the parcel model) for the clean case exhibits a higher supersaturation than for the polluted case. This is expected and is a consequence of increased competition effects for the amount of available water vapor (Nenes et al., 2001) in polluted aerosol conditions that lead to lower supersaturations in clouds relative to the clouds observed in pristine environments. It is also noted that this reduction in cloud water vapor supersaturation is expected to decrease the overall driving force for GCCN growth, thereby reducing the possibility of dust GCCN to grow and

become efficient collector drop in polluted clouds compared to pristine clouds. This is also discussed briefly in section 6.5.2. Similar behavior with lower cloud water vapor supersaturation associated with polluted environments for ASTEX-2 and CRYSTAL-FACE is also observed (not shown).
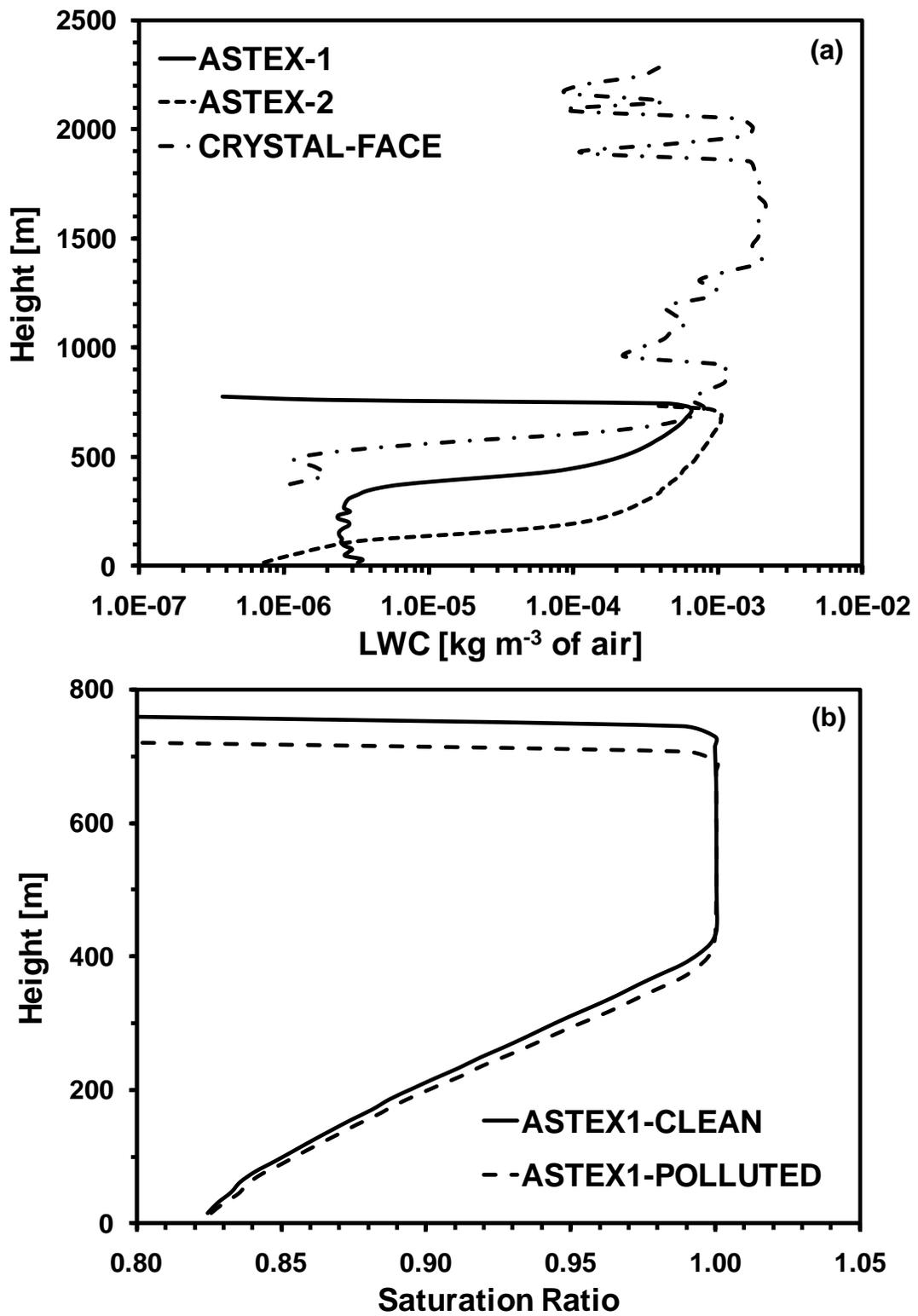
Figure 6.1: **(a)** LWC profiles observed during ASTEX-1, ASTEX-2, and CRYSTAL-FACE. **(b)** Simulated cloud water vapor supersaturation profiles in clean and polluted aerosol conditions during ASTEX-1.

209

6.5.2 *Effect of Dry Size on Dust GCCN Growth*

The analysis presented here and in following sections is performed to address the effect of adsorption activation on dust GCCN growth. In terms of the microphysical evolution of the cloud, the size of GCCN inside the cloud field is of importance because GCCN larger than 40 µm can act as effective collector drops (Feingold et al., 1999).

Figure 6.2 presents the average growth of dust GCCN with dry sizes of 1 µm, 2.5 µm, 5 µm, and 10 µm under pristine (dashed lines) and polluted (solid lines) conditions for cloud types observed during ASTEX-1 (Fig 6.2a), ASTEX-2 (Fig 6.2b), and CRYSTAL-FACE (Fig 6.2c). Simulations shown in Fig. 6.2 are performed for A_{FHH} = 2.25 and B_{FHH} = 1.20; adsorption parameters representative of dust aerosol (Kumar et al., 2010). Simulations suggest that as GCCN dry size increases, the resulting GCCN droplet size inside the cloud field also increases. This implies that dust aerosols with dry sizes between 1 µm to 10 µm (and greater) representative of coarse mode dust can grow by adsorption activation mechanism, and possess potential to reach sizes of 40 µm or greater in the presence of sufficient water vapor supersaturation levels. This confirms that the dust GCCN can affect the aerosol-cloud-precipitation linkage in both low level stratocumulus clouds and deep convective clouds. This result is of significant importance as it confirms that fresh dust entrained in boundary layer interacting with low level stratocumulus clouds or long-range transported dust interacting with deep convective clouds can affect the cloud microphysics with implications to precipitation efficiency.

It can be also seen from Fig. 6.2 that for all three cases of ASTEX-1, ASTEX-2, and CRYSTAL-FACE, the resulting GCCN droplet sizes under pristine conditions are significantly greater than the simulated sizes for the polluted environments. This is

consistent with greater supersaturation levels observed in pristine conditions (Fig. 6.1b) and explains the difference in observed droplet growth. Furthermore, for simulations representative of pristine conditions, the dust GCCN can grow to sizes greater than the threshold size of 40 µm in ASTEX-2 (Fig. 6.2b). This implies that dust GCCN, with B_{FHH} equal to 1.20 and with a dry size as low as 1 µm can act as an efficient collector drop in clouds representative of low level heavy-drizzling marine stratocumulus type. A similar behavior is also observed under pristine condition of ASTEX-1, where dust GCCN grows to up to 35 - 38 µm, and much higher than those simulated under polluted conditions of ASTEX-1. As 40 µm is only an approximate indicator of collector drops and can vary from cloud to cloud, it can be assumed that for certain low level stratocumulus clouds even a droplet size of up to 35 µm may be efficient to make GCCN an efficient collector drop. This implies that dust GCCN when present under clean conditions, may have the potential to change the cloud from a non-precipitating to precipitating state. This also suggests that Niger dust (B_{FHH} = 1.27), representative of African dust embedded in low level marine stratus clouds observed during ASTEX, can serve as collector drop with implications to precipitation.

Figure 6.2c shows that dust GCCN can grow to sizes greater than 40 µm under pristine conditions of CRYSTAL-FACE for B_{FHH} equal to 1.20 representative of fresh dust aerosol. As dust ages during long-range transport, it is expected to become more hydrophilic. This implies that aged Niger dust GCCN would grow to sizes greater than (40 µm) those simulated for pristine conditions of CRYSTAL-FACE and can also affect cloud microphysics of deep convective clouds. Furthermore, the increased collector drop potential of dust GCCN under clean conditions of deep convective clouds can also affect

ice and graupel formation in ice and mixed phase clouds respectively, with more water being retained in liquid phase.

Simulations performed for polluted conditions of ASTEX-1, ASTEX-2, and CRYSTAL-FACE indicate that dust GCCN growth is inhibited with observed maximum size much lower than the critical threshold of 40 µm in both (low level) stratocumulus and (high level) convective clouds. This implies that for low level marine stratocumulus clouds (drizzling or non-drizzling) embedded with high CCN concentrations (of dust or other aerosol types) observed off northwest coast of Africa, or deep convective clouds associated with long-range transport of African dust, dust GCCN if present may not affect drizzle formation by serving as a collector drop, for conditions considered in this study.
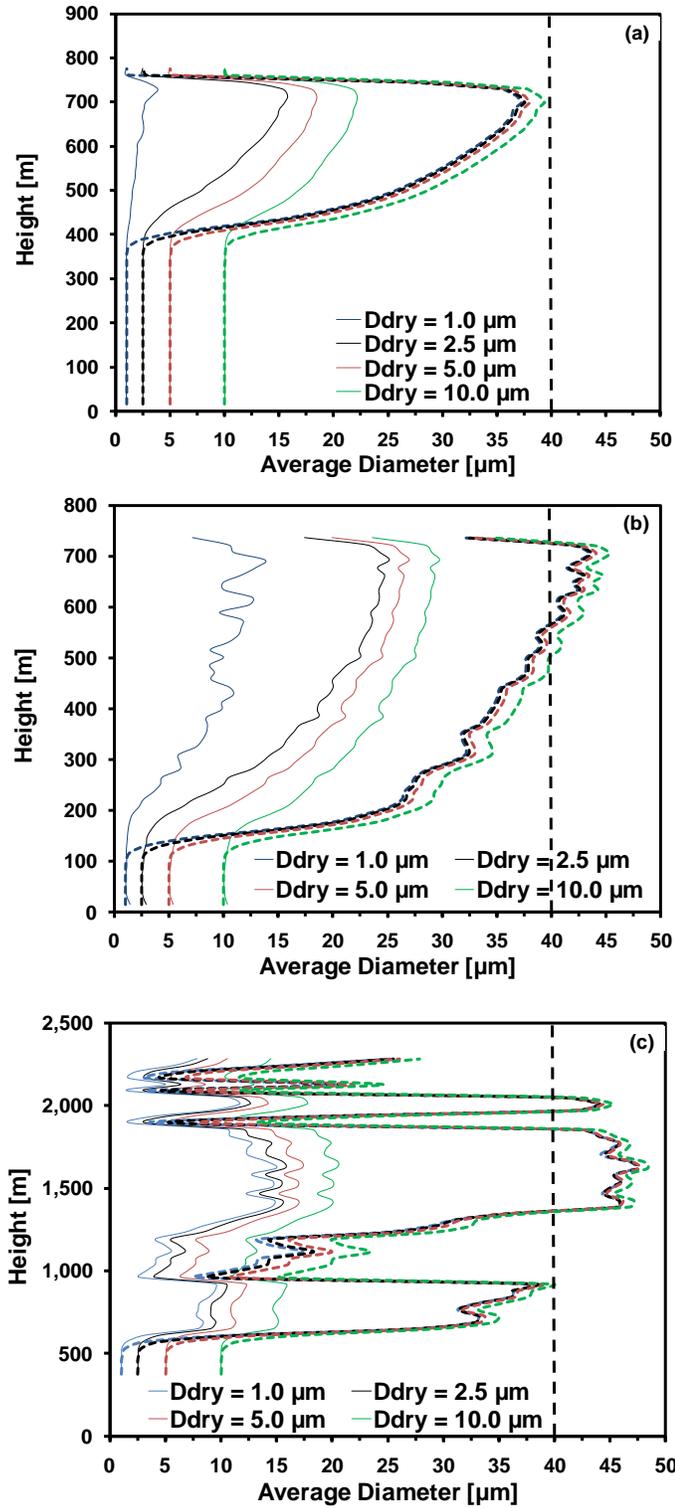
Figure 6.2: Average growth of dust GCCN with $A_{FHH} = 2.25$ and $B_{FHH} = 1.20$ for **(a)** ASTEX-1, **(b)** ASTEX-2, and **(c)** CRYSTAL-FACE. Solid and dashed lines represent polluted and pristine aerosol conditions, respectively.

6.5.3   *Effect of CCN Concentration and Activation Physics on Dust GCCN Growth*

All studies to date on dust GCCN cloud precipitation linkages address the affect of dust GCCN activation and its subsequent growth by Köhler Theory (KT; Köhler, 1936). However, based on the dependence of critical superstation with dust dry diameter, Kumar et al. (2010) found that FHH-AT is a better description of fresh dust CCN activity. Therefore, this study also addresses the effect of activation physics on the growth of dust GCCN, and its implications to cloud precipitation efficiency.

Figure 6.3 presents simulations for the average growth of dust GCCN of dry sizes equal to 1 µm, 2.5 µm, 5 µm, and 10 µm activated by FHH-AT (dashed lines) and by KT (solid lines) for clean and polluted conditions for cloud types observed during ASTEX-1 (Fig 6.3a, 6.3d), ASTEX-2 (Fig 6.3b, 6.3e), and CRYSTAL-FACE (Fig 6.3c, 6.3f). Simulations are performed for $A_{FHH} = 2.94$ and $B_{FHH} = 1.27$, representative of adsorption parameters determined for Niger dust aerosol (Kumar et al., 2010). The KT activation in ASTEX-1 an ASTEX-2 is parameterized by the hygroscopicity parameter, κ (Petters and Kreidenweis, 2007) equal to 0.02 for Niger dust (Kumar et al., 2010). It can be seen from Fig. 6.3 that dust GCCN growth is different under polluted and clean conditions for the same cloud type. For instance, under relatively clean conditions observed during ASTEX-1 (Fig. 6.3a), ASTEX-2 (Fig. 6.3b), and CRYSTAL-FACE (Fig. 6.3c), growth of GCCN by FHH-AT produces droplets of sizes almost equal to or greater than 40 µm. However, dust GCCN growth is inhibited under polluted conditions (Fig. 6.3d, 6.3e, 6.3f) with droplet of sizes much lower than 40 µm being simulated. This suggests that dust GCCN under polluted conditions may not affect precipitation efficiency, but if present in pristine environment, dust GCCN can serve as collector drops and increase precipitation

efficiency. These results of increased precipitation efficiency by dust GCCN in clean environments are consistent with the findings of Rosenfeld et al. (2001) and Van den Heever et al. (2006) that dust suppressed precipitation efficiency under conditions with enhanced CCN concentrations.

It can be also seen in Fig. 6.3 that activation by KT or FHH-AT has different effects on the dust GCCN growth in clouds with identical supersaturation levels (or identical CCN concentrations). For instance, under pristine conditions of ASTEX-1 (Fig. 6.3a) and ASTEX-2 (Fig. 6.3b), dust GCCN growth by KT has a relatively smaller impact on precipitation efficiency with observed GCCN droplet sizes for Niger dust either smaller or of the same order as those predicted when growth is described by FHH-AT. This implies that if dust GCCN activates by KT, it may incorrectly inhibit GCCN growth under clean conditions with implications to reduced precipitation efficiency. The impact of activation physics is more pronounced under polluted environments (Fig. 6.3d, 6.3e) where dust activation by KT can make GCCN droplets size appear larger than what they actually should be when activated by FHH-AT. For instance, simulations performed on stratocumulus clouds under polluted conditions of ASTEX-2 indicated that dust GCCN if activated by KT can increase precipitation efficiency by inaccurately growing dust GCCN to sizes of efficient collector drops. This is contradictory to findings by previous studies, and confirms the inappropriateness of using KT to represent the dust GCCN activation. In addition, as GCCN dry size increases from 1 μm to 10 μm, the impact of KT to dust GCCN growth is more pronounced than FHH-AT. This is because as the dry size of the dust GCCN increases, the corresponding solute volume fraction (for KT) increases, but surface area to volume ratio (for FHH-AT) decreases. This can be seen

in Fig. 6.3e, where the observed droplet sizes of dust GCCN activated by KT are inaccurately simulated to be as large as 40 µm with implications to cloud precipitation processes.

In this study, we also address the effect of KT and FHH-AT on dust GCCN growth in deep convective clouds observed during CRYSTAL-FACE. Simulations performed (not shown) for Niger dust using KT (with $\kappa = 0.02$) and dust GCCN of dry sizes equal to 1 µm, 2.5 µm, 5 µm and 10 µm under pristine and polluted conditions of CRYSTAL-FACE indicated negligible growth. Therefore, simulations were repeated with $\kappa = 0.03$, and are compared against those by FHH-AT as shown in Fig. 6.3c and 6.3f. Based on the results (Fig. 6.3c, 6.3f), it can be concluded that if dust activates according to KT (i.e. parameterized using κ representative of fresh dust), dust GCCN should not affect cloud precipitation efficiency (and cloud microphysics) in convective clouds under both polluted and pristine environments. However, when dust GCCN activation is described with FHH-AT, it is found that under pristine conditions (Fig. 6.3c), dust GCCN can increase precipitation efficiency. These results are consistent with previous studies on dust GCCN in CRYSTAL-FACE clouds (e.g., Van den Heever et al., 2006), suggesting that dust particles can promote precipitation under pristine conditions. Furthermore, the analysis performed here also questions previous studies on dust GCCN effect on cloud microphysics, with activation described by KT.
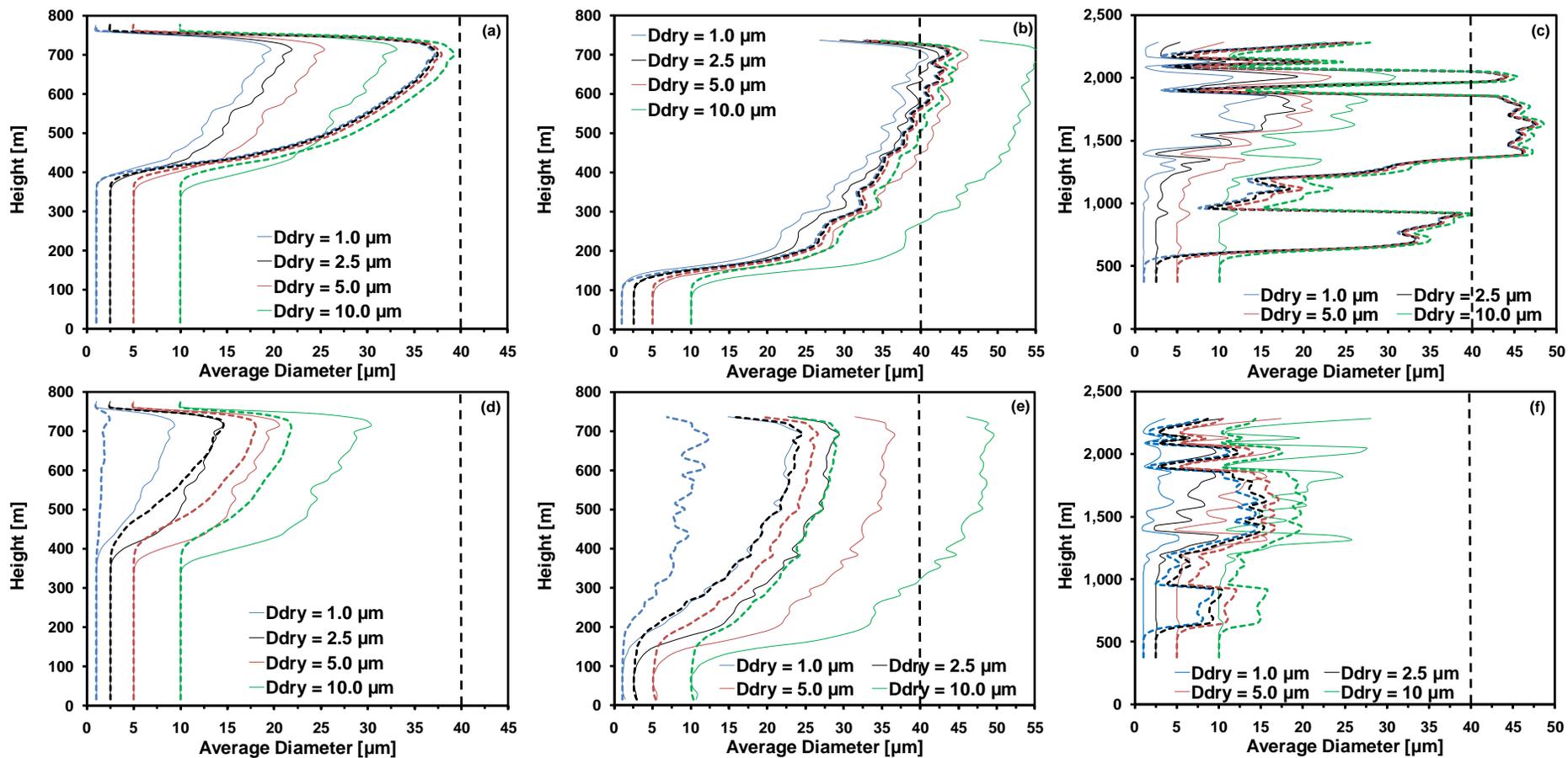
Figure 6.3: Average growth of dust GCCN with $A_{FHH} = 2.25$ and $B_{FHH} = 1.20$ for **(a,d)** ASTEX-1, **(b,e)** ASTEX-2, and **(c,f)** CRYSTAL-FACE. Top and bottom panels correspond to pristine and polluted aerosol conditions, respectively. Solid and dashed lines refer to growth by KT and FHH-AT, respectively. $\kappa = 0.02$ for **(a)**, **(b)**, **(d)**, **(e)**, and $\kappa = 0.03$ for **(c)**, **(f)**.

217

6.5.4   *Effect of B_{FHH} on Dust GCCN Growth*

The adsorption parameter B_{FHH} controls the hydrophilicity of dust GCCN. Based on laboratory measurements of dust CCN activity, Kumar et al. (2010) found B_{FHH} equal to 1.20 ± 0.10 for mineral aerosol, with lower B_{FHH} values corresponding to a more hydrophilic dust. As non-drizzling marine stratocumulus clouds are most ubiquitous in the atmosphere, the effect of B_{FHH} on the dust GCCN growth required to translate cloud from a non-drizzling to a precipitating state is investigated in this section. The effect of B_{FHH} on the dust GCCN growth in clean condition observed during ASTEX-1 is simulated and is shown in Fig. 6.4a. It can be seen that as B_{FHH} decreases from 1.30 to 1.10, the resulting driving force for condensational growth in Eq. (8) increases consequently. This results in larger wet size of the dust GCCN in cloud for $B_{FHH} = 1.10$ when compared to less hydrophilic dust GCCN (with $B_{FHH} = 1.30$) for the same dry diameter. A similar behavior of increasing hydrophilicity with decreasing B_{FHH} is also observed for polluted environments of ASTEX-1 as well as clean and polluted conditions of ASTEX-2 (not shown). The effect of B_{FHH} on dust GCCN droplet size is also explored under the clean and polluted conditions observed during CRYSTAL-FACE. Consistent with the above results, an increase in GCCN droplet size with a reduction in B_{FHH} value was found under both clean (not shown) and polluted conditions (Fig. 6.4b) of CRYSTAL-FACE.

The data shown in Fig. 6.4a suggest that in low level marine clean stratocumulus clouds, a 10 μm dust GCCN can act as an efficient collector drop (by growing to droplet size ~ 40 μm) when B_{FHH} is reduced from 1.30 to 1.10. Consequently, this can change the cloud microphysics and dynamics of low level stratocumulus cloud from a non-

precipitating to precipitating state. A comparison of B_{FHH} values for different regional soils representative of global dust regions reveals that certain Asian soils (with B_{FHH} ~ 1.10 – 1.20) can act as more efficient collector drops compared to African dust (B_{FHH} = 1.27) and Arizona Test dust (B_{FHH} = 1.28). Furthermore, these results demonstrate that B_{FHH} has a negligible effect on the precipitation efficiency of deep convective clouds (CRYSTAL-FACE). This is because under clean conditions, less hydrophilic dust GCCN with B_{FHH} = 1.30 can grow to a droplet size greater than 40 µm, while more hydrophilic dust GCCN with B_{FHH} = 1.10 is unable to grow in excess of 40 µm under polluted conditions. The results in this section imply that dust particles from different source regions most likely have different impacts on precipitation efficiency when interacting with low level stratocumulus clouds and should be parameterized appropriately by regional models. Whether or not the effect of varying dust B_{FHH} on dust-cloud interaction has an impact on global precipitation cycle remains to be answered by future studies.
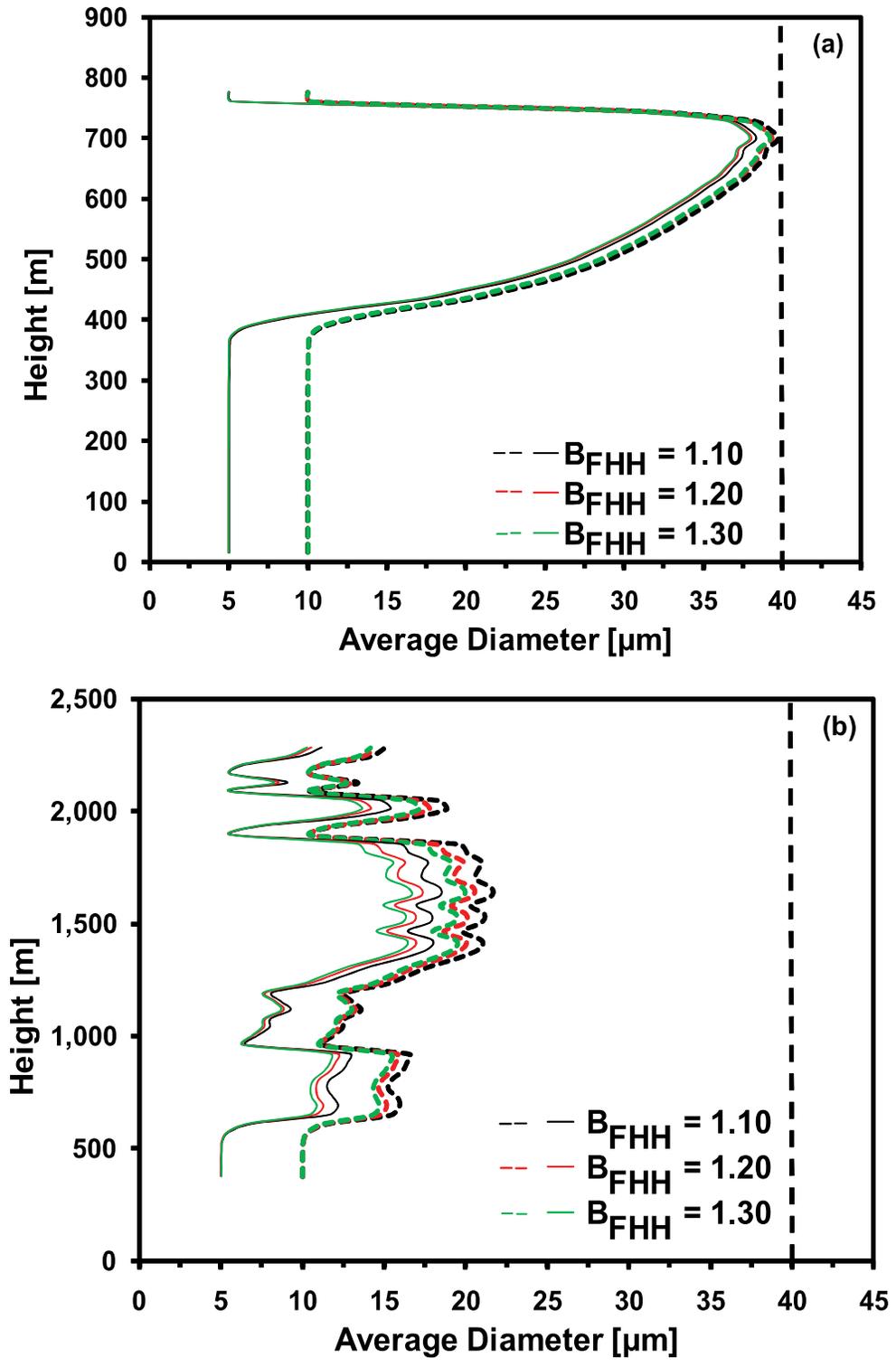
Figure 6.4: Average growth of dust GCCN **(a)** ASTEX-1: clean condition **(b)** CRYSTAL-FACE: polluted condition. Solid and dashed lines refer to dry size equal to 5 μm and 10 μm, respectively.

6.5.5 *Effect of Water Vapor Mass Transfer Coefficient on Dust GCCN Growth*

Kumar et al. (2010) found that mineral dust exhibits a $30 - 80\%$ lower water vapor mass transfer coefficient, α_c, compared to ammonium sulfate aerosol based on dust kinetics measurements. Thus, the effect of α_c on dust GCCN growth is also investigated in this study. The effect of α_c to condensational growth in Eq. (8) is introduced into $D_v^{'}$ as given by Eq. (9). A higher α_c implies a reduced water vapor mass transfer resistance and that translates to an increase in dust GCCN droplet size.

Figure 6.5 presents simulations for the average growth of dust GCCN of dry sizes of 5 μm and 10 μm for clean conditions observed during ASTEX-1. Simulations are performed for A_{FHH} = 2.25 and B_{FHH} = 1.20, and for different values of α_c: 0.042 (representative of $(NH_4)_2SO4$ aerosol), 0.025 (representative of dust aerosol) and 0.1 (upper limit of $(NH_4)_2SO4$ aerosol). It can be seen from Fig 6.5 that α_c does not have an appreciable impact on dust GCCN growth and consequently reduces the GCCN droplet size by less than 5%. A similar behavior of reduced droplet size is also observed for polluted conditions of ASTEX-1 as well as clean and polluted conditions of ASTEX-2 and CRYSTAL-FACE (not shown). These results suggest that the reduced α_c for dust GCCN does not have an appreciable effect on the activation kinetics of a single dust particle when present in shallow stratocumulus or deep convective clouds. Whether reduced dust α_c affects water vapor competition in CCN populations consisting of both KT and FHH particles requires further quantification.
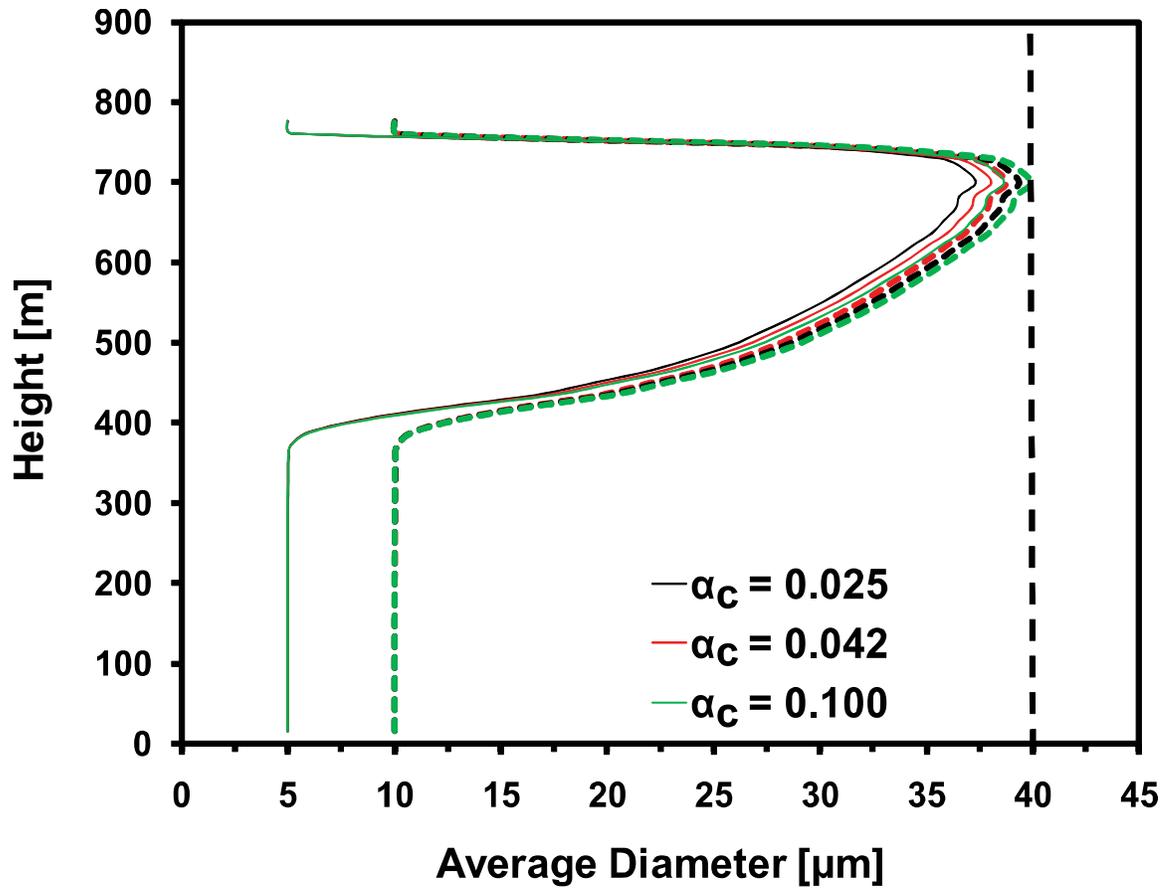
Figure 6.5: Average growth of dust GCCN during ASTEX-1 with clean condition. Solid and dashed lines refer to dry size equal to 5 µm and 10 µm, respectively. Simulations are performed for $A_{FHH} = 2.25$ and $B_{FHH} = 1.20$.

6.6   Conclusions

In this study, the effect of adsorption activation on the growth of dust GCCN within a low level stratocumulus and deep convective clouds was investigated using the trajectory ensemble model (TEM) approach of Stevens et al. (1996). Three different trajectories, two representing shallow stratocumulus (non-drizzling and heavily drizzling) observed during ASTEX and one representative of deep convective clouds during CRYSTAL-FACE were used to study the interaction of dust GCCN with low and high level clouds, respectively. Furthermore, two different aerosol conditions - one typical of clean and other polluted environment - were simulated for each of three cloud cases to study the behavior of dust GCCN growth in two contrasting environments.

The ability of dust GCCN to affect cloud microphysics was assessed by its effectiveness to act as collector drops. In our approach, we used a threshold diameter of 40 μm to classify dust GCCN as a collector drop. Simulations demonstrated that dust GCCN with dry sizes equal to 1 μm and above can activate and grow by adsorption mechanism. The results also indicated that under sufficient water vapor supersaturations, dust GCCN can serve as collector drops in both low and high level stratocumulus and convective clouds, respectively.

This study shows that the conditions to exceed the threshold of 40 μm was a function of cloud supersaturation history (i.e., whether dust GCCN were present under pristine or polluted conditions). Simulations indicated that under pristine conditions, dust GCCN has potential to act as efficient collector drops in both stratocumulus and convective clouds. However under polluted conditions, dust GCCN growth was inhibited, implying that dust particles in polluted environments may have a reduced effect on cloud

precipitation efficiency. A comparison of simulations derived for ASTEX-1 (typical of non-precipitating stratocumulus cloud) in pristine and polluted conditions indicated that dust GCCN when present under clean conditions, may have the potential to change the cloud from a non-precipitating to precipitating state. This result is of significant importance and illustrates that dust GCCN may be influencing the microphysical evolution of clouds to a greater extent that previously assumed by climate models.

The impact of activation physics on the growth of dust GCCN was also investigated in this study. Different droplet sizes were observed when dust GCCN growth was represented by KT and FHH-AT. Simulation performed for stratocumulus clouds indicated that under polluted condition of ASTEX-2, dust GCCN activated by KT can increase precipitation efficiency by inaccurately growing dust GCCN to sizes of efficient collector drops. On the other hand, results for dust GCCN activation by KT incorrectly reduced precipitation efficiency by inhibiting dust GCCN growth under clean conditions. The impact of activation physics on dust GCCN growth was more pronounced in CRYSTAL-FACE (deep convective clouds), with simulation indicating that dust GCCN growth was inhibited under both clean and polluted conditions when activation was represented by KT. However, dust GCCN was found to serve as an effective collector drop under clean conditions when activated by FHH-AT. The latter is expected and has been observed by previous studies. These results indicate that activation physics has strong implications to dust aerosol-cloud-precipitation linkages in stratocumulus and convective clouds.

The effect of B_{FHH} on the dust GCCN growth was also examined in this study. Simulations indicated that as dust hydrophilicity was increased (by decreasing B_{FHH}),

resulting dust GCCN droplet sizes were found to increase. The impact of decreasing B_{FHH} on cloud microphysics was more profound for clean stratocumulus clouds that could be transformed from a non-precipitating to drizzle forming cloud in the presence of dust GCCN. The results also demonstrated that B_{FHH} has a negligible effect on the precipitation efficiency of polluted deep convective clouds (CRYSTAL-FACE) as droplet sizes were much lower than the threshold size even as B_{FHH} value was reduced. The results imply that dust particles from different source regions may have different impacts on precipitation efficiency when interacting with low level stratocumulus clouds and should be parameterized appropriately by regional models.

Finally, the effect of α_c on dust GCCN growth was also addressed and was found to have a negligible impact on dust GCCN activation kinetics for conditions observed during ASTEX-1, ASTEX-2, and CRYSTAL-FACE. Whether reduced dust α_c affects water vapor competition in GCCN populations consisting of both KT and FHH particles is left for future study.

6.7   Acknowledgements

6.8   References

Albrecht, B. A.: Aerosols, cloud microphysics, and fractional cloudiness, Science, 245, 1227 – 1230, 1989.

Albrecht, B. A., Bretherton, C. S., Johnson, D., Scubert, W. H., and Frisch, A. S.: The Atlantic Stratocumulus Transition Experiment: ASTEX, Bull. Am. Meteorol. Soc., 76, 889 – 904, 1995.

Andreae, M. O., Rosenfeld, D., Artaxo, P., Costa, A. A., Frank, G. P., Longo, K. M., and Silva-Dias, M. A. F.: Smoking rain clouds over the Amazon, Science, 303, 1337 – 1342, 2004.

Chazette, P., Pelon, J., Moulin, C., Dulac, F., Carrasco, I., Guelle, W., Bousquet, P., and Flamant, P. H.: Lidar and satellite retrieval of dust aerosols over the azores during SOFIA/ASTEX, Atmos. Environ., 35, 4297 – 4304, 2001.

Clarke A. D., Porter J. N., Valero F. P. J., and Pilewskie P.: Vertical profiles, aerosol microphysics, and optical closure during the Atlantic Stratocumulus Transition Experiment: Measured and modeled column optical properties, J. Geophys. Res. 101, 4443 - 4453, 1996.

DeMott, P. J., Sassen, K., Poellot, M. R., Baumgardner, D., Rogers, D. C., Brooks, S. D., Prenni, A. J., and Kreidenweis, S. M.: African dust aerosols as atmospheric ice nuclei, Geophys. Res. Lett., 30(14), 1732, doi:10.1029/2003GL017410, 2003.

Feingold, G., Cotton, W. R., Kreidenweis, S. M., and Davis, J. T.: The impact of giant cloud condensation nuclei on drizzle formation in stratocumulus: implication for cloud radiative properties, J. Atmos. Sci., 56, 4100 - 4117, 1999.

Feingold, G., Stevens, B., Cotton, W. R., and Frisch, A. S.: On the relationship between drop in-cloud residence time and drizzle production in stratocumulus clouds. J. Atmos. Sci., 53, 1108 – 1122, 1996.

Fukuta, N. and Walter, L. A.: Kinetics of hydrometer growth from the vapor; spherical model, J. Atmos. Sci., 27, 1160–1172, 1970.

Huang, J., Lin, B., Minnis, P., Wang, T., Wang, X., Hu, Y., Yi, Y., and Ayers, J. K.: Satellite based assessment of possible dust aerosols semi-direct effect on cloud water path over East Asia, Geophys. Res. Lett., 33, L19802, doi:10.1029/2006GL026561, 2006.

Jensen, E., Starr, D. O. C., and Toon, O. B.: Mission investigates tropical cirrus clouds, Eos Trans. AGU, 84(5), 45, 50, 2004.

Kallos, G., Astitha, M., Katsafados, P., and Spyrou, C.: Long-Range Transport of Anthropogenically and Naturally Produced Particulate Matter in the

Mediterranean and North Atlantic: Current State of Knowledge, J. Appl. Meteor. Climatol., 46, 1230 – 1251, 2007.

Karyampudi, V. M.: A detailed synoptic-scale study of the structure, dynamics, and radiative effects of the Saharan air layer over the eastern tropical Atlantic during GARP Atlantic Tropical Experiment, M.S. thesis, pp. 136, Dep. of Meteorol., Pa. State Univ., 1979.

Karyampudi, V. M., Palm, S. P., Reagen, J. A., Fang, H., Grant, W. B., Hoff, R. M., Moulin, C., Pierce, H. F., Torres, O., Browell, E. V., and Melfi, S. H.: Validation of the Saharan dust plume conceptual model using Lidar, Meteosat, and ECMWF data, Bull. Amer. Meteor.Soc., 80, 1045 - 1074, 1999.

Köhler, H., The nucleus in and the growth of hygroscopic droplets, Trans. Faraday Soc., 32(2), 1152 - 1161, 1936.

Kouimtzis, T., and Samara, C.: Airborne Particulate Matter, pp. 339, Springer, New York, 1995.

Kumar, P., Sokolik, I. N., and Nenes, A.: Parameterization of cloud droplet formation for global and regional models: including adsorption activation from insoluble CCN, Atmos. Chem. Phys., 9, 2517 - 2532, 2009, http://www.atmos-chem-phys.net/9/2517/2009/.

Kumar, P., Sokolik, I. N., and Nenes, A.: Measurements of cloud condensation nuclei activity and droplet activation kinetics of fresh unprocessed regional dust samples and minerals, Atmos. Chem. Phys. Discuss., 10, 31039 – 31081, 2010, www.atmos-chem-phys-discuss.net/10/31039/2010/.

Levin, Z., and Cotton, W. R.: Aerosol Pollution Impact on Precipitation: A scientific review, Springer Press., pp. 382, 2008.

Levin, Z., Ganor, E., and Gladstein, V.: The effects of dust particles coated with sulfate on rain formation in the Eastern Mediterranean, J. Appl. Meteorol., 35, 1511 - 1523, 1996.

Li, X., Maring, H., Savoie, D., Voss, K,. and Prospero, J. M.: Dominance of mineral dust in aerosol light-scattering in the North Atlantic trade winds, Nature, 380, 416 – 419, 1996.

Mahowald, N. and Kiehl, L.: Mineral aerosols and clouds, Geophys. Res. Lett., 30(9), doi:10.1029/2002GL016762, 2003.

Medina, J., and Nenes, A.: Effects of Film Forming Compounds on the growth of Giant CCN: Implications for cloud microphysics and the aerosol indirect effect, J. Geophys. Res.,109, D20207, doi:10.1029/2004JD004666, 2004.

227

Nenes, A., Ghan, S. J., Abdul-Razzak, H., Chuang, P. Y., and Seinfeld, J. H.: Kinetic limitations on cloud droplet formation and impact on cloud albedo, Tellus, Ser. B, 53, 133 – 149, 2001.

Paluch, I. R., and Lenschow, D. H.: Stratiform cloud formation in the marine boundary layer. J. Atmos. Sci., 48, 2141 – 2158, 1991.

Perry, K., Cahill, T., Eldred, R., Dutcher, D. D., and Gill, T. E.: Long-range transport of North African dust to the eastern United States, J. Geophys. Res., 102, 11,225 – 11,238, 1997.

Petters, M. D., and Kreidenweis, S. M.: A single parameter representation of hygroscopic growth and cloud condensation nucleus activity, Atmos. Chem. Phys., 7, 1961 – 1971, 2007, http://www.atmos-chem-phys.net/7/1961/2007/.

Pruppacher, H. R. and Klett, J. D.: Microphysics of Clouds and Precipitation, 2nd edn., Kluwer Academic Publishers, Boston, MA, 137 – 144, 1997.

Rudich, Y., Khersonsky, O., and Rosenfeld, D.: Treating clouds with a grain of salt, Geophys. Res. Lett., 29 (22), 2060, doi:10.1029/2002GL016055, 2002.

Rosenfeld, D.: TRMM observed first direct evidence of smoke from forest fires inhibiting rainfall, Geophys. Res. Lett., 26, 3105 – 3108, 1999.

Rosenfeld, D.: Suppression of rain and snow by urban and industrial air pollution, Science, 287, 1793 – 1796, 2000.

Rosenfeld, D., Rudich, Y., and Lahav, R.: Desert dust suppressing precipitation: A possible desertification feedback loop, Proc. Natl. Acad. Sci. U.S.A., 98(11), 5975 - 5980, 2001.

Sassen, K.: Indirect climate forcing over the western US from Asian dust storms, Geophys. Res. Lett., 29, 1465, doi:10.1029/2001GL014051, 2002.

Sassen, K., DeMott, P. J., Prospero, J. M., and Poellet, M. R.: Saharan dust storms and indirect aerosol effects on clouds: CRYSTAL-FACE results, Geophys. Res. Lett., 30, 1633, doi:10.1029/2003GL017371, 2003.

Savoie, D. L., and Prospero, J. M.: Aerosol concentration statistics for the northern tropical Atlantic, J. Geophys. Res., 82, 5954 – 5964, 1997.

Seinfeld, J. H., and Pandis, S. N.: Atmospheric Chemistry and Physics, John Wiley, New York, USA, 767 – 773, 2006.

Stevens, B., Feingold, G., Cotton, W., and Walco, R.: Elements of the microphysical structure of numerically simulated nonprecipitating stratocumulus, J. Aerosol Sci., 53, 980 – 1006, 1996.

Stevens, B., Cotton, W., and Feingold, G.: Large-eddy simulations of strongly precipitating, shallow, stratocumulus-topped boundary layers. J. Atmos. Sci., 55, 3616 – 3638, 1998.

Teller, A., and Levin, Z.: The effects of aerosols on precipitation and dimensions of subtropical clouds; a sensitivity study using a numerical cloud model, Atmos. Chem. Phys., 6, 67 - 80, 2006, http://www.atmos-chem-phys.net/6/67/2006/.

Toon, O. B.: African dust in Florida clouds Nature, 424, 623-624, 2003.

Twohy, C. H., Kreidenweis, S. M., Eidhammer, T., Browell, E. V., Heymsfield, A. J., Bansemer, A. R., Anderson, B. E., Chen, G., Ismail, S., DeMott, P. J., and Van Den Heever, S. C.: Saharan dust particles nucleate droplets in eastern Atlantic clouds, Geophys. Res. Lett., 36, L01807, 1 - 6, doi:10.1029/2008GL035846, 2009.

Twomey, S.: Minimum size of particle for nucleation in clouds, J. Atmos. Sci., 34, 1832 – 1835, 1977.

Van den Heever, S. C., Carrio, G., Cotton, W. R., DeMott, P. J., and Prenni, A. J.: Impacts of Nucleating Aerosol on Florida Storms. Part I: Mesoscale Simulations, J. Atmos. Sci., 63, 1752 – 1775, 2006.

Whitby, K. T.: The physical characteristics of sulfur aerosols, Atmos. Environ., 12, 135 – 159, 1978.

Yin, Y., Wurzler, S., Levin, Z., and Reisin, T. G.: Interactions of mineral dust particles and clouds: Effects on precipitation and cloud optical properties, J. Geophys. Res., 107(D23), 4724, doi:10.1029/2001JD001544, 2002.

Zhu, L., Nenes, A., Wine, P., and Nicovich, J. M.: Effects of Aqueous Organo-Sulfur Chemistry on Speciation and Particulate MS-to-NSS Ratios, J.Geophy. Res., 111, D05316, doi:10.1029/2005JD006326, 2004.

CHAPTER 7

CONCLUSIONS, IMPLICATIONS, AND RECOMMENDATIONS

FOR FUTURE WORK

7.1 Conclusions

This thesis addresses the role of dust as CCN and GCCN with the goal of improving our understanding of dust-warm cloud interactions, and their representation in regional and global climate models. Chapter 2 examined the importance of water vapor adsorption effects to dust aerosol hygroscopicity and CCN activity, and explored a new thermodynamic approach to describe cloud droplet activation from hydrophilic dust particle by combining multilayer Frenkel-Halsey-Hill (FHH) physical adsorption isotherm and curvature (Kelvin) effects.

A new method of aerosol generation from insoluble mineral particles for CCN activation measurements was developed in this thesis (see Chapter 3). This new method is based on the soft-saltation technique, and generates mineral aerosol with a distribution that resembles the size distributions of dust plumes generated in the natural source region. FHH adsorption activation theory (FHH-AT) was corroborated by measurements of CCN activity of aerosols dry generated from clays, calcite, quartz, and desert soil samples from Northern Africa, East Asia/China, and Northern America in Chapter 3. Based on the dependence of critical supersaturation, s_c, with particle dry diameter, D_{dry}, the appropriateness of FHH-AT and well-established Köhler theory (KT) to mineral dust aerosol was quantified. The experimental exponent, x_{exp}, derived from the measured s_c-

D_{dry} relationship for (fresh and unprocessed) regional dust samples and mineral aerosols was found to be in excellent agreement with FHH-AT (within 10%), with one set of adsorption parameters ($A_{FHH} \sim 2.25 \pm 0.75$, $B_{FHH} \sim 1.20 \pm 0.10$) that adequately reproduced the measured CCN activity for all species considered, and also explained the range of dust-water interactions reported in the literature. The correction to dust CCN activity due to multiply charged particles and dust non-sphericity was also applied. Including multiple charge corrections significantly increased D_{dry} and decreased x_{exp}. Dust non-sphericity corrections were performed by using the dynamic shape factor, $\chi = 1.3 \pm 0.2$, as this range accounted for values for dust reported in the literature. Dust non-sphericity corrections involved correcting for surface area available for water vapor adsorption. This was done by converting from electrical mobility diameter to surface area equivalent diameter. It was found that while the application of the shape factor corrections to CCN activation data changes the dry activation diameters, it does so uniformly so that the magnitude of the exponent derived from the s_c-D_{dry} relationship (hence the implied activation physics) is not substantially affected with a deviation as low as 5%.

In Chapter 4, measurements of CCN activity and number size distributions of aerosol wet generated (from atomization of a dust aqueous suspension) from mineral samples (clays and regional soils used in Chapter 3) were reported. Number size distributions obtained from wet generated dust samples indicated unimodal distributions with particle sizes that were up to 10 times smaller those generated by dry technique. For wet generated clays and mineral aerosol, bimodal number size distributions were obtained for kaolinite, illite, calcite, while a unimodal distribution was observed for

montmorillonite clay. Based on the comparisons with the number size distribution generated by the dry technique, it was suggested that the second observed peak in the wet generation method could be a consequence of the external mixture containing more hygroscopic smaller particles and the less hydrophilic bigger particles. Measurements of the CCN activity indicated that the wet generated dust particles were significantly more CCN active than those generated from the dry soft-saltation technique with κ ranging between 0.15 - 0.61. For almost all wet generated regional dust aerosols, x_{exp} is ~ -1.5 (with the exception of ATD), while a much lower x_{exp} ~ -(0.9 ± 0.2) was observed for dry generated dust aerosol. For wet generated clays and mineral aerosols, measurement indicated that smaller particles generated in the more hygroscopic peak follow CCN activation by KT, while the larger peak is less hydrophilic with activation similar to dry generated dust that follow FHH-AT. This confirmed that FHH-AT describes fresh (and unprocessed) dry dust-CCN interactions, while KT is suitable for describing wet generated (processed) dust CCN activity.

The appropriateness of FHH-AT to fresh dust-CCN activation measurements was further substantiated by Ion Chromatography (IC) measurements of regional dust samples which indicated negligible soluble fractions. A comparison of κ_{CCN}, the hygroscopicity parameter determined from dry dust CCN activation measurements with κ_{mix}, hygroscopicity inferred from theory demonstrated that the inferred κ_{mix} for all considered samples was much smaller than the κ_{CCN}. These results confirmed that the presence of soluble fractions alone cannot explain fresh dust CCN activity, and support that water vapor adsorption is the prime source of CCN activity in the fresh dust.

Based on threshold droplet growth analysis (Chapters 3 and 4), dry generated dust CCN was found to have a reduced growth compared to $(NH_4)_2SO_4$ aerosol at the same instrument supersaturation. This implies slower activation kinetics of fresh dust relative to ammonium sulfate aerosol. These delays in activation by dust CCN, when parameterized in terms of the water vapor uptake coefficient, α_c, translated to a 30 - 80% (average = 50%) reduction in α_c (relative to the ammonium sulfate aerosol). Wet generated mineral aerosols, however, display similar activation kinetics to ammonium sulfate. This is consistent with longer time scales associated with adsorption than absorption.

The collected fresh dust CCN activation data were used to develop a new parameterization framework of cloud droplet formation for regional and global climate models by including the effect of adsorption activation on insoluble dust CCN. The new parameterization presented in Chapter 5 considers cloud droplet formation within an ascending air parcel containing insoluble (but wettable) particles activating by FHH-AT, externally mixed with aerosol population containing an appreciable soluble fraction with activation described through KT. This new parameterization is the first of its kind for insoluble CCN such as dust and is developed for sectional and lognormal representations of the aerosol size distribution. To facilitate the analytical development of the parameterization, we further developed FHH-AT by *i*) determining the combinations of A_{FHH} and B_{FHH} for atmospherically-relevant behavior, and, *ii*) linking s_c with D_{dry} using a simple power law expression determined from numerical solutions to the FHH equilibrium curves. The parameterization was tested by comparing predictions of droplet number, N_d, and parcel maximum supersaturation, s_{max}, against detailed cloud parcel

model simulations. The evaluations were performed for a range of updraft velocities, water vapor uptake coefficients relevant to dust CCN, ambient temperature, relative humidity, parameters of aerosol size distributions, and A_{FHH} and B_{FHH}. The parameterization closely followed the parcel model simulations with a mean relative error varying between 2% and 20%, depending on aerosol distribution type with an average relative error of 10% and $R^2 \sim 0.98$.

In this thesis, we also proposed a new unified framework of dust CCN activation that accounted for concurrent effects of solute and adsorption on dust (see Chapter 4). The framework is based on a core-and-shell model and describes equilibrium supersaturation as a function of adsorption parameters, hygroscopicity parameter of the soluble fraction, the size of the dry particle, and the insoluble and soluble volume fraction. An analysis into the framework revealed that as insoluble volume fraction decreased, the x_{exp} changed from -0.85 (FHH-AT limit) and to -1.50 (KT limit). The new framework is ideally suited to describe the CCN activity of aged dust, dry lakebed dust mixed with salts (e.g., Owens Lake, Texcoco, and Aral Sea), and more generally dust particles with significant amounts of soluble materials.

Finally, the ability of dust GCCN to affect cloud microphysics by adsorption activation mechanism was examined in Chapter 6. This was performed by assessing the effectiveness of dust GCCN to act as collector drops within low level stratocumulus and deep convective clouds using a trajectory ensemble model (TEM) approach. Results demonstrate that dust GCCN with dry sizes equal to 1 µm and above activate through water vapor adsorption to become collector drops. It was found that under pristine aerosol conditions, dust GCCN acted as collector drops in both shallow stratocumulus and deep

convective clouds. However under polluted aerosol conditions, dust GCCN growth was inhibited. Furthermore, the impact of activation physics on the dust GCCN growth was investigated. The results show that different droplet sizes were observed when dust GCCN activation was represented by KT and FHH-AT. The effect of B_{FHH} on the dust GCCN growth was also examined, and it was found that as dust hydrophilicity increased (by decreasing B_{FHH}), resulting dust GCCN droplet sizes also increased. It was also shown that the reduced water vapor accommodation properties associated with dust aerosol had negligible impact on activation kinetics of dust GCCN growth within stratocumulus and convective clouds.

7.2   Implications

The results of this thesis confirm that dust particles do not require deliquescent material to act as CCN in the atmosphere. One major implication is that freshly emitted dust and mineral aerosols can act as CCN through the effects of water adsorption alone. Conclusions support that FHH-AT provides a more realistic representation of fresh dust CCN activity than KT in the atmosphere.

The samples investigated in this thesis (see Chapter 3) are representative of major regional dust sources, and the adsorption activation parameters determined can be used to express their CCN activation potential in the cloud droplet formation parameterization presented in Chapter 5. These parameterizations are valid for fresh dust in the dust source regions and for transported dust, if it will not undergo significant atmospheric processing. In some cases, 100 nm dust particles can exhibit comparable hygroscopicity to an organic species with $\kappa \sim 0.05$ or a particle with ammonium sulfate volume fraction of 10%.

An important finding is that the process of wet generation for mineral aerosol leads to significant artifacts in measurements of physical and chemical properties with implications to dust CCN activity (see Chapter 4). These results question the atmospheric relevance of recent studies on mineral dust aerosol generated with the wet atomization method. The method however, still generates a less hydrophilic peak, with the degree of hydrophilicity similar to dry dust, implying that the process of wetting and drying of dust particles do not have a major affect on its hydrophilicity. This contradicts some of the previous studies that tend to show wetting makes dust a better CCN (and likely to some degree is an experimental artifact).

Faster activation kinetics of wet generated dust compared to dry dust would imply that the fresh dust at its source region and cloud processed dust downwind of its source region would behave differently when exposed to the same levels of supersaturation. This carries important implications for both Saharan and Asian dusts, given that large regions of the world are affected by their mid- and long-range transport. Whether a fresh or cloud processed dust has more significant impact on cloud droplet number would also depend on activation physics and time scales of cloud formation.

Another major conclusion of this thesis is that the activation physics carries important implications for cloud droplet number determined from mineral aerosol, even if consistent hygroscopicity and adsorption parameters (i.e., derived from the same experimental data) are used. In certain cases applicable to dust, CCN concentrations can differ by a factor of 10, which may result in up to a 40% difference in predicted cloud droplet number concentration between the two theories (see Chapter 2).

An equally important implication of adsorption activation to dust GCCN growth is that under clean conditions, dust GCCN may have the potential to change a marine stratocumulus cloud from a non-precipitating to precipitating state. Furthermore, the activation of dust GCCN by FHH-AT in deep convective clouds under pristine environments can affect dust-cloud-precipitation linkages with impacts on precipitation efficiency. This result introduces strong implications associated with dust aerosol indirect effect, as earlier studies have assumed dust activation by KT and found negligible effects on convective clouds. These results are of significant importance and suggest that dust GCCN may be influencing the microphysical evolution of clouds to a greater extent that previously assumed by climate models.

An important contribution made by this thesis to understanding aerosol-cloud-climate interactions is that the new FHH-AT framework provides an ideal platform for describing hydrophilic properties of tropospheric aerosols other that mineral dust such as (insoluble) volcanic ash in climate models. This has been recently demonstrated by Lathem et al. (2011) who found that the ash-water interactions in water vapor supersaturated environments associated with volcanic eruptions can be parameterized by FHH-AT with adsorption parameters similar (but less hydrophilic) to dust aerosol. The adsorption parameters determined can be used in atmospheric models with the end goal to improve predictions of ash microphysics, transport and impacts of volcanic aerosols.

An equally important contribution of this thesis is that the new cloud droplet parameterization framework has already been incorporated in both regional (COSMO-ART) and global (NASA-GMI) climate models to address dust aerosol indirect effects. The incorporation of the new parameterization framework provides, for the first time, the

most comprehensive treatment of dust aerosol in climate models. Preliminary results obtained from NASA-GMI study indicate up to a 15% change in cloud droplet number concentration from dust activation by FHH-AT (Karydis et al., 2011). Similarly, the contribution of Saharan dust to cloud droplet activation by FHH-AT over Western Europe is being accounted for in the regional climate model, COSMO-ART (Bangert et al., 2011).

7.3   Recommendations for future work

An important recommendation is that the experiments must be designed to examine the strong size dependence of mineral aerosol to CCN activity. The current dry generation technique is based on the soft-saltation method that generates fine mineral aerosol by shaking the soil sample (present in all possible size ranges) using the wrist-action shaker. The technique should be modified such that soil samples can be separated between the fine and coarse mode aerosol, and using the fine and coarse mode dust separately to generate mineral aerosol CCN. This would allow us to determine any possible size dependence on dust CCN activity. Any differences observed can then be related to differences in mineralogy between the fine and coarse mode for the soil samples collected at the source region. Furthermore, the information collected can be used in regional models to parameterize cloud droplet nucleation from regional soils. It is also proposed to simulate droplet activation in the CCN instrument (CFSTGC) at supersaturations less than 0.1%. This would allow us to experimentally evaluate droplet nucleation behavior of dust particles in sizes representing the lower size spectrum of the coarse mode dust aerosol.

It is recommended to measure morphology of mineral aerosol. This should be pursued by performing simultaneous measurements of dynamic shape factor (χ) or Aspect Ratio (AR). Performing shape measurements would provide more appropriate values required to correct for dust non-sphericity in CCN activation diameters for mineral aerosol.

Experiments should also be designed to examine the effect of residual water (potentially present on particle surface) to dust CCN activation measurements. Such measurements can be performed by introducing fresh (dry) dust into a chamber saturated with water vapor, and then passing the moist aerosol stream through a heated chamber that can operate at different relative humidity (RH). By operating chamber at RH between 5% and 95%, and then measuring the CCN activity downstream of this heated chamber, the effect of residual water coverage on dust CCN activation can be investigated. These measurements would enable constraining the effects of stochastic nature of dust CCN inside the cloud as it undergoes multiple activation/evaporation cycles.

The effect of RH on dust CCN can also be investigated using Environmental Scanning Electron Microscopy (ESEM). ESEM is used to collect data on hygroscopic transformation of individual particles when exposed to RH between 5 - 100%. These measurements will determine the minimum RH at which spontaneous growth of water over particles occurs, which is indicated by the quick disappearance of particle images and blurring on the entire field-of-view. These measurements will indicate critical RH at which the first onset of water vapor monolayer is observed and will provide evidence for water vapor adsorption of mineral aerosol.

Experiments should also examine the possible dependence of the residence time in the CFTGC. The residence time of a particle exposed to controlled water vapor supersaturation depends on the aerosol flow rate through the instrument. The residence can be increased by the decreasing the flow through the instrument to investigate the effect of long equilibration time scales associated with adsorption process.

A number of previous studies have observed coatings of soluble species like sulphates on dust aerosol (Levin et al., 1996; Pratt et al., 2010). CCN experiments should also be designed to elucidate the role of soluble material on the activation of processed mineral aerosol. This would require a modified dust aerosol generation setup to enable heterogeneous chemistry to occur, for instance, between the calcite in dust aerosol and the reactive gaseous specie such as sulphates. Such measurements can provide information on the role of various coatings and the potential for gas phase reactions on the surface of these particles to alter cloud droplet nucleation ability of dust. Coatings should try to reproduce realistic conditions in the atmosphere of reactive gaseous species to get an accurate prediction of dust aging. An example would be Saharan dust mixed with substantial sulfate amounts that is observed over the Eastern Mediterranean. It is also proposed to utilize these measurements to verify the unified dust activation framework proposed in this study (see Chapter 4) for dust aerosol with a coating of soluble salt.

The parameterization of cloud droplet formation from mineral aerosol developed in this thesis is suitable to treat an external mixture of aerosol consisting of soluble Köhler and insoluble FHH-AT particles. It is proposed to extend the parameterization framework to account for the effects of aged dust or dust coated with sufficient solutes.

This may be possible by including the unified dust activation framework in cloud droplet activation parameterization to quantify the contribution of dust with soluble species to cloud droplet activation.

It is also well established that Asian dust can undergo long-range transport across the Pacific Ocean, and has been observed over parts of Hawaii. Hence, it is proposed to extend and investigate the effect of adsorption activation on the growth of dust GCCN representative of Asian dust. This can be performed by using cloud trajectories typical for clouds observed over parts of Hawaii to generate supersaturation profiles, and using adsorption parameters representative of Asian dust aerosol to drive GCCN growth in the cloud parcel model.

Furthermore, it is proposed to combine dust adsorption activation with cloud precipitation parameterizations to simulate the effect of dust aerosol on the cloud precipitation efficiency. This approach will provide a more comprehensive understanding of dust aerosol-cloud-precipitation linkages.

7.4   References

Bangert, M., Nenes, A., Vogel, B., Vogel, H., Barahona, D., and Kumar, P.: The impact of mineral dust particles on cloud formation during a Saharan dust event over Western Europe simulated with an online coupled regional model framework, 2011 (manuscript in preparation).

Karydis, V., Kumar, P., Barahona, D., Sokolik, I. N., and Nenes, A.: On the effect of insoluble dust particles on global CCN and droplet number, 2011 (manuscript in preparation).

Lathem, T. L., Kumar, P., Nenes, A., Dufek, J., Sokolik, I. N., Trail, M., and Russell, A.: Hygroscopic Properties of Volcanic Ash, Geophys. Res. Lett., 2011 (in review)

Levin, Z., Ganor, E., and Gladstein, V.: The effects of dust particles coated with sulfate on rain formation in the Eastern Mediterranean, J. Appl. Meteorol., 35, 1511 - 1523, 1996.

Pratt, K. A., et al.: Observation of playa salts as nuclei in orographic wave clouds, J. Geophys. Res., 115, D15301, doi:10.1029/2009JD013606, 2010.

VITA

PRASHANT KUMAR

Prashant was born in London, United Kingdom (UK) in 1983. He grew up in Delhi, India, and completed high school from Delhi Public School, R. K. Puram, New Delhi in 2001. He moved back to UK for graduation, and earned a B.Eng. (Bachelors in Engineering) in Chemical Engineering from University of Bath in UK in 2006 with first class honors. In 2004 – 2005, he completed 12 months of industrial placement working as a process engineer for DuPont Teijin Films, Ltd. at Middlesbrough, UK. He then moved to Georgia Institute of Technology in January of 2007 to pursue a Ph.D (Doctor of Philosophy) in Chemical Engineering. He joined research groups of Dr. Athanasios Nenes and Dr Irina N. Sokolik. During his Ph.D, he has authored and co-authored 8 peer-reviewed publications (5 as first authors). He received awards for the best research presentation (2nd place) at the 2010 Chemical & Biomolecular Engineering Annual Symposium, and also for the best Teaching Assistant in spring 2010. He will graduate with a Ph.D in May 2011.